Final Report

# MECHANISM IN THE DETONATION REGIME

by

J. A. Nicholls
T. H. Pierce
L. Dye
R. Fry
K. Kearney
M. Liou

Gas Dynamics Laboratories
Department of Aerospace Engineering
The University of Michigan
Ann Arbor, Michigan

for

# FOREWORD

This work was conducted under Contract No. DAAA 21-73-C-0571 at the Gas Dynamics Laboratories, The University of Michigan, in the period 24 May 1973 through December 31, 1973. The research program was directed by Professor J.A. Nicholls, Aerospace Engineering, and the project monitor was Dr. N. Slagg, Explosives Lab., Picatinny Arsenal. Other contributors to this study include the following:

| | |
|---|---|
| T. H. Pierce | Postdoctoral |
| L. Dye | Graduate Student |
| R. Fry | Graduate Student |
| K. Kearney | Undergraduate Student |
| M. Liou | Graduate Student |

# ABSTRACT

A vertical detonation tube was used to study the blast initiated detonation of various liquid fuels, including some monopropellants, in a few different oxygen-nitrogen atmospheres. The fuels tested included n-propyl nitrate, nitropropane, nitromethane, and decane. All fuel drops were of the same size and a range of mixture ratios were tested. The blast wave was initiated by a detonative combustion driver. Much work was done in calibrating the driver in so far as it approximated idealized planar blast wave behavior. Attention was given to the influence of diaphragm thickness, ignition point location in the driver, and charge gas equivalence ratio in the driver. Also, the rate of decay of the blast wave for various spray loadings in the inert atmosphere of the driven section was determined. The experiments were guided by a theoretical analysis which treated the necessary conditions required for self sustained heterogeneous detonation. Further, an approximate theory was developed for the initiation criteria for gas phase and heterogeneous detonation. Experimental results are presented which indicate when detonation was realized, the detonation velocity attained, and some pressure-time profiles. NPN was probably the most easy to detonate, even in air.

Experiments were also conducted in a sectored chamber, wherein cylindrical blast waves were generated by a condensed explosive and electric detonators. The details of individual drop breakup and ignition

were observed using streak schlieren optical techniques. Normal propyl nitrate and decane drops of 384 $\mu$m and 768 $\mu$m diameter were shocked by blast waves of Mach 2 to 6, in ambient atmospheres of 100% $O_2$, 50% $O_2$- 50% $N_2$, and Air at standard conditions. Qualitatively, the results conclusively show that the time history of the drop breakup and ignition was extended due to the rapidly decaying local dynamic conditions behind the incident blast waves.

# LIST OF FIGURES

# LIST OF TABLES

# TABLE OF CONTENTS

# I. INTRODUCTION

The objective of this program was to study the behavior of certain fuel drops in different oxidizing atmospheres when subjected to a blast wave. The program was subdivided into two major phases; studies relating to the initiation of self-sustaining heterogeneous detonations in a vertical tube; and studies relating to the breakup and ignition of liquid fuel drops in a sectored tube. Many variables were of interest, including the strength of the incident shock wave, the fuel, the oxidizer, the fuel drop size and spacing, and the number of fuel streams. Velocity, pressure, and photographic data were desired. The combination of these variables of interest implied a considerable number of tests, many of which could be ruled out on the basis of known information. Accordingly, a rather extensive theoretical analysis was performed which treated the necessary conditions required in order that heterogeneous detonations in the vertical tube be initiated and self-sustaining. This was of immeasurable help in guiding the experiments and reducing the data.

The existing vertical detonation tube was altered so that a true planar blast wave could impact on the two-phase cloud. Most of the experimentation was done in this tube. The sectored shock tube supplied data on cylindrical blast waves impacting fuel drops. While it required no modifications, streak schlieren and fuel drop generation systems required some time to finalize.

1

The investigation is described in detail in the following sections. The reader is referred to Tables II and III for a quick review of the experimental conditions treated in the vertical and sectored tubes, respectively, as well as a brief summary of the findings.

# II. THEORETICAL ASPECTS

The experiments to be described in Section III of this report demonstrate the detonability of the several monopropellants tested in various atmospheres. Initiation was attempted in all cases with an axial detonation-mode combustion driver, using premixed stoichiometric hydrogen and oxygen at an initial mixture pressure of 50 psig. This initiator was intended to approximate a blast wave, and is discussed in detail in Section III. In those tests for which the monopropellant detonation did occur, the detonability of the particular spray/oxidizer combination was established. However, in those combinations which failed to detonate, the failure may be traced either to insufficient energy release, or to an inadequate initiation source. It was therefore considered of significance in the present study to investigate the nature of the limits which correspond to these two causes for detonation failure.

## A. MINIMUM REACTANT ENERGY REQUIREMENTS

A freely propagating detonation is possible only when the net energy release within the reaction zone (after losses to the surroundings) is sufficient to sustain a shock front that is capable of continually igniting fresh reactants. The magnitude of the minimum shock front strength is not well defined, but it is believed to be associated with shock temperatures below which reaction rates would become excessively slow.

An indication of expected detonation Mach number for a given energy release in a two-phase detonation can be obtained from the conservation equations. Written between point (1), which is at the leading shock, and point (3), which is at the Chapman-Jouguet point, these are

$$\rho_3 a_3 - \rho_1 U_s = \omega_s \rho_1 U_s \qquad (1)$$

$$\rho_3 a_3^2 \left(\frac{\gamma_3 + 1}{\gamma_3}\right) - \rho_1 \left(U_s^2 + \frac{a_1^2}{\gamma_1}\right) = U_s^2 \omega_s \rho_1 + \frac{b}{A_c} \int_0^{x_R} \tau_\omega \, dx \qquad (2)$$

$$\rho_3 a_3^3 \left(\frac{\gamma_3 + 1}{\gamma_3 - 1}\right) - \rho_1 U_s \left(\frac{2a_1^2}{\gamma_1 - 1} + U_s^2\right) = \omega_s \rho_1 U_s (2e_s + U_s^2)$$

$$+ \frac{2b}{A_c} \int_0^{x_R} \tau u \, dx + 2\epsilon \omega_s \rho_1 U_s - \frac{2b}{A_c} \int_0^{x_R} \dot{q} \, dx \qquad (3)$$

In these equations, $\rho_1$ is the density of the "carrier gas" in which the spray is initially suspended, $U_s$ is the propagation velocity of the leading shock, $\gamma$ is the ratio of specific heats, b is the perimeter of the duct in which the spray/carrier system is confined, whose cross-sectional area is $A_c$, and $x_R$ is the reaction zone length, $\tau$ is the shear stress at the duct wall, and $\dot{q}$ is the heat transfer rate to the wall. The "loading factor", $\omega_s$, is the ratio of the entire quantity of mass per unit volume that is initially in the condensed

4

phase, $\rho_s$, to the density of the carrier gas, $\rho_1$; i.e., $\omega_s = \rho_s/\rho_1$. The

energy released by combustion within the reaction zone has been designated

in writing these forms by the product $\rho_1 \omega_s \epsilon$, which is the same as $\rho_s \epsilon$.

Hence, the symbol $\epsilon$ carries the meaning of energy liberated per unit mass

of the <u>entire</u> condensed phase, regardless of its chemical nature or geo-

metric form (e.g., spray, film).

Equation (1)-(3) are similar to those given by Ragland et al.[1] except

that they are more general. However, following Ragland we introduce

$$C_D \equiv b \int_0^{x_R} \tau \, dx \, / \, (\tfrac{1}{2} \rho_2 u_2^2 A_s) \tag{4}$$

and

$$C_H \equiv b \int_0^{x_R} \dot{q} \, dx \, / \left[ \rho_2 u_2 A_s \left( h_2 + \frac{u_2^2}{2} - h_w \right) \right] \tag{5}$$

in which $A_s$ is the surface area in the duct that is wetted by the reaction

zone, $h_w$ is the gas enthalpy at the wall (recovery enthalpy). Point (2) is

located just downstream of the leading shock so that $\rho_2$, $u_2$, and $h_2$ are the

density, absolute velocity, and enthalpy there. Then assuming that

$$\int_0^{x_R} \tau u \, dx \approx U_s \int_0^{x_R} \tau \, dx \tag{6}$$

5

and also that $h_w \doteq h_2$, Eq. (1)-(5) can be solved to give

$$\left(\frac{U_s}{U_{s_0}}\right)^2 = \cfrac{1}{1 + \left[C_D + 2(\gamma_3^2 - 1) C_H\right]\left(\frac{x_R/r_h}{1 + \omega_s}\right)\cfrac{u_2^2}{U_s (U_s - u_2)}} \tag{7}$$

in which

$$U_{s_0}^2 = 2(\gamma_3^2 - 1) \omega_s \, \epsilon \, / \, (1 + \omega_s) \tag{8}$$

and $r_h \equiv A_c/b$ is the hydraulic radius. If the further assumptions are made that $C_H = 2 C_D$ and

$$\frac{u_2^2}{U_s (U_s - u_2)} \doteq 3.0 \tag{9}$$

Eq. (7) can be additionally simplified to

$$M_s^2 = \frac{2(\gamma_3^2 - 1) \omega_s \, \epsilon/a_1^2}{1 + \omega_s + 6 C_H \gamma_3^2 x_R / r_h} \tag{10}$$

which is adequate for reasonably approximate use.

In the case of a two-phase detonation in which the condensed phase and the carrier gas together form a reactive system, and in which the condensed phase does not add energy by its own dissociation, the "loading factor" assumes the meaning of a global fuel/oxidizer ratio, $\phi_0$. The energy liberated per unit mass of condensed phase reactant is then simply its heat of combustion, $\mathcal{H}_c$. Thus, $\omega_s = \phi_0$ and $\epsilon = \mathcal{H}_c$ in this case, and so Eq. (10) becomes

$$M_s^2 = \frac{2(\gamma_3^2 - 1)\,\phi_o \mathcal{H}_c / a_1^2}{1 + \phi_o + 6C_H\,\gamma_3^2\, x_R/r_h} \tag{11}$$

which is the form obtained by Ragland.

On the other hand, if the condensed phase reactant is a monopropellant, the carrier gas may or may not contribute to the total energy release. A global fuel/oxidizer ratio cannot be defined for purposes of computing $M_s$ using the form of Eq. (11). Instead, Eq. (10) must be used.

For a spray/carrier system, the loading factor $\omega_s$ can be written in terms of the number density of the spray, $n_s$, and the drop size in the spray, $D_s$ (presuming it is monodispersed), as

$$\omega_s = \left(\frac{\pi}{6}\frac{\rho_\ell}{\rho_1}\right) n_s\, D_s^3 \tag{12}$$

where $\rho_\ell$ is the condensed phase mass density. Hence, if a minimum Mach number is defined, below which detonation is not expected to occur, Eq. (10) and (12) allow for computation of a locus in the $n_s$-$D_s$ plane that corresponds to the minimum required droplet number density at each drop size.

Now, the reaction zone length in Eq. (10) can be approximated by the semi-empirical expression[2]

$$x_R \doteq \frac{10\,D_o}{u_2}\sqrt{\frac{\rho_\ell}{\rho_2}}\,U_s \tag{13}$$

7

in which $D_0$ is the drop size in the spray. It is easy to show that for

$M_s > 3$, this is a weak function of Mach number. Hence, Eq. (10) shows

that as $\omega_s \rightarrow \infty$, the detonation Mach number should asymptotically approach

$$M_s^2 \rightarrow 2 \, (\gamma_3^2 - 1) \, \epsilon \, / \, a_1^2 \tag{14}$$

provided that $\epsilon$ = constant. This would in fact be the case for a monopro-

pellant in a nonreactive carrier, for which $\epsilon = \mathcal{H}_D$, the dissociation energy.

On the other hand, if the carrier is exothermally reactive with the mono-

propellant, then $\epsilon = \epsilon \, (\omega_s)$. As $\omega_s$ is increased above zero, $\epsilon = \mathcal{H}_c$, the heat

of combustion, until stoichiometric proportions (approximately) are reached.

Thereafter $\epsilon$ would decrease monotonically toward $\mathcal{H}_D$ and the Mach number

would again asymptotically approach the value in Eq. (14) (with $\epsilon = \mathcal{H}_D$) as

$\omega_s \rightarrow \infty$.

If the Mach number computed from Eq. (14) is less than the defined

minimum, using $\epsilon = \mathcal{H}_D$, then a freely propagating detonation in a system

composed of the liquid monopropellant and a non-reactive carrier cannot be

expected. In general, $\mathcal{H}_c > \mathcal{H}_D$, and so it may be possible for the same

monopropellant to detonate in a reactive carrier. This would have to be

checked by Eq. (10) and (12).

## B. INITIATION REQUIREMENTS

The detonability of a reactive system and its initiation by a particular source must be considered separately. A system that is not detonable cannot be initiated by any source; on the other hand, a detonable system cannot be initiated by _every_ source. Of interest in the present study is the initiation potential of blast waves, which may occur in the detonable medium as the result of a spark discharge, an exploding wire, a focused pulsed laser, or an exploded charge, for example.

The decay rate of a blast wave is a function of the energy deposited by the source, the geometry of the source, and the physical properties of the medium in which it occurs. If the medium consists of both a gas phase component and a condensed phase component, the magnitude of the decay rate will in general be increased above that which would obtain in the absence of the condensed phase. This is due to the increased effective density of the medium and to loss of latent heat if the condensed phase vaporizes. Blast wave characteristics for a two-phase system therefore cannot be properly assessed from gas-phase formulations, and initiation requirements for the two systems must be developed separately. However, the physical ideas leading to an initiation criterion will be common to both, and the two-phase system will accordingly be treated as an extension of the gas-phase formulation.

## 1. Initiation of Gas-Phase Reactants

A blast wave of energy $E_0$ consists of a shock front whose radius is described by $R_s(t)_2$ and an expansion region which extends from the shock front to the position of original energy deposition (center of explosion). In the expansion region, the gas that was accelerated by the shock front is brought to rest. The blast wave velocity, $U_s(t) = d R_s/dt$, monotonically decreases from infinity at the center of explosion to the sonic velocity as $R_s \to \infty$.

While the blast wave is very strong, the reactive gas into which it is expanding is ignited, with an extremely short induction zone. If $E_0$ is large, the blast wave is subsequently observed to transform into a detonation wave, approaching the Chapman-Jouguet propagation velocity, $U_{CJ}$, in a monotonic fashion. For somewhat lower $E_0$, the blast wave velocity decays below $U_{CJ}$, reaches a minimum, and then slowly returns to $U_{CJ}$. Both of these cases are included in what Bach et al.[3], term a "supercritical" regime.

For still lower $E_0$, the induction zone length does not remain small throughout the transformation. Rather, as $U_s$ decays toward Mach numbers $M_s \to 3$, the induction zone length increases exponentially. A critical blast wave energy, $E_0 = E_{0c}$, exists below which this growth in induction zone length does not terminate and the blast wave simply decays to a Mach wave without effecting initiation. This is the "subcritical" regime.

When $E_0 = E_{0_c}$, the blast wave decays until it reaches a critical Mach number, $M_c$, whose value is $M_c \sim 3$. The reaction zone at this point has separated substantially from the leading shock, but this separation remains finite. It is observed in this case that the wave will propagate in a quasi-stable fashion for some time before it will begin to accelerate towards $U_{CJ}$. This is the "critical" regime. The three regimes are illustrated in Fig. 1.

In a more recent work, Bach et al.[4] have analyzed a decaying reactive blast wave by modifying Sakurai's formulation[5] to include the time varying energy release. Computed profiles similar to the sketches in Fig. 1 are obtained from which $E_{0_c}$ can be determined by identifying the lowest value of $E_0$ for which $U_s \rightarrow U_{CJ}$ as $t \rightarrow \infty$. This procedure yields useful results but is rather cumbersome. For many purposes, the $U_s(t)$ curve is not required and the value of $E_{0_c}$ is all that is sought. In the present work, a direct means of estimating $E_{0_c}$ is developed.

Near the center of explosion, most of the gas within a blast wave is contained in the region just behind the leading shock. During subsequent expansion, this mass is carried out of this zone and is distributed throughout the expansion region. In this manner, the thermal energy content in the vicinity of the shock is continually diminished. When a blast wave occurs in a reactive medium, however, energy is added at a rate which is a function of $u_s(t)$ and the chemical characteristics of the medium.

The blast wave in this case can be expected to decay until the rate of energy addition exceeds the energy depletion rate. This crossover may occur before or after the point at which $M_s = M_{CJ}$. However, it must occur before $M_s = M_c$. If at this point the net rate of energy accumulation in the extended induction zone is negative, the thermal content of the near-shock region will be insufficient to support further ignition. Hence, an estimate of $E_{0_c}$ can be derived from the conceptual argument that the blast wave produced by this particular amount of energy deposition will result in the occurrence of a balance of energy production and depletion rates within the induction zone at the point in time for which $M_s = M_c$. This may be expressed formally for each possible blast wave geometry, as follows. For a planar wave,

$$\rho_{F_1} \mathcal{H}_c \, U_{s_c} \, A_c = - A_c \frac{d}{dt} \int_0^{\Delta_c} \xi \, dx \tag{15}$$

in which $A_c$ is an arbitrary planar area, while for a cylindrical wave

$$\rho_{F_1} \mathcal{H}_c \, U_{s_c} \, 2\pi \, R_c \, L = - 2\pi \, R_c \, L \frac{d}{dt} \int_0^{\Delta_c} \xi \, dx \tag{16}$$

where L is an arbitrary length, and for a spherical wave

$$\rho_{F_1} \, \mathcal{H}_c \, U_{s_c} \, 4\pi \, R_c^2 = -4\pi \, R_c^2 \, \frac{d}{dt} \int_0^{\Delta_c} \xi \, dx \qquad (17)$$

In each of these expressions, the left hand side represents the energy production rate and the right hand side represents the depletion rate. The partial density of fuel vapor in the reactive gas is $\rho_{F_1}$, and the heat of combustion per unit mass of fuel is $\mathcal{H}_c$. The blast wave radius at the critical condition is $R_c$, the internal energy per unit volume in the induction zone is designated by $\xi(x)$, and the induction zone length is $\Delta_c$. Equations (15)-(17) are equivalent to

$$\rho_{F_1} \, \mathcal{H}_c \, U_{s_c} = -\frac{d}{dt} \int_0^{\Delta_c} \xi \, dx \qquad (18)$$

The internal energy of the gas mixture is $\xi = \rho e$, per unit volume, where $e \approx C_v T$. Then

$$\xi \doteq P/(\gamma_1 - 1) \qquad (19)$$

in the induction zone. The subscript (1) again refers to the gas ahead of the shock.

Presumably if the balance in Eq. (18) is established, the induction zone length would be unchanging at that moment; i.e., $d\,\Delta_c/dt = 0$ at the critical time, $t_c$. Hence the integral in Eq. (18) has "constant" limits.

13

Before carrying out the integration, some simple transformations are worth-while. Defining $\bar{P} \equiv P_2/P_1$ as the shock pressure ratio, $\zeta \equiv x/R_s$, $\tilde{P} \equiv P/P_2$, and $\delta^* \equiv \Delta_c/R_{s_c}$, we may write

$$\frac{d}{dt} \int_0^{\Delta_c} \xi \, dx = R_s \frac{d}{dt} \int_0^{\delta^*} \frac{P_1 \bar{P} \tilde{P}}{\gamma_1 - 1} \, d\zeta \tag{20}$$

Now, $\bar{P} = \bar{P}(t)$ only, while $\tilde{P} = \tilde{P}(\zeta, t)$ in general. In the case of a self-similar (strong) blast wave, $\tilde{P} = \tilde{P}(\zeta)$ (Ref. 6) only. Then Eq. (20) becomes

$$\frac{d}{dt} \int_0^{\Delta_c} \xi \, dx = \frac{R_s P_1}{\gamma_1 - 1} \frac{d\bar{P}}{dt} \int_0^{\delta^*} \tilde{P}(\zeta) \, d\zeta \tag{21}$$

Medium strength blast waves, with $M_s < 5$, approximately, are no longer self-similar. However, the departure from self-similarity does not become pronounced until $M_s \lesssim 3$. That is, changes in profile _shape_ do not occur rapidly in blast waves, above $M_s \sim 3$. Therefore Eq. (21) can be applied to the range $3 < M_s < \infty$ with acceptable accuracy, but the actual profile $\tilde{P}(\zeta)$ to be used should be taken from the blast wave theory appropriate to the regime near $M_s = M_c$.

The derivative $dP/dt$ contains the greatest information describing the blast wave decay rate. The usual blast wave notation is used to express this derivative in a convenient form; namely, $y \equiv M_s^{-2}$, $R_s = R_s/R_0$, and

$$R_0 = (E_\alpha/P_1)^{1/\alpha+1} \tag{22}$$

Here, $\alpha$ refers to the geometry of the blast wave, assuming the values $\alpha = 0, 1, 2$ for the planar, cylindrical, and spherical geometries, respectively. The parameter $E_\alpha$ represents the energy released at the center of explosion:

$$E_O = \text{energy per unit area}$$

$$2\pi E_1 = \text{energy per unit length} \qquad (23)$$

$$4\pi E_2 = \text{energy}$$

Following Sakurai[7] we also introduce

$$\lambda(y) \equiv \frac{R_s}{y} \frac{dy}{dR_s} \qquad (24)$$

so that

$$\frac{d\overline{P}}{dt} = \frac{dy}{dR_s} \frac{dR_s}{dt} \frac{d\overline{P}}{dy}$$

or

$$\frac{d\overline{P}}{dt} = \frac{U_s \lambda y}{R_o \overline{R}_s} \frac{d\overline{P}}{dy} \qquad (25)$$

Values of $\overline{R}_s(y)$ and $\lambda(y)$ are readily available from any blast-wave theory. The derivative $d\overline{P}/dy$ can be evaluated directly from the shock-wave relation,

$$\frac{d\overline{P}}{dy} = \frac{d}{dy}\left[\frac{2\gamma_1}{\gamma_1 + 1} \frac{1}{y} - \frac{\gamma_1 - 1}{\gamma_1 + 1}\right]$$

15

giving

$$\frac{d\bar{P}}{dy} = - \frac{2\gamma_1}{\gamma_1 + 1} y^{-2} \qquad (26)$$

Then, combining Eq. (18), (21), (25), and (26), there obtains

$$\rho_{F_1} \mathscr{U}_c = \left(\frac{2\gamma_1}{\gamma_1^2 - 1}\right) \frac{P_1 \, \lambda(y_c)}{y_c} I_1(\delta^*) \qquad (27)$$

in which

$$I_1(\delta^*) \equiv \int_0^{\delta^*} \tilde{P}(\zeta) \, d\zeta \qquad (28)$$

The integral $I_1(\delta^*)$ can be evaluated directly from explicit forms for $\tilde{P}(\zeta)$, in the case of strong blast waves. However, $M_c$ is more typically within the medium strength regime, for which closed form blast-wave solutions do not exist. It is not inconsistent with the approximate approach being followed here to avoid this complication by assuming that when $M_s = M_c$, $\delta^* \ll 1$. This is tantamount to taking $\tilde{P}(\zeta) = 1$ over the range $0 \leq \zeta \leq \delta^*$, and the result is $I_1(\delta^*) = \delta^*$. Then Eq. (27) simplifies to

$$\rho_{F_1} \mathscr{V}_c = \frac{2\gamma_1}{\gamma_1^2 - 1} \frac{P_1 \lambda(y_c)}{y_c} \frac{\Delta_c}{R_{0_c} \bar{R}(y_c)} \tag{29}$$

The product $\rho_{F_1} \mathscr{V}_c$ can be written in terms of the Chapman-Jouguet detonation velocity in the gas mixture, $U_{s_{CJ}}$, by noting that

$$U_{s_{CJ}}^2 \doteq 2(\gamma_3^2 - 1) \frac{\rho_{F_1} \mathscr{V}_c}{\rho_1} \tag{30}$$

where (3) refers to the burned gases. Hence, with $y_{CJ} \equiv M_{CJ}^{-2}$, Eq. (29) becomes

$$R_0 = \frac{4(\gamma_3^2 - 1) \lambda(y_c) y_{CJ} \Delta_c}{(\gamma_1^2 - 1) \bar{R}(y_c) y_c} \tag{31}$$

or, using Eq. (22),

$$\frac{E_{\alpha_c}}{P_1} = \left[ \frac{4(\gamma_3^2 - 1) \lambda(y_c) y_{CJ} \Delta_c}{(\gamma_1^2 - 1) \bar{R}(y_c) y_c} \right]^{\alpha+1} \tag{32}$$

In the notation of Bach et al.[4], $E_\alpha = E_0/K_\alpha$, where

$$K_\alpha = \begin{cases} 1 & , & \alpha = 0 \\ 2\pi & , & 1 \\ 4\pi & , & 2 \end{cases} \tag{33}$$

and we can then write for the minimum critical energy release,

$$E_{o_c} = K_\alpha \gamma_1 P_1 \left(\frac{\Delta_c}{\delta_c}\right)^{\alpha+1} \qquad (34)$$

in which

$$\delta_c = \left(\frac{\gamma_1^2 - 1}{\gamma_3^2 - 1}\right)\left[\gamma_1^{\frac{1}{\alpha+1}}\frac{1}{4}\right]\left(\frac{\overline{R}(y_c)}{\lambda(y_c)}\right)\left(\frac{M_{CJ}}{M_c}\right)^2 \qquad (35)$$

Values of $\lambda(y)$ and $\overline{R}(y)$ for $\gamma_1 = 1.4$ appear in Fig. 2 and 3. These were

computed from Sakurai's linear particle velocity theory. The form of

Eq. (34) is identical to that obtained in Ref. 4. However, Eq. (35) provides

a direct means of computing the value of $\delta_c$.

In Ref. 4 there also appears some experimental data with which Eq. (34)

may be compared. For a stoichiometric mixture of $C_2H_2$ and oxygen at

$P_1 = 100$ mm Hg, it is found that for initiation of detonation by a spherical

blast wave, a minimum energy deposition of $E_{o_c} \doteq 0.3$ Joules is required.

To compute $E_{o_c}$ from Eq. (34) it is necessary first to specify $M_c$ (or $y_c$)

and to determine a value for $\Delta_c$. It should be pointed out that neither $\Delta_c$

nor $\delta_c$ carries the meaning in this study that is assigned to it in Ref. 4.

Here, $\Delta_c$ is the induction zone length when $M_s = M_c$, and it will be approxi-

mated from

$$\Delta_c \doteq \hat{U}_{2_c} \tau_c \qquad (36)$$

where $U_2$ is the velocity at which the shock separates from fluid particles

that have passed through it; i.e.

18

$$\hat{U}_2 \qquad U_s - U_2$$

and $U_{2_c}$ is its magnitude when $M_s = M_c$. The induction time at the critical

Mach number is $\tau_c$. In the present example, $\tau_c \approx 40 \ \mu sec$, $M_{CJ} \approx 8.0$, $\gamma_1 = 1.31$,

$\gamma_3 \approx 1.13$, and $a_1 \approx 1070$ ft/sec. The critical Mach number was taken as $M_c = 3.5$.

From these data we find $U_{2_c} = 770$ ft/sec and $\Delta_c = 3.08 \times 10^{-2}$ ft = 8.56 mm.

The approximate values of $\bar{R}(y_c)$ and $\lambda(y_c)$ are read from Fig. 2 and 3;

these are $\bar{R}(y_c) \doteq 0.525$ and $\lambda(y_c) \doteq 2.81$, at $y_c = 0.082$. Then, for $\alpha = 2$,

Eq. (35) gives $\delta_c = 0.685$ and Eq. (34) results in $E_{0_c} = 0.565$ Joules.

Although this result is reasonably close to the measured value, $E_{0_c} \doteq 0.3$

Joules, the intermediate calculations are indicative of difficulties in the theory.

The parameter $\delta*$ is not small, but indicates an allowable induction zone

length that actually exceeds the blast wave radius when $M_s = M_c$. While this

is possible if $M_s$ remains at $M_c$ for some period of time, it can certainly

not be the case at the first instant when $M_s$ has just reached $M_c$. Moreover,

because $\delta*$ is not small, the theoretical simplification $I_1(\delta*) = \delta*$ is not

corroborated.

It is believed however that these difficulties are not inherent in the basic

approach to the initiation criterion, but are traceable to the simplifications

in expressing energy release rates and in computing the critical induction

zone length, $\Delta_c$. As to the first of these, the energy release rate was taken

in the derivation to be $\rho_{F_1} \mathcal{H}_c U_s$, per unit shock-wave area. This is the

rate of accumulation of maximum potential chemical energy within the blast wave at a given instant. The energy release rate may, however, be substantially lower than this.

Second, a gas particle that ignites at the instant when $M_s = M_c$ must have passed through the shock at an earlier time, when $M_s > M_c$. The difference between these two Mach numbers can be substantial. Hence the induction time for this particle is shorter than that computed for a particle subjected to conditions corresponding to $M_s = M_c$. That is, $\Delta_c$ is less than that given by Eq. (36).

## 2. Initiation of Two-Phase Reactants

More work is needed to resolve the difficulties in the model for gas-phase initiation. Until this can be completed, the extension to two-phase reactants should be postponed. However, any description of initiation in two-phase media will require knowledge of simple blast-wave behavior therein.

In the case of a two-phase system, it is clear that during the transition from a blast-wave to a detonation wave, the flow downstream of the shock must at all times be able to effect the conversion of the liquid phase reactant to its vapor phase. In the following derivations, therefore, it will be assumed that the "shock" consists of the entire zone in which the conversion occurs. The symbol (1) will refer to conditions upstream of the leading shock wave, and (3) to those at the end of the conversion zone, whose length is $x_B$. At point (3), a homogeneous mixture of evaporate and initial carrier gas exists.

The conservation equations written between these two points are

$$\rho_3 \hat{U}_3 = \rho_1 U_s (1 + \omega_s) \tag{37}$$

$$P_1 + \rho_1 U_s^2 (1 + \omega_s) = P_3 + \rho_3 \hat{U}_3^2 \tag{38}$$

and

$$h_1 - \omega_s (\mathcal{L} - e_s) + \frac{1}{2}(1 + \omega_s) U_s^2 = (1 + \omega_s)\left(h_3 + \frac{\hat{U}_3^2}{2}\right) \tag{39}$$

In these equations, $\omega_s$ is the loading factor of the condensed phase, $\hat{U}_3$ is the gas velocity at point (3) relative to the leading shock, h represents static enthalpy, $\mathcal{L}$ is defined by

$$\mathcal{L} \equiv \mathcal{L}^* - (C_{v_s} - C_s) T_b \tag{40}$$

and $e_s = C_s T_1$. The constant volume specific heat of the vaporized liquid is $C_{v_s}$, and its specific heat in the condensed phase is $C_s$. The latent heat of the liquid at its boiling point, $T_b$, corresponding to pressure $P_1$, is $\mathcal{L}^*$.

Now we define

$$\phi \cong 1 + \omega_s \tag{41}$$

and

$$\psi \equiv \omega_s (\mathcal{L} - e_s) \tag{42}$$

21

Then the "shock" equations, Eq. (37)-(40), take the simplier form

$$\phi \rho_1 U_s = \rho_3 \hat{U}_2 \tag{43}$$

$$P_1 + \rho_1 \phi U_s^2 = P_3 + \rho_3 \hat{U}_3^2 \tag{44}$$

and

$$\frac{a_1^2}{\gamma_1 - 1} - \psi + \frac{1}{2} \phi U_s^2 = \phi \frac{a_3^2}{\gamma_3 - 1} + \frac{1}{2} \phi \hat{U}_3^2 \tag{45}$$

After some manipulation, these algebraic equations can be solved for $\rho \equiv \rho_3/\rho_1$,

$$\bar{\rho} = \frac{\dfrac{\gamma_3}{\gamma_3 - 1} \phi (1 + \zeta) \pm \phi \, \nu^{1/2}}{2 \left[ \dfrac{\gamma_1}{\gamma_1 - 1} - \gamma_1 \, \tau + \dfrac{1}{2} \zeta \right]} \tag{46}$$

in which

$$\nu = \left( \frac{\gamma_3}{\gamma_3 - 1} \right)^2 (1 + \zeta)^2 - 4\zeta \left[ \frac{\gamma_1}{\gamma_1 - 1} - \gamma_1 \, \tau + \frac{1}{2} \zeta \right] \left[ \frac{\gamma_3}{\gamma_3 - 1} - \frac{1}{2} \right] \tag{47}$$

and

$$\tau \equiv \psi/a_1^2 \tag{48}$$

$$\zeta \equiv \gamma_1 \phi M_s^2 \tag{49}$$

22

Equation (46) is the "exact" form for the shock density ratio. It is simplified when

$$\left| \gamma_1 \tau \right| \ll \frac{\gamma_1}{\gamma_1 - 1} + \frac{1}{2}\zeta$$

can be assumed, which is equivalent to

$$\left| \frac{\omega_s (\mathscr{X} - e_s)}{a_1^2} \right| \ll \frac{1}{\gamma_1 - 1} + \frac{(1 + \omega_s)}{2} M_s^2$$

This is valid for sufficiently large $M_s$ and/or very small $\omega_s$. If $\omega_s$ is large, the assumption requires

$$M_s^2 \gg 2 \left| \frac{\mathscr{X} - e_s}{a_1^2} \right|$$

Using this assumption, Eq. (47) gives

$$\nu = \frac{1}{(\gamma_3 - 1)^2} \left[ \zeta^2 + 2\zeta \frac{(\gamma_1 - \gamma_3^2)}{(\gamma_1 - 1)} + \gamma_3^2 \right] \tag{50}$$

Now, for purposes of assessing the value of $\nu$ in Eq. (50), it can readily be demonstrated that for typical values of $\gamma_1$ and $\gamma_3$, the error incurred by replacing the term in brackets by $(\zeta - \gamma_3)^2$ is $O(M_s^{-2})$. Hence, with this simplification,

$$\nu \approx \left( \frac{\zeta - \gamma_3}{\gamma_3 - 1} \right)^2$$

and then Eq. (46) becomes

$$\bar{\rho} = \frac{\left(\dfrac{\gamma_3}{\gamma_3 - 1}\right) \phi \, (1 + \zeta) \pm \phi\left(\dfrac{\zeta - \gamma_3}{\gamma_3 - 1}\right)}{2\left[\dfrac{\gamma_1}{\gamma_1 - 1} + \dfrac{1}{2}\zeta\right]} \tag{51}$$

The non-trivial solution is recovered by taking the + sign in the numerator, yielding

$$\bar{\rho} = \frac{\beta_2 \, \phi \, M_s^{\,2} \, (\gamma_1 + \beta_1)}{2 + (\gamma_1 - 1) \, \phi \, M_s^{\,2}} \tag{52}$$

in which $\beta_1 \equiv \gamma_1 / \gamma_3$ and

$$\beta_2 \equiv \frac{\gamma_3}{\gamma_1}\left(\frac{\gamma_1 - 1}{\gamma_3 - 1}\right) \tag{53}$$

Note that this reduces to the ordinary shock relation when $\gamma_1 = \gamma_3$ and $\phi = 1$ $(\omega_s = 0)$.

Equations (43)-(45) also give $\bar{U} \equiv \hat{U}_3 / U_s$ and $\bar{P} \equiv P_3 / P_1$ rather directly in terms of $\rho$,

$$\bar{U} = \phi / \bar{\rho} \tag{54}$$

and

$$\bar{P} = 1 + \gamma_1 \, M_s^{\,2} \, \frac{\phi}{\bar{\rho}} \, (\bar{\rho} - \phi) \tag{55}$$

24

When Eq. (51) is inserted into Eq. (54) and (55) there obtains

$$\overline{U} = \frac{2}{\beta_2 \, \phi \, (\gamma_1 + \beta_1) \, M_s^2} + \frac{\gamma_1 - 1}{\beta_2 \, (\gamma_1 + \beta_1)} \tag{56}$$

and

$$\overline{P} = \gamma_1 \, \phi \, M_s^2 \left[ 1 - \frac{\gamma_1 - 1}{\beta_2 \, (\gamma_1 + \rho_1)} \right] + \left[ 1 - \frac{2\gamma_1}{\beta_2 \, (\gamma_1 + \beta_1)} \right] \tag{57}$$

Also, the ratio of the absolute gas velocity at point (3) to the shock velocity is

$$\frac{U_3}{U_s} = 1 - \frac{\gamma_1 - 1}{\beta_2 \, (\gamma_1 + \beta_1)} - \frac{2}{\beta_2 \, (\gamma_1 + \beta_1) \, \phi \, M_s^2} \tag{58}$$

With the "shock" relations, Eq. (51) and (56)-(58), we are now in a position to describe the motion of a blast wave in the initially two-phase medium. Again, it is emphasized that, by assumption, the condensed phase is completely vaporized at point (3) so that the properties of the gas mixture within the blast wave are in general different from those at point (1). Moreover, condensation within the blast wave is not considered, and it is also assumed that $x_B/R_s$ is small enough to ignore the conversion (or, "breakup") zone.

The derivation that follows is an extension of Sakurai's linear particle velocity blast wave formulation to the two-phase medium, under the above assumptions. Accordingly, we write the Euler equations for the flow within the blast wave in the forms,

$$\frac{\partial U}{\partial t} + u \frac{\partial U}{\partial r} = -\frac{1}{\rho} \frac{\partial p}{\partial r} \tag{59}$$

$$\frac{\partial \rho}{\partial t} + U \frac{\partial \rho}{\partial r} = -\rho \left( \frac{\partial U}{\partial r} + \frac{\alpha U}{r} \right) \tag{60}$$

and

$$\frac{\partial}{\partial t} \left( \frac{P}{\rho^{\gamma_3}} \right) + U \frac{\partial}{\partial r} \left( \frac{P}{\rho^{\gamma_3}} \right) = 0 \tag{61}$$

The boundary conditions at $r = R_s$ are simply the shock relations, Eq. (51), (57), and (58), which are now re-written by defining $\beta_3 \equiv \beta_2 \, (\gamma_1 + \beta_1)$ in the form

$$(U)_{r=R_s} = U_s \left[ 1 - \frac{\gamma_1 - 1}{\beta_3} - \frac{2}{\beta_3 \, \phi \, M_s^2} \right] \tag{62}$$

$$(P)_{r=R_s} = P_1 \left[ \gamma_1 \, \phi \, M_s^2 \left( 1 - \frac{\gamma_1 - 1}{\beta_3} \right) + \left( 1 - \frac{2\gamma_1}{\beta_3} \right) \right] \tag{63}$$

and

$$(\rho)_{r=R_s} = \rho_1 \left[ \frac{\beta_3 \phi^2}{\dfrac{2}{M_s^2} + (\gamma_1 - 1) \, \phi} \right] \tag{64}$$

Note that when $\gamma_1 = \gamma_3$ (which is always the limit as $\omega_s \to 0$), $\beta_3 = \gamma_1 + 1$.

26

Equations (59)-(61) and $U_s = dR_s/dt$ form a set of four equations in the five unknowns, $p(r,t)$, $U(r,t)$, $\rho(r,t)$, $R_s(t)$, and $U_s(t)$. A solution requires a fifth equation, and this is supplied by the condition of conservation of total energy. That is, the integrated energy content within the blast wave at any instant $t > 0$ must be equal to the energy content in the same spacial volume when $t \leq 0$, plus the energy deposited at the center of explosion at $t = 0$. Formally, this is

$$\int_0^{R_s} (\rho\bar{e} + \frac{1}{2}\rho\,U^2)\,r^\alpha\,dr = \int_0^{R_s} (\rho_1\,\bar{e}_1 + \rho_s\,\bar{e}_s)\,r^\alpha\,dr + E_\alpha \qquad (65)$$

in which $\rho\bar{e}$ is the internal energy per unit volume of the gas mixture within the blast wave and $\rho_1\bar{e}_1$ and $\rho_s\bar{e}_s$ are the initial internal energies of the carrier gas and the condensed phase, respectively. When the appropriate expressions for $\bar{e}$, $\bar{e}_1$, and $\bar{e}_s$ are inserted in Eq. (65), and conservation of species is invoked, there results

$$E_\alpha = \int_0^{R_s} (\rho\,C_v\,T + \frac{1}{2}\rho\,U^2)\,r^\alpha\,dr - \frac{R_s^{\alpha+1}}{\alpha+1}\rho_1\,C_{v_1}\,T_1$$

$$+ \frac{R^{\alpha+1}}{\alpha+1}\rho_1\,\omega_s\,(\mathscr{L}-e_s)$$

27

or

$$E_\alpha = \int_0^{R_s} \left( \frac{1}{2} \rho u^2 + \frac{P}{\gamma_3 - 1} \right) r^\alpha \, dr - \frac{\theta P_1 R_s^{\alpha+1}}{(\gamma_1 - 1)(\alpha + 1)} \tag{66}$$

in which

$$\theta \equiv 1 + \frac{\gamma_1 (\gamma_1 - 1) \omega_s}{a_1^2} \left[ C_s T_1 + (Cv_s - C_s) T_b - \mathscr{L}* \right] \tag{67}$$

Note that the integral in Eq. (66) is not equal to the left-hand integral in Eq. (65). The value of $\int_0^{R_s} P/(\gamma_s - 1) \, r^\alpha dr$ exceeds the total integrated internal energy of the gas within the blast wave by an amount equal to

$$\frac{P_1 R_s^{\alpha+1} \gamma_1 \omega_s}{(\alpha + 1) a_1^2} \left[ C_s T_1 + (Cv_s - C_s) T_b - \mathscr{L}* \right]$$

due to the phase change of the liquid. The value of $\theta$ can therefore be positive or negative depending on the magnitudes of the parameters appearing in Eq. (67). Although the equivalent term was dropped in the shock relations derivation, here it must be retained because the integration continually increases its effect as $R_s$ increases.

Now, following Sakurai, we introduce the independent non-dimensional variables

$$\left. \begin{array}{l} x = x(r, R(t)) \equiv r/R_s \\[2mm] y = y(t) \equiv M_s^{-2} \end{array} \right\} \tag{68}$$

and nondimensional dependent variables f, g, and h through

$$U = U_s \, f(x,y)$$

$$P \cdot P_1 \, y^{-1} \, g(x,y) \tag{69}$$

$$\rho = \rho_1 \, h(x,y)$$

The boundary conditions, Eq. (62)-(64), become

$$f(1,y) = 1 - \frac{\gamma_1 - 1}{\beta_3} - \frac{2y}{\beta_3 \phi} \quad , \tag{70}$$

$$g(1,y) = \gamma_1 \phi \left(1 - \frac{\gamma_1 - 1}{\beta_3}\right) + y \left(1 - \frac{2\gamma_1}{\beta_3}\right) \tag{71}$$

and

$$h(1,y) = \frac{\beta_3 \, \phi^2}{2y + (\gamma_1 - 1)\phi} \tag{72}$$

Similarly, Eq. (66) transforms to

$$y \left(\frac{R_o}{R_s}\right)^{\alpha+1} = \int_0^1 \left(\frac{\gamma_1}{2} hf^2 + \frac{g}{\gamma_3 - 1}\right) x^\alpha \, dx - \frac{\theta y}{(\gamma_1 - 1)(\alpha + 1)} \quad , \tag{73}$$

By substituting Eq. (70)-(72) in Eq. (66) and dividing by $P_1 R_s^{\alpha+1}$.

Now, noting that

$$\frac{\partial}{\partial r} = \frac{\partial}{\partial x} \frac{\partial x}{\partial r} = \frac{1}{R} \frac{\partial}{\partial x}$$

$$\frac{\partial}{\partial t} = \frac{\partial}{\partial x} \frac{\partial x}{\partial t} + \frac{\partial}{\partial y} \frac{\partial y}{\partial t}$$

and that

$$\frac{\partial x}{\partial t} = \frac{\partial}{\partial t} \left( \frac{r}{R_s} \right) = - \frac{x U_s}{R_s}$$

$$\frac{\partial y}{\partial t} = \frac{\partial y}{\partial R_s} \frac{dR_s}{dt} = U_s \frac{dy}{dR_s}$$

and

$$\frac{dU_s}{dt} = \frac{dU_s}{dR_s} \frac{dR_s}{dt} = U_s \frac{dU_s}{dR_s}$$

Eq. (59) and (60) transform to

$$- \frac{1}{2} \lambda f + (f - x) \frac{\partial f}{\partial x} + \lambda_y \frac{\partial f}{\partial y} = - \frac{1}{\gamma_1 h} \frac{\partial g}{\partial x} \tag{74}$$

and

$$(f - x) \frac{\partial h}{\partial x} + \lambda_y \frac{\partial h}{\partial y} = - h \left( \frac{\partial f}{\partial x} + \frac{\alpha f}{x} \right) \tag{75}$$

where $\lambda$ was defined in Eq. (24). Finally, differentiating Eq. (73) with respect to y gives

$$\lambda = \frac{(\alpha + 1) J - \frac{\theta}{\gamma_1 - 1} y}{J - y \frac{dJ}{dy}} \tag{76}$$

30

where

$$J(y) \equiv \int_0^1 \left( \frac{\gamma'_1}{2} hf^2 + \frac{g}{\gamma_3 - 1} \right) x^\alpha \, dx \quad . \tag{77}$$

This completes the basic formulation. The effect of an initially condensed phase is felt in the boundary conditions, Eq. (70)-(72), and in the conservation of total energy, Eq. (73) or (76), but not in the _form_ of the transformed differential equations, Eq. (74) and (75). Of course, the system of equations and boundary conditions regress to those of Sakurai when $\omega_s = 0$.

The assumption of linear particle velocity is made at this point, so that $f \propto x$. This is the equivalent of reducing the number of unknowns, and so one less equation is needed. The Euler energy equation, Eq. (61), is excluded. The assumption of a linear velocity profile is quite reasonable above $M_s \approx 2$ in gas-phase systems. Also, continuing with Sakurai's arguments, the term $\lambda y \, \partial h / \partial y$ is dropped in mass conservation equation, Eq. (75). This term is zero when $y = 0$ and also when $y = 1$ ($\lambda = 0$), and it is presumed to be small at intermediate values of $y$ without _a priori_ justification.

With these two simplifications we immediately obtain

$$f = f_0(y) \, x \tag{78}$$

for which the boundary condition at $x = 1$, Eq. (70), yields

$$f_0 = 1 - \frac{\gamma_1 - 1}{\beta_3} - \frac{2y}{\beta_3 \phi} \quad . \tag{79}$$

But, Eq. (75) with $\lambda y\, \partial h/\partial y = 0$ and using Eq. (78) gives

$$\frac{1}{h}\frac{\partial h}{\partial x} = \left[\frac{f_0\,(\alpha + 1)}{1 - f_0}\right]\frac{1}{x}$$

This can be integrated with respect to x, producing

$$h = h_0\, x^m \tag{80}$$

with

$$m \equiv \frac{f_0\,(\alpha + 1)}{1 - f_0} \tag{81}$$

The boundary condition of Eq. (72) can be applied to this result, and we find,

$$h_0 = \frac{\beta_3\, \phi^2}{2y + (\gamma_1 - 1)\,\phi} \tag{82}$$

Now both f and h are known functions of x and y, and so Eq. (74) can be reduced to

$$\frac{\partial g}{\partial x} = \gamma_1\, h_0\, x^{m+1}\left[f_0\,(1 + \tfrac{1}{2}\lambda - f_0) + \lambda y\left(\frac{2}{\beta_3\,\phi}\right)\right]$$

which integrates to the form

$$g = \frac{\gamma_1\, h_0\, x^{m+2}}{m + 2}\left[f_0\,(1 + \tfrac{1}{2}\lambda - f_0) + \lambda y\left(\frac{2}{\beta_3\,\phi}\right)\right] + C(y)$$

Then, invoking Eq. (71) to solve for $C(y)$, this becomes finally

$$g = A \left(x^{m+2} - 1\right) + g \tag{83}$$

in which

$$A \equiv \frac{\gamma_1 \, h_o}{m+2} \left[ f_o \left(1 + \frac{1}{2}\lambda - f_o\right) + \lambda y \left(\frac{2}{\beta_3 \, \phi}\right) \right] \tag{84}$$

and

$$g_o \equiv \gamma_1 \, \phi \left(1 - \frac{\gamma_1 - 1}{\beta_3}\right) + y \left(1 - \frac{2\gamma_1}{\beta_3}\right) \tag{85}$$

Since f, g, and h have now been obtained, the integration indicated in Eq. (73) or (77) can be carried out, giving $R_o/R_s$ as a function of y. However, the variable g contains $\lambda(y)$, which remains at this point an unknown function. Therefore the integration will result in $J = J(\lambda(y), y)$. The form of $\lambda(y)$ must be determined by inserting the integrated form of J into Eq. (76) to obtain a differential equation for $\lambda$.

Proceeding in this fashion, J(y) is integrated and reduced to the form

$$J(y) = \frac{1}{m+3+\alpha} \left[ \frac{\gamma_1}{2} h_o \, f_o^2 + \frac{A}{\gamma_3 - 1} \right] + \frac{g_o - A}{(\gamma_3 - 1)(\alpha + 1)}$$

in which the dependence on $\lambda$ appears in A(y). In fact, this can be written out in detail as

$$J(y) = S + \lambda Q \tag{86}$$

in which

$$S(y) = \frac{\gamma_1 h_o f_o}{m + 3 + \alpha} \left[ \frac{f_o}{2} + \frac{(1 - f_o)}{(m + 2)(\gamma_3 - 1)} \right] + \frac{1}{(\gamma_3 - 1)(\alpha + 1)} \left[ g_o - \frac{\gamma_1 h_o f_o}{m + 2} (1 - f_o) \right] \quad (87)$$

and

$$Q(y) = \frac{\gamma_1 h_o}{(\gamma_3 - 1)(m + 2)} \left[ \frac{f_o}{2} + \frac{2y}{\beta_3 \phi} \right] \left[ \frac{1}{m + 3 + \alpha} - \frac{1}{\alpha + 1} \right] \quad (88)$$

Instead of inserting Eq. (86) in Eq. (76) and solving for $\lambda$, it has proved more direct to eliminate $\lambda$ between the two equations, which gives

$$\frac{dJ}{dy} = \frac{J}{y} \left( 1 - \frac{\alpha + 1}{\lambda} \right) + \frac{\theta}{(\gamma_1 - 1) \lambda} \quad (89)$$

or

$$\frac{dJ}{dy} = \frac{J}{y} \left( 1 - \frac{(\alpha + 1) Q}{J - S} \right) + \frac{\theta Q}{(\gamma_1 - 1)(J - S)} \quad (90)$$

Assuming that Eq. (90) can be solved, $R_s/R_o$ can thereafter be evaluated from Eq. (73) when it is put in the form

$$\frac{R_s}{R_o} = \left[ \frac{J}{y} - \frac{\theta}{(\gamma_1 - 1)(\alpha + 1)} \right]^{-(1/\alpha + 1)} \quad (91)$$

34

Equation (90) must be numerically integrated. A difficulty is presented

by the fact that, at $y = 0$, $\lambda = \alpha + 1$, according to Eq. (76), because $dJ/dy$

must remain finite there. But Eq. (89) then shows indeterminancy at $y = 0$.

To resolve this, L'Hospital's rule is applied to the first term on the right

hand side of Eq. (89), resulting in

$$\left.\frac{dJ}{dy}\right|_0 = \frac{J(0)}{\alpha + 1} \left.\frac{d\lambda}{dy}\right|_0 + \frac{\theta}{(\gamma_1 - 1)(\alpha + 1)} \tag{92}$$

However, differentiating Eq. (86) and evaluating the result at $y = 0$ gives

$$\left.\frac{dJ}{dy}\right|_0 = \mu_0 + Q(0) \left.\frac{d\lambda}{dy}\right|_0 \tag{93}$$

where

$$\mu_0 \equiv \left.\frac{dS}{dy}\right|_0 + (\alpha + 1) \left.\frac{d\phi}{dy}\right|_0 \tag{94}$$

Then, combining Eq. (93) and (92) gives

$$\left.\frac{d\lambda}{dy}\right|_0 \left[\frac{J(0)}{\alpha + 1} - Q(0)\right] = \mu_0 - \frac{\theta}{(\gamma_1 - 1)(\alpha + 1)} \tag{95}$$

but

$$J(0) - (\alpha + 1) Q(0) = J(0) - \lambda(0) Q(0) = S(0)$$

so Eq. (95) becomes

$$\left.\frac{d\lambda}{dy}\right|_0 = \frac{1}{S(0)} \left[(\alpha + 1) \mu_0 - \frac{\theta}{\gamma_1 - 1}\right]$$

35

so the Eq. (93) can be written

$$\left.\frac{dJ}{dy}\right|_0 = \mu_0 + \frac{(\alpha + 1) Q(o)}{S(o)} \left[\mu_0 - \frac{\theta}{(\gamma_1 - 1)(\alpha + 1)}\right] \qquad (96)$$

Using Eq. (96), a numerical integration of Eq. (90) can be initiated.

Five parameters which characterize the two-phase medium and the geometry of the blast-wave present themselves in this formulation. These are $\alpha$, $\omega_s$, $\gamma_1$, $\gamma_3$, and the group

$$\epsilon \equiv \left[C_s T_1 + (Cv_s - C_s) T_b - \mathcal{L}*\right] / a_1^2 \quad,$$

which enters in the computation of $\theta$. Of course, $\gamma_3 = \gamma_3(\omega_s)$, and in fact as $\omega_s \rightarrow \infty$, $\gamma_3$ approaches that of the vapor, while for $\omega_s \rightarrow 0$, it approaches that of the carrier gas. The parameter $\epsilon$ contains the effects of the phase change, which include the loss of latent heat, $\mathcal{L}*$, and the change in specific heat of the fuel.

Although a full parametric study of the above formulation has not been carried out, some limited calculations were made. These show that the presence of a spray in substantial quantities ($\omega_s \sim O(1)$) results in appreciably accelerated blast wave decay rates, as can be seen for example on Fig. 4. Therefore, a continued exploration of detonation initiation in two-phase systems must utilize results of this type in their formulation. Also,

it can be anticipated that for a fixed blast wave energy, a maximum loading factor may exist above which the decay rate of the blast wave would be too great to allow for initiation. Corresponding to this loading factor, a locus in the $n_s$ - $D_s$ plane, calculated from Eq. (12) would exist as an upper limit. This would be in addition to the $n_s$ - $D_s$ curve corresponding to minimum reactant energy requirements, and the space between the two loci would indicate the range of number densities at each drop size for which a self-sustaining detonation can be initiated.

# III. EXPERIMENTAL STUDIES IN THE VERTICAL DETONATION TUBE

The major portion of the experimental research was conducted in essentially three phases, which were:

(a)  facility modifications to accommodate the requirements of the proposed word,

(b)  investigation and establishment of the characteristics of the detonation tube, with modifications, under test conditions, and

(c)  investigation of the detonability characteristics of the fuels of interest.

Under phase (a) above, a combustion driver was installed at the lower end of the tube and an adapter and flame arrestor assembly were designed, constructed, and installed at the upper end of the tube. In phase (b), the ability of the flame arrestor to attenuate detonations of various strengths was tested. Also, the properties of the wave produced by the driver was investigated for various conditions and compared to the predictions of strong blast wave theory. Under (c), the fuels propyl nitrate, nitropropane, nitro methane, and decane were tested at various mixture ratios, using the combustion driver as a blast initiator. Distance-time data necessary for the determination of velocities and pressure-time data were recorded for each run. The work conducted under these different phases will now be discussed.

# A. EXPERIMENTAL ARRANGEMENT AND PROCEDURES

## 1. Facility Description

The vertical steel detonation tube used for these studies is the same
one that has been used for many years. The internal cross section of this
tube is 1 5/8 in. by 1 5/8 in. Access ports are provided at approximately
9 in. intervals to provide for pressure switches, pressure transducers,
or heat transfer gages. The drop generator is located at the top of the
tube so that the drops produced, of the desired size and amount, can fall
vertically through the tube. The gaseous environment in the tube is appro-
priately controlled by means of mixing tanks, vacuum pumps, and valving
systems. The tube is always evacuated before charging in order to
minimize contamination.

In the earlier studies ignition of the two phase mixture was achieved
by a small combustion driver which would inject a shock wave in a direc-
tion perpendicular to the axis of the tube and at the upper end. The cross
sectional area of this driver was only 8% of that of the tube. While this
was generally sufficient to ignite two phase spray detonations in hydro-
carbon-oxygen systems, it was believed that it would be inadequate for
the fuels and high gaseous nitrogen concentrations of interest here.
Further, it was desired to simulate, as closely as possible, blast wave
ignition of these sprays. Accordingly, a reasonable facsimile to a blast
wave igniter was provided by affixing a 12 in. long detonative combustion

driver at the bottom of the tube. The cross section of this driver matched that of the tube. Thus the driver transmitted a shock-expansion wave system, similar to a blast wave, upward into the main tube. Under the right conditions, detonation would then be realized and propagate supersonically in the upward direction. This led to another problem and necessity for further modification to the tube. The upward travelling detonation posed serious damage potential to the drop generating system and other upper end components. Thus it was deemed essential to attenuate the detonation. Towards this end, the tube was fitted with a large port vent and an associated flame arrestor assembly at its upper end. Experience showed that this did significantly reduce the danger of damage.

The major means of data accumulation were from pressure switches and acoustic rod type pressure transducers. Time of arrival data (and hence velocities) were measured by placing pressure switches along the tube at roughly 1.5 ft intervals. The first pressure switch, located 0.5 ft from the driver diaphragm, was used to start a set of ten CMC microsecond timers. Each succeeding switch was shorted to ground by the wave and stopped the counter. Thus since the distances between pressure switches was known and the corresponding time interval was determined from the elapsed time data, the velocity was calculable. Pressure time data was obtained from a photograph of the pressure transducer output on the face of an oscilloscope.

## 2. Calibration of Combustion Driver

Inasmuch as the driver was to simulate blast wave initiation of detonation, it was deemed important to assess the performance of the driver and how this performance varied with certain key variables. Principally, the rate of Mach number decay with increasing distance from the diaphragm (which separates the driver from the driven section) was observed. This was compared with the theoretical rate of decay of a medium to weak blast wave in an analysis given by Sakurai.

For each condition investigated, velocity-distance data as well as pressure-time data were obtained. The procedure followed for obtaining the data for each run was as follows:

1. Clear the inside wall of the detonation tube-driver assembly.

2. Place a diaphragm of the appropriate thickness between the driver and the main tube and secure the driver to the main tube.

3. Evacuate the driver and main tube.

4. Charge the detonation tube with the appropriate gas; charge the driver with the appropriate mixture.

5. Evacuate the buffer lines between the main tube, driver, and charge gas sources.

6. Secure the test cell and reset instrumentation.

7. Start run sequence timer.

8. Record elapsed times from the interval meters and remove scope traces (pressure-time records) from the oscilloscope cameras.

The various parameters investigated include the following:

1.  Driver charge pressure.

2.  Axial location of the driver ignition point.

3.  Diaphragm thickness, .006-.025 in.

4.  Charge gas stoichiometry, range of equivalence ratios, 0.167-2.44.

5.  Detonation tube charge gas composition—air, nitrogen, argon.

6.  Spray density effect on wave velocity in an inert carrier gas—

    kerosene fuel—nitrogen carrier.

## 3. Heterogeneous Detonation Experiments.

An experimental program was devised to investigate the detonability

characteristics of various fuel mass loadings* of a number of fuels. The

major portion of the work was concentrated near the lean end of the scale.

An investigation of the entire range of loadings of which the facility is capable

would have been a very lengthy program and was not feasible at this time.

However, the experimental conditions selected were guided by the theoretical

treatment of Section II, which considered minimum energy density for

detonation as well as initiation requirements.

Fuel needle sizes of 0.008 and 0.016 in., corresponding to drop diameters

of 384 and 768 microns, were selected and the 768 micron drops were chosen

as the base for the study. Fuel mass loading was then varied by increasing

---

*Mass loading ≡ lbs fuel/lb carrier gas in the fuel-carrier gas mixture.

the number of .016 needles. Then by selecting the proper number of jets

and the frequency, the same mass loadings as were investigated using the

0.016 jets were investigated using the 0.008 jets. Each jet size was

investigated in three different atmospheres, or carrier gas mixtures.

A driver pressure of 50 psi, corresponding to a shock wave of initial

Mach number 4.5, was selected and held constant for nearly all runs. Tests

were then conducted in a relatively systematic fashion.

To prepare the detonation tube for each test, the inside surfaces were

thoroughly cleaned and dried. Next the tube and the driver were separated

by a .006 in. Mylar diaphragm and each evacuated. The driven section was

charged with the carrier gas. The fuel spray system was then lined up

to deliver the appropriate drop size and drop number density, and the driver

was charged with a stoichiometric mixture of hydrogen and oxygen. All buffer

lines leading to the charge gas system were then evacuated and the cell secured.

Instrumentation, cameras, scopes, and timers were reset and the firing sequence

executed. The formation of the fuel-oxidizer and the ignition of the combustion

driver were controlled by a run sequence timer. The chain of events was as

follows:

t = 0            Fuel solenoids open and remain open long enough for the

fuel to form a stable spray and to reach the driver diaphragm.

t = 1.4 sec     Nitrogen begins to blow through the drop generator head:

this forms a fuel oxidizer mixture whose detonability

is very low, thus making detonation damage to the viewing

section windows less probable.

43

t = 4.06 sec    Scope camera shutters open.

t = 4.2 sec    Spark plug fires igniting the combustion driver; fuel

solenoids close.

t = 4.36 sec    Manifold dumps open relieving pressure in the fuel

system and arresting fuel flow immediately.

Within 5 milliseconds after the spark has been initiated, the wave has traversed

the length of the tube. Now the time intervals are recorded from the CMC Time-

interval-meters and pressure traces removed from the scope cameras. The

tube is then cleaned and the cycle repeated for the next point.


B. RESEARCH RESULTS AND DISCUSSION

1. Combustion Driver

The experimental work conducted on the combustion driver was outlined

in Section III. A. 2. The first sequence of tests were conducted to determine

the Mach number-charge pressure relationship for the driver in the test

configuration. Air was the charge gas in the detonation tube while the driver

contained a stoichiometric mixture of hydrogen and oxygen, separated from

the detonation tube by 0.005 in. diaphragm. The results obtained are

shown in Fig. 1. The difficulty in obtaining Mach numbers much higher

than 7 is quite apparent. The station 0.915 ft from the diaphragm was

chosen since it is the station nearest the diaphragm at which the velocity can

be measured. The behavior of the plot is roughly parabolic, having the

form $P = (20/7)(M^2 - 1)$, in the region $0 \leq P \leq 100$ and cubic, having

the form $P = (20/43)(M^3 - 1)$, in the region $100 \leq P \leq 140$. While some

scatter in the data is apparent, in general the curve is fairly well defined.

Testing was limited to the maximum pressure shown since the structural

limits of the drive charge system, which must withstand the detonation

pressure of the $H_2$-$O_2$ mixture in the driver, were being approached.

In addition to observing the velocity at the 0.915 station, the velocity

was obtained over the entire length of the tube (during the driver experi-

ments the tube was twelve (12) ft long; later it was extended to 18 ft).

These data were plotted as shown in Figs. 6, 7, 8, and 9 in the form

Mach number versus distance from the driver diaphragm.

In order to assess driver performance in terms of planar blast wave

theory, an analytical model was needed. A version of Sakurai's theory[7],

which assumes that the velocity profile behind the shock wave behaves in

a linear fashion, and that the upstream pressure is negligible compared

to the pressure behind the shock wave, was chosen in that it provided a

ready calculation of Mach number versus non-dimensional wave radius

and was a good approximation to strong planar blast wave theory. This

model was programmed for the IBM 360/67 computer and theoretical results

obtained. Knowing the Mach number versus non-dimensional wave radius

from the theory, one could, knowing the speed of sound and the character-

istic radius, $R_o$, for a particular driver test, calculate a curve of velocity

(or Mach number) versus radius for the theoretical case. Thus from the

theory we have

$$R_o = E_\alpha / P_1$$

$$R_o = Hm/(A_c P_1)$$

(97)

where $\quad E_\alpha \equiv$ energy released per unit area at the blast center.

$\qquad H \equiv$ energy per unit mass of the explosive.

$\qquad m =$ mass of driver charge.

$\qquad A_c =$ driver cross sectional area.

$\qquad P_1 =$ pressure ahead of the shock wave.

$\qquad R_o =$ characteristic radius for the given energy release.

H was obtained by assuming that the process by which the energy was released was detonation. Computations of H were made using the NASA program of Gordon and McBride. Since the energy release was a function of driver charge pressure, the $R_o$, and hence the theoretical velocity profile, were also a function of charge pressure. So each charge pressure required that a new theoretical detonation Mach number and energy release be calculated. Figures 6, 7, 8 and 9, show typical plots of Mach number versus distance for both the theoretical and experimental cases. In each case it can be noted that the initial decay rate of Mach number with distance is much greater for the blast wave than for the driver. The calculated Mach number of detonation in the driver is indicated on each curve. As would be expected, the predicted Mach number is higher than experimental at small distances. However, they do intersect later and, at least for the lower driven pressures, are then in reasonable agreement.

A further comparison of the driver characteristics with theoretical

blast wave model can be effected by non-dimensionalizing the M vs distance

plots and displaying them against the blast wave M vs $R_s/R_o$ plots. This

is shown in Fig. 10. As expected, as the driver pressure is lowered the

velocity or Mach number profile is lowered. Also for all pressures,

the initial slope of the curve is less steep for the driver than for the

theoretical model. Note also that the experimental Mach number decay

with distance is less than the blast model until the two curves intersect,

but thereafter the driver approaches the blast wave in decay rate; i. e.

the driver curve and the blast wave curve have about the same slope but

that portion of the driver curve is shifted to the right in dimensionless

space by some constant. Again note that driver pressure (or driven energy)

enters as a parameter in Mach number-dimensionless displacement space.

This can be seen to be peculiar to the driver wave since for a given energy

only one curve is needed to describe the ideal blast wave. As the driven

wave propagates away from the source, however, it begins to approach the

blast wave more closely. This is evident in the "blending" of the experi-

mental curves beyond their intersection with the blast wave curve. In that

region of the waves history the effects of the driver charge pressure appear to have dissipated. It appears that if one were to continue plotting driver wave curves for higher pressures a new curve parallel and to the right of the blast wave curve could be drawn (through the last point of each experimental curve) representing the behavior of the drive wave at distances large compared to the length of the driver. Along that curve initial driver pressure would be a very weak parameter.

a.   Effect of Diaphragm Thickness

The effects of diaphragm thickness on the shock Mach number close to the driver diaphragm and on the Mach number as a function of distance from the diaphragm are shown in Figs. 11 and 12. Figure 11 shows the Mach number at the first station at which it can be measured (0.915 ft). The trend indicates that thinner diaphragms produce appreciably higher initial Mach numbers. Figure 12 shows the effect of the diaphragm on the Mach number at larger distances. For the first 4.5 ft it is clearly evident that thinner diaphragms produce higher Mach numbers while at greater distances the effects of diaphragm thickness are minimal.

b.   Axial Location of the Ignition Point

Most of the shock wave Mach number versus distances plots showed inflection points at about four to five feet from the diaphragm. This leads to the belief that a reflected wave was catching up with the initial shock wave which was formed when the diaphragm broke. To further explore this

48

phenomena the ignition point in the driver was changed from the opposite end from the diaphragm to the axial mid-point on one side. The results are shown in Fig. 13. The curve for mid-point ignition shows a pronounced inflection at a much earlier location than for the end point ignition and thereafter a sharp rise followed by a monotonically decreasing Mach number as it propagated away from the diaphragm. As seen, at large distances from the diaphragm there is no effect of the ignition location.

c.   Effect of Charge Gas Equivalence Ratio

A number of experiments were conducted wherein the stoichiometry of the driver gas was varied. This, of course, changes the energy level, temperature level, molecular weight, and sound speed of the combustion products. Accordingly, the strength of the transmitted shock wave will be different. Curves of shock Mach number versus distance for lean and rich driver gas compositions are shown in Figs. 14, 15, and 16. The excellent agreement between experiment and theory for the lean driver case, Fig. 14, is to be noted. The excellent agreement at shorter distances for the very rich case, Fig. 16, is of interest. This would appear to indicate that if the reflected wave from the driver could be eliminated, we would have very good simulation of a planar blast wave over a large distance. Figure 17 shows the shock Mach number variation with driver equivalence ratio for 2 discrete locations in the tube. As observed, up to a certain point it pays to go on the rich side. Presumably, this is attributable to the large amount of $H_2$ with its low molecular weight.

d.  Effect of Spray Loading on Shock Wave Attenuation.

The dynamics of a wave propagating into a spray-gas mixture is considerably different from that of a wave propagating through a gas alone. To investigate this effect the driver was discharged into a kerosene drop-nitrogen mixture for two fuel loadings, where the fuel loading, $\omega_s$, is defined as lbs fuel/lb carrier gas in the fuel carrier gas mixture. The results of this work are shown in Fig. 18. The graph shows, be sides the two fuel loading curves, a plot for the wave in the carrier gas alone. The fuel used was in the form of 1010 $\mu$m kerosene drops and the gas was nitrogen, so that no combustion took place. Of course, acceleration and aerodynamic shattering of the drops would occur. It is readily noted that higher spray loadings substantially increase the rate of decay of the blast wave. This is of particular importance to cloud ignition considerations wherein too great a rate of decay of the blast wave over distances measured in terms of the reaction zone length will preclude ignition. This aspect has been treated in Section II. B. 2.

2.  Detonation Experiments

In a steady self-sustaining detonation, the temperature rise across the leading shock must be high enough to cause the fuel oxidizer mixture to react rapidly. This implies a minimum Mach number, below which the detonation will not propagate. The Mach number for a two-phase detonation (liquid fuel plus gaseous oxidizer) in terms of spray loading, heat of

50

combustion, and wall losses, was presented in Eq. (11) wherein, for this case, $\omega_s = \phi_o$. The equation is:

$$M_s^2 = \frac{2(\gamma_3^2 - 1)\, \omega_s\, H_c/a_1^2}{1 + \omega_s + 6C_H\, \gamma_3^2\, x_R/r_h} \tag{98}$$

where $\quad M_s^2$ = detonation Mach number

$\gamma_3$ = ratio of specific heats in the products

$\omega_s$ = fuel/oxidizer mass ratio

$H_c$ = heat of combustion, or heat liberated due to chemical reaction

$a_1$ = speed of sound in the unburned gas

$C_H$ = heat loss coefficient

$x_R$ = reaction zone length

$r_h$ = hydraulic radius of the detonation tube

For the case of no losses to the walls of the tube, the Mach number can be expressed as

$$M_s^2 = \frac{2(\gamma_3^2 - 1)\, \omega_s\, H_c/a_1^2}{1 + \omega_s} \tag{99}$$

Solving for $\omega_s$,

$$\omega_s = \frac{M_s^2}{2(\gamma_3^2 - 1)\, H_c/a_1^2 - M_s^2} \tag{100}$$

Now if the minimum Mach number of propagation were known, the lower

limit for the fuel/oxidizer ratio would also be known. A criteria for

determining the minimum Mach number of propagation has not yet been

developed but experience from many tests in the past has shown that it

is approximately $M_s = 3$. Hence, using this value, an approximate

lower limit, $\omega_{s_{min}}$, was set. Using this value of $\omega_{s_{min}}$, a jet size which

would give this value of $\omega_s$ for a single stream of droplets was selected.

Fuel loadings for each test point were then simply multiples of $\omega_{s_{min}}$

Tests were conducted on four fuels; propyl nitrate, nitro propane,

nitro methane, and decane. Three atmospheres were used; oxygen, air,

and a 10% oxygen-90% nitrogen mixture, the last being referred to

simply as 10:90. The physical and chemical properties of the fuels are

listed in Table I. A summary of all of the tests conducted is given in

Table II. For each test the information given includes the following:

the fuel, oxidizer, fuel drop size, number of needles or jets producing

the drops, drop number density, frequency for disturbing the fuel flow,

the spray loading factor, equivalence ratio, the driver charge pressure,

whether it detonated or not (plus for yes and minus for no), and the measured

detonation velocity. The velocity and pressure data for practically all of

the runs are shown in Figs. 19 through 39. The runs for which a figure

is not included are indicated by an asterisk in Table II. In examining the

velocity and pressure records of Figs. 19-39, it is usually obvious as to

Table No. I.  Physical Properties of Fuels

| | Propyl Nitrate | Nitro Propane | Nitro Methane | Decane |
|---|---|---|---|---|
| Density ($slugs/ft^3$) | 2.0375 | 1.9069 | 2.1906 | 1.407 |
| Surface Tension (lb/ft) | $2.31 \times 10^{-3}$ | $2.39 \times 10^{-3}$ | $2.52 \times 10^{-3}$ | $2.54 \times 10^{-3}$ |
| Viscosity ($lb\ sec/ft^2$) | $1.17 \times 10^{-5}$ | $1.57 \times 10^{-5}$ | $1.38 \times 10^{-5}$ | $1.74 \times 10^{-5}$ |
| Molecular Weight | 105.09 | 89.09 | 61.04 | 142 |
| Molecular Composition | $CH_3 (CH_2)_2\ O\ NO_2$ | $(CH_3)_2\ CH\ NO_2$ | $CH_3\ NO_2$ | $C_{10} H_{22}$ |
| Heat of Combustion (BTU/lbm) | 8284 | 9655 | 4995 | 20445 |

53

whether detonation occurred or not. However, there are instances where some doubt exists. Some of the pressure traces are quite interesting, particularly as to how some change at different locations in the tube. As seen, some of the pressures measured are very high. Also, in some cases, the detonation waves appear to be still accelerating.

A review of Table II shows that propyl nitrate was very detonable. Detonations were observed for all points tested in $O_2$ and air. Detonation was not achieved in the 10:90 for the larger drop size but it was realized with the 384 $\mu$m drops at the highest equivalence ratio.

Nitropropane was relatively easy to detonate also, although it never went in 10:90, even for the smaller drop sizes and very rich mixtures. No tests were run with higher driver pressures in order to pursue this point through.

The fuel nitro methane proved to be most difficult to detonate so the normal sequence of runs was modified. Higher fuel loadings, and in some cases, high initiator energies were used in order to achieve detonations. The interesting part of the nitro methane work was the detonations in 10:90. An approximation to the minimum fuel loading was made using the recombination energy, or self oxidizing energy, of the monopropellant. To insure adequate initiator energy, driver pressure was raised to 90-100 psi. For a fuel loading of $\omega_s = 0.352$, Run No. 81a, detonation was achieved. However, it was not achieved for the identical

54

## Table II.  Detonation Test Summary
### Vertical Tube

| Run No. | Fuel | Oxidizer | $D_0$ Drop Diameter $\mu m$ | No. Jets | $n_1$ Drop Number Density per $ft^3 \times 10^{-3}$ | $f_r$ cps | $\omega_s$ | $\phi$ | $P_D$ | Detonated? | Velocity Experimental ft/sec |
|---|---|---|---|---|---|---|---|---|---|---|---|
| 1 | Propyl Nitrate | $O_2$ | 768 | 1 | 6.12 | 1400 | 0.047 | 0.046 | 50 | + | 6382 |
| 2 | | | 768 | 2 | 12.2 | 1400 | 0.094 | 0.092 | 50 | + | 6800 |
| 4 | | Air | 768 | 1 | 6.12 | 1400 | 0.047 | 0.197 | 50 | + | 3760 |
| 5 | | | 768 | 2 | 12.2 | 1400 | 0.094 | 0.395 | 50 | + | 4000 |
| 6 | | | 768 | 3 | 18.4 | 1400 | 0.141 | 0.592 | 50 | + | 5050 |
| 7 | | 10 $O_2$ 90 $N_2$ | 768 | 1 | 6.12 | 1400 | 0.047 | 0.449 | 50 | - | |
| 8 | | | 768 | 2 | 12.2 | 1400 | 0.094 | 0.899 | 50 | - | |
| 9 | | | 768 | 3 | 18.4 | 1400 | 0.141 | 1.348 | 50 | - | |
| 10 | | $O_2$ | 384 | 4 | 56.0 | 1400 | 0.047 | 0.046 | 50 | - | |
| 11 | | | | 8 | 112.0 | 1400 | 0.094 | 0.092 | 50 | + | 4590 |
| 12 | | | | 12 | 168.0 | 1400 | 0.141 | 0.138 | 50 | + | 3940 |
| 13 | | Air | 384 | 4 | 50 | 1400 | 0.047 | 0.197 | 50 | - | |
| 14 | | | 384 | 8 | 112 | 1400 | 0.094 | 0.395 | 50 | + | 5080 |
| 15 | | | 384 | 12 | 168 | 1400 | 0.141 | 0.592 | 50 | + | 4780 |
| 16 | | 10% $O_2$ 90% $N_2$ | 384 | 4 | 56 | 1400 | 0.047 | 0.449 | 50 | - | |
| 17 | | | 384 | 8 | 112 | 1400 | 0.094 | 0.899 | 50 | - | |
| 18 | | | 384 | 12 | 168 | 1400 | 0.141 | 1.348 | 50 | + | 5200 |
| 19 | Nitro Propane | $O_2$ | 768 | 1 | 7.55 | 1440 | 0.047 | 0.0633 | 50 | - | |
| 20 | | | 768 | 2 | 15.1 | 1440 | 0.095 | 0.128 | 50 | - | |
| 21 | | | 768 | 3 | 22.6 | 1440 | 0.142 | 0.191 | 50 | + | 5535 |
| 22 | | Air | 768 | 1 | 7.55 | 1440 | 0.047 | 0.272 | 50 | - | |
| 23 | | | 768 | 2 | 15.1 | 1440 | 0.095 | 0.549 | 50 | - | |
| 24 | | | 768 | 3 | 22.6 | 1440 | 0.142 | 0.820 | 50 | + | 5050 |
| 27 | | 10% $O_2$ 90% $N_2$ | 768 | 3 | 22.6 | 1440 | 0.142 | 0.820 | 50 | - | |
| 73* | | $N_2$ | 768 | 16 | 121 | 1440 | 0.712 | 9.351 | 50 | - | |
| 28 | | $O_2$ | 384 | 8 | 121 | 1440 | 0.095 | 0.128 | 50 | - | |
| 29 | | | 384 | 12 | 181 | 1440 | 0.142 | 0.191 | 50 | + | 5068 |
| 30 | | | 384 | 16 | 242 | 1440 | 0.190 | 0.256 | 50 | + | 5725 |
| 31 | | Air | 384 | 8 | 121 | 1440 | 0.095 | 0.549 | 50 | - | |
| 32 | | | 384 | 12 | 181 | 1440 | 0.142 | 0.820 | 50 | + | 4950 |
| 33 | | | 384 | 16 | 242 | 1440 | 0.190 | 1.098 | 50 | + | 5034 |
| 34 | | 10% O 90% $N_2$ | 384 | 8 | 121 | 1440 | 0.095 | 1.247 | 50 | - | |
| 36 | | | 384 | 16 | 181 | 1440 | 0.190 | 2.495 | 50 | - | |
| 56 | Nitro Methane | $O_2$ | 768 | 2 | 15.3 | 1700 | 0.046 | 0.118 | | - | |
| 57 | | | 768 | 3 | 23.0 | 1700 | 0.069 | 0.176 | | + | 3900 |
| 59 | | Air | 768 | 2 | 15.3 | 1700 | 0.046 | 0.118 | | - | |
| 74 | | $O_2$ | 768 | 6 | 61.4 | 1700 | 0.352 | 0.139 | | + | 5000 |
| 75 | | | 768 | 5 | 38.3 | 1700 | 0.294 | 0.115 | | + | 5136 |
| 76 | | | 768 | 4 | 30.7 | 1700 | 0.235 | 0.097 | 50 | + | |
| 60 | | Air | 768 | 3 | 23.0 | 1700 | 0.176 | 0.297 | | + | 4731 |
| 77 | | | 768 | 5 | 30.7 | 1700 | 0.294 | 0.496 | 50 | + | 5136 |
| 78 | | | 768 | 4 | 30.7 | 1700 | 0.235 | 0.396 | 50 | + | 4854 |
| 79 | | 10% $O_2$ 90% $N_2$ | 768 | 16 | 123 | 1700 | 0.940 | 3.603 | 90 | + | 5084 |
| 80 | | | 768 | 12 | 92.1 | 1700 | 0.705 | 2.702 | 100 | + | 4688 |
| 81a | | | 768 | 6 | 61.4 | 1700 | 0.352 | 1.349 | 100 | + | 5190 |
| 81b | | | 768 | 6 | 61.4 | 1700 | 0.352 | 1.349 | 50 | - | |
| 82* | | | 768 | 12 | 122.8 | 1700 | 0.705 | 2.702 | 50 | + | 3739 |
| 46 | Decane | $O_2$ | 384 | 6 | | 1387 | 0.049 | 0.170 | 50 | + | 4573 |
| 47 | | | 384 | 9 | | 1387 | 0.072 | 0.252 | 50 | + | 5102 |
| 48 | | | 384 | 12 | | 1387 | 0.097 | 0.340 | 50 | + | 5882 |
| 49 | | Air | 384 | 6 | | 1387 | 0.049 | | 50 | - | |
| 50 | | | 384 | 9 | | 1387 | 0.072 | 1.08 | 50 | - | |
| 51 | | | 384 | 12 | | 1387 | 0.097 | 1.46 | 50 | + | 5046 |
| 52 | | 10 $O_2$ 90% $N_2$ | 384 | 6 | | 1387 | 0.049 | 1.66 | 50 | - | |
| 53 | | | 384 | 9 | | 1387 | 0.072 | 2.46 | 50 | - | |
| 54 | | | 384 | 12 | | 1387 | 0.097 | 3.32 | 50 | - | |

conditions when the driver pressure was reduced to 50 psi (Run 81b).

Detonations were achieved for high fuel loadings, such as indicated by

Runs 79, 80, and 82. In Run 82, this was true even though the driver

pressure was reduced to 50 psi.

The runs with decane were more limited and only the smaller drop

size was tested. As can be seen, it went easily in $O_2$, had to be quite

rich in air, and didn't detonate in 10:90.

Detonability of a monopropellant in air oxidizing atmosphere takes

on the character of a two-phase detonation. However the nature of the

energy release in oxidizers with very low concentrations of oxygen,

and ultimately in an inert carrier gas, changes from that of an oxygen

consuming fuel to that of a self-oxidizing fuel. Run No. 73 was the only

run conducted with no oxygen present and it was desired to see if it

would detonate. As noted, in Table II, it did not for the one attempt.

Certainly this type of problem warrants a more thorough investigation.

# IV. EXPERIMENTAL STUDIES IN THE SECTORED SHOCK TUBE

## A. INTRODUCTION

Closely controlled experiments were conducted on the blast wave breakup and ignition of a single stream of fuel drops. The blast waves were generated by condensed explosive and electric detonators. The advantage of this facility is that away from the origin the shock behaves as a true cylindrical blast wave.

A description of the experimental facility follows in Section B. A discussion of the test conditions examined appears in Section C. The details of individual drop breakup and, for sufficient conditions, ignition were observed using streak schlieren techniques. The results of these observations and associated fundamental calculations are plotted and discussed in Section C as well.

## B. EXPERIMENTAL ARRANGEMENT

The ignition and shattering characteristics of fuel drops were examined by using the convective flow established behind the incident blast wave in a pie-shaped chamber. A single stream of mono-disperse fuel drops under free fall conditions crossed the tube perpendicular to the direction of flow. Through variation of the strength of the incident blast wave and the initial test section composition the fuel drops could be exposed to hot oxidizing or inert environments under various conditions of dynamic pressure.

All experiments were conducted using normal propyl nitrate (NPN) and decane as the fuels. A summary of the properties of these fuels are given in Table I. In this section a discussion will be given of 1) the shock tube used to produce the ambient conditions surrounding the fuel drops, 2) the method of producing the uniform sized fuel drops, 3) the instrumentation used to record the various data, and 4) the experimental procedure.

A schematic of the sectored chamber used in this study is shown in Fig. 40. The detonation chamber, without the breech-like explosive charge holder, is 28 3/4 in. along the centerline. The top and bottom bars diverge at a $20^{\circ}$ total included angle. The inside dimensions of the chamber are 2.05 in. wide, 1 in. high at the narrow end, and 11 in. high at the open end. A breech, which contains the blast energy source, is mounted to the narrow upstream end of the chamber. The breech is constructed of 3-in. -diameter round steel stock 4 in. in length. In the initial design, the breech included a cylindrical cavity 7/8 in. in diameter and 2 1/2 in. deep in which the explosive charge was placed. One end of this cavity was open to the test chamber; at the rear of this cavity a hole was drilled to hold the detonator cap. An additional smaller diameter hole was bored the remaining distance allowing the detonator lead wires to be fed through a conax sealing unit. The breech was pressed into a small aluminum plate which can be bolted to the chamber backplate and sealed with an O-ring seal.

Dupont electric ignitors, type E106 containing a 2 grain PETN primary charge, were used in conjunction with varying amounts of Dupont Detasheet 'C' type plastic explosive to achieve varying strength blast waves. The largest blast source energy used to date yields Mach numbers in excess of 40 near the breech, and values reaching 6 at the drop location depicted in Fig. 40. Typical values of Mach number at the drop location were $2 \leq M \leq 5$. The performance of this facility in comparison with strong blast wave theory is quite satisfactory. Details of this comparison are available in previous publications[8-11]

The test section shown in Fig. 40, has two 3/4 in. x 5 3/4 in. schlieren quality windows 1 in. thick through which the streak data was observed. The inset in Fig. 40 displays the relative locations of the reference wires seen in the streak photographs, and the stream of fuel drops. The uniform size fuel drops are produced through the standard application of the Rayleigh instability criteria for a capillary jet. A small jet of fluid is caused to oscillate at a critical frequency which causes the jet to break up into small drops having approximately twice the diameter of the jet itself. The details of construction of this particular system are given elsewhere[8]. Once formed, the stream of drops fall vertically across the chamber terminating at the bottom.

All drop breakup and ignition data reported upon herein was the result of an analysis of streak schlieren photographic records. The

optical system used to obtain these records is displayed schematically

in Fig. 41. Using this system, a great deal of detail was produced in

the records, providing more than enough information. The streak

schlieren system employed a 12 in. diameter, 60 in. focal length para-

bolic mirror and appropriate lenses in conjunction with a xenon flash

tube for the light source and a high speed drum camera. A slit was

placed along. the length of the test chamber window, and properly sized

to ensure that only one drop would be visible. The usable streak schlieren

records obtained from the system described are given in Figs. 42-46.

They are discussed in more detail in the following section.

In an experimental run the following sequence of events would occur;

1) Visual check made to ensure uniform drops are being established
at the desired operating conditions. Fuel shut off.

2) Ignitor/explosive combination to produce desired strength blast
wave is positioned in breech.

3) Test chamber is sealed up, evacuated and pressurized to 1 atm
with desired oxidizing atmosphere.

4) The automatic event sequencer is started, initiating fuel drop
production, blast source energy release and optical system
spark light source.

Between experimental runs the chamber walls were cleansed with solvent

to prevent superfluous combustion.

## C. RESEARCH RESULTS AND DISCUSSION

The experimental conditions considered in this investigation encompass those under which blast initiated two-phase detonations have been observed to propagate. The strength of the incident blast wave which interacts with the fuel drops was varied between Mach 2 and 6. The lower limit was determined approximately by the flammability limit of the fuel drops and the minimum achievable blast wave source energy. The upper limit was established by safety considerations regarding the maximum allowable source energy. The size of the fuel drops used were $384\mu$, and $768\mu$. The fuels examined were normal-propyl nitrate and decane. The ambient atmosphere in the chamber consisted of 100% $O_2$, 50% $O_2$-50% $N_2$, Air, and 100% $N_2$ at atmospheric pressure. Selection of the 50% $O_2$-50% $N_2$ mixture in place of the suggested 10% $O_2$-90% $N_2$ is discussed in later sections with reference to the data obtained. The Weber and Reynolds numbers under these conditions are sufficiently large to ensure the drop shattering mode was of the stripping type.

In the following sections photographic data is presented which show the interaction of the fuel drop and blast wave under a variety of initial conditions for both reacting and non-reacting cases. The methods and equations used to obtain fundamental breakup, stripping and ignition results are presented. The results themselves are then given in both tabular and plotted form in conjunction with any appropriate discussion.

# 1. Blast Wave/Drop Interaction

An important phase in the dynamic process of an explosion in an unconfined two-phase fuel air mixture is the breakup and ignition of the liquid fuel drops. In order to formulate a satisfactory analytic model of the entire unconfined fuel air explosion problem, the drop shattering phase must be considered. Heretofore, considerable effort has been expended studying the fundamental problem of aerodynamic shattering and to a lesser extent, ignition of liquid fuel drops. Standard shock tube techniques were generally used throughout all such work. However, in doing so an important physical change in the drop shattering process, unique to the problem of blast initiated explosions in two-phase fuel air clouds, was not considered. A significant difference exists in the pressure profile behind the usual supported shock wave and a blast wave. In the former case the pressure behind the incident shock is constant, if the shock tube has been properly designed, during the drop shattering process, whereas in the latter case the pressure decays with time. The affect of this dependency on time is to produce varying drop dynamic conditions throughout the duration of the shattering and ignition process. Therefore, the results of the aforementioned studies into drop aerodynamic shattering and ignition cannot in general be applied to the problem of unconfined explosions in liquid fuel air mixtures without first examining how these results are altered, if at all, by this effect.

Experimental data was obtained in the form of numerous streak schlieren photographs so as to examine the nature of incident blast wave formation, bow shock/wake shock formation and drop stripping, breakup, ignition and blast wave formation. Streak records used to obtain the data reported upon herein are given in Figs. 42-46. In the records the time axis is running horizontally, for right running shock, with the distance axis running from bottom to top. The three horizontal lines are reference wires at 1 in. intervals. On the time axis 1 in. corresponds to approximately 50 $\mu$sec. The fuel drop enters the field of view from the left, it is impacted by the shock entering from the bottom. The drop is subsequently accelerated in the downstream direction, simultaneously shattered and, provided proper conditions exist, ignited. Approximately seventy experimental runs were performed. All essential information regarding the above processes was obtained by digitizing 8 1/2 in. x 11 in. enlargements of the 35 mm streak record film strips. The digitized data was then placed on file and each run in turn was subsequently analyzed by a universal computer program designed to yield nearly all dimensional and non-dimensional parameters common to drop shattering and ignition studies. Once in working order, this program reduced data from all seventy runs in a matter of minutes. The techniques employed by the program and the parameters computed and reported upon herein will now be described.

The computer program which analyzes the streak schlieren photo-
graphic records is organized into the following computational code:

(a) Establish physical parameters characterizing fuel and atmos-
phere being used.

(b) Establish time and distance scales and convert x, y data to
r, t data.

(c) Perform computations associated with the following phenomena
as needed for a given run:

(i) Incident shock front
(ii) Drop trajectory - leading edge
(iii) Drop trajectory - trailing edge
(iv) Convective gas flow trajectories
(v) Drop trajectory calculations dependent upon knowledge of
local convective gas flow conditions.

Operations performed in steps (a) and (b) were very straightforward and
are not worth elaborating upon. Each of the sub-sections of step (c) do,
however, merit further discussion. In order to design an effective and
workable, automated data reduction scheme, it was necessary to repre-
sent much of the shock and drop trajectory behavior mathematically.
This involved approximating such behavior as shock r, t, trajectories
by equations derived by least squares techniques. In doing so, some
simplifying assumptions were made for computational purposes; these
assumptions will be pointed out where applicable.

To begin, computations associated with the incident shock front
involved approximating its r, t trajectory behavior by a second order
least squares fit. The derived equation was then used to represent
the shocks' displacement and velocity behavior with time in subsequent

computations. Comparison of approximate with exact trajectory data

was always exceptionally good. Computations associated with the

leading edge of the drop trajectory involved a similar approximation.

A second order least squares fit of drop radial displacement was per-

formed with time as the independent variable. Again, comparison with

exact drop location showed good agreement. The derived relationship

was similarly used throughout all subsequent computations. Knowing

the drop initial location, the incident shock wave performance was

then computed from the previously mentioned shock approximation.

Further computations regarding the drop were forestalled at this point,

owing to the fact that not all streak records had visible convective gas

flow streamlines; as the latter were used to establish experimentally

the locally decaying dynamic flow conditions.

The drop trailing edge was located in the digitized streak records

solely for the purpose of determining drop stripping times and distances.

Considerable scatter in such data was observed with subsequent analysis.

It was observed that the approximate locations of convective gas

flow streamlines could be digitized due to the relative impurity of the

blast wave energy source. The trajectories of micron-sized particles

were thus traced at somewhat regular intervals. These trajectories

were then approximated, as before, by second order least squares fit;

again with these approximating equations representing each of the n-number

of paths obtained for each run in all subsequent computations. Such approximating equations allowed for an experimental determination of the decay of local dynamic flow conditions.

The final and most important computational sub-section involved those drop parameters which were dependent upon local convective gas flow conditions. Such conditions, experienced by the constantly accelerating drop, were computed from the previously mentioned approximating equations. Knowing the equations of drop trajectory and those for convective gas flow streamlines for each run, the local flow conditions were calculated by taking derivatives of the appropriate trajectores and hence obtaining relative velocities. One final approximation was made at this point. The local convective gas flow velocity, $u_2$, easily determined experimentally as a function of time, was approximated by a first order least squares fit. The drop breakup time was then computed mathematically by comparing $u_{2_{drop}}$ and $u_{2_{gas}}$, using the appropriate corresponding approximation, until the condition that

$$u_{2_{drop}} \geq 0.60 \, u_{2_{gas}} \qquad (101)$$

was established. The corresponding time was then equated to breakup time. Given this time and the approximating function of $u_2 = u_2(t)$, the local convective gas velocity at breakup could then be determined.

This velocity, $u_{2_{brkp}}$, was then used to non-dimensionalize or calculate

66

all parameters associated with drop breakup. A similar routine was

followed for conditions at the drop stripping point, i.e. $u_{2_{strip}}$ was

computed. This point is that where the wake first starts to form rapidly.

Finally, those conditions which have been referred to as 'initial' were

computed on the basis of simple normal shock relations and the knowledge

of the incident experimental blast wave strength. Such conditions

refer to those which the drop experiences immediately behind the

shock front. The fundamental results of the computations outlined here

are given in Table III.

## 2. Breakup of Fuel Drops

Prior to discussing the results of observed fuel drop breakup phenomena,

the basic performance of the facility will be outlined. The fundamental

blast wave strength produced in the chamber at a fixed radial location,

R = 24 in., is displayed in Fig. 47 as a function of the size of the energy

source, in grams of Detasheet 'C', and oxidizing atmosphere. The data

reveals conclusive, but scattered, results that Mach number, $M_{R=24\ in.}$,

increases with increasing source energy. Increasing the concentration

of $O_2$ in the atmosphere above that contained in air has little effect until

the concentration of 100% $O_2$ is approached. At this high $O_2$ concentra-

tion a slight, but noticable improvement in Mach strength is seen at a

given source energy. This is probably due to both the increased density

of the medium and a more complete combustion of the Detasheet.

## Table III.  Experimental Test Summary
## Sectored Shock Tube

| Run Number | Fuel | Drop Diameter $D_o$ (μm) | Oxidizer | Energy (gms) | $M_{s_i}$ | $M_{R=24\,in.}$ | $t_b$ (μsec) | $t_b/D_o$ (msec/in.) | $\bar{t}_b$ | $x_b$ (in.) | $\bar{x}_b$ | $t_{st}$ (μsec) | $t_{st}/D_o$ (msec/in.) | $\bar{t}_{st}$ | $x_{st}$ (in.) | $\bar{x}_{st}$ |
|---|---|---|---|---|---|---|---|---|---|---|---|---|---|---|---|---|
| 2 | Propyl Nitrate | 768 | Air | 0.00 | 2.036 | 2.036 | 128.55 | 4.25 | 3.079 | 0.45 | 14.841 | 9.565 | 0.316 | 0.374 | 0.024 | 0.784 |
| 3* | | | | | 2.127 | 2.210 | 197.54 | 6.53 | 4.045 | 0.57 | 18.975 | 9.009 | 0.298 | 0.409 | 0.006 | 0.197 |
| 4 | | | | | 1.998 | 2.029 | 93.81 | 3.10 | 1.320 | 0.19 | 6.328 | 9.104 | 0.301 | 0.399 | 0.0 | 0.0 |
| 5 | | | | 0.50 | 2.745 | 2.778 | 84.44 | 2.79 | 4.081 | 0.48 | 15.877 | 5.714 | 0.189 | 0.317 | 0.0 | 0.0 |
| 6 | | | | | 2.786 | 2.869 | 85.44 | 2.83 | 3.827 | 0.48 | 15.825 | 25.601 | 0.847 | 1.532 | 0.0 | 0.0 |
| 7 | | | | 0.00 | 2.154 | 2.270 | 77.29 | 2.56 | 1.214 | 0.18 | 6.056 | 2.582 | 0.085 | 0.153 | 0.005 | 0.177 |
| 8 | | | | 1.00 | 3.173 | 3.296 | 40.53 | 1.34 | 1.678 | 0.20 | 6.594 | 1.382 | 0.046 | 0.120 | 0.002 | 0.068 |
| 9 | | | | 1.50 | 3.080 | 3.080 | 58.91 | 1.94 | 3.881 | 0.38 | 12.591 | 19.023 | 0.629 | 1.431 | 0.0 | 0.0 |
| 14* | | | | 2.00 | | 4.529 | | | | | | | | | | |
| 15 | | | | 2.50 | 4.393 | 4.951 | 80.58 | 2.66 | 6.431 | 0.67 | 22.084 | 8.373 | 0.277 | 1.011 | 0.0 | 0.0 |
| 22 | Propyl Nitrate | 768 | 50%$O_2$ 50%$N_2$ | 1.50 | 3.270 | 3.274 | 54.65 | 1.81 | 4.138 | 0.53 | 17.421 | | | | | |
| 23 | | | | 0.50 | 2.962 | 2.962 | 43.30 | 1.43 | 1.705 | 0.21 | 6.861 | 6.932 | 0.229 | 0.505 | 0.0 | 0.0 |
| 24* | | | | 1.00 | | 3.823 | | | | | | | | | | |
| 25 | | | | 1.25 | 3.204 | 3.204 | 45.61 | 1.51 | 3.498 | 0.43 | 14.205 | 3.673 | 0.121 | 0.296 | 0.0 | 0.0 |
| 26 | | | | 1.75 | 3.409 | 3.409 | 55.21 | 1.83 | 4.563 | 0.31 | 10.383 | 4.507 | 0.149 | 0.390 | 0.0 | 0.0 |
| 27 | | | | 1.00 | 3.677 | 3.776 | 62.97 | 2.08 | 3.934 | 0.45 | 14.777 | 5.310 | 0.176 | 0.624 | 0.001 | 0.039 |
| 10* | Propyl Nitrate | 768 | $O_2$ | 0.50 | | 2.788 | | | | | | | | | | |
| 11 | | | | | 2.991 | 3.165 | 80.66 | 2.67 | 4.397 | 0.59 | 19.513 | 25.119 | 0.831 | 1.666 | 0.043 | 1.437 |
| 12 | | | | 1.00 | 3.575 | 3.625 | 53.12 | 1.76 | 3.912 | 0.28 | 9.349 | | | | | |
| 16 | | | | 1.50 | 3.601 | 3.606 | 58.71 | 1.94 | 3.940 | 0.20 | 6.760 | 7.251 | 0.240 | 0.753 | 0.015 | 0.492 |
| 17 | | | | 0.75 | | 3.197 | | | | | | | | | | |
| 18 | | | | 0.875 | 3.704 | 4.091 | 34.07 | 1.13 | 2.600 | 0.21 | 7.058 | | | | | |
| 19 | | | | 0.70 | 2.949 | 2.949 | 64.08 | 2.12 | 2.840 | 0.35 | 11.506 | 6.654 | 0.220 | 0.507 | 0.0 | 0.003 |
| 20* | | | | 0.60 | | 3.186 | | | | | | | | | | |
| 21 | | | | 0.90 | 3.303 | 3.321 | 54.83 | 1.81 | 2.824 | 0.22 | 7.193 | 4.955 | 0.164 | 0.497 | 0.0 | 0.0 |
| 64 | Propyl Nitrate | 384 | 50%$O_2$ 50%$N_2$ | 0.00 | 1.901 | 1.901 | 119.13 | 7.88 | 6.069 | 0.46 | 30.282 | 9.112 | 0.603 | 0.747 | 0.009 | 0.579 |
| 65* | | | | 1.00 | | 3.319 | | | | | | | | | | |
| 66 | | | | 0.50 | 2.768 | 2.768 | | | | | | | | | | |
| 67 | | | | 1.00 | 3.060 | 3.165 | 53.45 | 3.54 | 6.413 | 0.31 | 20.563 | | | | | |
| 68 | | | | 1.50 | 3.522 | 3.569 | 38.04 | 2.52 | 5.037 | 0.21 | 13.582 | 9.451 | 0.625 | 1.863 | 0.0 | 0.0 |
| 28 | Propyl Nitrate | 384 | $O_2$ | 0.50 | 2.754 | 2.789 | 53.50 | 3.54 | 7.506 | 0.43 | 28.192 | 6.182 | 0.409 | 0.949 | 0.0 | 0.0 |
| 29 | | | | 1.50 | 3.460 | 3.460 | 28.55 | 1.89 | 4.618 | 0.29 | 19.409 | 2.307 | 0.153 | 0.410 | 0.0 | 0.0 |
| 30 | | | | 1.00 | 3.461 | 3.515 | 64.65 | 4.28 | 9.822 | 0.31 | 20.683 | 4.408 | 0.292 | 0.836 | 0.0 | 0.0 |
| 31* | | | | 2.00 | | 3.521 | | | | | | | | | | |
| 32* | | | | 2.00 | | 3.823 | | | | | | | | | | |
| 33 | | | | 1.25 | 3.487 | 3.506 | 36.27 | 2.40 | 5.623 | 0.29 | 18.904 | | | | | |
| 13 | Propyl | 768 | $N_2$ | 0.50 | 2.781 | 2.811 | 65.32 | 2.16 | 1.767 | 0.22 | 7.229 | 10.844 | 0.359 | 0.691 | 0.005 | 0.151 |
| 1 | | | Air | 0.0 | | 2.198 | | | | | | | | | | |

*Indicates the streak record of that run is not supplied due to its poor quality.
**Indicates no ignition occurred.
--Indicates insufficient data for determination.

| $t_{ig}$ | $x_{ig}$ | $q_i$ | $Re_i$ | $We_i$ | $T_{2_i}$ | $q_b$ | $Re_b$ | $We_b$ | $q_b/q_i$ | $Re_b/Re_i$ |
|---|---|---|---|---|---|---|---|---|---|---|
| (μsec) | (in.) | (psi) | x 10$^{-5}$ | x 10$^{-5}$ | (°R) | (psi) | x 10$^{-5}$ | x 10$^{-4}$ | | |
| ** | ** | 46.39 | .2243 | .0536 | 890.4 | 25.768 | .1671 | .2976 | .5555 | .7453 |
| ** | ** | 55.96 | .2406 | .0617 | 930.2 | 18.83 | .1395 | .2076 | .3366 | .5802 |
| ** | ** | 42.70 | .2174 | .0504 | 874.3 | 8.898 | .0992 | .1049 | .2084 | .4565 |
| ** | ** | 146.1 | .3456 | .1273 | 1240. | 104.8 | .2928 | .9137 | .7180 | .8479 |
| 74.72 | 0.49 | 153.6 | .3523 | .1323 | 1263. | 89.68 | .2682 | .7721 | .5838 | .7641 |
| | | 58.85 | .2451 | .0640 | 940.0 | 11.08 | .1063 | .1204 | .1882 | .4351 |
| -- | -- | 238.0 | .4183 | .1864 | 1522. | 77.01 | .2379 | .6034 | .3236 | .5689 |
| -- | -- | 216.9 | .4034 | .1734 | 1463. | 194.9 | .3824 | 1.558 | .8988 | .9481 |
| -- | -- | 602.1 | .6103 | .3969 | 2477. | 286.0 | .4207 | 1.885 | .4753 | .6893 |
| 41.56 | 0.48 | | | | | | | | | |
| 32.32 | 0.18 | 252.0 | .4143 | .1936 | 1584. | 257.5 | .4189 | 1.978 | 1.0220 | 1.0109 |
| ** | ** | 184.9 | .3671 | .1520 | 1389. | 69.67 | .2254 | .5726 | .3767 | .6138 |
| 46.18 | 0.60 | 237.3 | .4047 | .1847 | 1544. | 264.2 | .4271 | 2.057 | 1.1135 | 1.0553 |
| -- | -- | 287.3 | .4368 | .2151 | 1690. | 306.8 | .4514 | 2.297 | 1.0680 | 1.0335 |
| 43.81 | 0.27 | 359.8 | .4784 | .2581 | 1895. | 175.3 | .3340 | 1.258 | .4873 | .6981 |
| ** | ** | 209.1 | .3911 | .1706 | 1412. | 133.5 | .3124 | 1.089 | .6385 | .7991 |
| 44.98 | 0.30 | 360.1 | .4853 | .2627 | 1810. | 243.6 | .3988 | 1.774 | .6755 | .8219 |
| 52.72 | 0.13 | 371.3 | .4913 | .2693 | 1844. | 202.3 | .3627 | 1.467 | .5451 | .7383 |
| -- | -- | | | | | | | | | |
| -- | -- | 401.4 | .5070 | .2867 | 1917. | 261.6 | .4093 | 1.869 | .7047 | .8074 |
| 59.82 | 0.31 | 198.9 | .3834 | .1640 | 1380. | 88.26 | .2554 | .7277 | .4438 | .6662 |
| 61.81 | 0.48 | 282.9 | .4400 | .2160 | 1603. | 119.2 | .2856 | .9100 | .4213 | .6491 |
| ** | ** | 33.54 | .0963 | .0209 | 851.0 | 29.14 | .0898 | ,1818 | .8689 | 9322 |
| 34.57 | 0.15 | 148.2 | .1686 | .0641 | 1278. | 117.3 | .1500 | .5073 | | |
| 34.78 | 0.15 | 206.2 | .1916 | .0828 | 1456. | 161.6 | .1696 | .6490 | .7840 | .8854 |
| 25.56 | 0.12 | 316.2 | .2269 | .1161 | 1770. | 196.9 | .1791 | .7232 | .6227 | 7891 |
| 57.13 | 0.68 | | | | | | | | | |
| ** | ** | 159.0 | .1759 | .0691 | 1270. | 221.0 | .2075 | .9602 | 1.3905 | 1.1792 |
| 33.58 | 0.50 | 328.6 | .2338 | .1219 | 1731 | 293.9 | .2211 | 1.091 | .8943 | 9457 |
| 69.15 | 0.51 | 325.8 | .2328 | .1209 | 1716. | 259.2 | .2076 | .9617 | .7955 | .8919 |
| -- | -- | 335.6 | .2357 | .1240 | 1748. | 269.9 | .2114 | .9968 | .8040 | .8967 |
| | | 149.9 | .3529 | .1292 | 1280. | 32.86 | .1652 | .2832 | .2192 | .4682 |

# Table III. Continued.

| Run Number | Fuel | Drop Diameter $D_o$ ($\mu$m) | Oxidizer | Energy (gms) | $M_{s_i}$ | $M_{R=24 \text{ in.}}$ | $t_b$ ($\mu$sec) | $t_b/D_o$ (msec/in.) | $\bar{t}_b$ | $x_b$ (in.) | $\bar{x}_b$ | $t_{st}$ ($\mu$sec) | $t_{st}/D_o$ (msec/in.) | $\bar{t}_{st}$ | $x_{st}$ (in.) | $\bar{x}_{st}$ |
|---|---|---|---|---|---|---|---|---|---|---|---|---|---|---|---|---|
| 59 | Decane | 768 | 50%$O_2$ 50%$N_2$ | 0.00 | 2.007 | 2.028 | 70.29 | 2.32 | 2.070 | 0.23 | 7.596 | 6.696 | 0.221 | 0.337 | 0.003 | 0.091 |
| 60 | | | | 1.00 | 2.814 | 2.814 | 39.48 | 1.31 | 2.353 | 0.18 | 5.805 | 4.889 | 0.162 | 0.420 | 0.001 | 0.038 |
| 61* | | | | 0.00 | | | | | | | | | | | | |
| 62 | | | | 0.50 | 2.470 | 2.970 | 47.71 | 1.58 | 2.713 | 0.30 | 9.969 | 12.108 | 0.400 | 0.986 | 0.011 | 0.351 |
| 63 | | | | 1.50 | 3.276 | 3.338 | 46.45 | 1.54 | 3.172 | 0.20 | 6.450 | 6.712 | 0.222 | 0.799 | 0.0 | 0.0 |
| | | | | | | | | | | | | | | | | |
| 52 | Decane | 768 | $O_2$ | 0.00 | 2.011 | 2.011 | 97.09 | 3.21 | 3.020 | 0.34 | 11.395 | | | | | |
| 53 | | | | 1.50 | 3.417 | 3.440 | 64.21 | 2.12 | 5.098 | 0.33 | 10.930 | 5.657 | 0.187 | 0.661 | 0.005 | 0.164 |
| 54* | | | | 1.00 | 3.693 | 3.848 | | | | | | | | | | |
| 55 | | | | 0.50 | 3.061 | 3.244 | 71.24 | 2.36 | 4.825 | 0.46 | 15.224 | 6.878 | 0.227 | 0.701 | 0.0 | 0.0 |
| 56 | | | | 1.25 | 2.918 | 2.918 | 57.02 | 1.89 | 4.566 | 0.26 | 8.679 | 5.662 | 0.187 | 0.627 | 0.0 | 0.015 |
| 57 | | | | 0.75 | 3.421 | 3.475 | 54.25 | 1.79 | 4.472 | 0.44 | 14.658 | 3.585 | 0.119 | 0.394 | 0.009 | 0.285 |
| 58 | | | | 0.25 | 2.374 | 2.376 | 74.22 | 2.45 | 3.321 | 0.37 | 12.343 | 6.098 | 0.202 | 0.505 | 0.0 | 0.0 |
| | | | | | | | | | | | | | | | | |
| 37 | Decane | 384 | 50%$O_2$ 50%$N_2$ | 0.00 | 2.096 | 2.096 | 61.99 | 4.10 | 3.794 | 0.19 | 12.522 | 6.172 | 0.408 | 0.713 | 0.0 | 0.0 |
| 38* | | | | 3.00 | | 3.482 | | | | | | | | | | |
| 41 | | | | 1.50 | 3.304 | 3.469 | 43.29 | 2.86 | 7.723 | 0.42 | 27.991 | 3.339 | 0.221 | 0.783 | 0.001 | 0.059 |
| 42 | | | | 1.00 | 3.286 | 3.286 | 66.42 | 4.39 | 10.716 | 0.35 | 23.208 | 13.691 | 0.906 | 3.193 | 0.0 | 0.0 |
| 45* | | | | 0.50 | | 2.430 | | | | | | | | | | |
| 46 | | | | 0.50 | 2.548 | 2.548 | 57.98 | 3.84 | 5.995 | 0.41 | 27.086 | 0.699 | 0.046 | 0.115 | 0.0 | 0.0 |
| 47 | | | | 0.25 | 2.232 | 2.247 | 49.64 | 3.28 | 4.735 | | | | | | | |
| 48* | | | | 1.50 | 3.167 | 3.210 | | | | | | | | | | |
| 49 | | | | 1.50 | 2.846 | 2.850 | 49.06 | 3.25 | 6.577 | 0.35 | 23.080 | | | | | |
| 50* | | | | 1.50 | | 2.994 | | | | | | | | | | |
| | | | | | | | | | | | | | | | | |
| 34 | Decane | 384 | $O_2$ | 1.50 | 3.712 | 3.758 | 25.70 | 1.70 | 5.314 | 0.26 | 17.112 | 33.175 | 2.194 | 6.060 | 0.252 | 16.642 |
| 35 | | | | 0.00 | 1.889 | 1.889 | 71.05 | 4.70 | 4.797 | 0.40 | 26.726 | | | | | |
| 36* | | | | 3.00 | | 5.923 | | | | | | | | | | |
| 39 | | | | 3.00 | 4.160 | 4.166 | 18.78 | 1.24 | 4.422 | 0.18 | 11.852 | | | | | |
| 40 | | | | 1.50 | 3.551 | 3.590 | 52.37 | 3.46 | 10.290 | 0.46 | 30.157 | 5.946 | 0.393 | 1.423 | 0.009 | 0.628 |
| 43* | | | | 1.00 | | 3.280 | | | | | | | | | | |
| 44 | | | | 0.50 | 2.883 | 2.986 | 57.71 | 3.82 | 7.938 | 0.29 | 18.953 | 11.249 | 0.744 | 1.774 | 0.0 | 0.0 |
| 51 | | | | 1.50 | 3.607 | 3.607 | | | | | | 48.631 | 3.217 | 6.746 | 0.505 | 33.420 |

| $t_{ig}$ | $x_{ig}$ | $q_i$ | $Re_i$ | $We_i$ | $T_{2_i}$ | $q_b$ | $Re_b$ | $We_b$ | $q_b/q_i$ | $Re_b/Re_i$ |
|---|---|---|---|---|---|---|---|---|---|---|
| ($\mu$sec) | (in.) | (psi) | x $10^{-5}$ | x $10^{-5}$ | (°R) | (psi) | x $10^{-5}$ | x $10^{-4}$ | | |
| ** | ** | 42.86 | .2118 | .0726 | 893.5 | 26.92 | .1674 | .4560 | .6281 | .7925 |
| 78.76 | 1.31 | 156.3 | .3441 | .1928 | 1301. | 110.2 | .2889 | 1.359 | .7050 | .8397 |
| ** | ** | 186.5 | .3683 | .2209 | 1393. | 100.3 | .2701 | 1.188 | .5377 | .7333 |
| 57.62 | 0.58 | 253.6 | .4154 | .2810 | 1590. | 144.6 | .3138 | 1.603 | .5704 | .7553 |
| 188.9 | 1.43 | 42.21 | .2226 | .0798 | 895.3 | 30.01 | .1775 | .5073 | .6358 | .7974 |
| 79.8 | 0.72 | 314.6 | .4592 | .3396 | 1690. | 195.6 | .3621 | 2.112 | .6218 | .7886 |
| 106.7 | 1.34 | 224.5 | .4020 | .2602 | 1452. | 142.3 | .3200 | 1.650 | .6339 | .7962 |
| 65.76 | 0.67 | 192.2 | .3784 | .2306 | 1362. | 199.0 | .3850 | 2.387 | 1.0352 | 1.0748 |
| 56.78 | 0.64 | 315.4 | .4597 | .2357 | 1691. | 210.8 | .3758 | 2.275 | .6684 | .8176 |
| 143.4 | 1.39 | 93.08 | .2871 | .1328 | 1064. | 62.12 | .2345 | .8860 | .6674 | .8169 |
| ** | ** | 52.30 | .1139 | .0422 | 942.2 | 29.05 | .0849 | .2346 | .5554 | .7453 |
| 30.07 | 0.32 | 263.9 | .2113 | .1454 | 1632. | 246.8 | .2044 | 1.360 | .9355 | .9672 |
| -- | -- | 257.5 | .2091 | .1424 | 1606. | 201.9 | .1851 | 1.116 | .7841 | .8855 |
| 48.49 | 0.43 | 111.5 | .1514 | .0746 | 1161. | 82.90 | .1305 | .5546 | .7433 | .8621 |
| | | 67.53 | .1253 | .0511 | 1002. | 70.56 | .1281 | .5342 | 1.0450 | 1.0226 |
| | | 164.4 | .1756 | .1005 | 1336. | 139.4 | .1618 | .8520 | .8481 | .9210 |
| <u>35.46</u> | <u>0.55</u> | | | | | | | | | |
| 20.48 | 0.23 | 402.2 | .2541 | .2078 | 1916. | 331.7 | .2303 | 1.708 | .8246 | .9062 |
| ** | ** | 326.7 | .0995 | .0296 | 849.7 | 35.36 | .1035 | .3209 | 1.0820 | 1.0404 |
| | | 555.2 | .2898 | .2705 | 2296. | 430.0 | .2550 | 2.095 | .7745 | .8801 |
| 49.33 | 0.61 | 356.9 | .2418 | .1884 | 1809. | 299.5 | .2215 | 1.581 | .8390 | .9160 |
| 67.98 | 0.64 | 186.4 | .1872 | .1128 | 1353. | 146.7 | .1660 | .8882 | .7872 | .8873 |
| | | 374.9 | .2468 | .1962 | 1859. | | | | | |

A method of discussing the extent of decay of the drop dynamic conditions, i.e. localized convective gas flow conditions, was required to help distinguish the results obtained herein from the conventional shock tube results reported upon elsewhere. The ratio of dynamic pressure just behind the incident shock front to that at drop breakup was evaluated from the experimental data and is given in Fig. 48. This ratio is plotted versus incident blast wave Mach number for two drop sizes, 768 $\mu$m and 384 $\mu$m. The results plainly show, in spite of a few spurious points, the decrease in dynamic pressure behind the blast wave. Further, this decrease is more severe for the larger drop size. This latter result is to be expected due to the extended duration of the breakup process for the larger drop. No definite trends with incident Mach number are noted, but this may be due to the data scatter or to the method of computation of the ratio $q_b/q_i$. The initial drop local dynamic pressure, $q_i$, was derived from the experimental incident shock speed and normal shock relations. The local dynamic pressure at breakup, $q_b$, was evaluated at the downstream drop breakup position from an experimental determination of $u_2$ as a function of distance behind the shock front. Local gas density was evaluated immediately behind the shock and used for both cases. See Section C.1, for further detail on this computation. Hence a parameter established both by experiment and theory, $q_i$, is being compared with one based solely on experiment, $q_b$. A cursory computation was made to seek a new semi-theoretical $q_b$ based upon $q_i$ and the known rate of decay

of convective gas flow behind strong blast waves,

$$v_2 = \frac{2}{\gamma_1 + 1} \frac{r}{t} \qquad (102)$$

This computation revealed that in general the experimental $q_b$ was higher than the semi-theoretical $q_b$. A contributor to this difference may be that the experimental value was based upon a $u_2$ found by differentiating the trajectory of impurities in the convective flow field behind the shock. Such impurities might have been traveling at speeds in excess of the true local convective flow. A second iteration on the reduction of drop data associated with the dynamic pressure seems in order, but has not been done, by making use of the above mentioned semi-theoretical dynamic pressure at breakup. This will undoubtedly remove some of the observed scatter and inconsistencies in the data such as values of $q_b/q_i > 1.0$. A discussion of plots made of $Re_b/Re_i$ as a function of incident shock Mach number reveal results similar to those for dynamic pressure ratio.

Following the initial shock/drop interaction, the next characteristic feature of the drop time history is the initial development of the drop wake. This condition has been referred to by many as the drop stripping point. Times and distances to this point have been tabulated. Results reveal a general decrease in stripping time and distance with increasing incident shock strength, if obviously outlying points are ignored. For NPN as the fuel, stripping occurs at approximately 9 $\mu$sec for a Mach 2.0

wave, decreasing to 4 $\mu$sec for a Mach 3.75 wave. The corresponding

stripping times for decane drops are 8 $\mu$sec and 4 $\mu$sec. Only slight

increases in $t_{st}$ are suggested by increasing drop size. The results

further show that the drop does not move in the downstream direction

prior to the stripping process.

The fundamental process of drop breakup was examined in light of

several data representations. The first, given in Fig. 49, shows dimen-

sional breakup time, $t_b$, as a function of incident shock Mach number. The

data reveals a general decrease in $t_b$ with increasing Mach number, with

the larger drop size yielding higher overall breakup times. Data for

decane shows less scatter than that for n-propyl nitrate, however, the

scatter throughout all the data seemed to be high. The addition of $O_2$

to the atmosphere indicates that slightly higher breakup times occur. This

trend is more easily seen in the decane data. For comparison, breakup

data reported by Kauffman[12] for diethylcyclohexane (DECH) fuel drops is

shown in Fig. 49b for specified conditions. The comparison seems to

suggest that the breakup times are only slightly increased, if at all, due to

the decaying dynamic conditions behind the blast wave. At this stage,

breakup times do not seem to be as highly affected as do the ignition

times, to be discussed in the next section. However, if this discussion

is examined in light of observed non-dimensional breakup distance,

$$\overline{x}_b = x_b/D_o \qquad\qquad (103)$$

versus Mach number, greater dependency is suggested. The latter data

is displayed in Fig. 50, where $6 \leq \overline{x}_b \leq 22$ for n-propyl nitrate and

$6 \leq \overline{x}_b \leq 28$ for decane. Additionally, $\overline{x}_b$ tends to decrease for increasing

Mach number, despite the usual scatter. It is also of interest to notice

that the values of $\overline{x}_b$ are slightly larger for smaller drops. All these

observations are in agreement with those of Kauffman[12], whose results

are given briefly in Table IV for comparison.

Table IV. Non-Dimensional Breakup Distances for DECH

| $D_o$ ($\mu$m) | Atm | $\overline{x}_b$ | $\overline{x}_{b_{mean}}$ |
|---|---|---|---|
| 932 | $O_2$ | 10-12 | 11.0 |
| 932 | $N_2$ | 11-16 | 13.5 |
| 1520 | $N_2$ | 9-14 | 11.5 |
| 2130 | $N_2$ | 8-14 | 11.0 |

Table IV shows $\overline{x}_{b_{mean}} \approx 12$ for all conditions examined by Kauffman,

with perhaps a slight decrease with increased $O_2$ concentration. The

results of the experiments on decane reported herein find that $\overline{x}_{b_{mean}} \approx 17$

for all conditions examined. This result suggests that the drop traveled

a greater distance downstream before breaking up, when impacted by a

blast wave. The reason for the lack of a corresponding difference in breakup times, as suggested earlier, is conceivably due to the fact that the experimentally determined local convective gas flow velocity at break-up, $u_{2_{brkp}}$, was higher than corresponding predicted values. Hence, a higher velocity when combined with a given breakup distance seemed to produce breakup times lower than expected. This is consistent since $u_{2_{brkp}}$ and $t_b$ both proved to be more sensitive functions of incident Mach number than $r_{brkp}$. The conclusion is that the breakup process does indeed seem to be extended due to the decaying local dynamic conditions behind the blast wave. Further analysis of the breakup time data should tend to substantiate the trends suggested by non-dimensional breakup distances.

Reduced breakup time, defined as

$$\tilde{t}_b = t_b/D_o \tag{104}$$

is shown plotted versus $q_b$ in Fig. 51. Observed data is compared with that reported elsewhere[13] for simple one-dimensional shock waves. The observed data tends to straddle the mean approximating line of the simple shock data. The difference in $\tilde{t}$ should presumably be more pronounced in light of the previous discussion. Examination of non-dimensional breakup times reveal $2.0 \leq \tilde{t}_b \leq 10.5$ with $\tilde{t}_{b_{mean}} \approx 4.5$ for decane and $1.25 \leq \tilde{t}_b \leq 10.0$ with $\tilde{t}_{b_{mean}} \approx 3.75$ for n-propyl nitrate. Here define

$\bar{t}_b$ as

$$\bar{t}_b = u_2 \, (\rho_2/\rho_f)^{1/2} \, t/D_o \qquad (105)$$

The range of scatter is evident. However, it is also clear from this and other data that n-propyl nitrate breaks up quicker than decane, and that the non-dimensionalization appears to be in satisfactory agreement with Kauffman's results who found $2.5 \leq \bar{t}_b \leq 5.0$ for DECH for all conditions examined.

A final representation of the drop breakup process is of key interest. Shown in Fig. 52 is breakup time plotted as a function of dynamic pressure ratio, $q_b/q_i$, for both fuels. Despite the usual scatter, the generally conclusive result that $t_b$ increases with decreasing $q_b/q_i$ is suggested. Similar effects are represented, but with much less data scatter, in Fig. 53 by plotting $t_b$ versus $Re_b/Re_i$, drop local Reynolds number ratio, where

$$Re_b = \rho_2 \, (u_{2_b} \, D_o)/\mu_1$$

and $\qquad (106)$

$$Re_i = \rho_2 \, (u_2 \, D_o)/\mu_1$$

Here $\mu_1$ was used in place of $\mu_2$ for computational simplicity. The conclusion derived from Figs. 52 and 53 is that the decrease in local drop dynamic conditions has a significant modifying effect upon the drops' time history to breakup. An increase in breakup time of nearly 100%

in some cases is observed if values of $t_b$ are compared for correspondingly decreasing values of $Re_b/Re_i$ or $q_b/q_i$. Recall that for simple one-dimensional shock wave without decay due to expansion waves, $Re_b/Re_i = 1$ and $q_b/q_i = 1$.

## 3. Ignition of Fuel Drops

Ignition is the final stage of development in the time history of a liquid fuel drop, impacted by a blast wave, which was examined in this study. Characteristic ignition delay times and distances were obtained for all experimental runs for which combustion was observed. An important difficulty encountered throughout the observations and subsequent analysis of some of the data runs was that of distinguishing between deflagrative and detonative combustion of the drop from the streak schlieren records. This problem, while of greater interest in the n-propyl nitrate experiments, did enter to a lesser degree in the decane experiments. The mere occurrence of blast waves, usually a good indicator of the detonative mode, was of no help in establishing combustion mode in some cases. Observed experimental evidence seems to substantiate the existence of multiple ignition centers, and perhaps suggests the occurrence of multiple combustion modes. The conditions under which the above occurred are given in Table V.

Table V. Observed Conditions of Multiple Ignition Center

| Fuel | $D_o$ ($\mu$m) | Oxidizer | Run No. | $M_{s_i}$ |
|------|------|------|------|------|
| n-propyl nitrate | 768 | 50% $O_2$-50% $N_2$ | 22 | 3.27 |
| | | | 23 | 2.96 |
| | 384 | 100% $O_2$ | 28 | 2.75 |
| | | 50% $O_2$-50% $N_2$ | 68 | 3.52 |
| decane | 384 | 50% $O_2$-50% $N_2$ | 34 | 3.71 |

Also given in Table III is a comparison of the observed multiple ignition delay times and distances for Run No.'s 23, 28, and 34. The numbers displayed above the small bars are those expected for the given initial conditions, with the lower numbers representing the second ignition center. No clear trends are evident at this writing.

Individual primary blast waves were observed for the ignition of decane at high dynamic pressure, i.e. $M \gtrsim 3$ in 100% $O_2$. At the same conditions but lower dynamic pressures a blast wave followed by a succession of recurring Mach waves were observed. This is in agreement with results of Kauffman. Such phenomena were not observed in n-propyl nitrate with any regularity. For the purposes of the remainder of the discussion in this section, ignition delay time, $t_{ig}$, was generally defined as that time

interval between the initial drop/blast interaction and first occurrence

of combustion blast waves in the drop wake. In most cases, combustion

was clearly of the detonative type.

It is of interest to discuss the ignition delay times observed in terms

of drop breakup. Drop breakup times are plotted against ignition delay

times in Fig. 54. The essential features displayed by the data are that

n-propyl nitrate drops are less destroyed at ignition than decane drops

for all conditions examined. The decane drops were considerably more

destroyed at ignition than would be expected from results reported by

Kauffman. These comments support the fact that the fundamental processes

are slowed due to the decaying local dynamic conditions. It is of interest

to note that the ignition delay data for decane suggests that combustion

occurred after the classically defined drop breakup time; whereas

n-propyl nitrate data suggests combustion occurred prior to corres-

ponding drop breakup times.

Figure 55 shows the results of plotting ignition delay times versus

incident blast wave strength. Also shown for comparison are the results

reported by Kauffman[12] for DECH drops and Lu and Slagg[14] for

n-propyl nitrate drops. The experiments conclusively yielded larger

ignition delay times than those suggested by the simple one-dimensional

shock experiments. Ignition delay times were found to decrease with

increasing Mach number, except for some n-propyl nitrate test conditions,

which could have easily been due to data scatter and too few points or uncertainty of combustion mode as pointed out earlier. Increased drop size had the expected effect of increasing ignition delay. However, the dilution of oxygen atmosphere by nitrogen seems, in some cases, to have the effect of decreasing ignition delay. This again may easily be associated with a corresponding change in combustion mode, and hence further analysis on this point is required. It is clear from all the ignition data that n-propyl nitrate ignites more readily than decane and is more substantially affected by the decaying dynamic conditions. An additional representation of the ignition delay times may be made against the reciprocal of static temperature. The results of this are shown in Fig. 56, where it is seen that some of the scatter has been removed. Trends similar to those in Fig. 55 are more easily seen. For the purposes of discussion, ignition delay times were considered to be related to the flow static temperature, in the classical sense, through the use of an Arrhenius rate law,

$$t_{ig} \propto \exp \left( \Delta E / RT \right) . \qquad (107)$$

A standard least squares fit to the available data was made on this basis. The results of this correlation are given in Table VI and compared with data reported by Kauffman and Lu and Slagg. The data shown for current tests represent those conditions for which sufficient data existed to support

## Table VI. Comparison of Activation Energy Data

| Fuel | $D_0$ | Atm | $\Delta E$ (kcal/gm-mole) |
|---|---|---|---|
| Decane | 768 | 100% $O_2$ | 2.173[1] |
| | 384 | 100% $O_2$ | 2.816[1] |
| DECH | 932 | 100% $O_2$ | 6.86[2] |
| | 1520 | 100% $O_2$ | 4.59[2] |
| | 1520 | 75% $O_2$-25% $N_2$ | 6.08[2] |
| | 2130 | 100% $O_2$ | 4.04[2] |
| n-Propyl Nitrate | 384 | 50% $O_2$-50% $N_2$ | 1.588[1] |
| | 768 | 100% $O_2$ | 1.338[1] |
| | 768 | 50% $O_2$-50% $N_2$ | 0.346[1] |
| | 1639 (multiple) | 100% $O_2$ | 10.22[3] |
| | 3000 | 100% $O_2$ | 2.96[3] |

[1] Current Tests
[2] Kauffman
[3] Lu and Slagg

a reasonable least squares regression. The results are encouraging in that $\Delta E$ decreases with increasing $D_o$ for both n-propyl nitrate and decane agreeing with the data of Kauffman, Lu and Slagg. The only effect of dilution on $\Delta E$ for the current tests is seen for n-propyl nitrate data, where no comparison is available.

A final representation of the ignition delay data was made relative to the ratio of dynamic pressures, and is given in Fig. 57. The results, while not being entirely conclusive, tend to suggest a general increase in ignition delay with decreasing $q_b/q_i$. Again recall, that this figure is based strictly upon experimental data. Had $t_{ig}$ been plotted against $q_{b_{theory}}$, nondimensionalized by $q_i$, then on the basis of an earlier discussion $q_{b_{theory}}$, the results would seem to suggest a conclusive dependency of ignition delay upon dynamic pressure decay.

The general conclusions to be drawn from this study suggest that the drop time history of breakup and ignition is indeed extended due to the decaying local dynamic conditions behind the incident blast wave. However, the great scatter in the data necessitates additional study before quantitative effects can be established with any confidence.

# REFERENCES

1. Ragland, K. W. , Dabora, E. K. , and Nicholls, J. A. , "Structure of Two-Phase Detonations," Phys. Fluids, Vol. 11, No. 11, Nov. 1968.

2. Dabora, E. K. , Ragland, K. W. , and Nicholls, J. A. , "Drop-Size Effects in Spray Detonations," Twelfth Symposium (International) on Combustion, Combustion Institute, 1969.

3. Bach, G. G. , Knystautas, R. , and Lee, J. H. , "Direct Initiation of Spherical Detonations in Gaseous Explosives," Twelfth Symposium (International) on Combustion, Combustion Institute, 1969.

4. Bach, G. G. , Knystautas, R. , and Lee, J. H. , "Initiation Criteria for Diverging Gaseous Detonations," Thirteenth Symposium (International) on Combustion, Combustion Institute, 1971.

5. Sakurai, A. , Exploding Wires (W. G. Chace and H. K. Moore, ed.), Plenum Press, 1959, p. 264 ff.

6. Sedov, L. I. , Similarity and Dimensional Methods in Mechanics, Academic Press, New York, 1959, p. 152 ff.

7. Sakurai, A. , "Blast Wave Theory," Basic Developments in Fluid Dynamics, Vol. 1, Academic Press, New York, 1965, p. 309 ff.

8. Nicholls, J. A. , Fry, R. S. , Glass, D. R. , Sichel, M. , VanderSchaaf J. , and Sternstein, A. J. , "Fundamental Aspects of Unconfined Explosions," Tech. Rept. AFATL-TR-72-39, AF Armament Lab. , Eglin AFB, Fla. , Mar. 1972.

9. Nicholls, J. A. , Sichel, M. , Fry, R. S. , Hu, C. , Glass, D. R. , DeSaro, R. , and Kearney, K. , "Fundamental Aspects of Unconfined Explosions," Tech. Rept. AFATL-TR-73-125, AF Armament Lab. , Eglin AFB, Fla. , Mar. 1973.

10. Nicholls, J. A. , Sichel, M. , Fry, R. , and Glass, D. R. , "Theoretical and Experimental Study of Cylindrical Shock and Heterogeneous Detonation Waves," Fourth International Colloquium on Gasdynamics of Explosions and Reactive Systems, San Diego, Calif. , 10-13 July 1973.

11. Fry, R. S. and Nicholls, J. A., "Blast Initiation and Propagation of Cylindrical Detonations in MAPP-Air Mixtures," presented at the AIAA 12th Aerospace Sciences Meeting, Jan. 30-Feb. 1, 1974, Washington, D. C., Preprint No. 74-149, accepted for publication in the AIAA J.

12. Kauffman, C. W., "Shock Wave Ignition of Liquid Fuel Drops," Ph. D. Thesis, University of Michigan, 1971.

13. Dabora, E. K., Ragland, K. W., Ranger, A. A., and Nicholls, J. A., "Two-Phase Detonations and Drop Shattering Studies," NASA CR-72225, April 1967.

14. Lu, P. -L. and Slagg, N., "Chemical Aspects in the Shock Initiation of Fuel Droplets," Astronautica Acta, 17, 1972, 693-720.
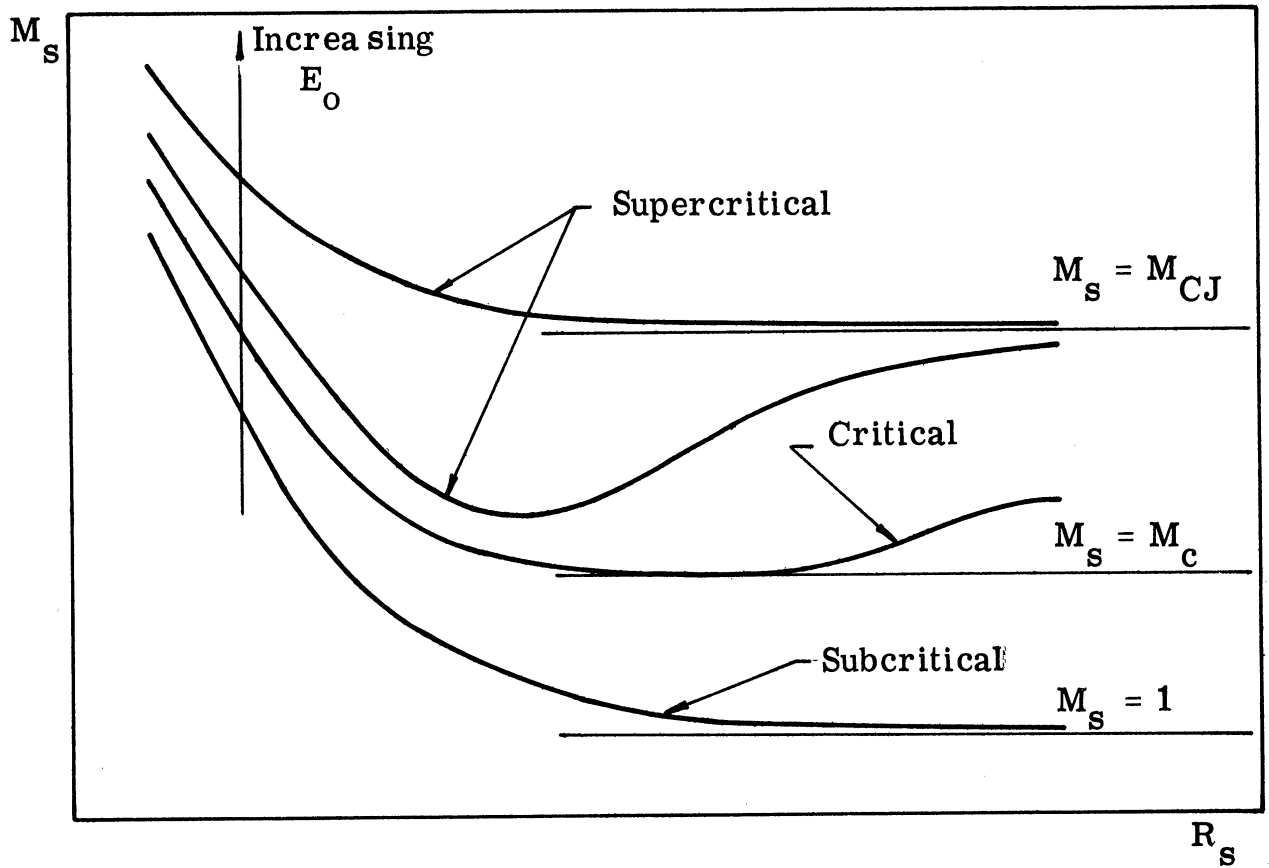
Figure 1.    Wave Mach Number vs Radius for Various Initiator Energy Levels; Combustible Atmosphere.
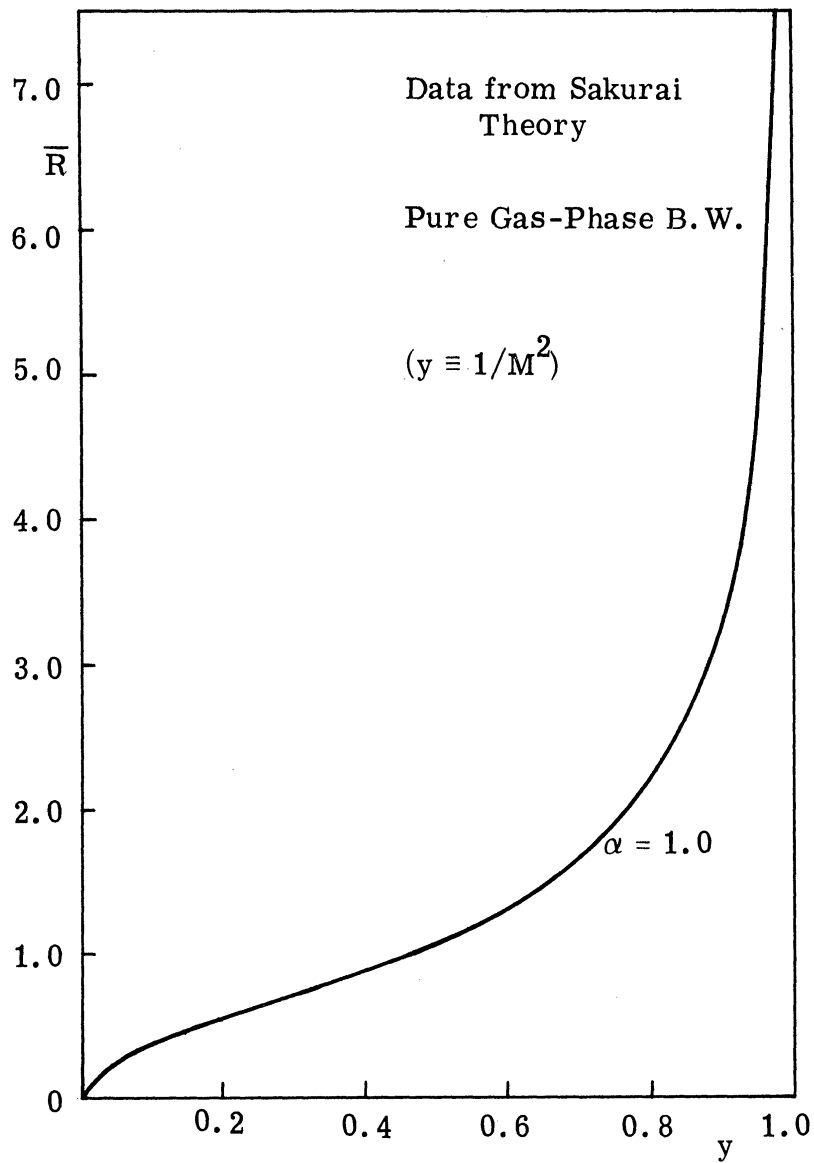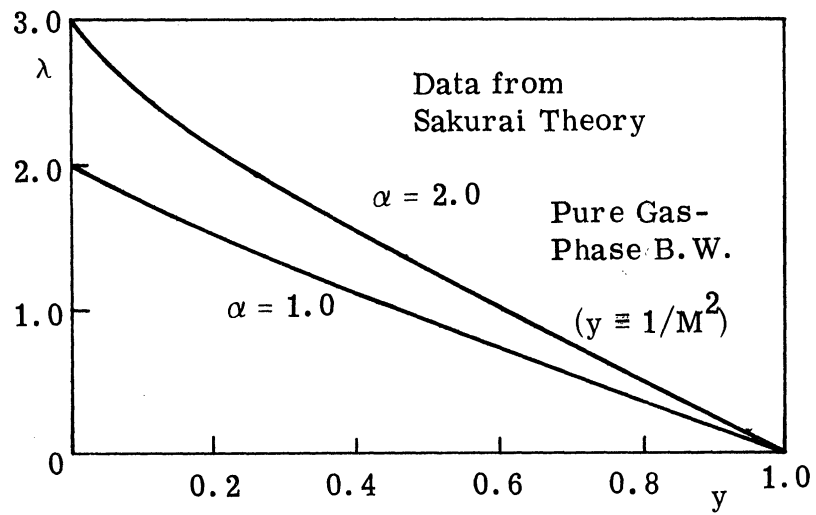
Figure 2.    $\lambda(y)$ vs y for a Pure Gas Phase Blast Wave.

Figure 3.    $\bar{R}(y)$ vs y for a Pure Gas Phase Blast Wave.
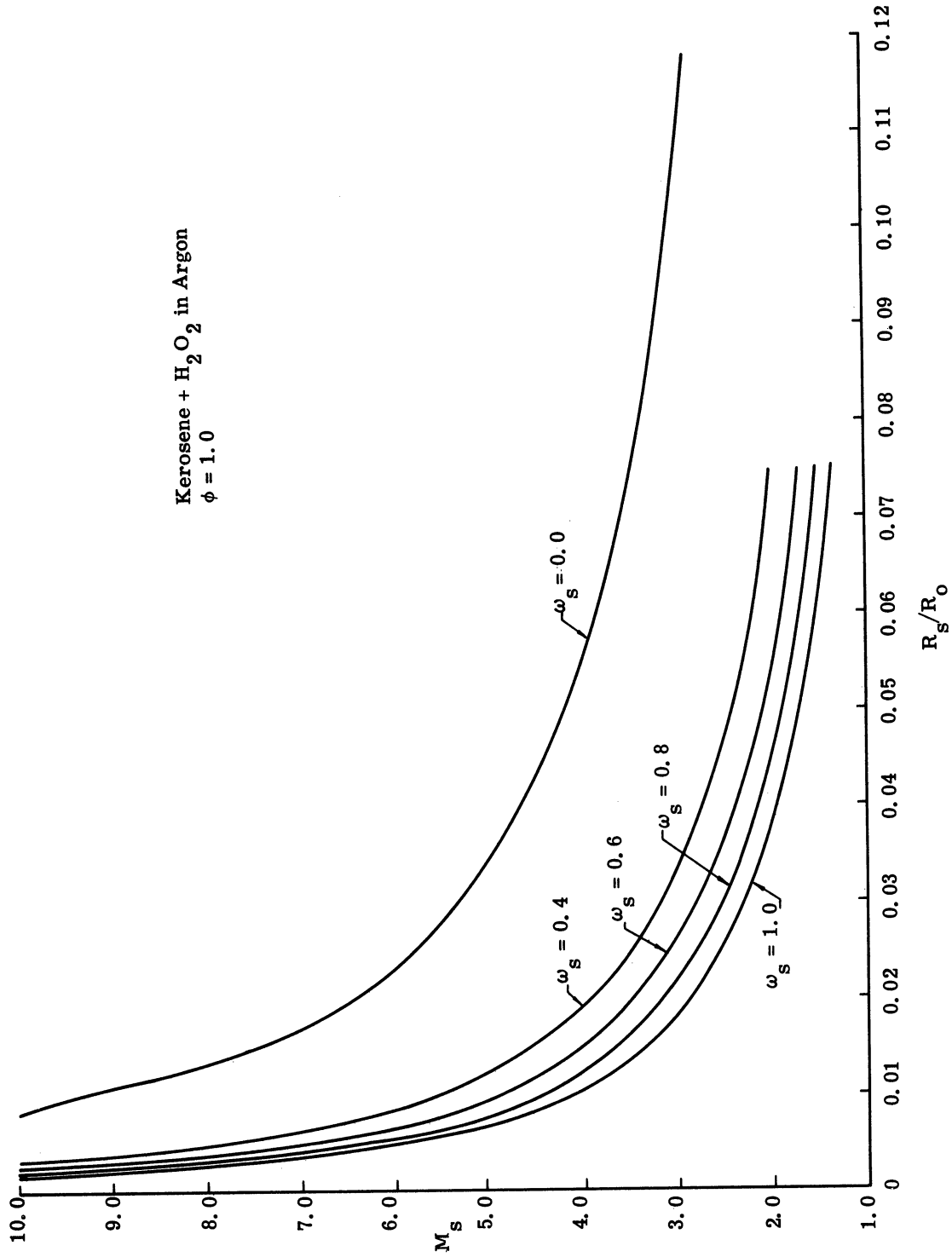
Figure 4.    Blast Wave Attenuation for Various Spray "Loading Factors".

88
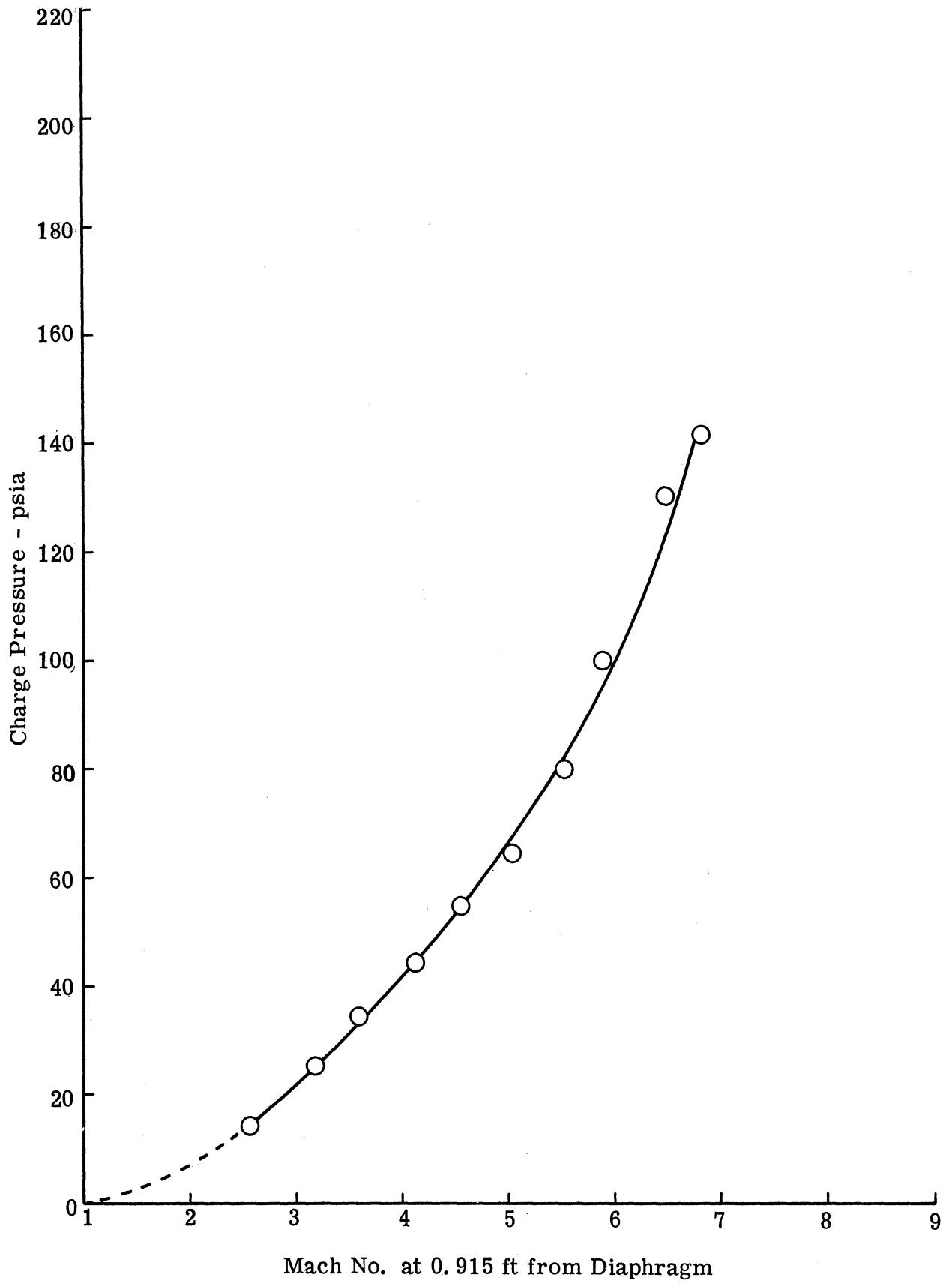
Figure 5. Transmitted Shock Number vs Driver Charge Pressure.
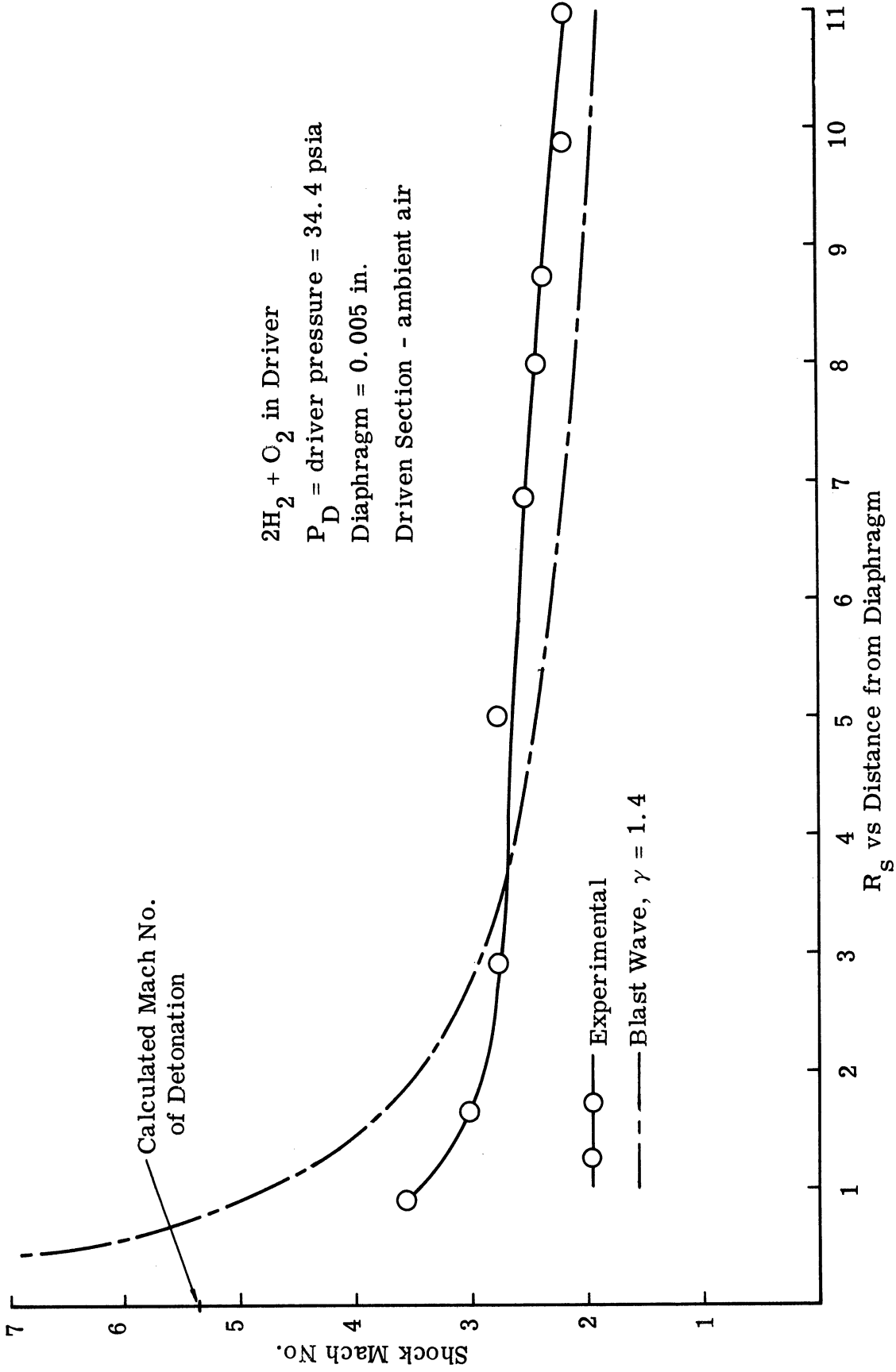
Figure 6. Transmitted Shock Mach Number vs Distance, $P_D = 34.4$ psia.
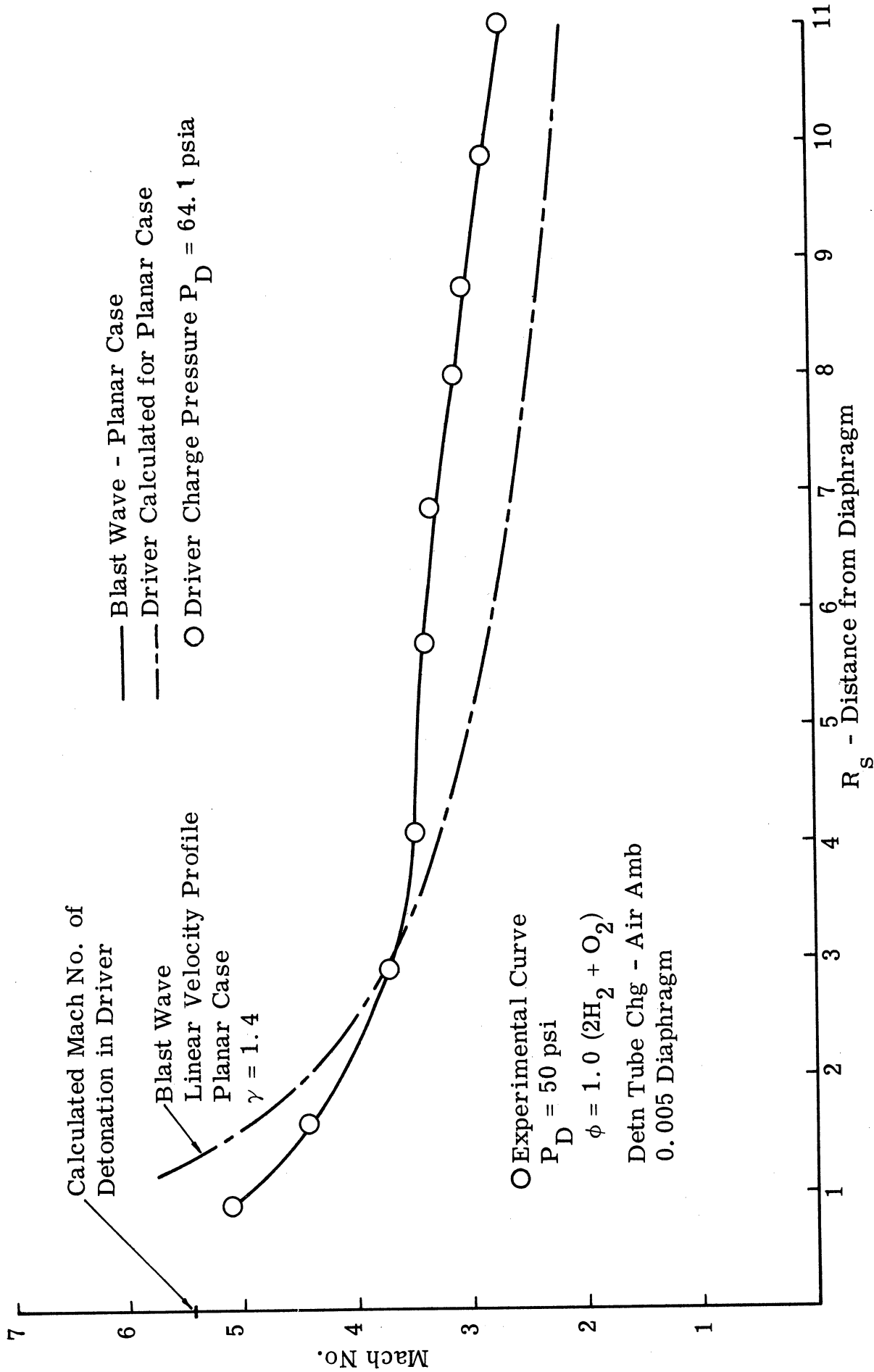
Figure 7.    Transmitted Shock Mach Number vs Distance,   $P_D$ = 64.1 psia.

91
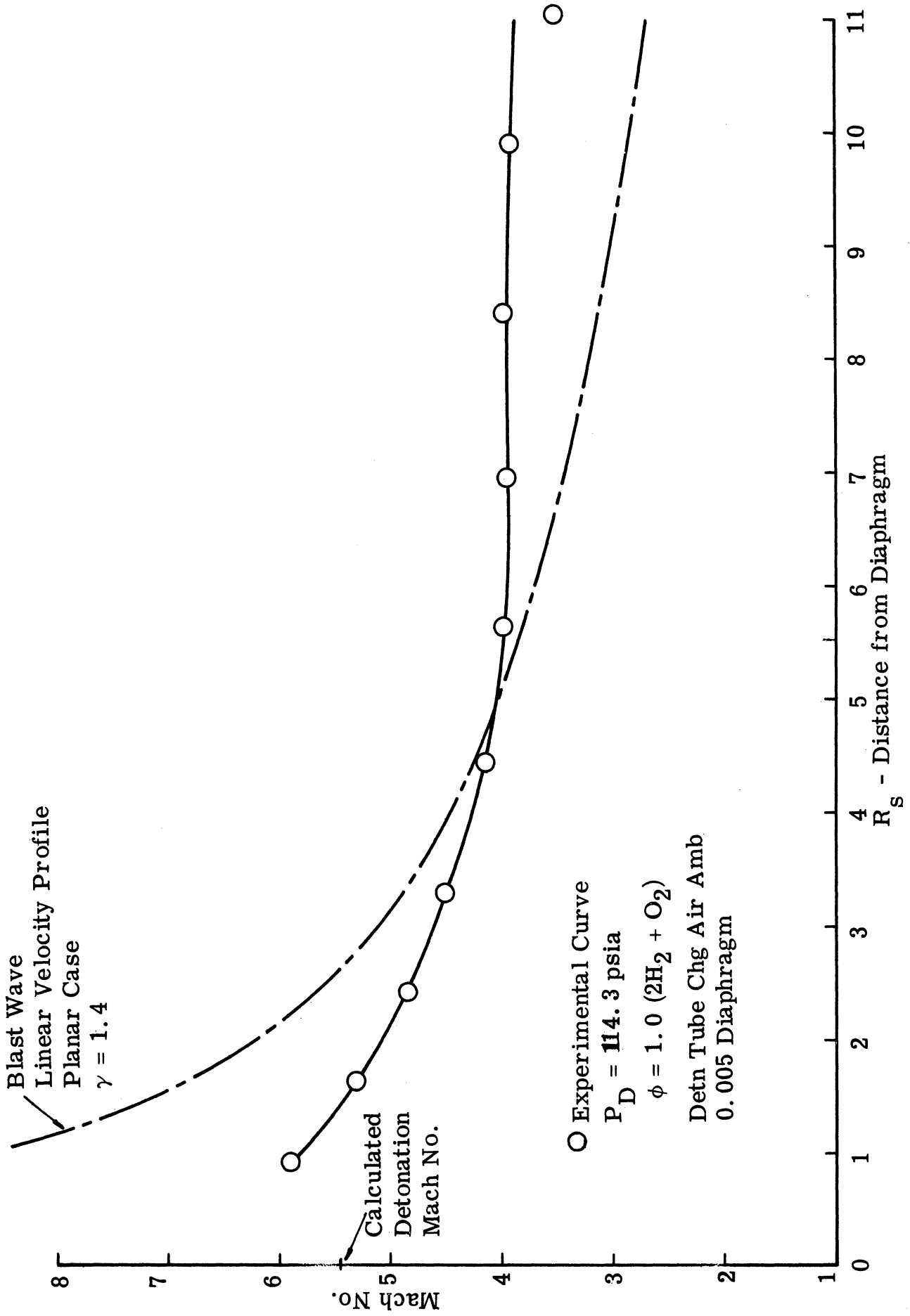
Figure 8.    Transmitted Shock Mach Number vs Distance, $P_D$ = 114.3 psia.
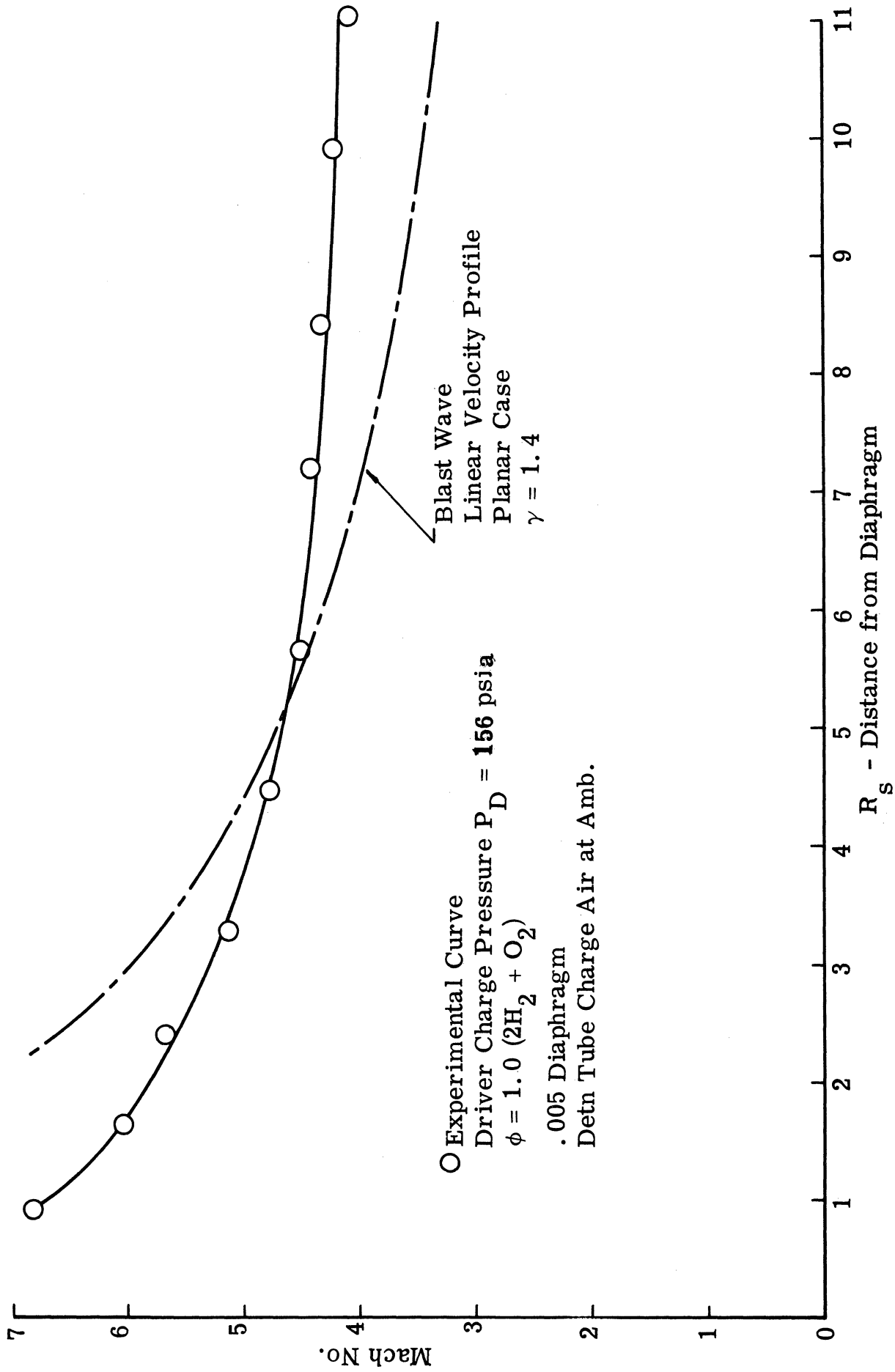
Figure 9.    Transmitted Shock Mach Number vs Distance,  $P_D = 156$  psia.

93

Figure 10.    M vs $R_s/R_o$ .

94
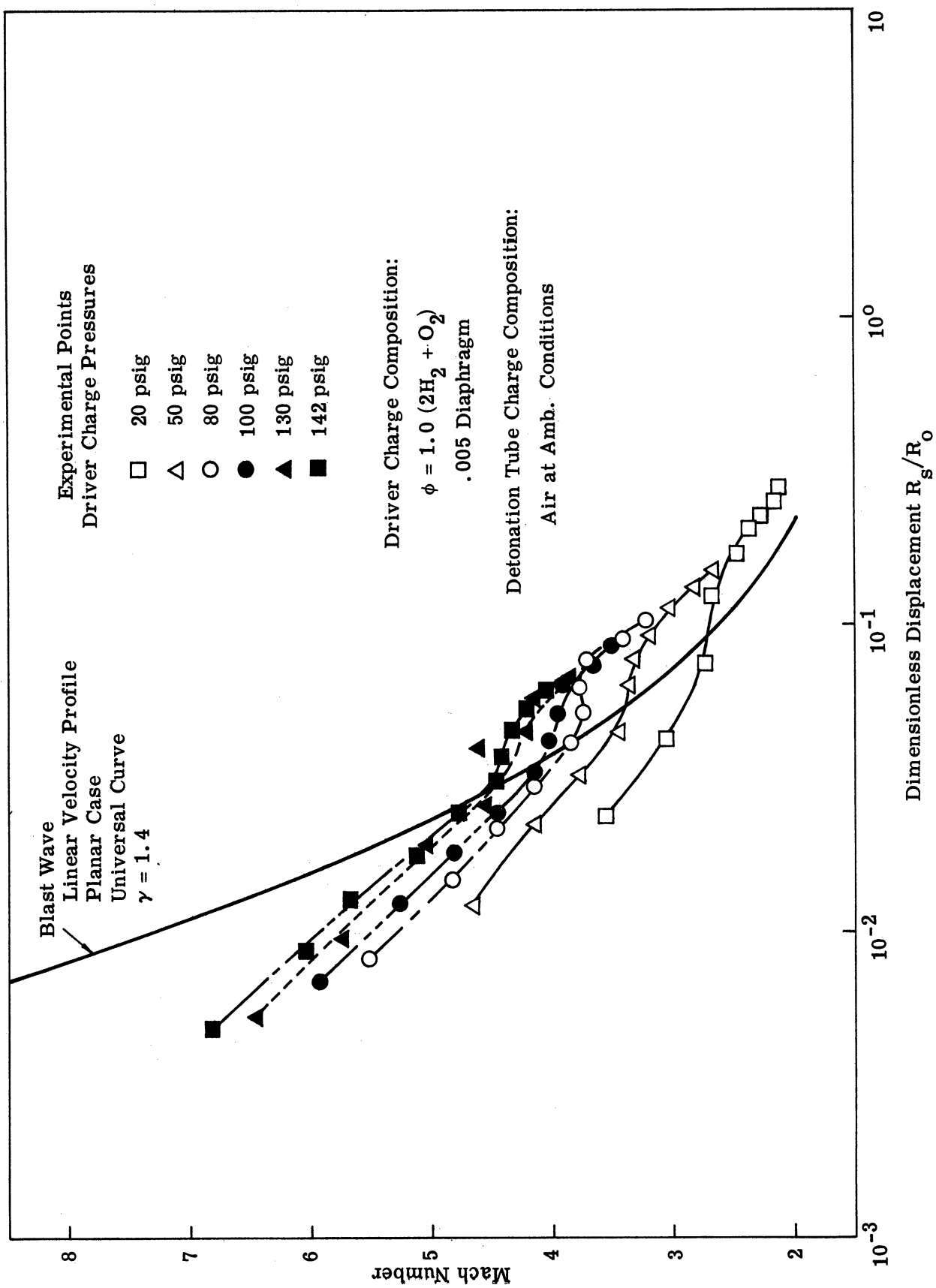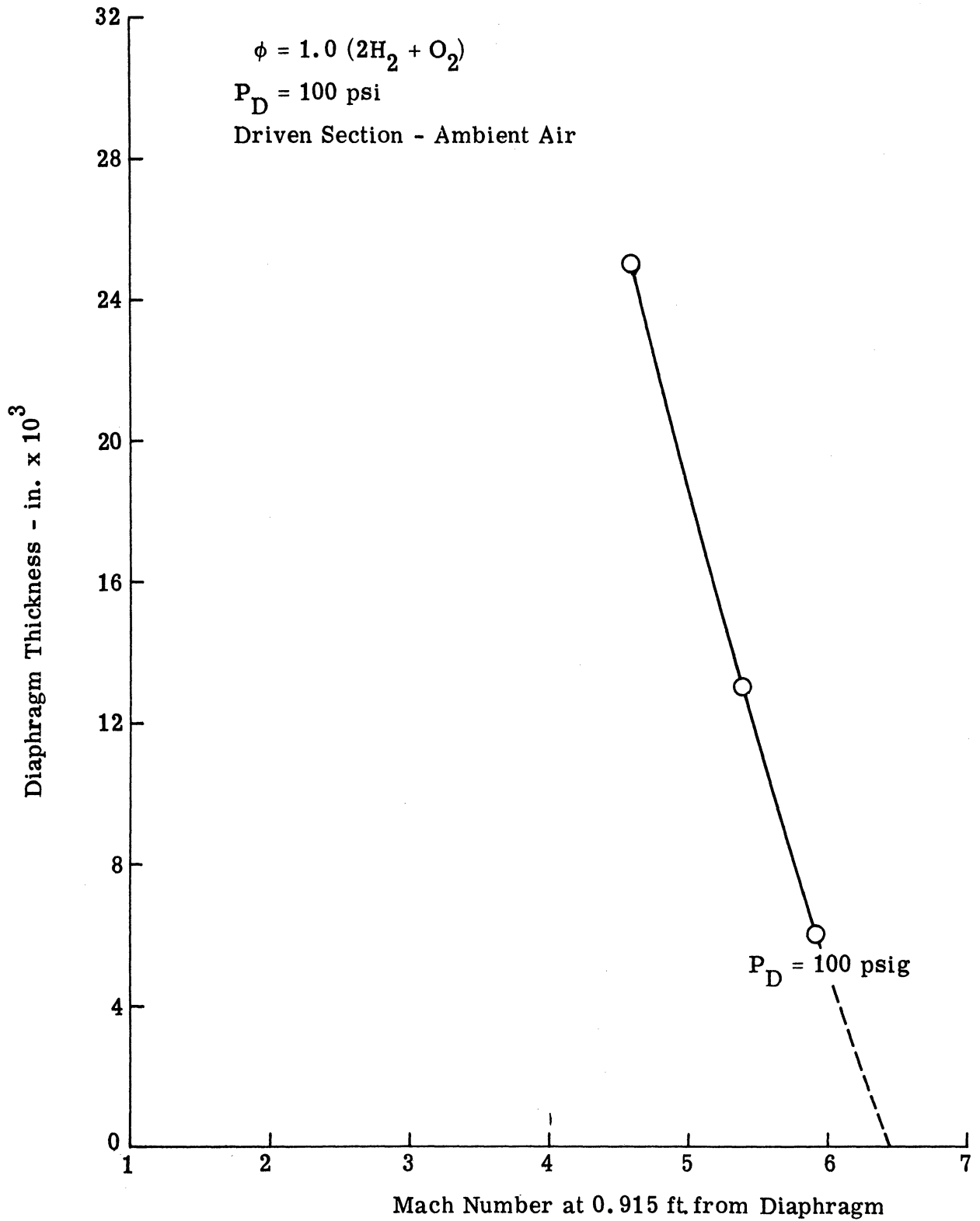
Figure 11.    M at 0.915 ft vs Diaphragm Thickness, $P_D$ = 100 psig.
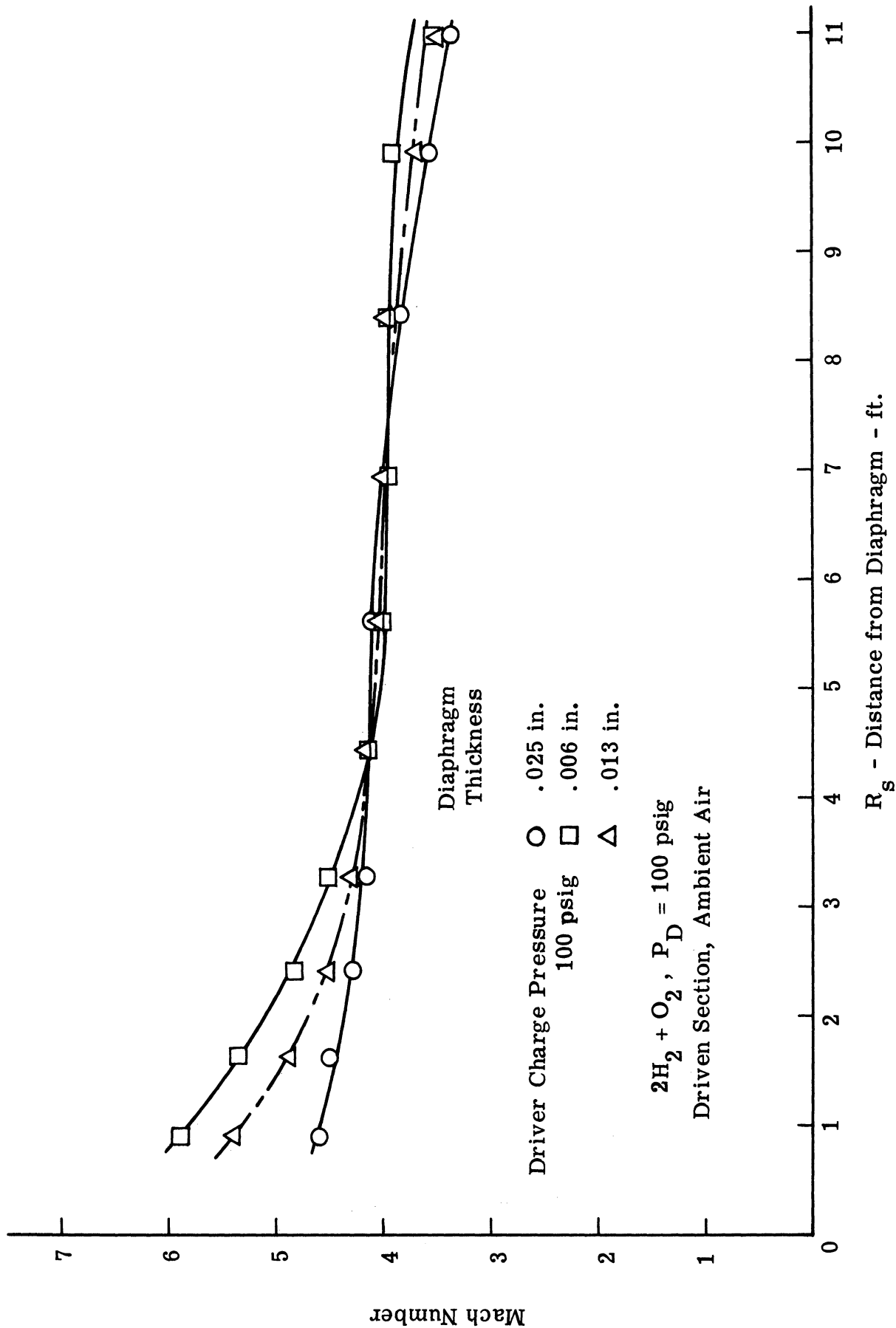
Figure 12. M vs x, $P_D = 100$ psig.
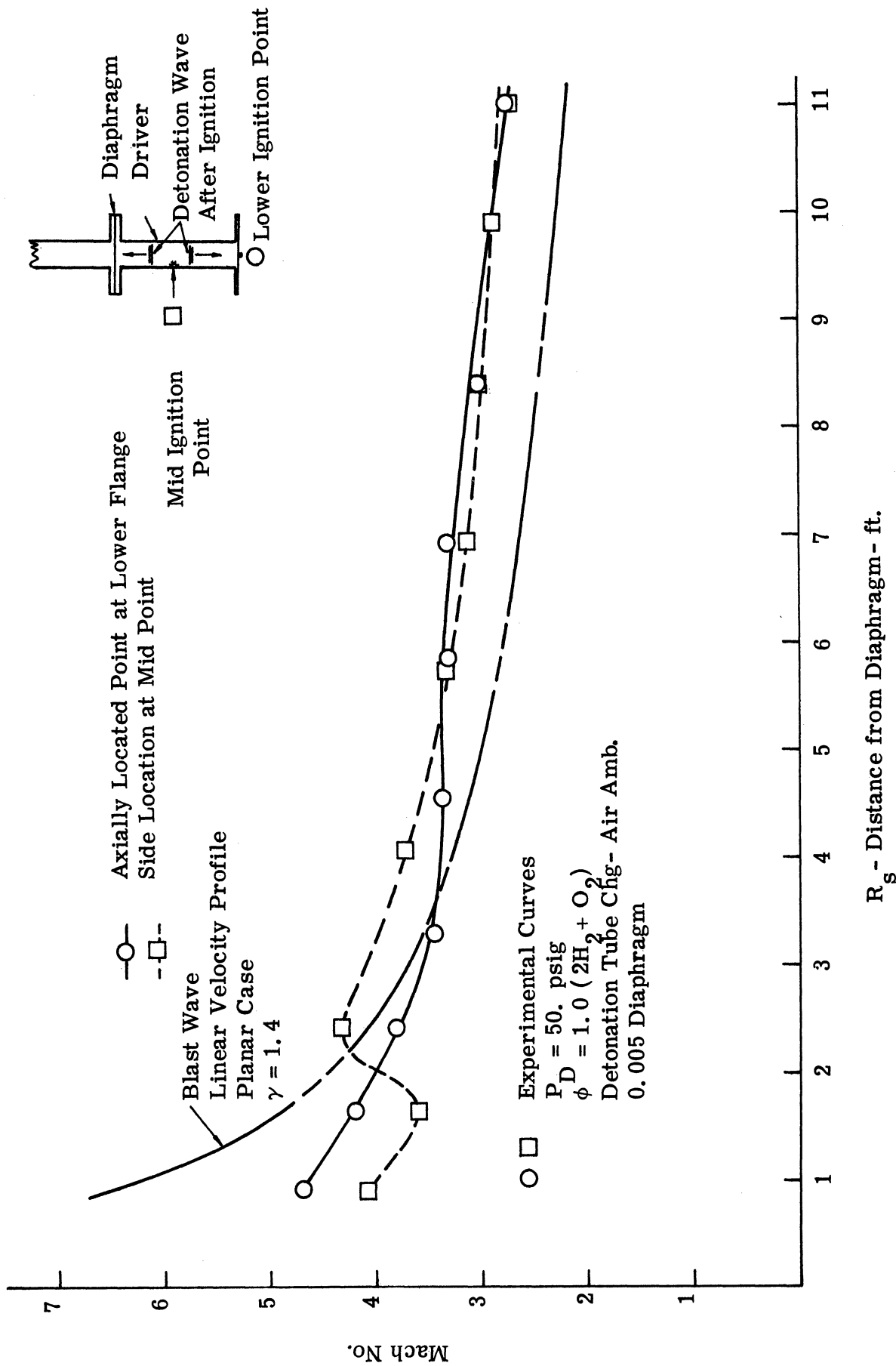
Figure 13.    M vs x - Ignition Point Location, $P_D$ = 50 psig.

$R_s$ - Distance from Diaphragm- ft.

Mach No.

Axially Located Point at Lower Flange
Side Location at Mid Point

Mid Ignition
Point

Blast Wave
Linear Velocity Profile
Planar Case
$\gamma = 1.4$

Experimental Curves
$P_D$ = 50. psig
$\phi = 1.0$ ($2H_2 + O_2$)
Detonation Tube Chg- Air Amb.
0.005 Diaphragm

Diaphragm
Driver
Detonation Wave
After Ignition
Lower Ignition Point
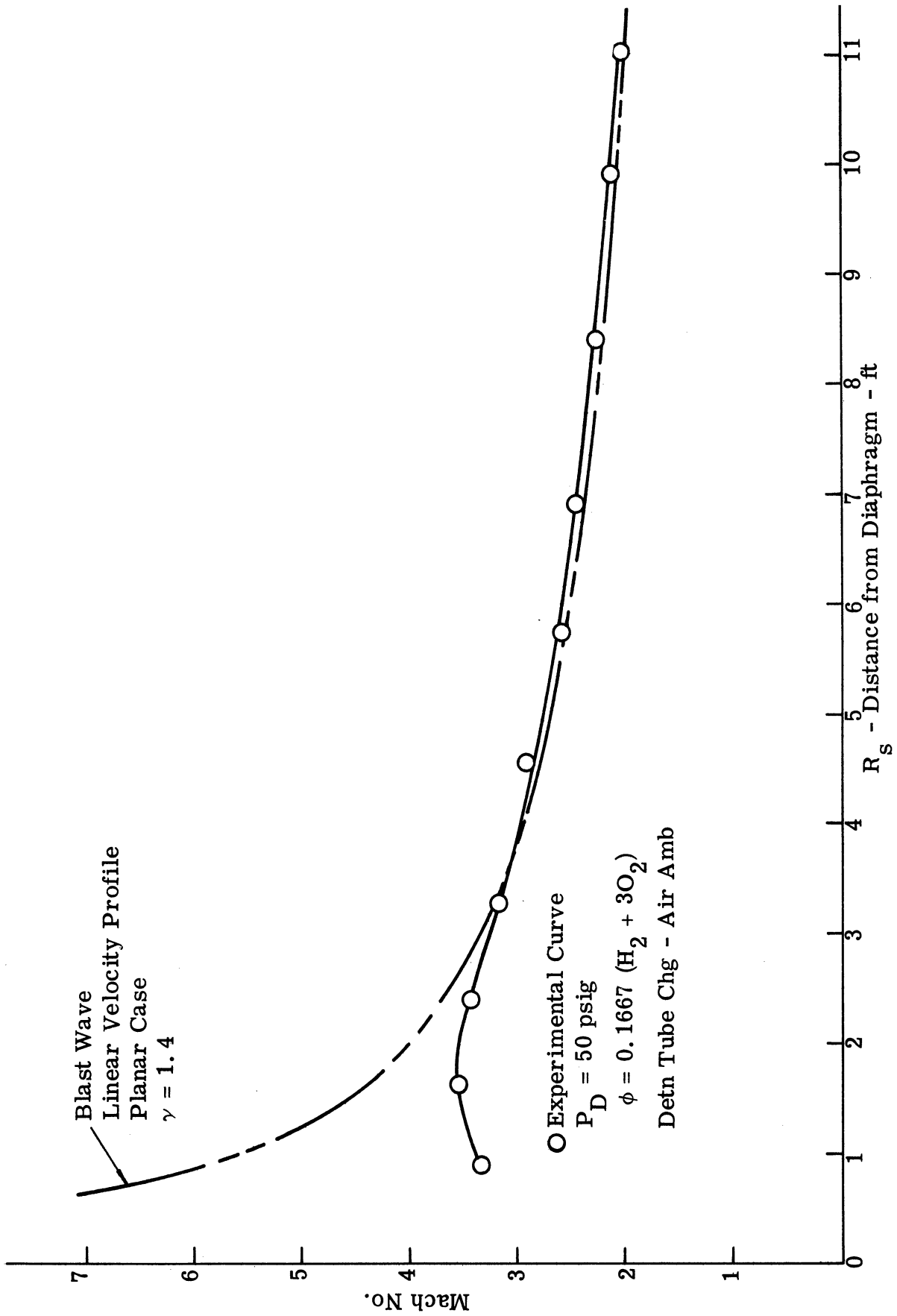
Figure 14.  M vs x - Lean Driver, $P_D$ = 50 psig.

98
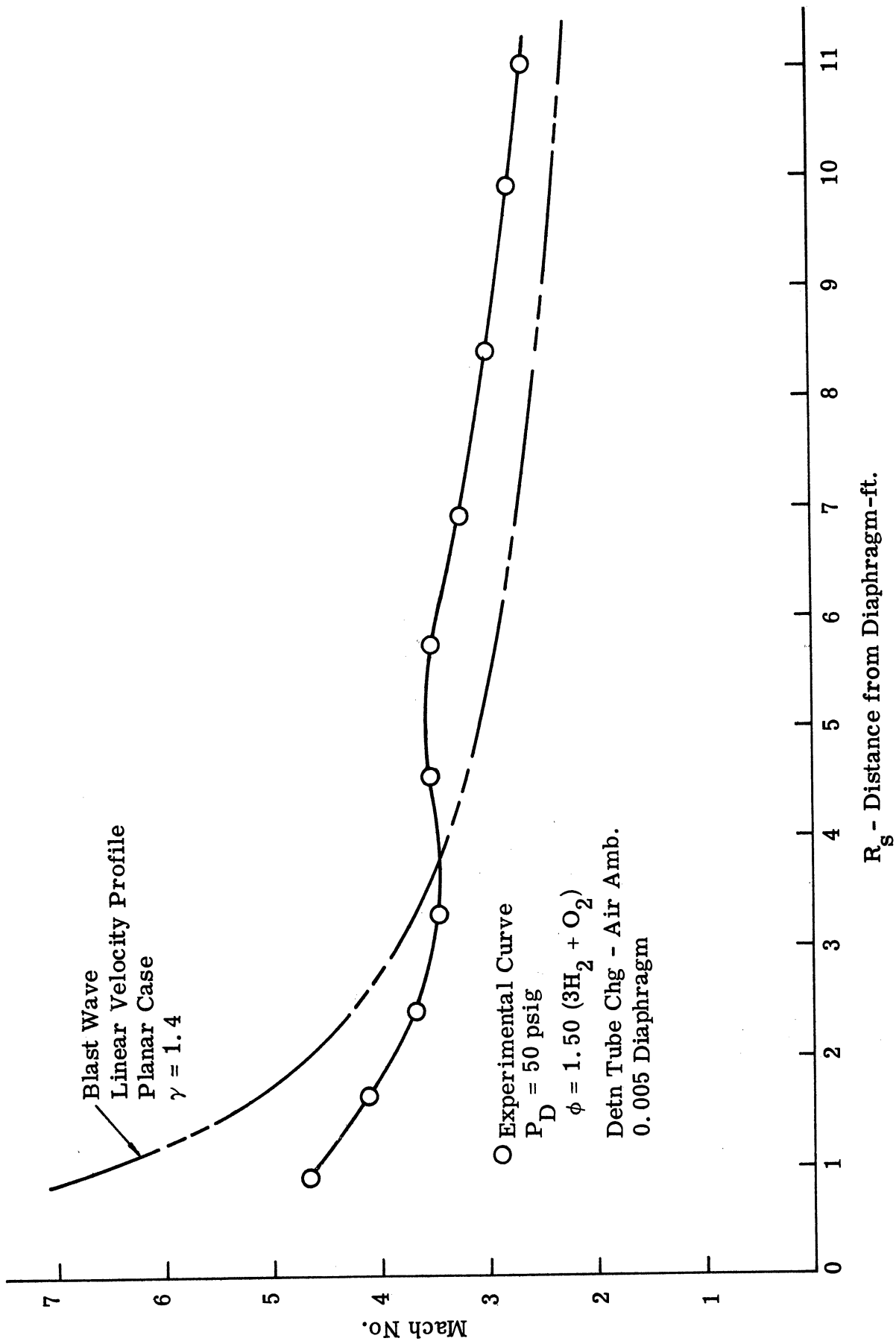
Figure 15.    M vs x - Rich Driver.

Figure 16.    M vs x - Rich Driver.

○ 0.915 ft from Diaphragm
□ Test Section 5.4 ft from Diaphragm
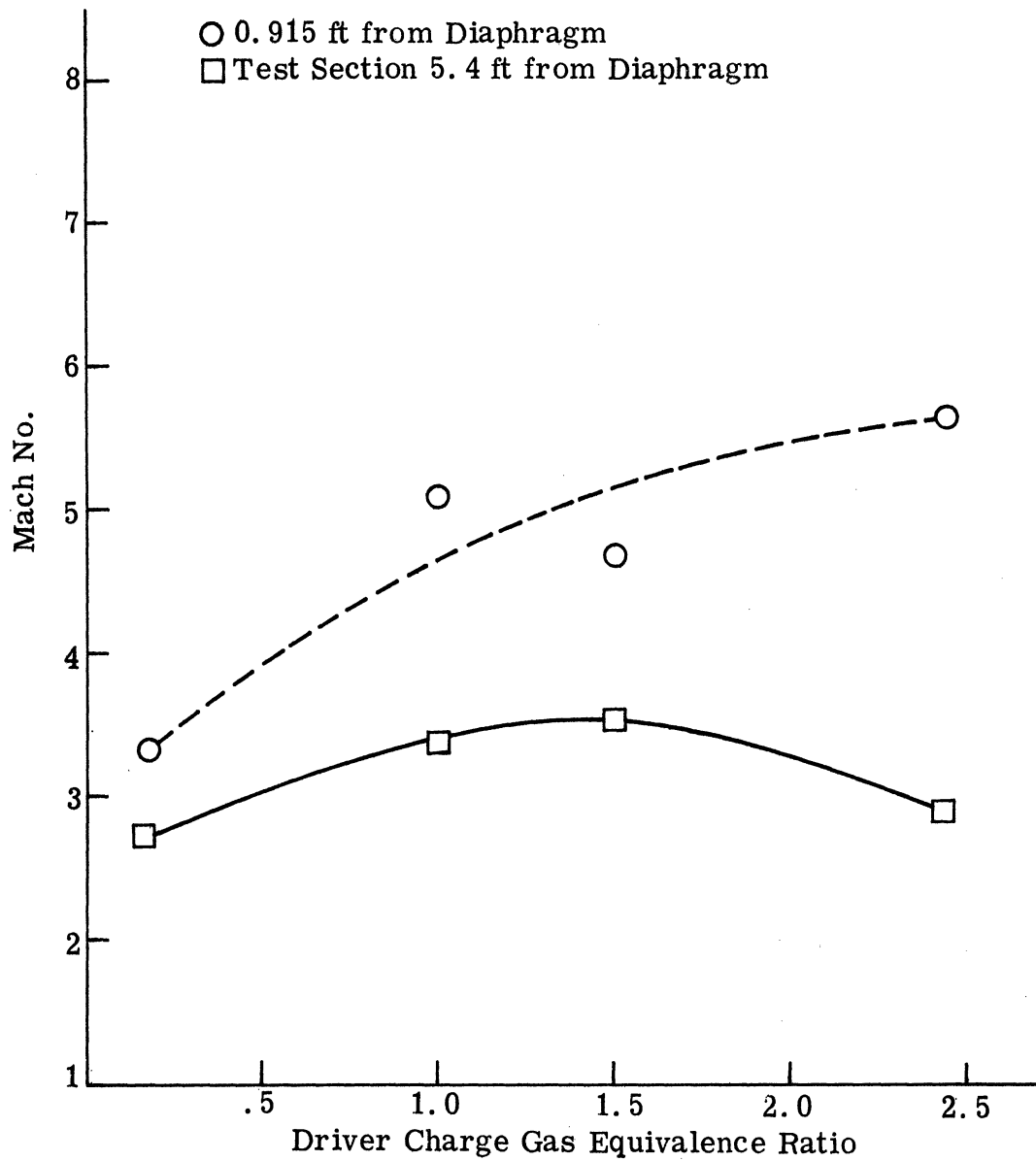
Figure 17.    M vs $\phi$ of Driver.

Figure 18.  M vs x – Effect of $\omega_s$.
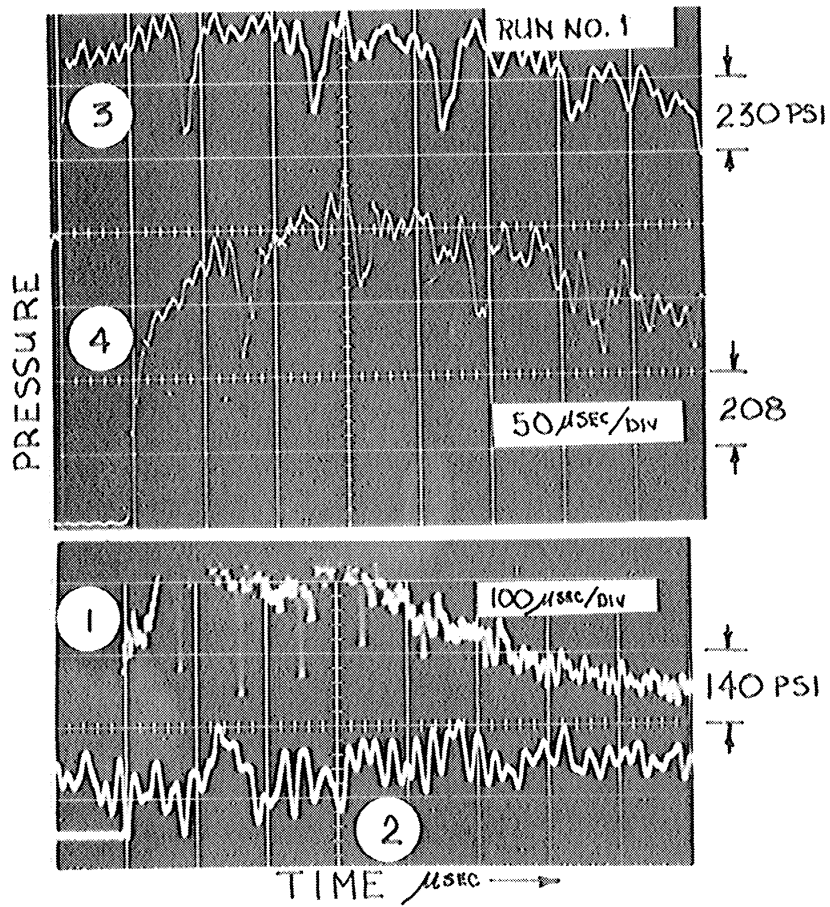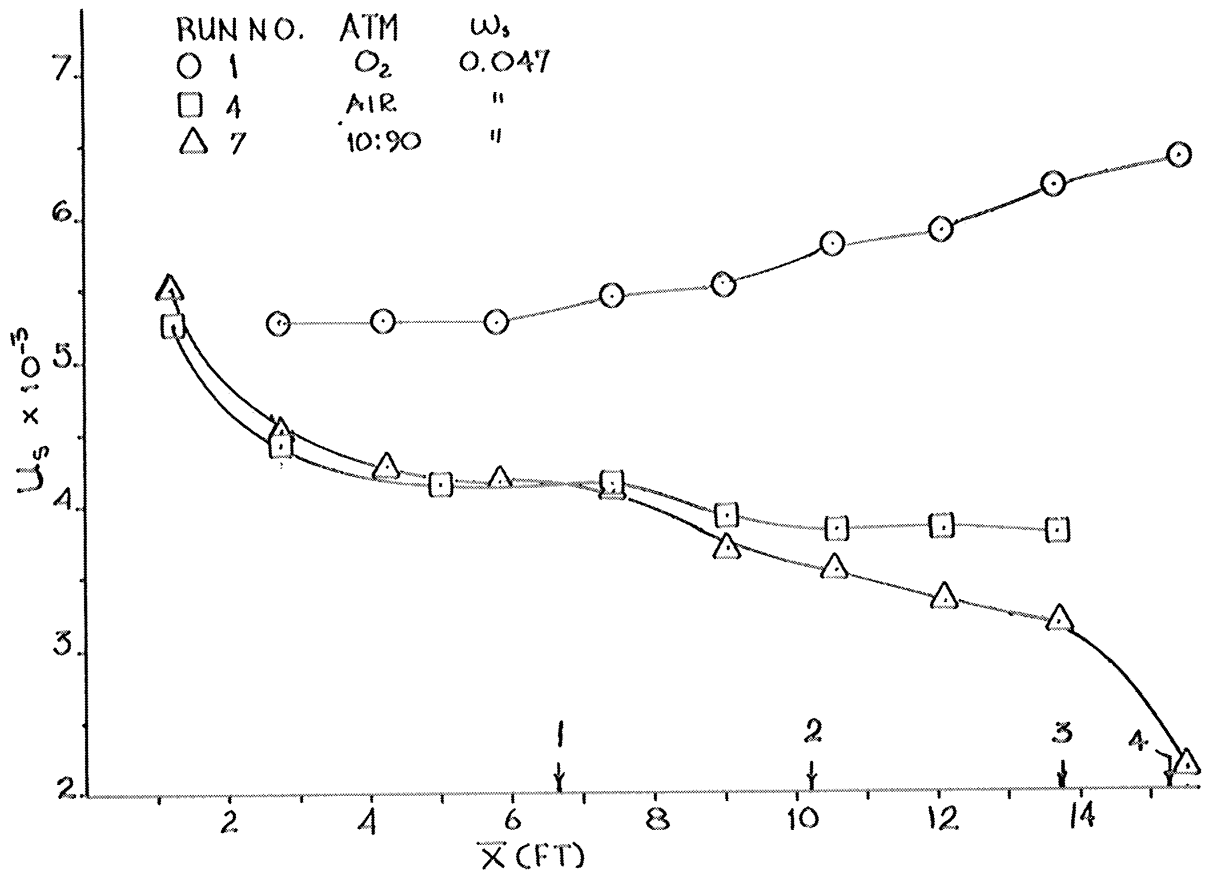
Figure 19.    Velocity and Pressure Results for Propyl Nitrate- Runs 1, 4, and 7.

103
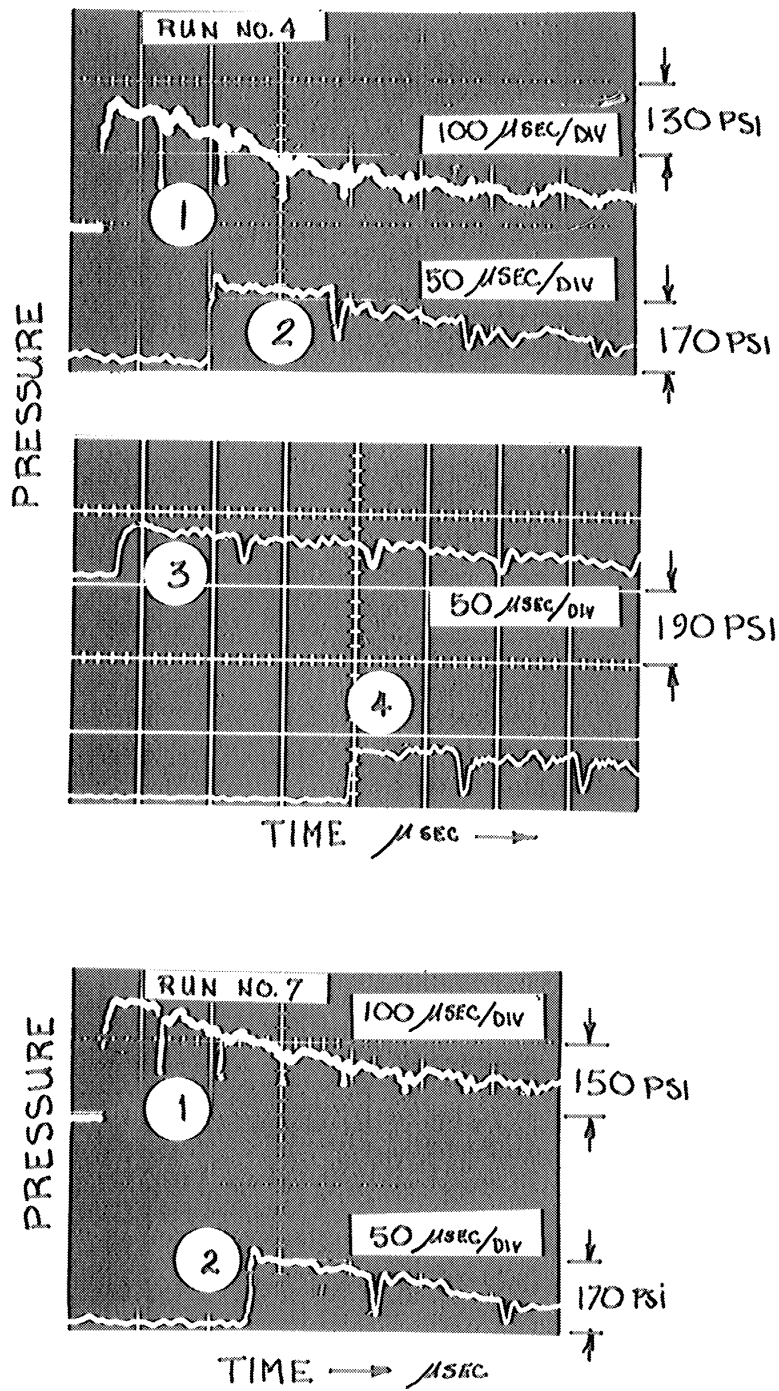
Figure 19.    (Continued) Velocity and Pressure Results for Propyl Nitrate--
Runs 1,  4,  and 7.

104
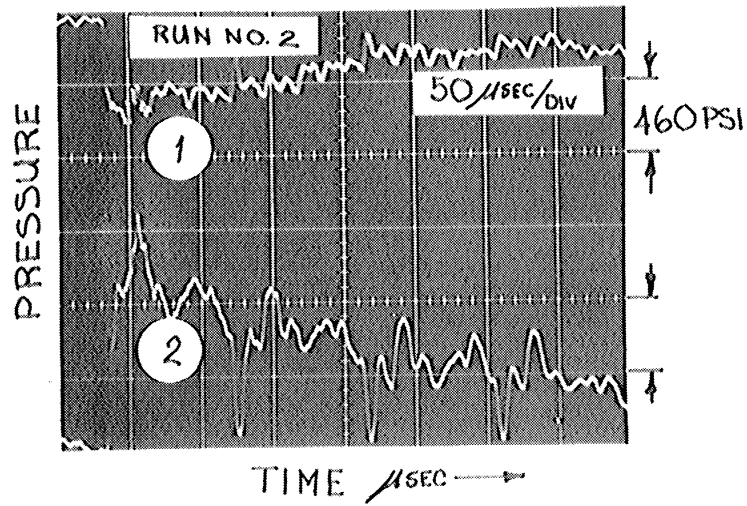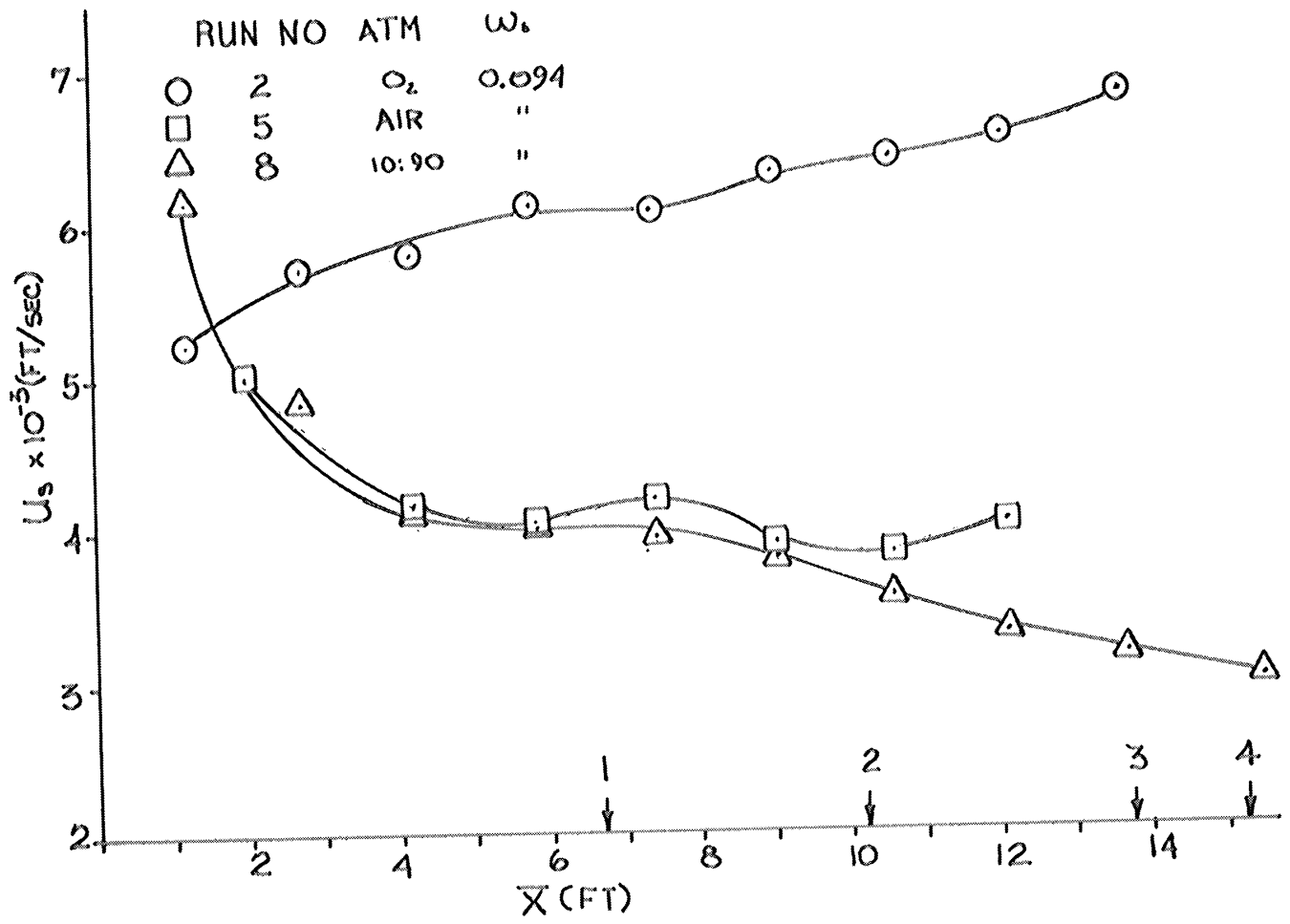
Figure 20.    Velocity and Pressure Results for Propyl Nitrate-Runs 2, 5, and 8.
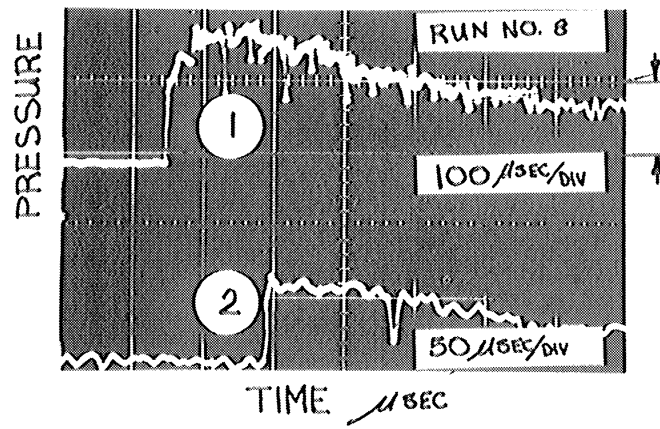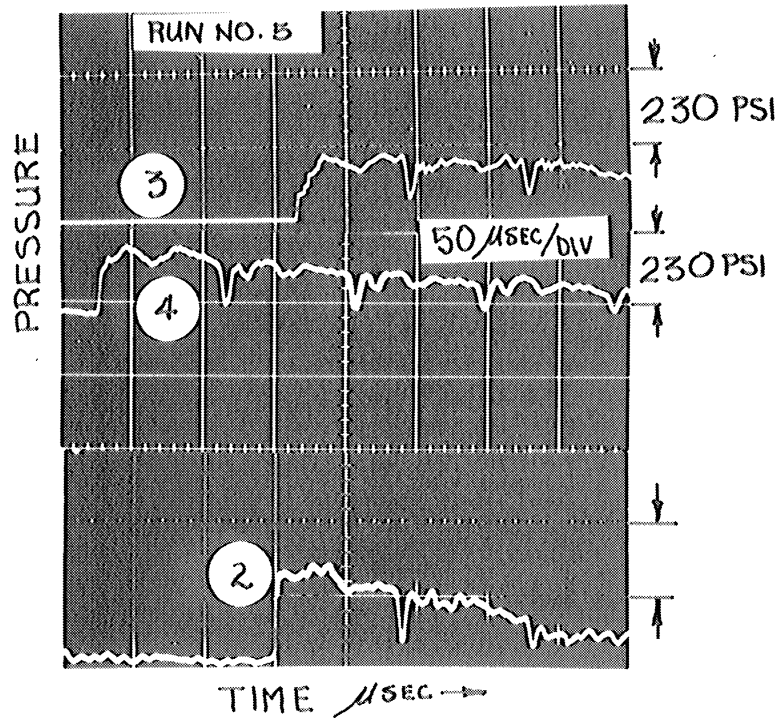
Figure 20.    (Continued) Velocity and Pressure Results for Propyl Nitrate-
Runs 2, 5, and 8.
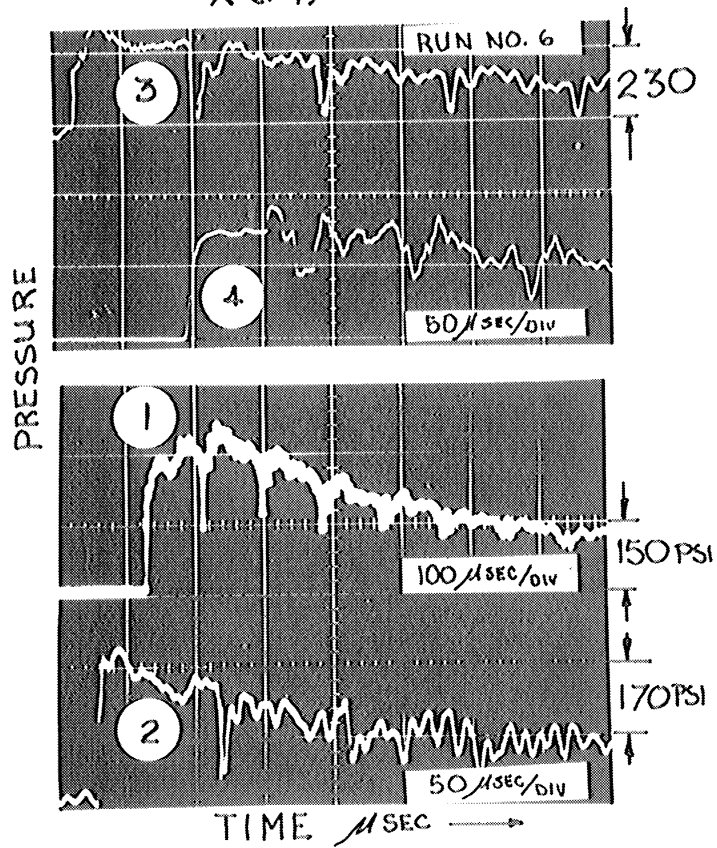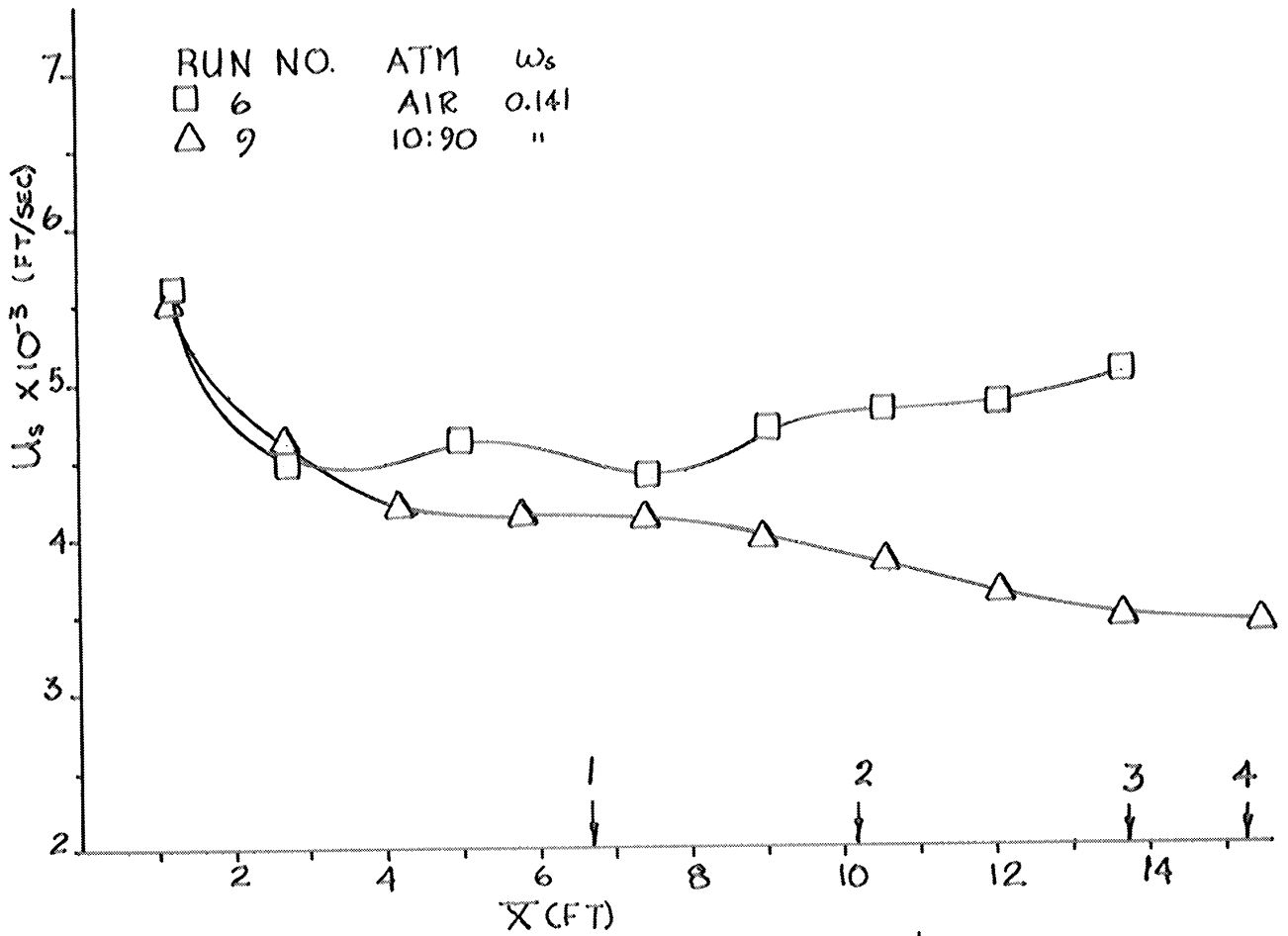
Figure 21. Velocity and Pressure Results for Propyl Nitrate- Runs 6 and 9.
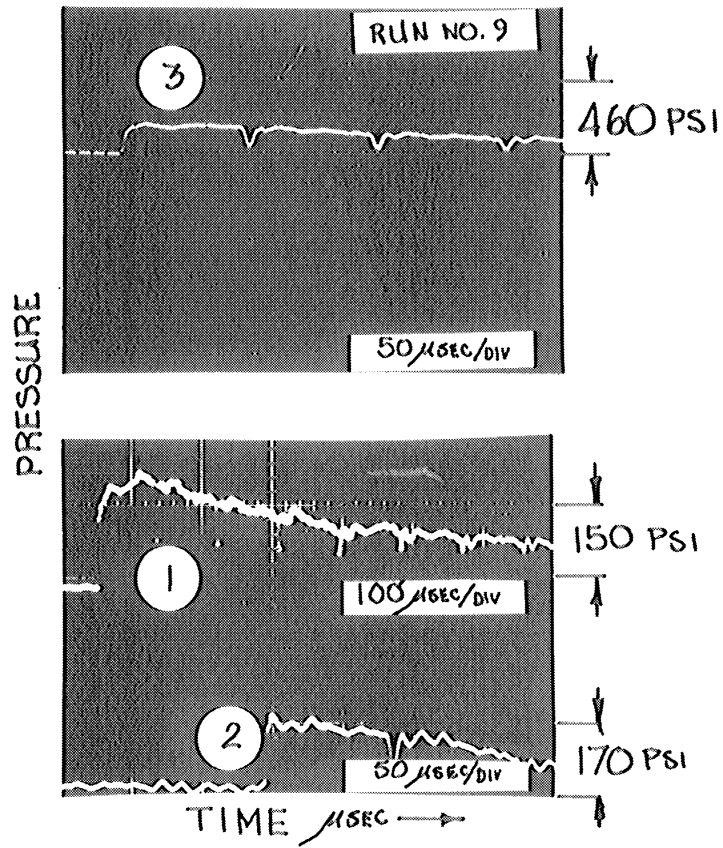
Figure 21.     (Continued) Velocity and Pressure Results for Propyl Nitrate-
Runs 6 and 9.
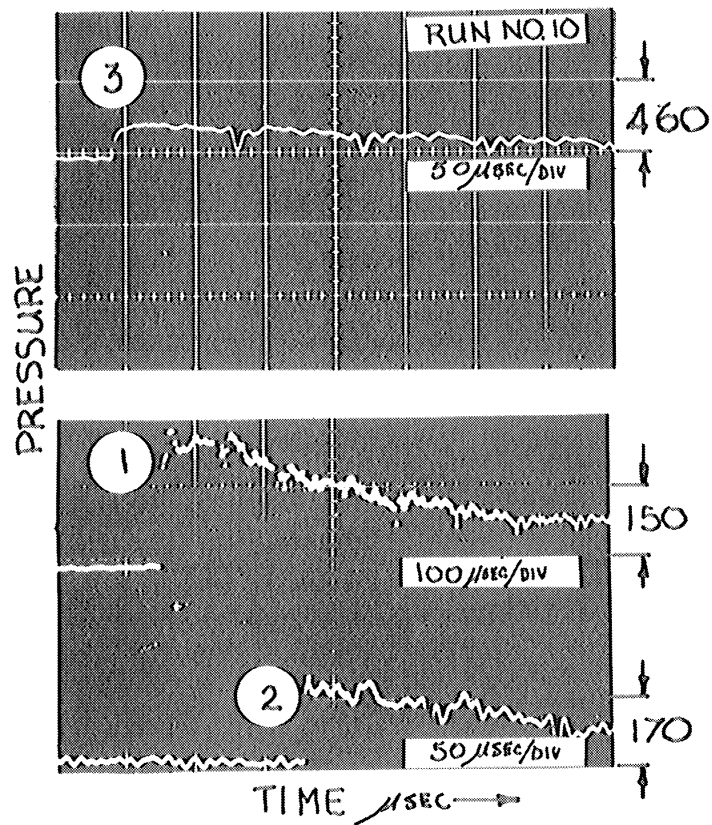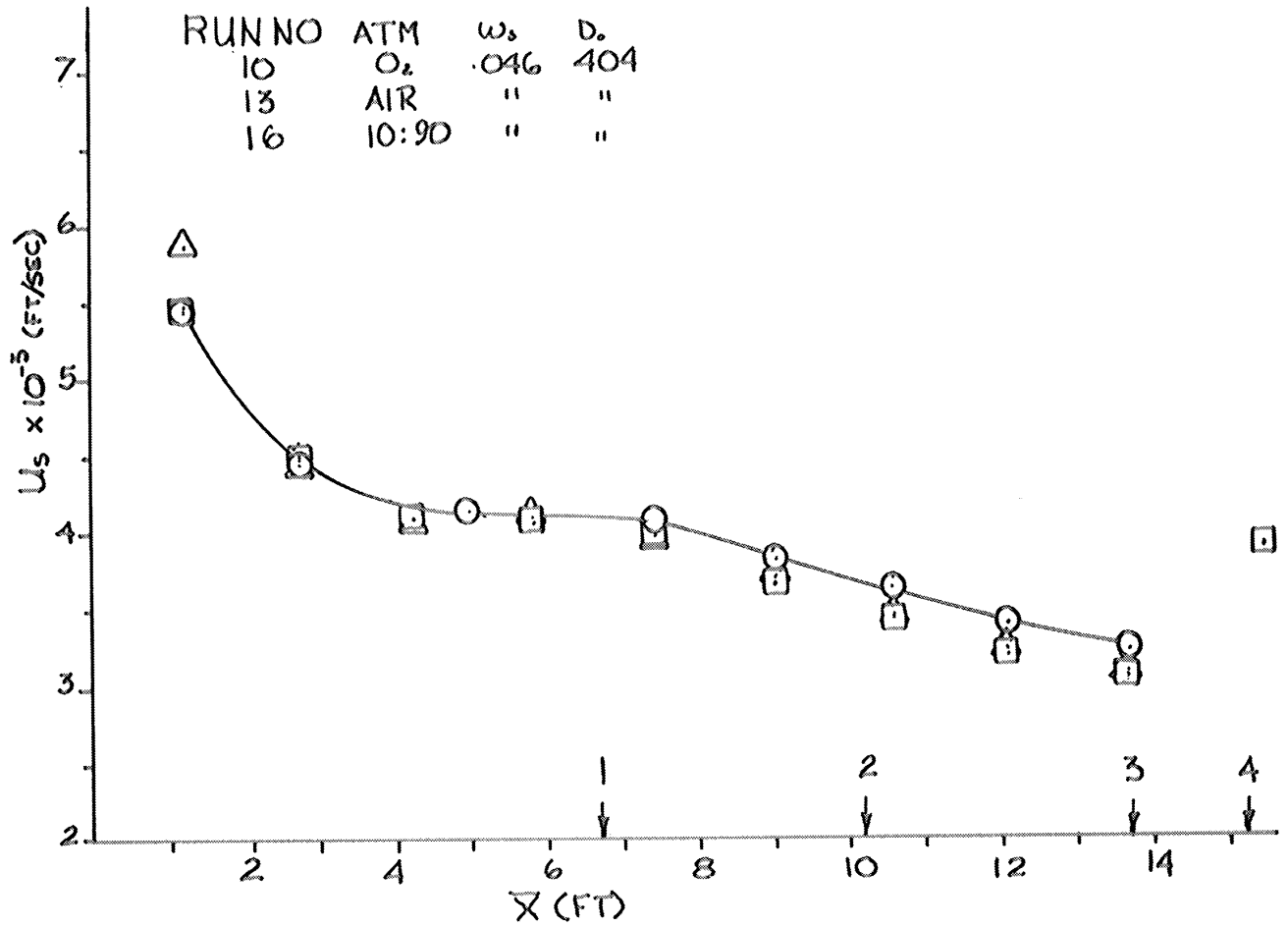
Figure 22.    Velocity and Pressure Results for Propyl Nitrate – Runs 10, 13 and 16.

109
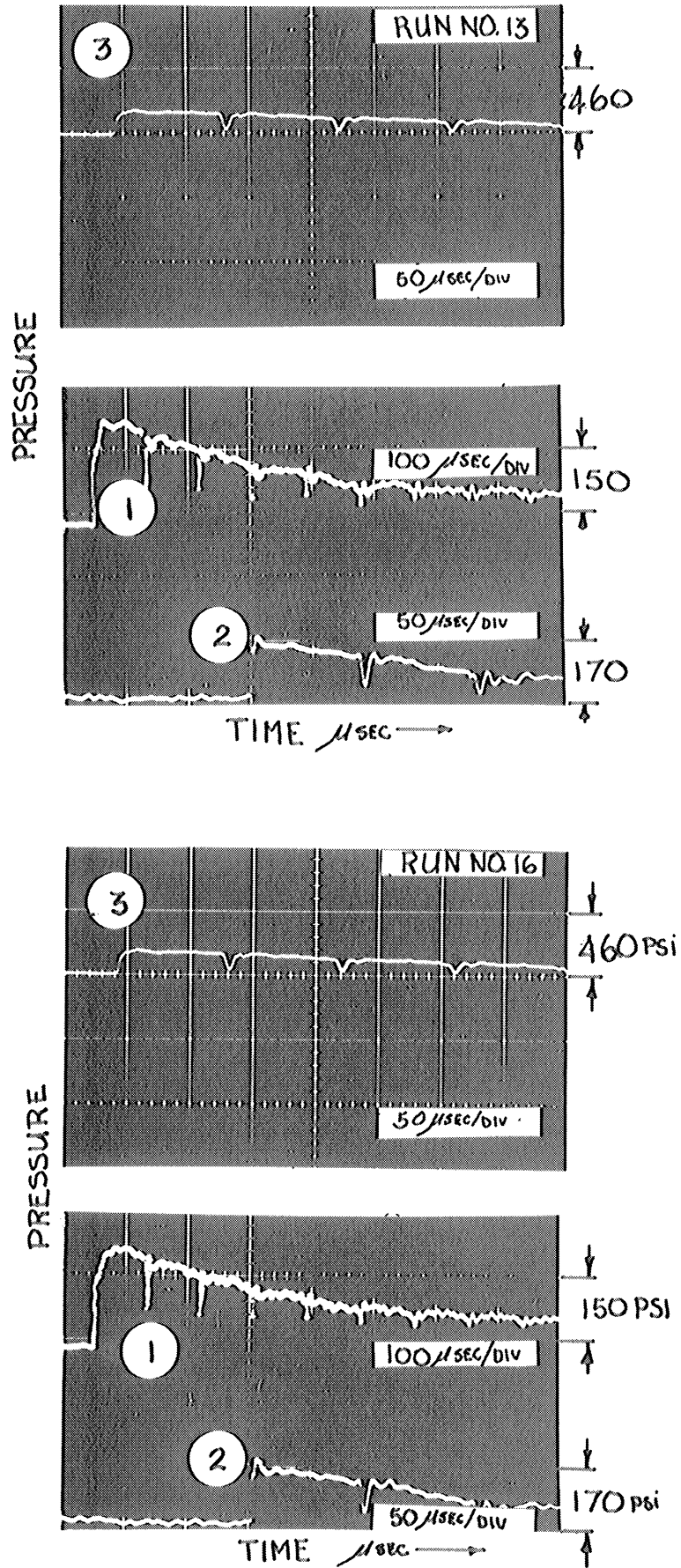
Figure 22.    (Continued) Velocity and Pressure Results for Propyl Nitrate-
Runs 10, 13, and 16.
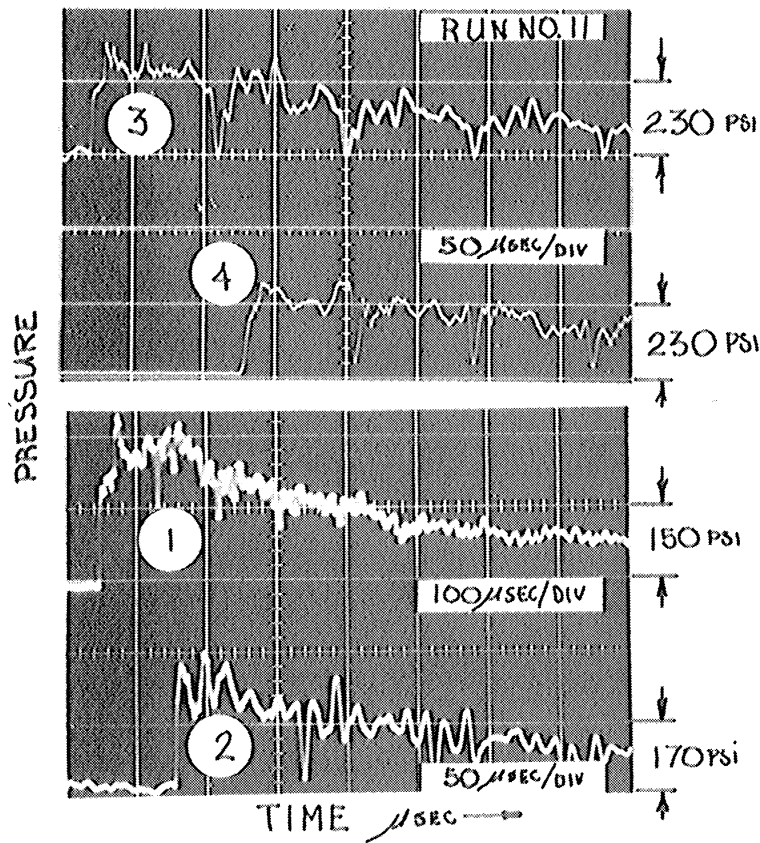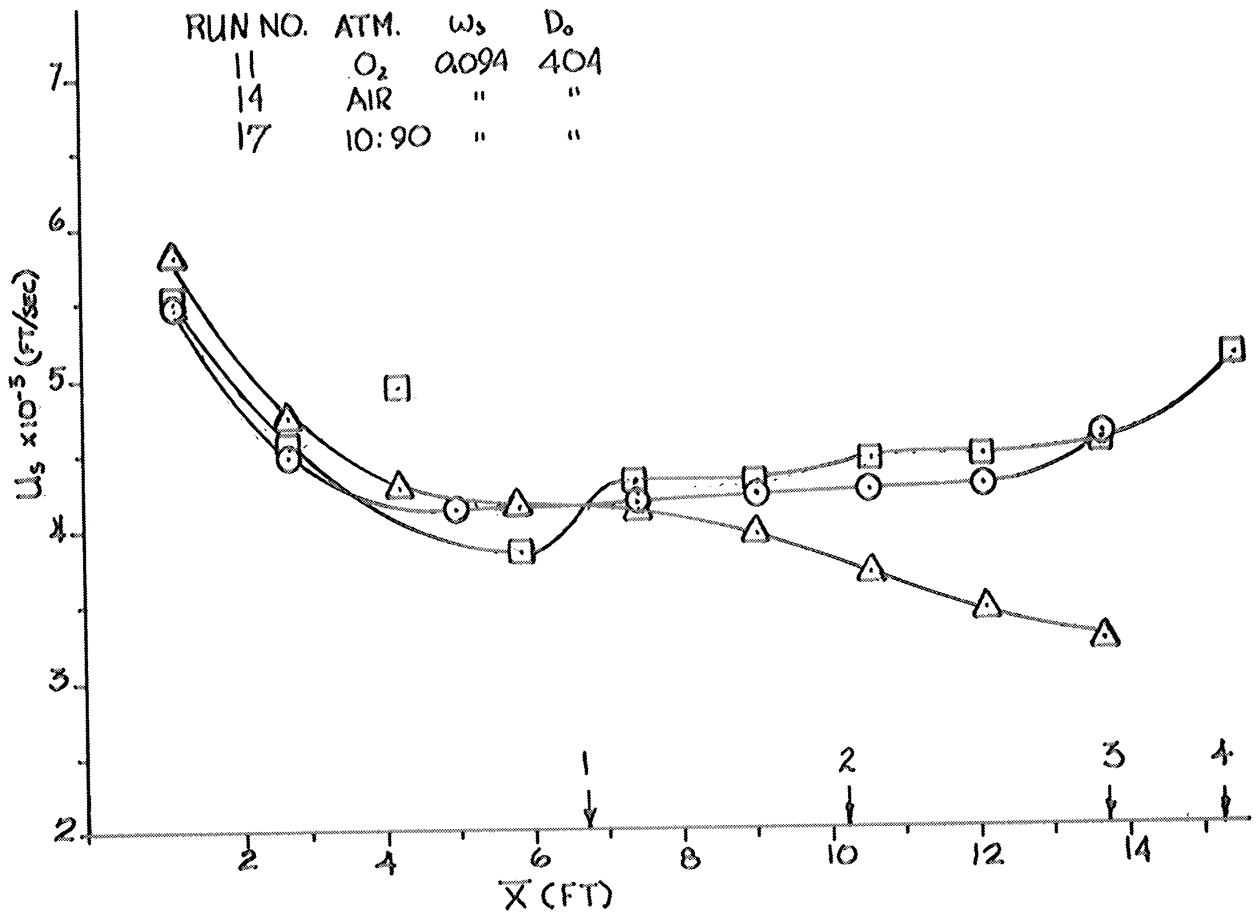
Figure 23.    Velocity and Pressure Results for Propyl Nitrate- Runs 11, 14, and 17.

111
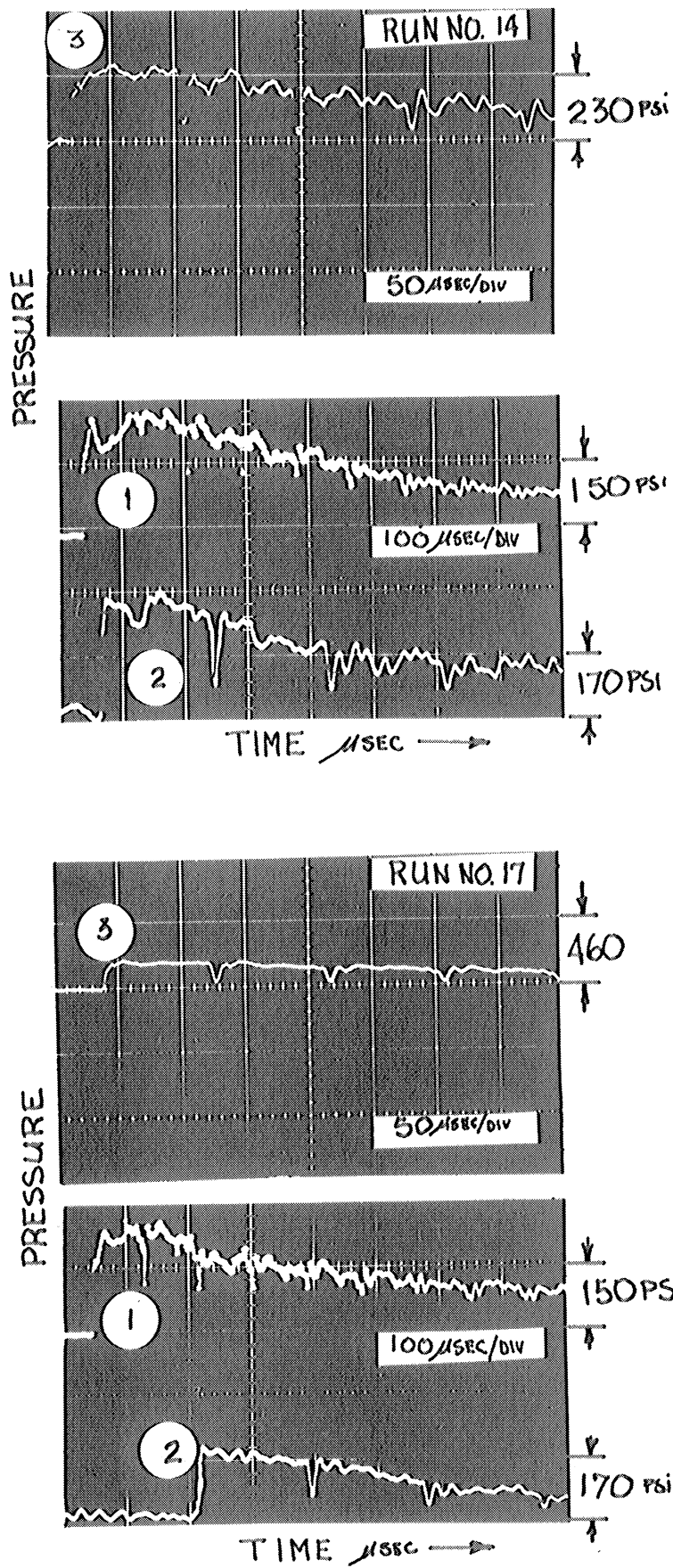
Figure 23.    (Continued) Velocity and Pressure Results for Propyl Nitrate-
Runs 11, 14, and 17.
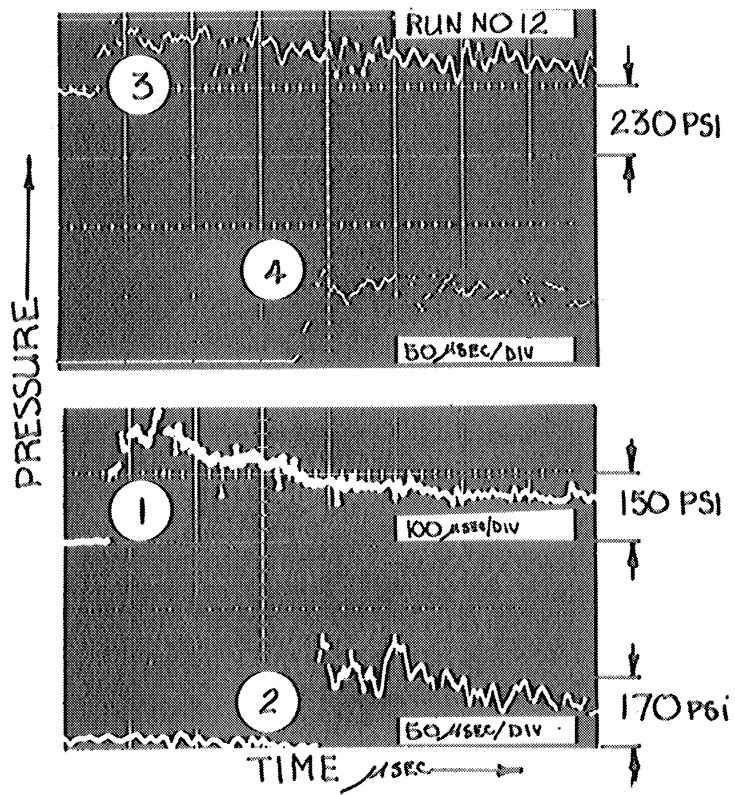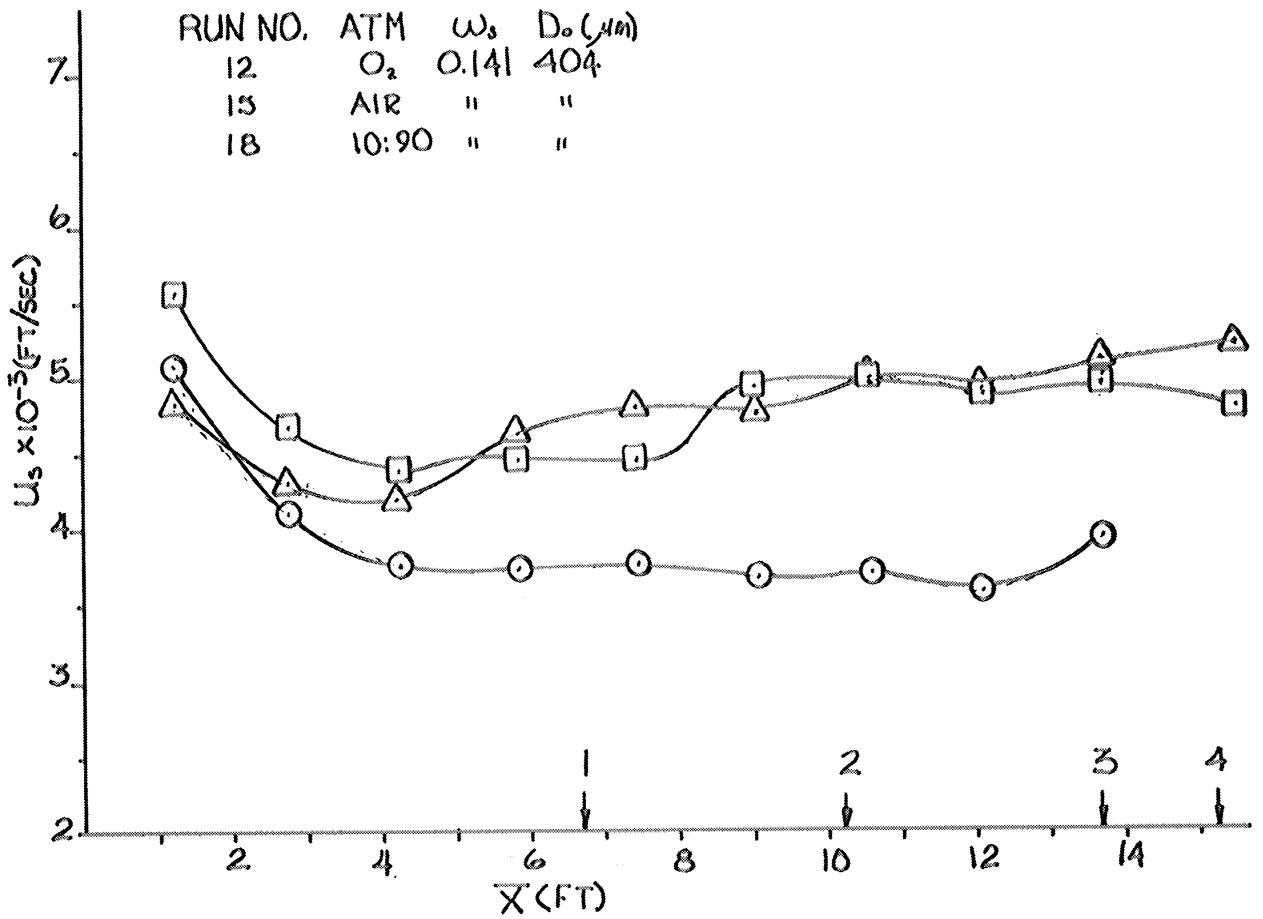
Figure 24.     Velocity and Pressure Results for Propyl Nitrate-- Runs 12, 15, and 18.
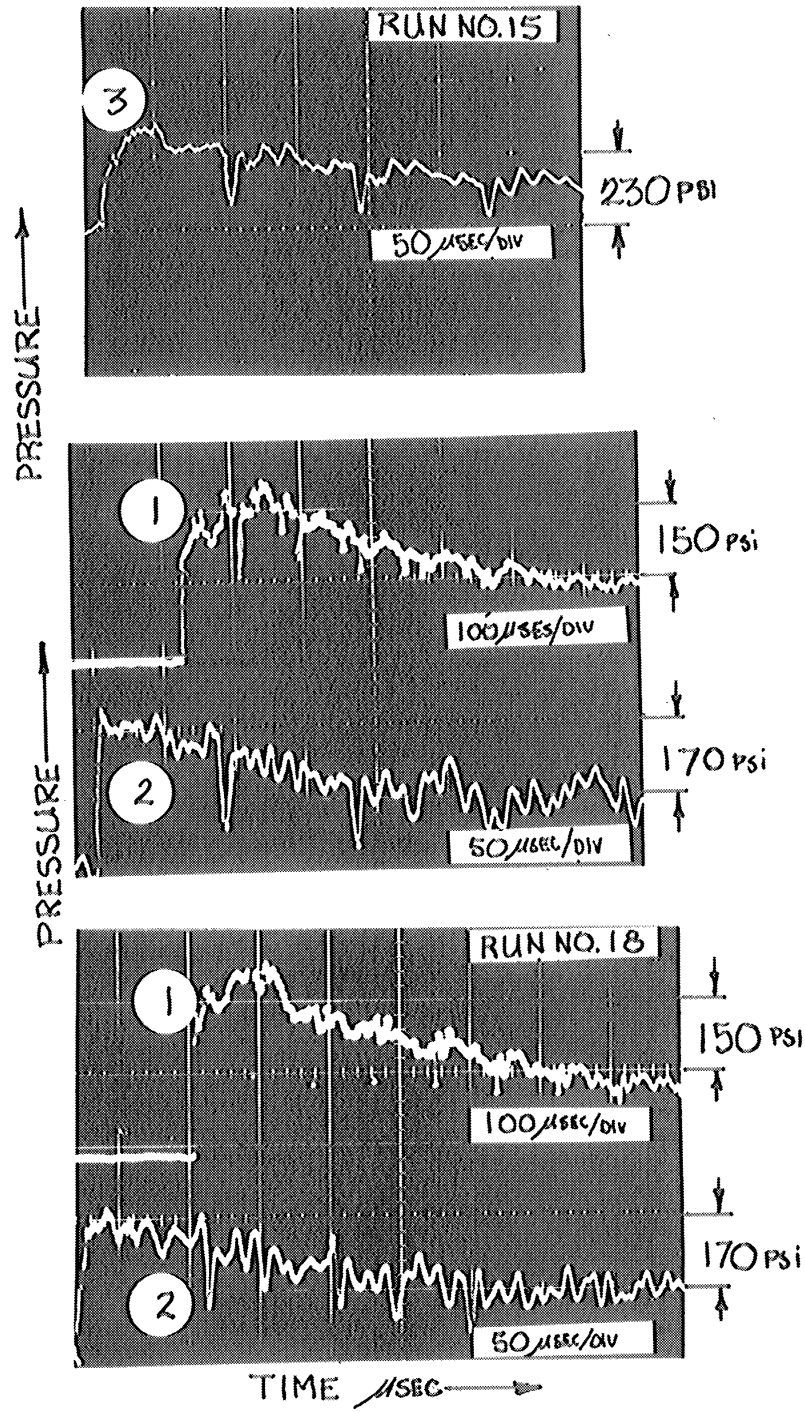
Figure 24.    (Continued) Velocity and Pressure Results for Propyl Nitrate-
Runs 12, 15, and 18.

114
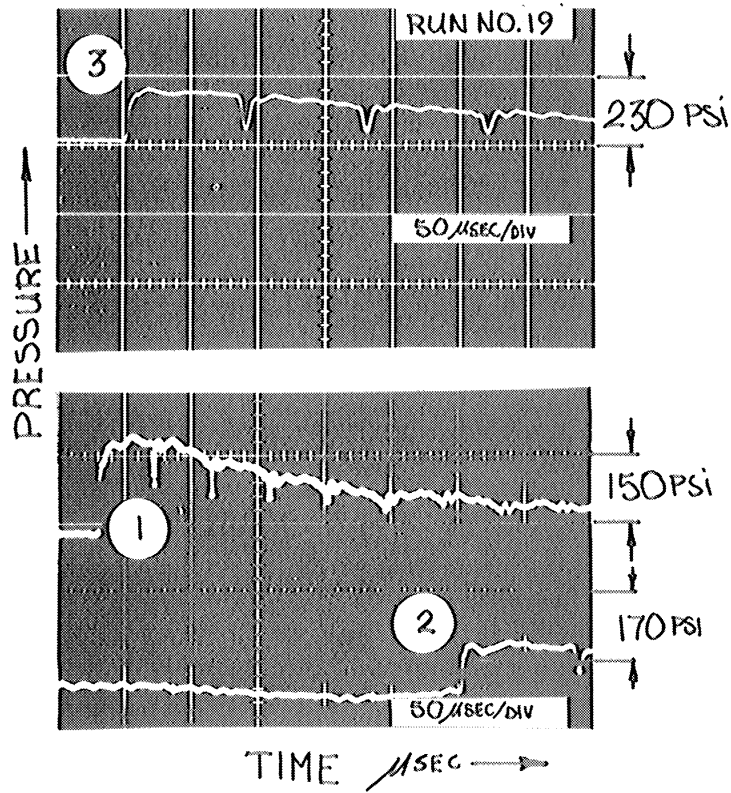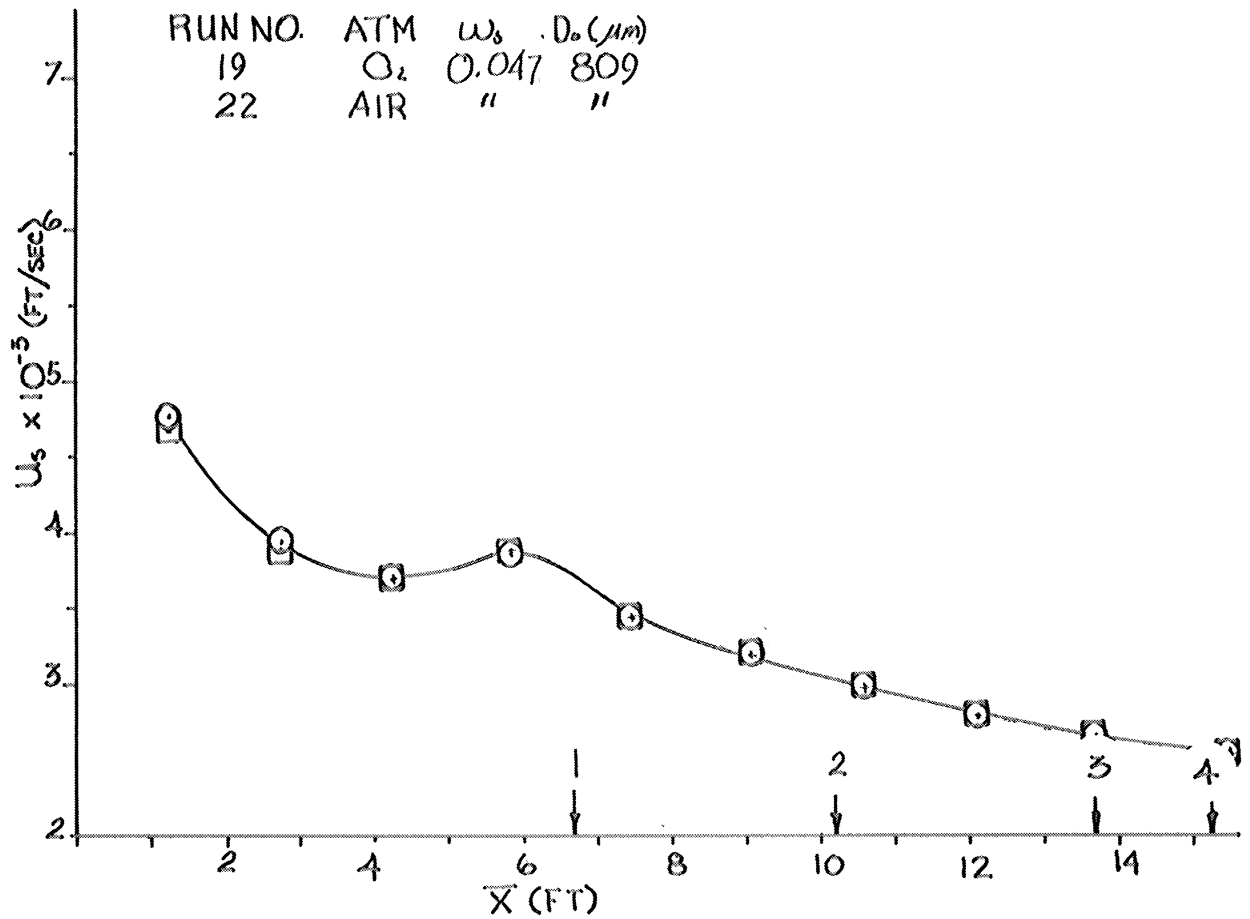
Figure 25.    Velocity and Pressure Results for Nitropropane- Runs 19 and 22.
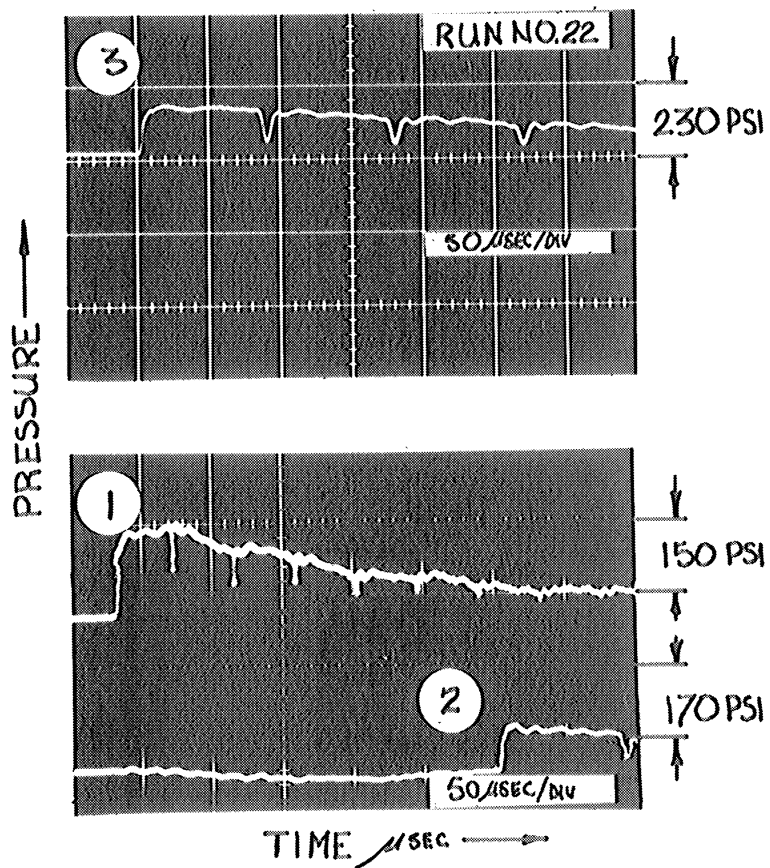
Figure 25.    (Continued) Velocity and Pressure Results for Nitropropane-
Runs 19 and 22.
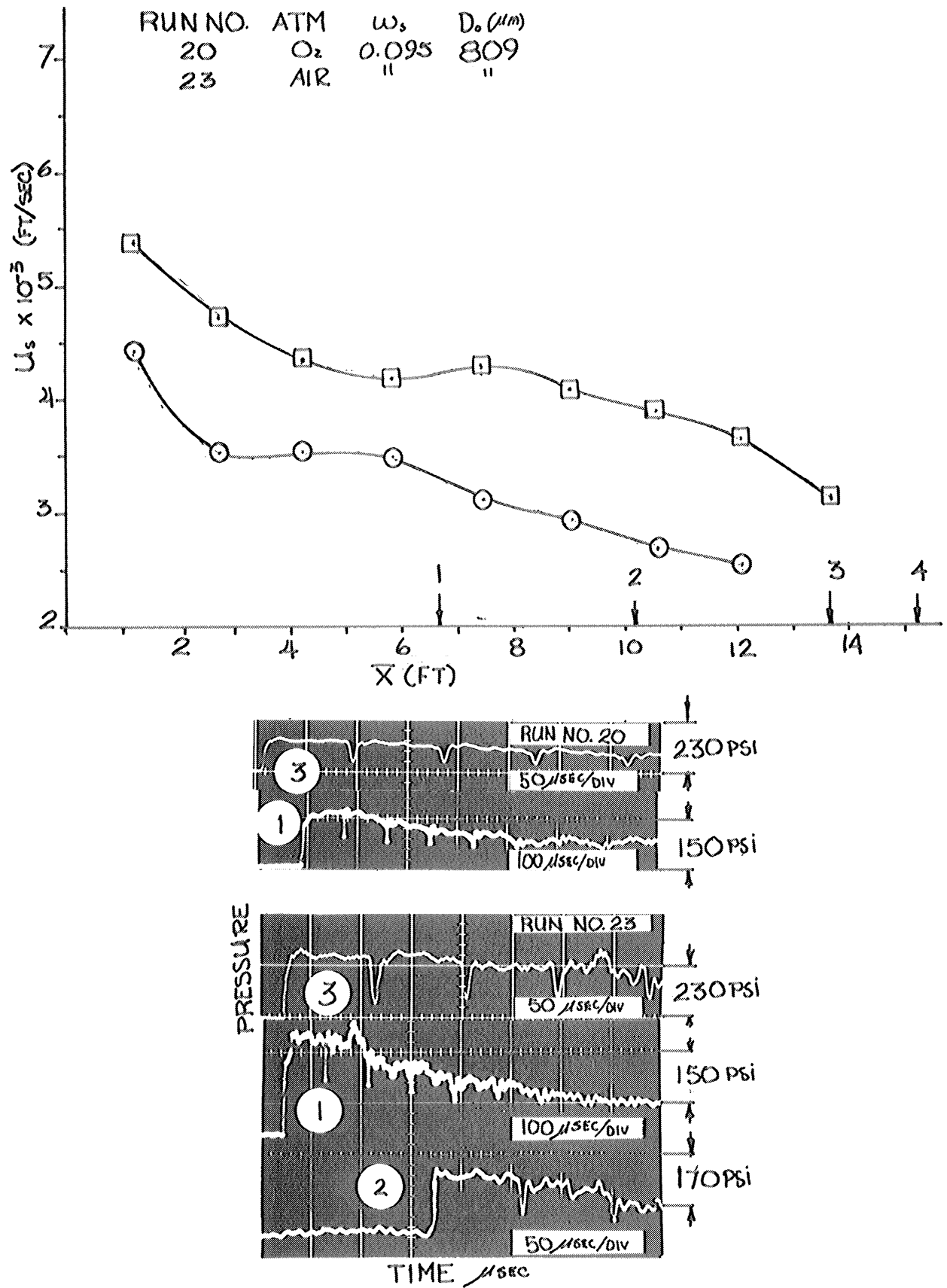
Figure 26. Velocity and Pressure Results for Nitropropane-- Runs 20 and 23.
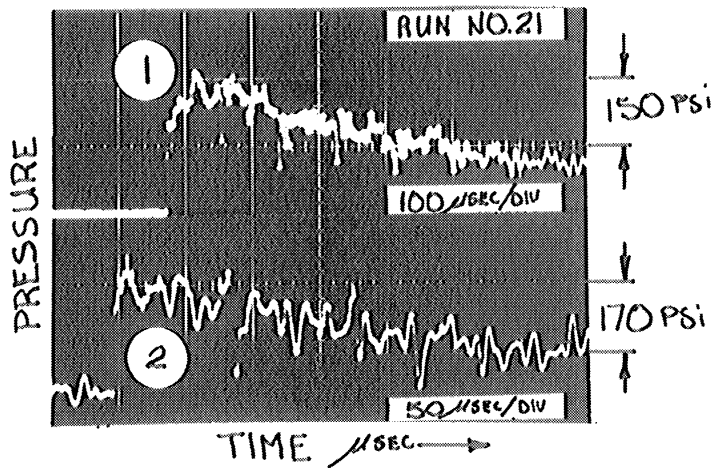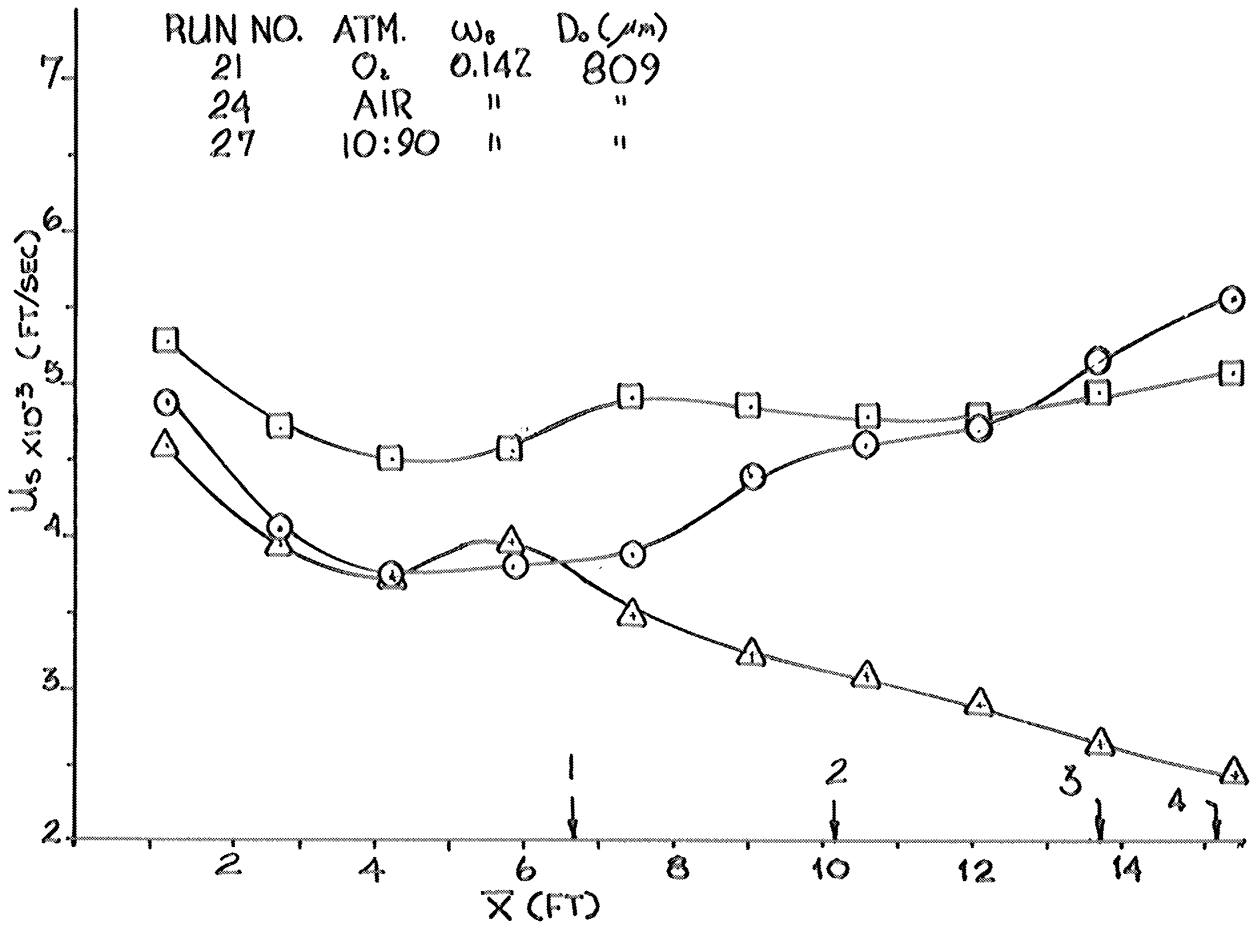
Figure 27.    Velocity and Pressure Results for Nitropropane- Runs 21, 24, and 27.

118
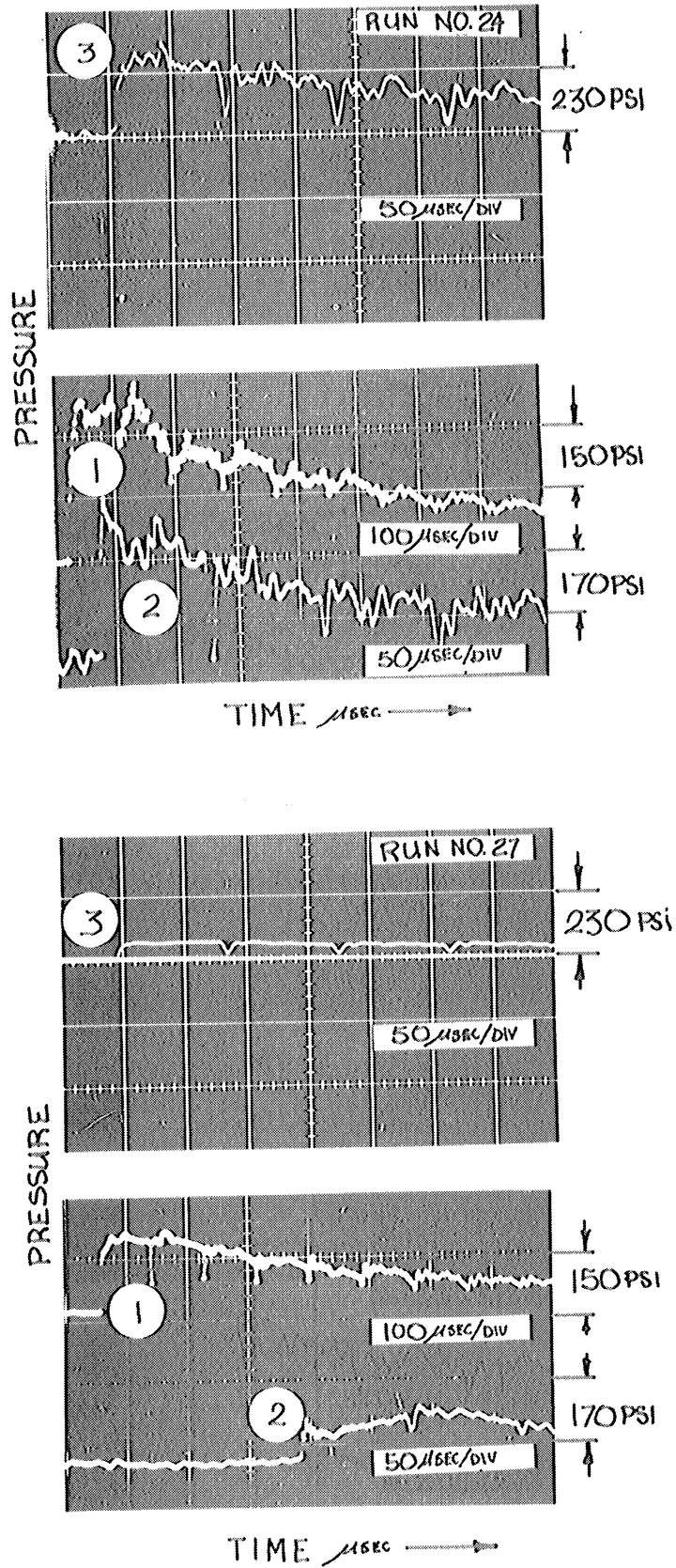
Figure 27.  (Continued) Velocity and Pressure Results for Nitropropane--
Runs 21, 24, and 27.

119
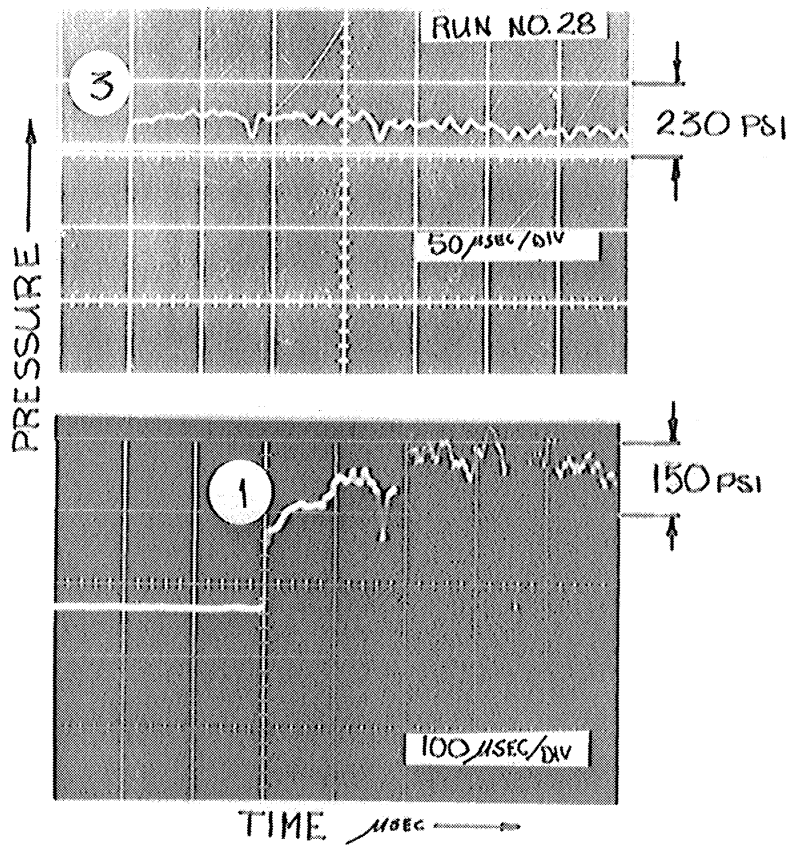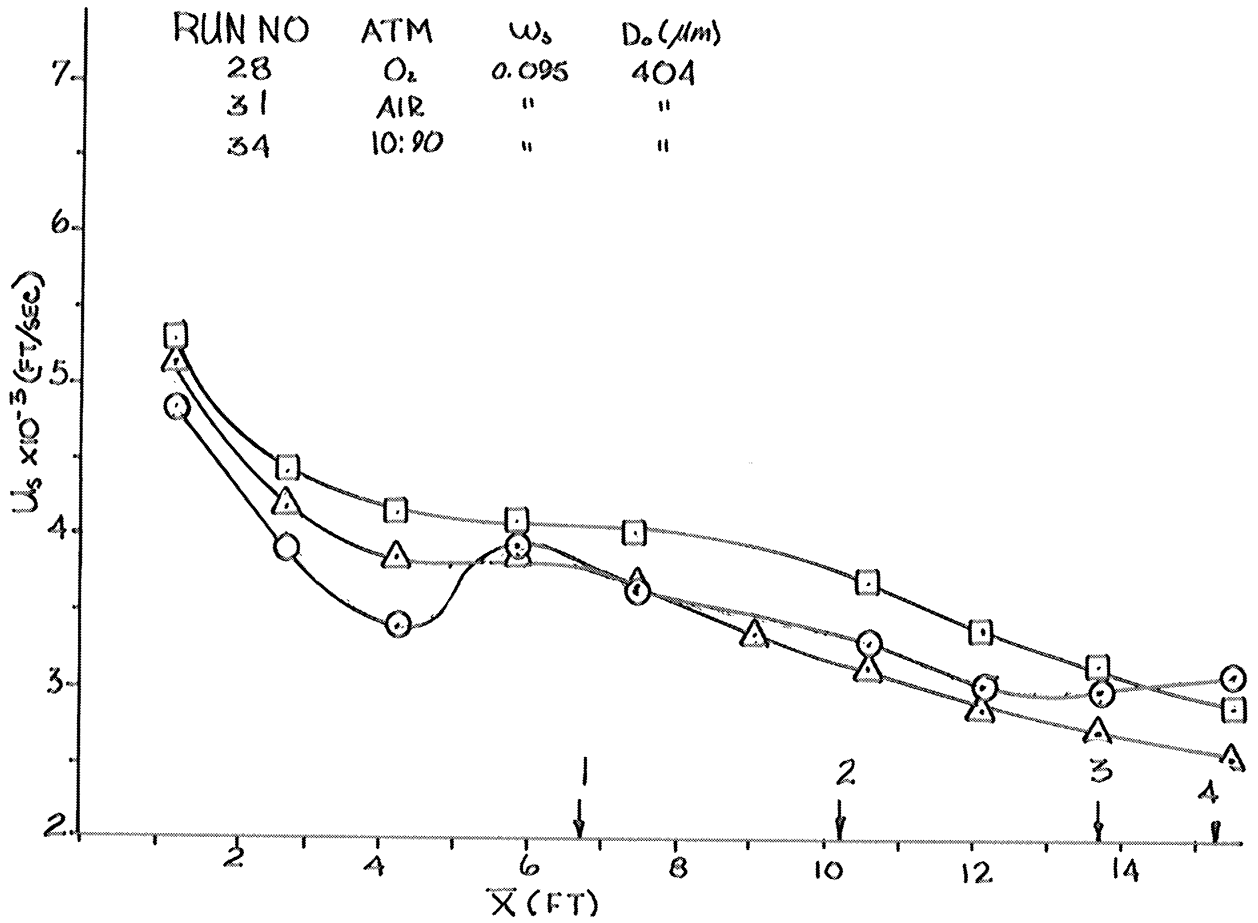
Figure 28.     Velocity and Pressure Results for Nitropropane-Runs 28, 31, and 34.
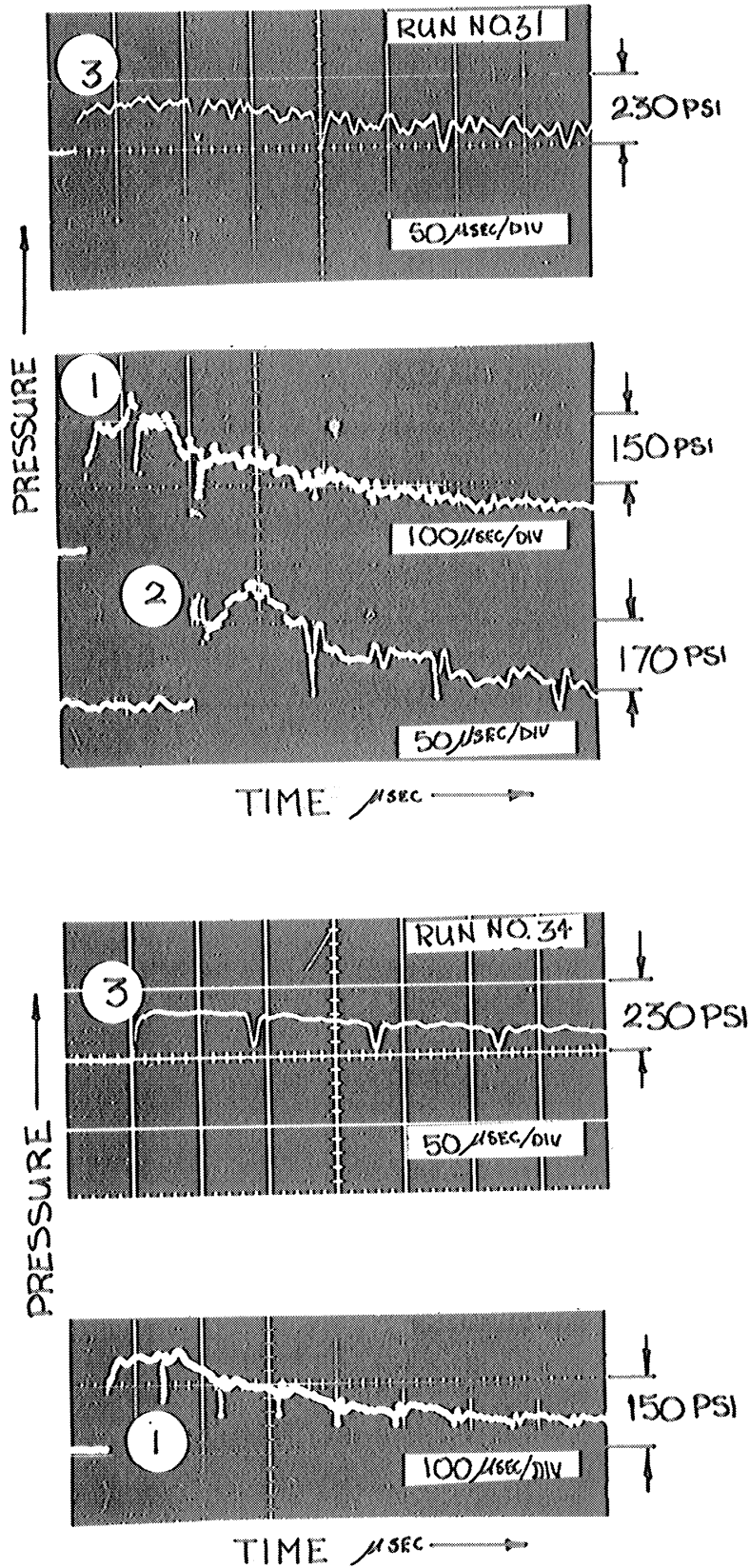
Figure 28. (Continued) Velocity and Pressure Results for Nitropropane-
Runs 28, 31, and 34.

121
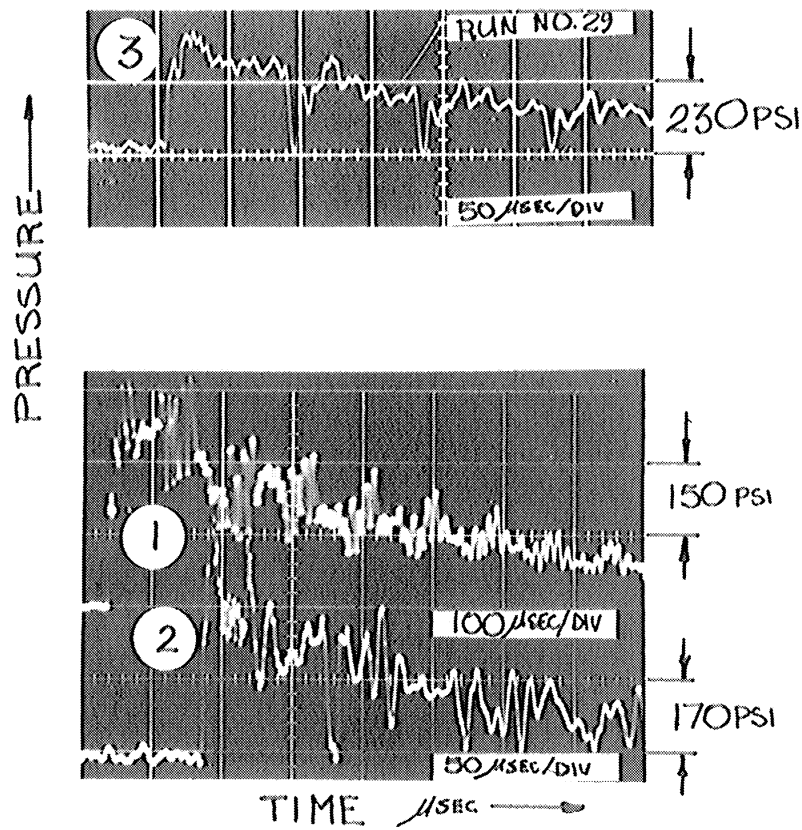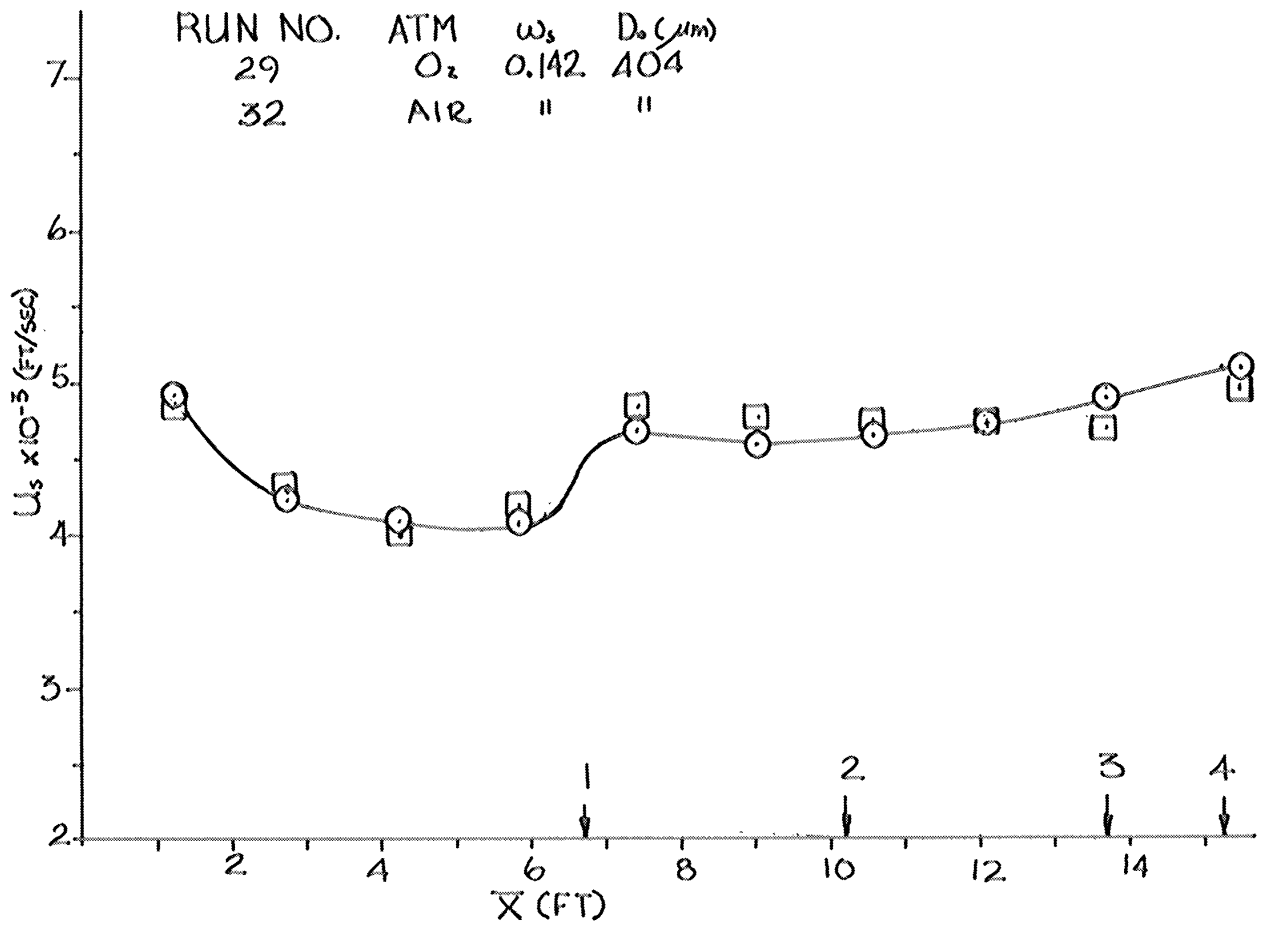
Figure 29.    Velocity and Pressure Results for Nitropropane- Runs 29 and 32.

122
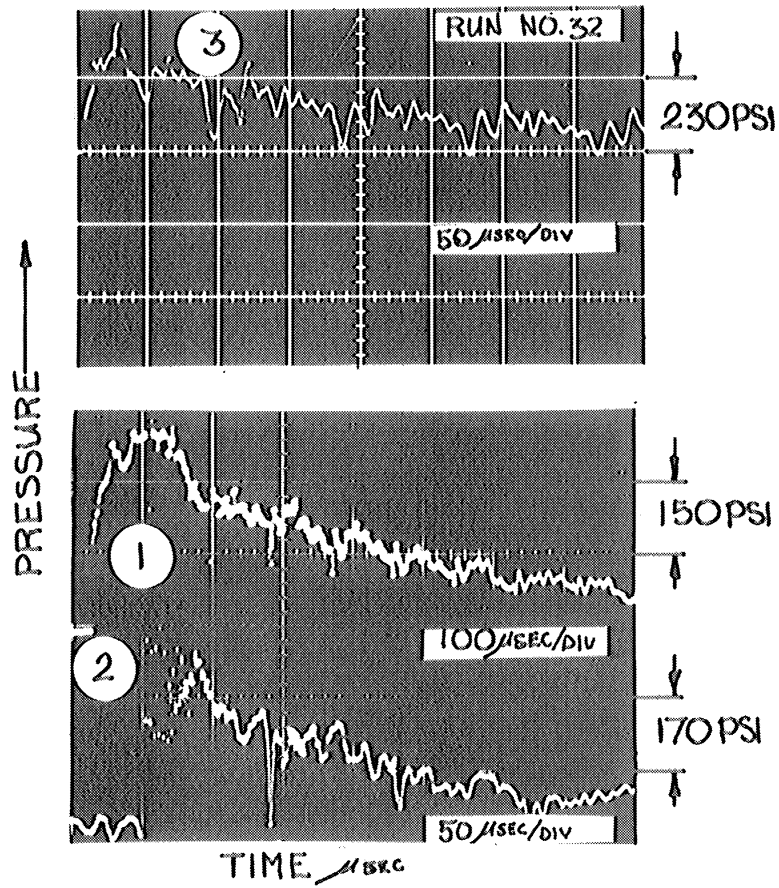
Figure 29.    (Continued) Velocity and Pressure Results for Nitropropane-
Runs 29 and 32.
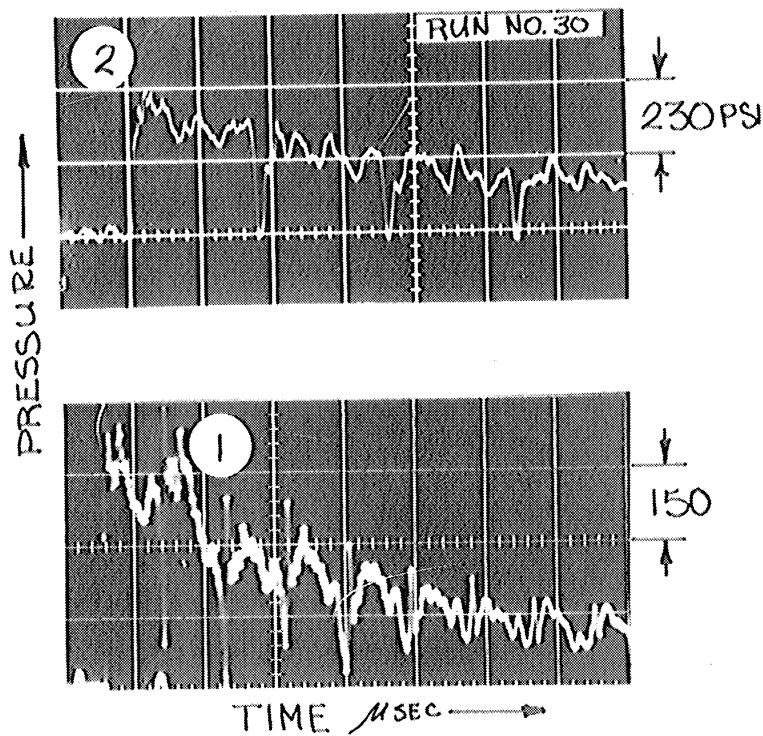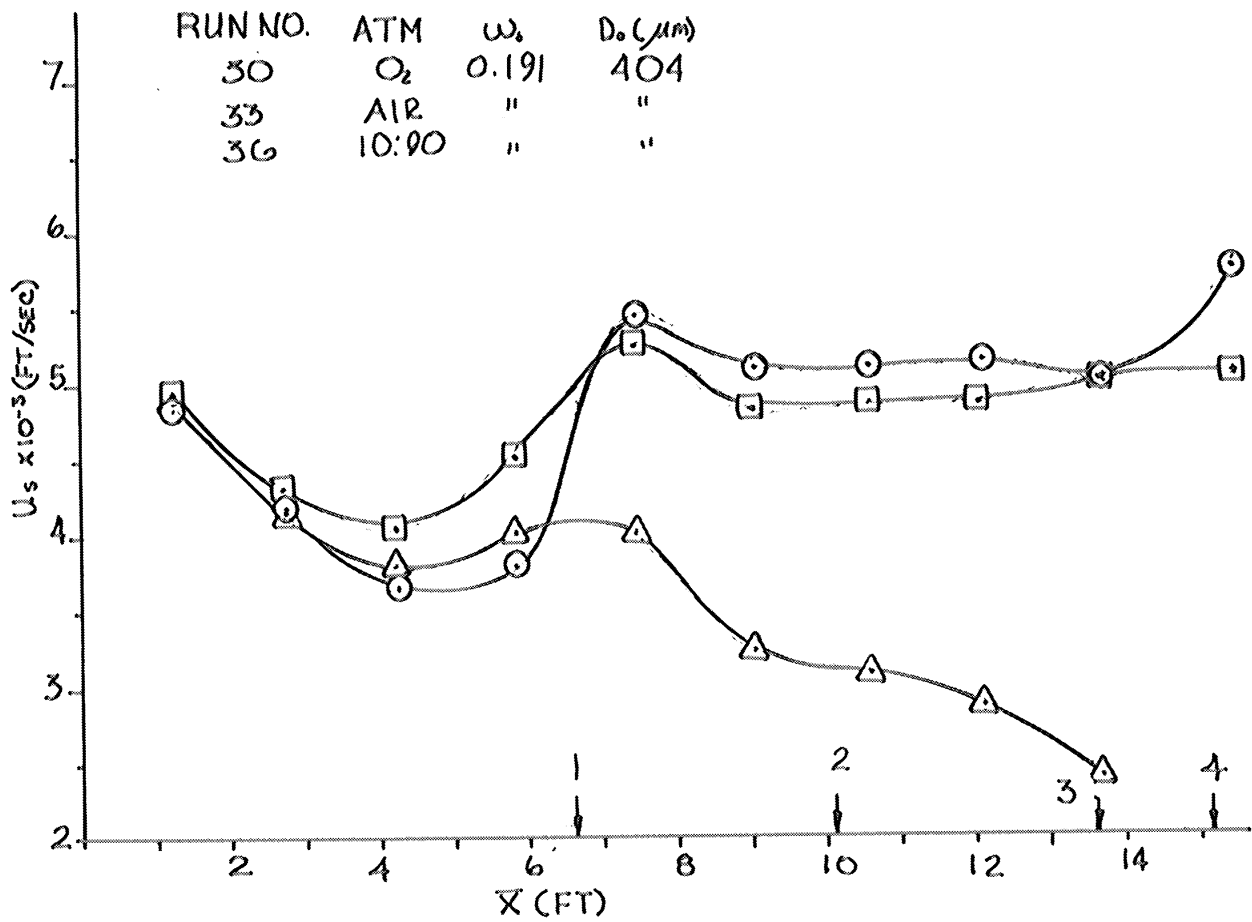
Figure 30.    Velocity and Pressure Results for Nitropropane–Runs 30, 33, and 36.
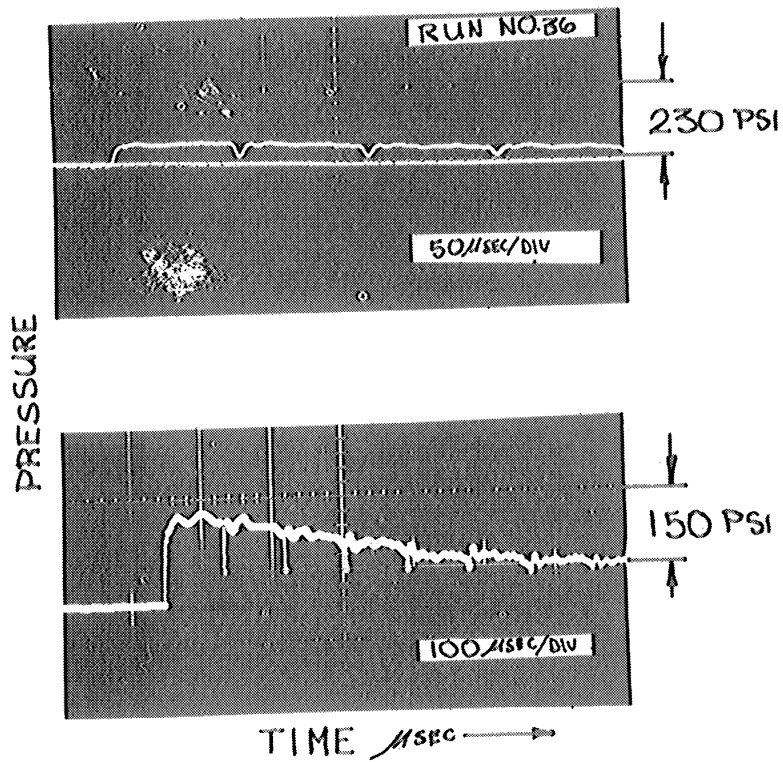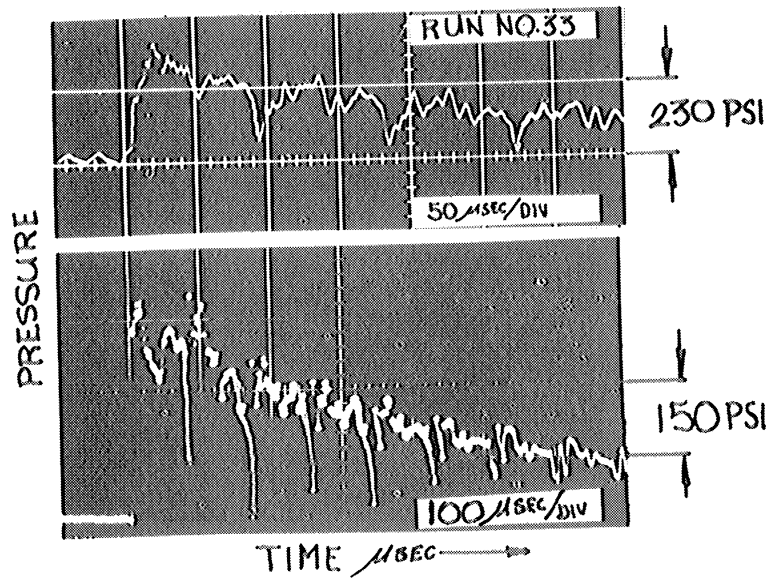
Figure 30.    (Continued) Velocity and Pressure Results for Nitropropane--
Runs 30, 33, and 36.
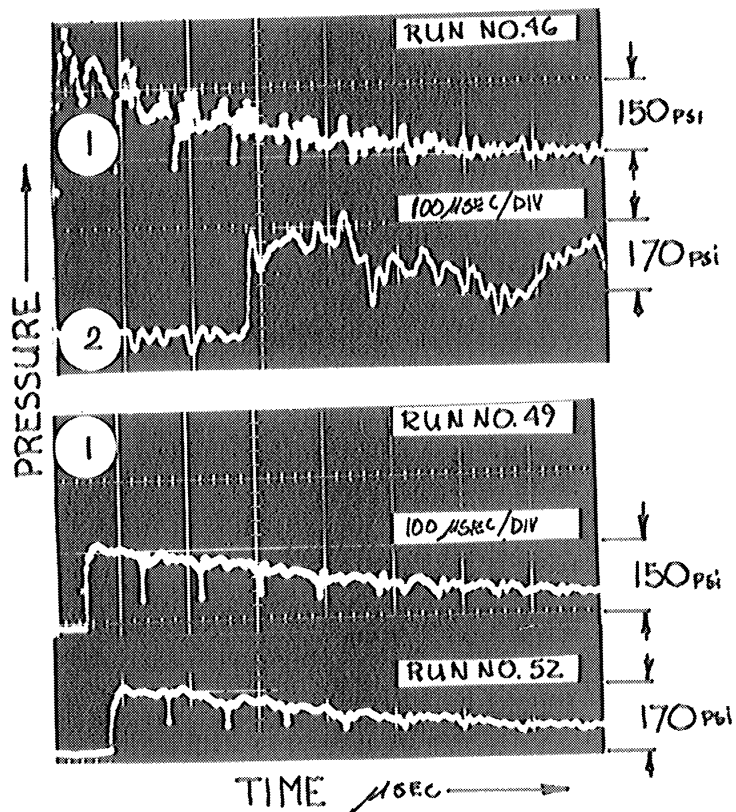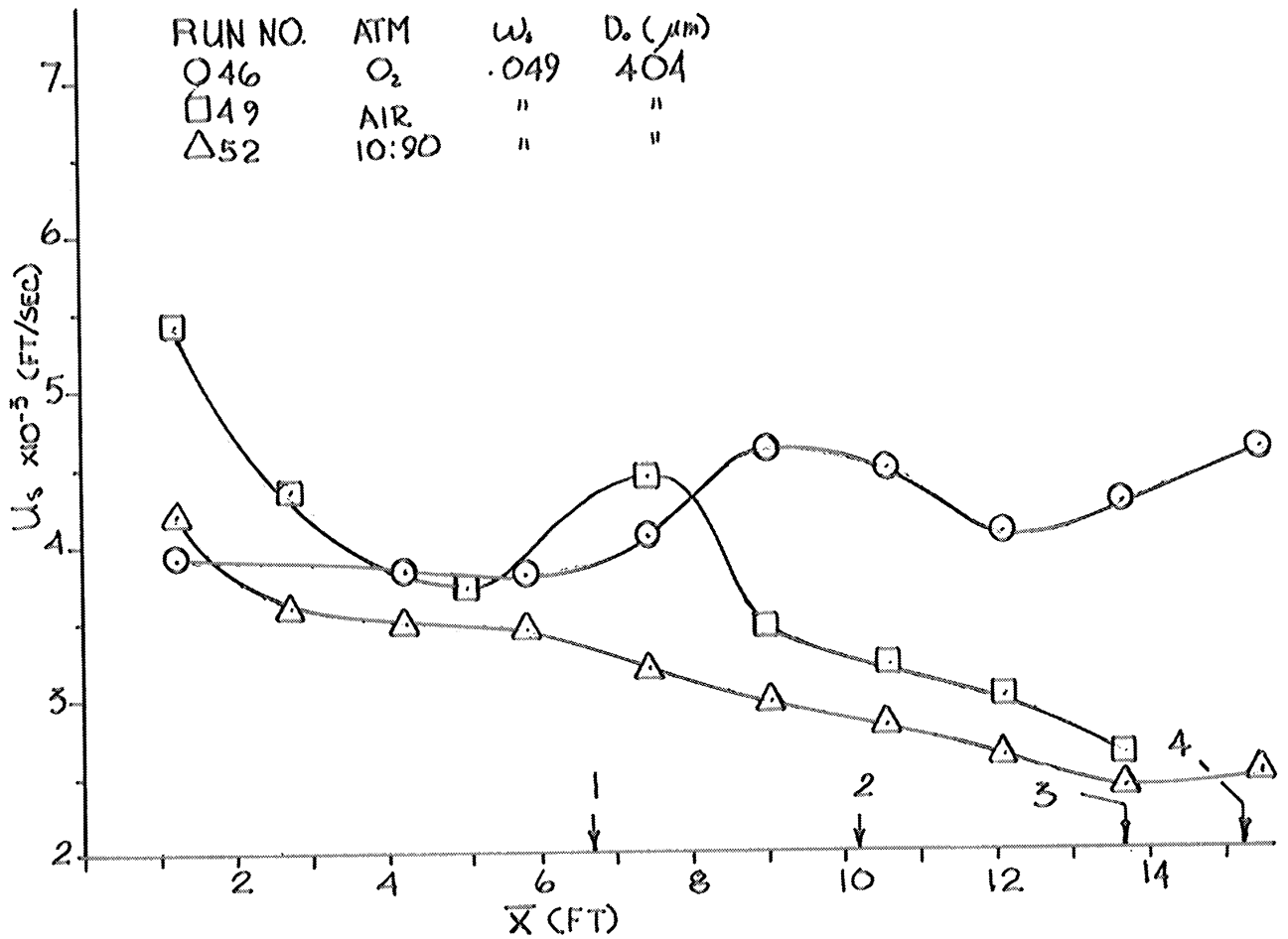
Figure 31.    Velocity and Pressure Results for Decane- Runs 46, 49, and 52.
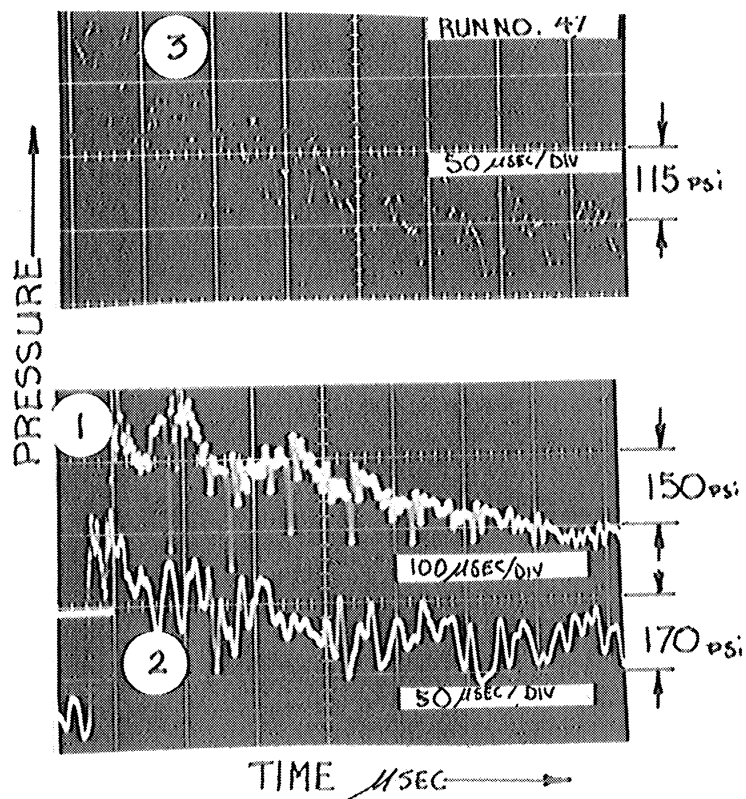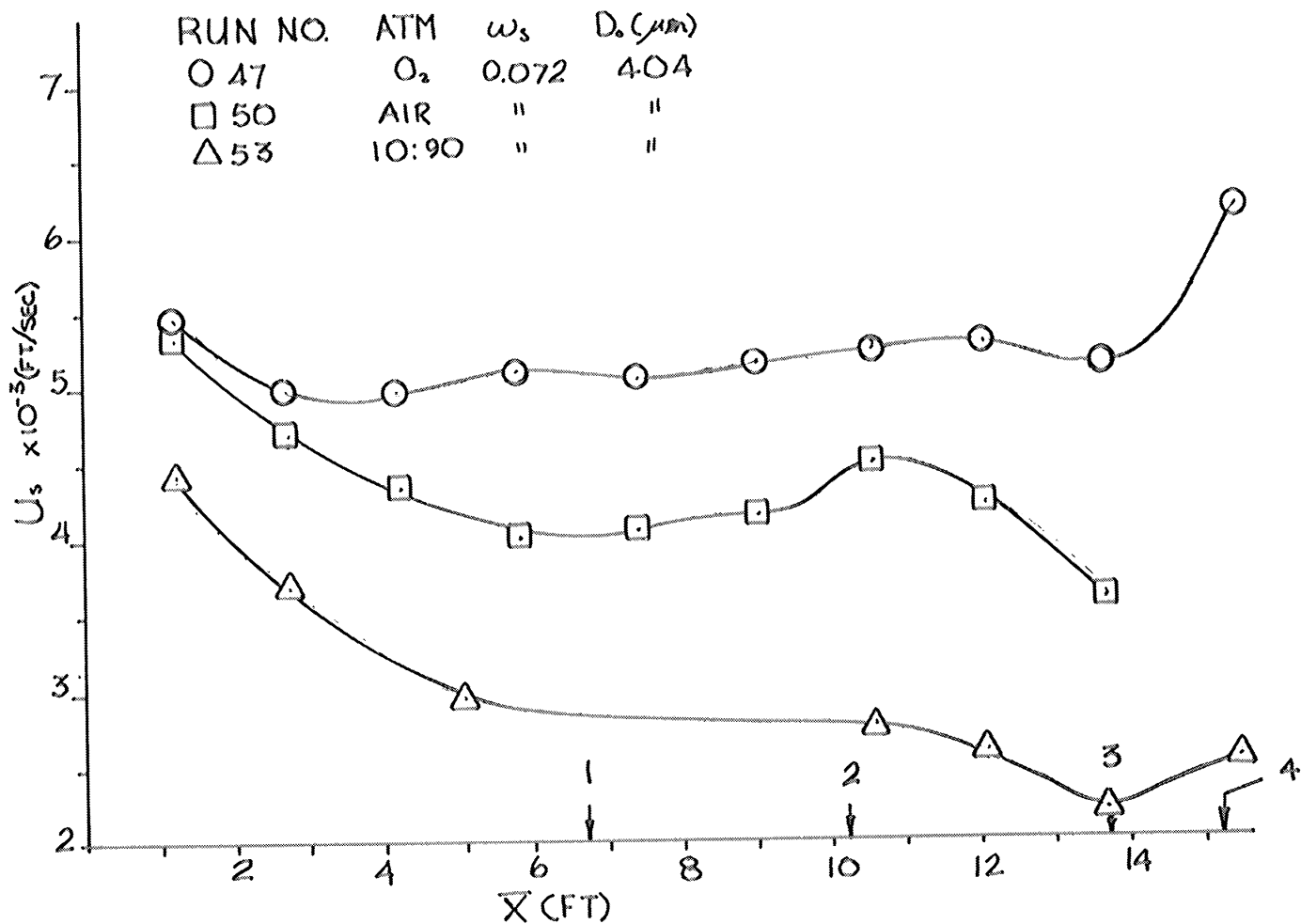
Figure 32.    Velocity and Pressure Results for Decane - Runs 47, 50, and 53.
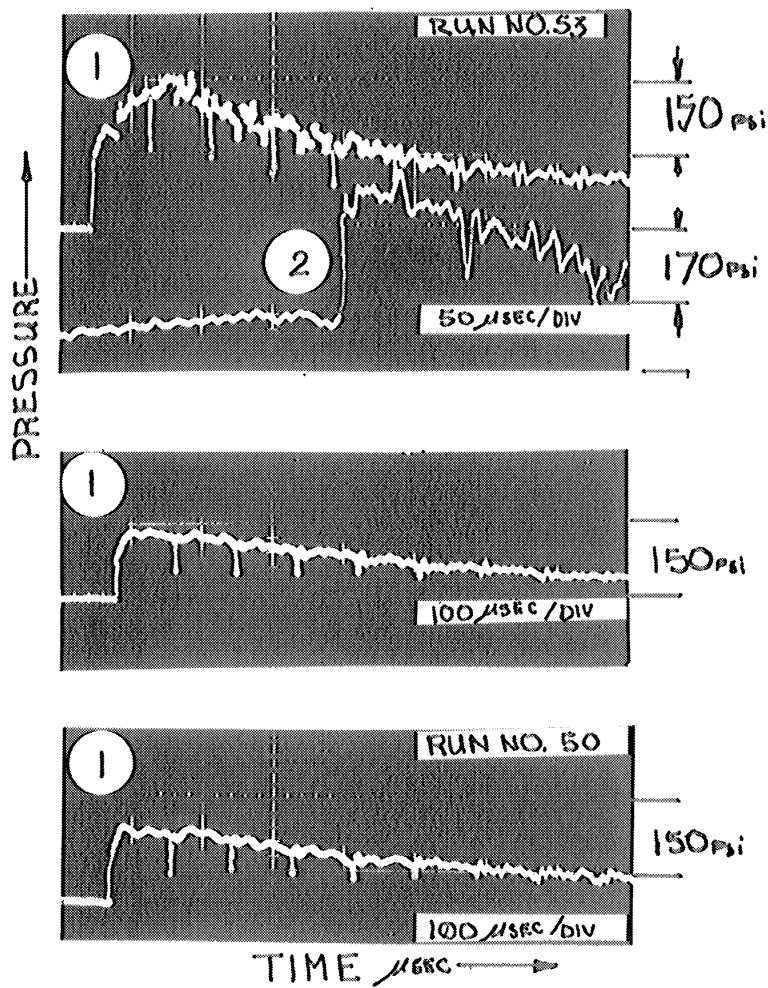
Figure 32.    (Continued) Velocity and Pressure Results for Decane-
Runs 47, 50, and 53.
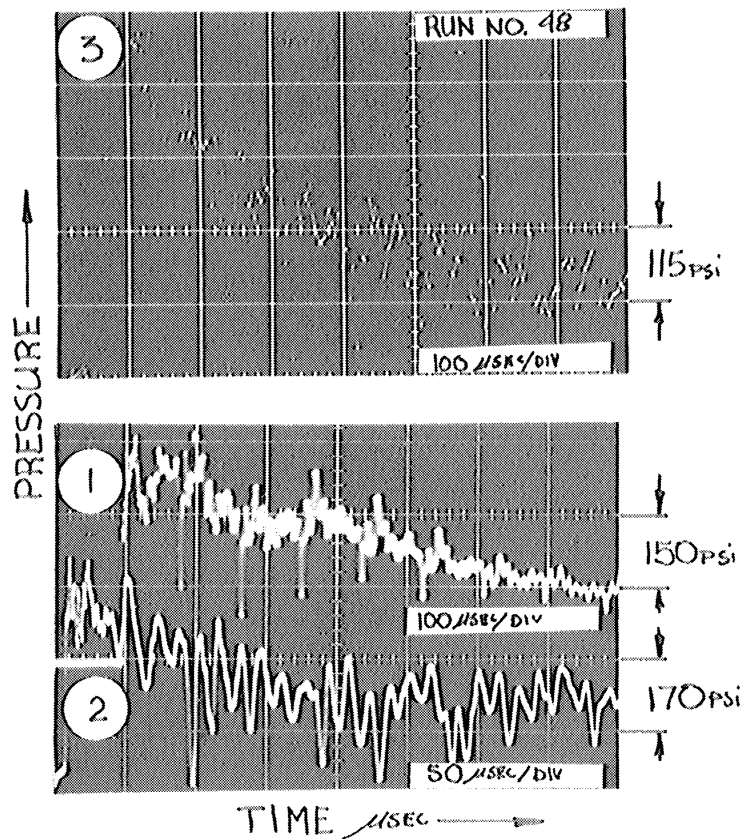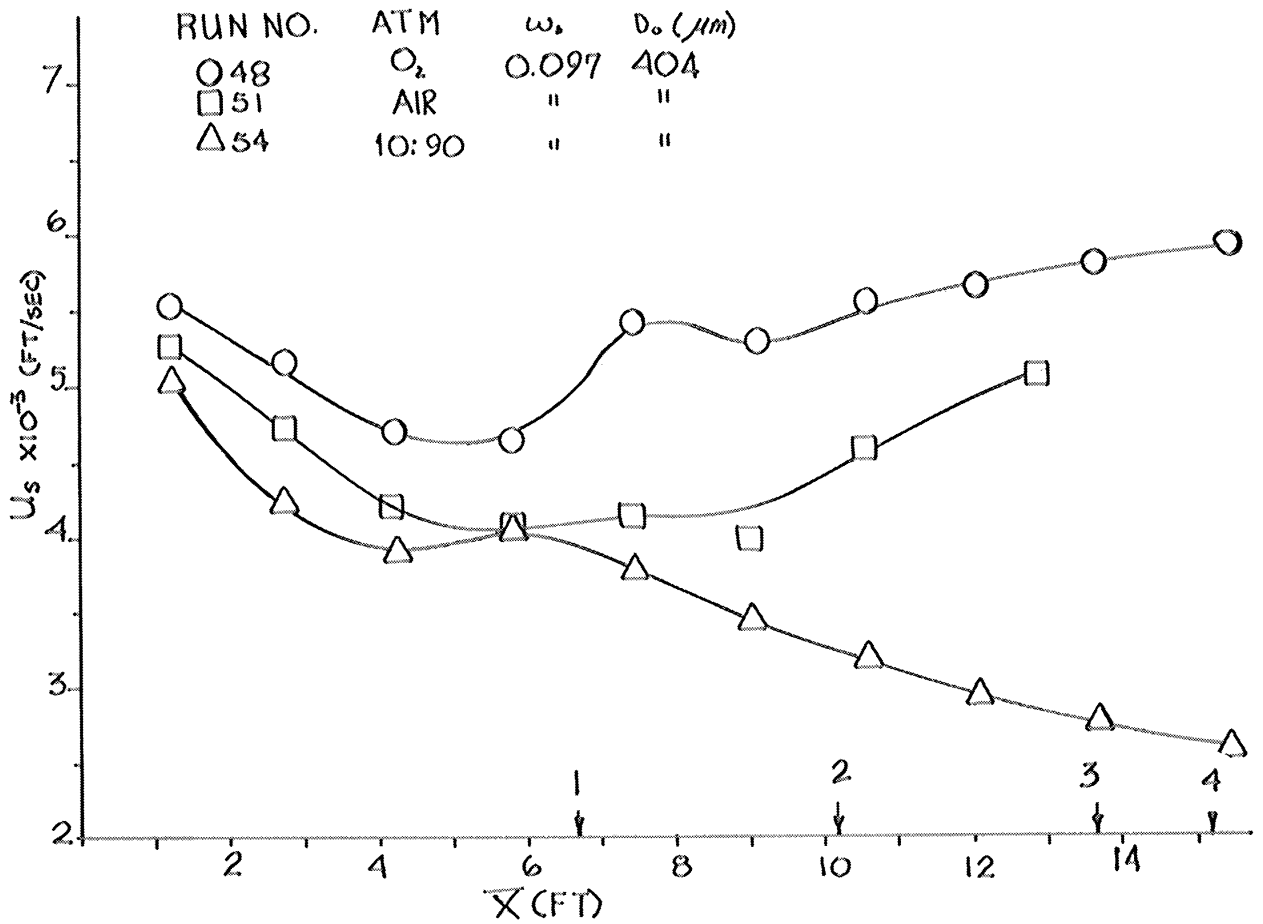
Figure 33. Velocity and Pressure Results for Decane-Runs 48, 51, and 54.
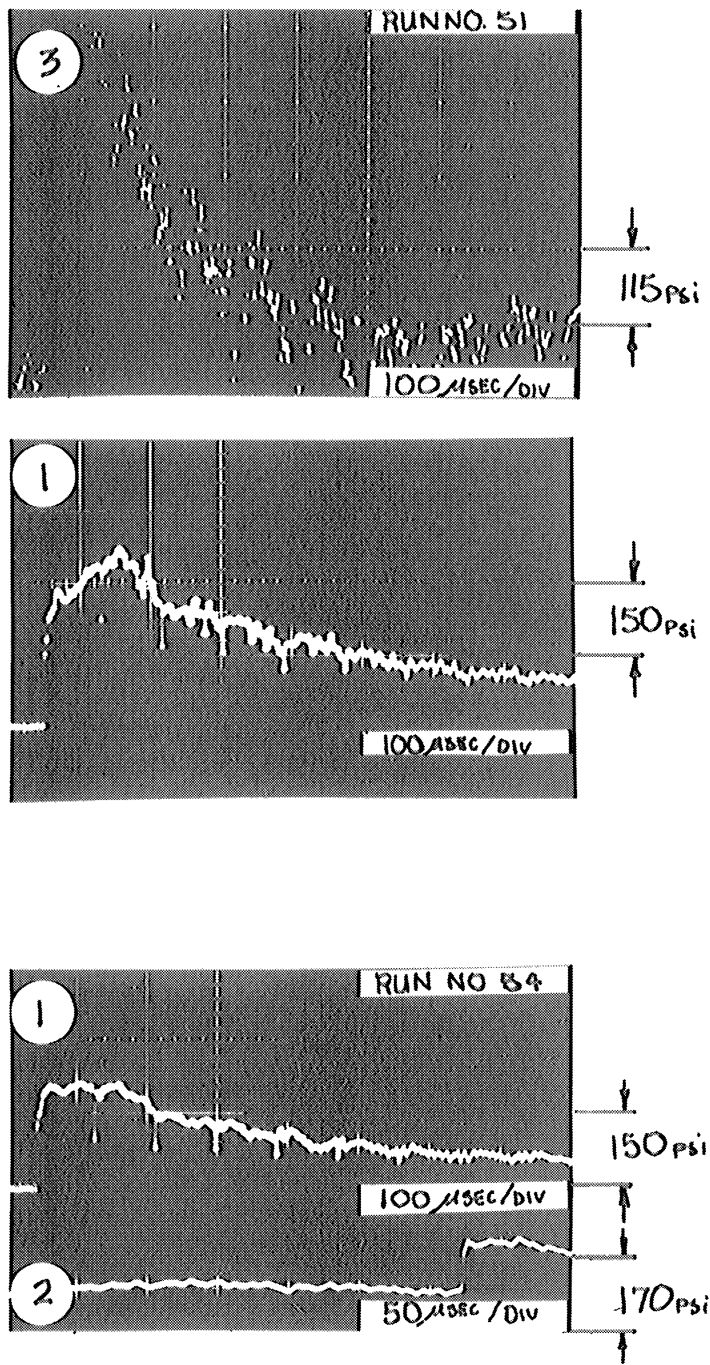
Figure 33.  (Continued) Velocity and Pressure Results for Decane-
Runs 48, 51, and 54.
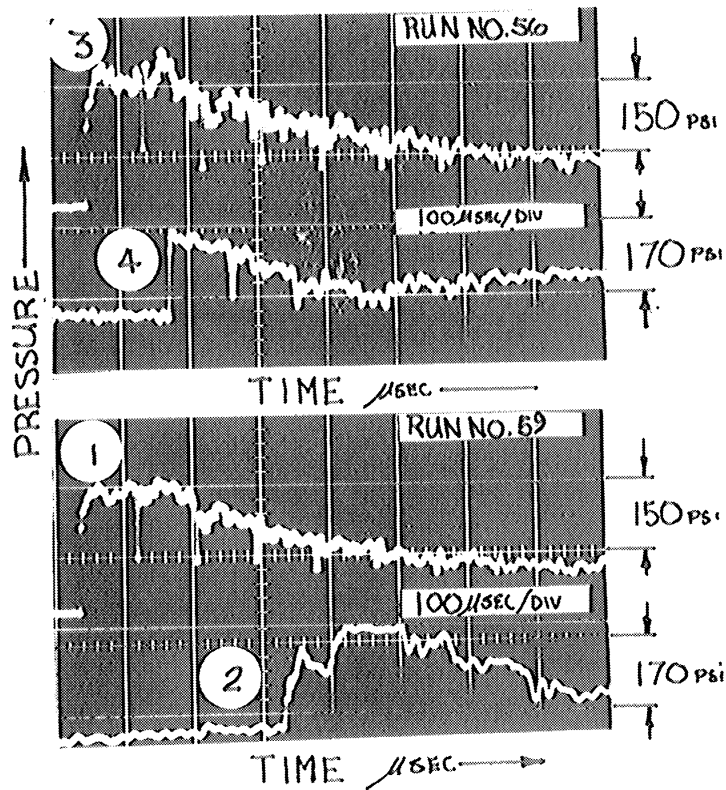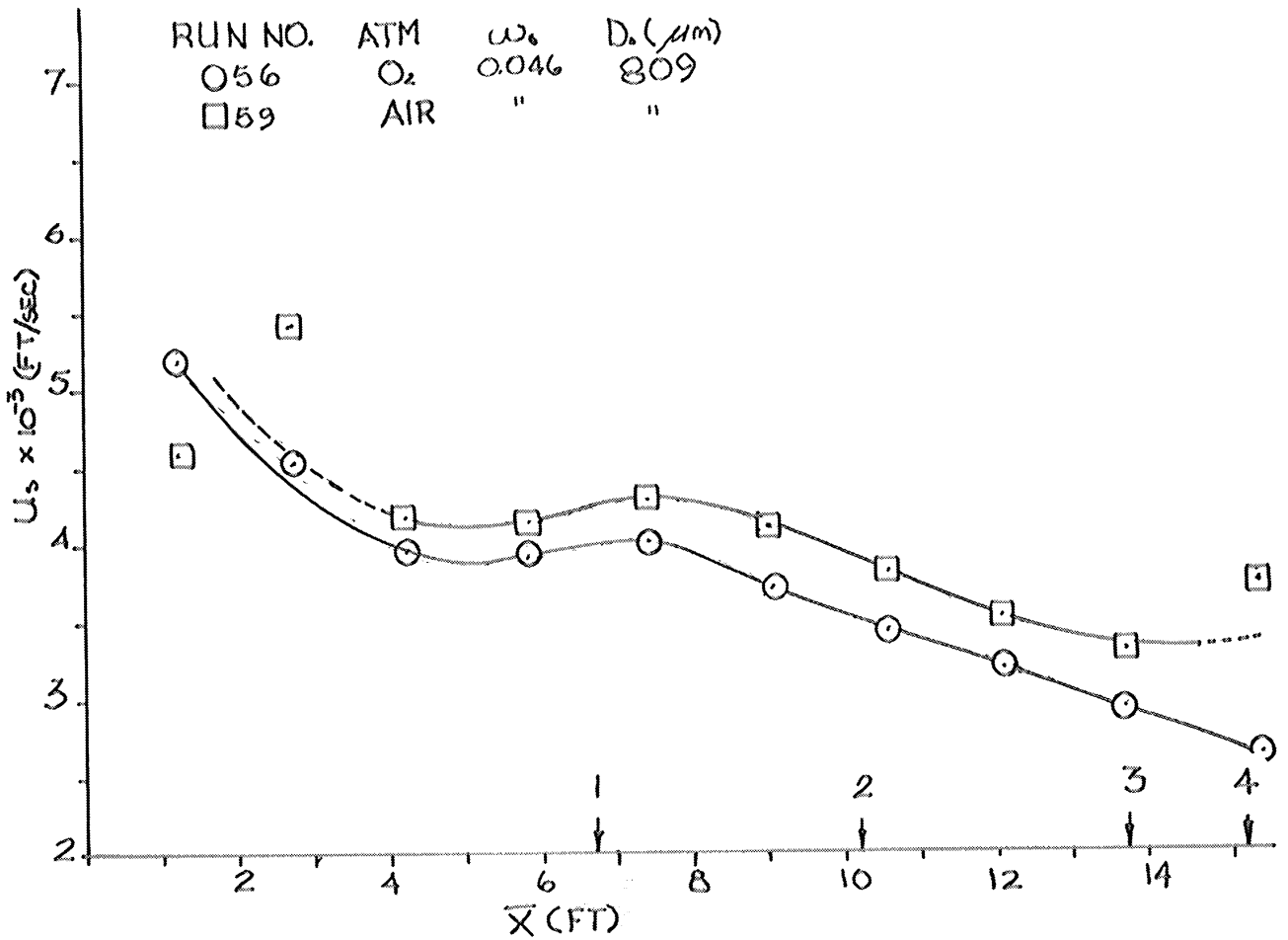
Figure 34.     Velocity and Pressure Results for Nitromethane-Runs 56 and 59.

131
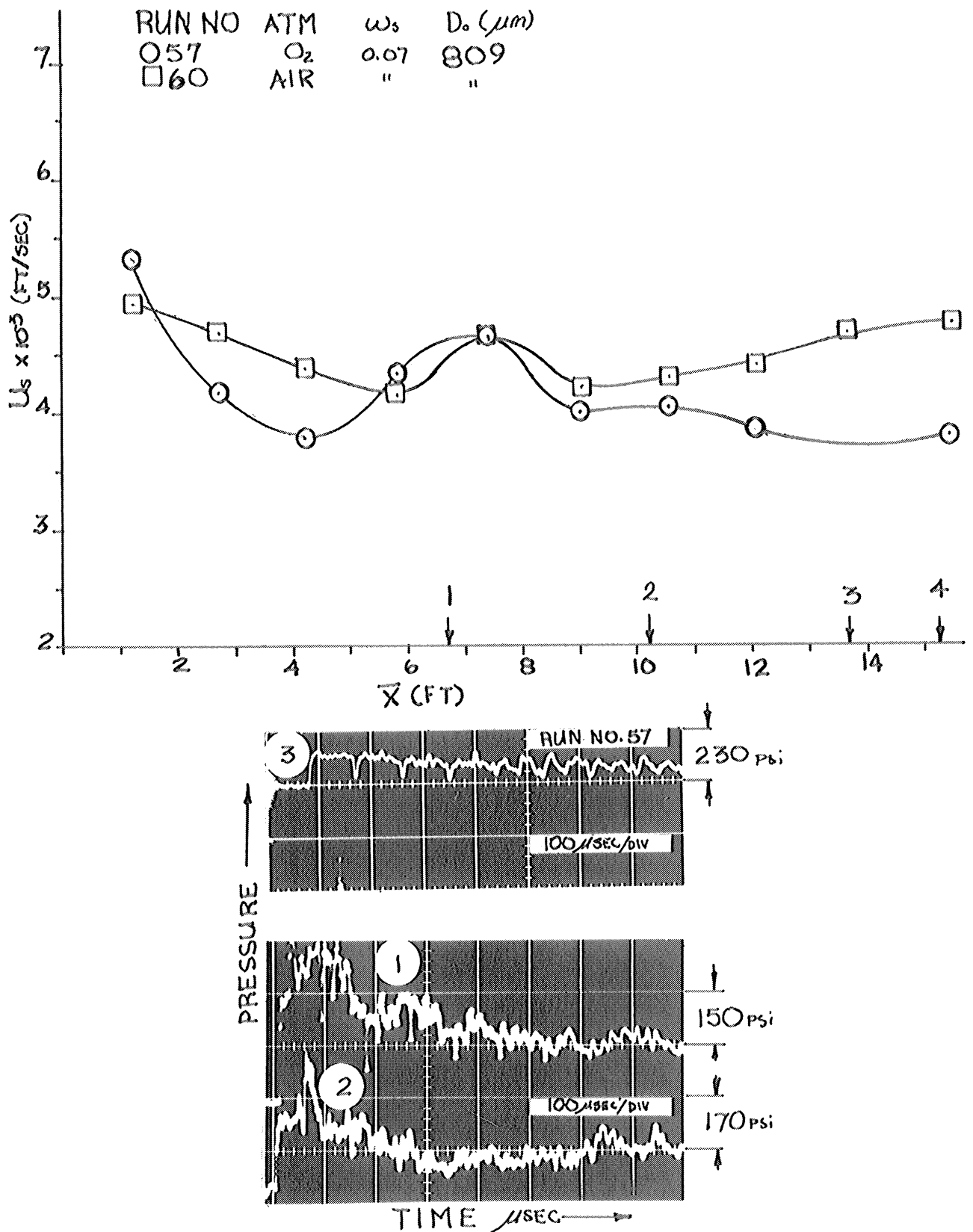
Figure 35.     Velocity and Pressure Results for Nitromethane-- Runs 57 and 60.
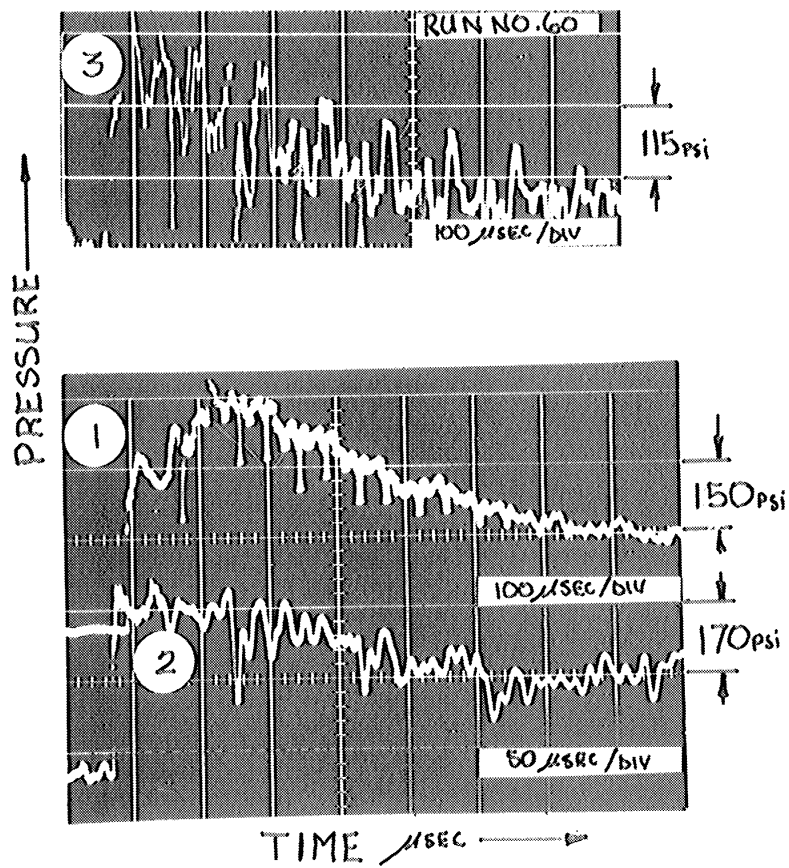
Figure 35.    (Continued) Velocity and Pressure Results for Nitromethane-
Runs 57 and 60.

133
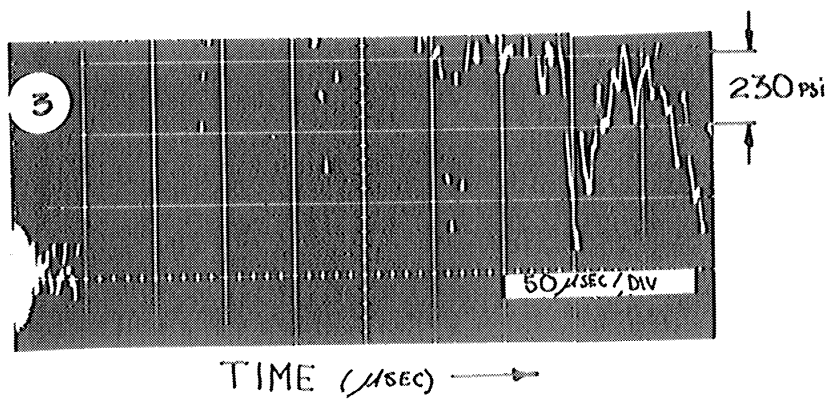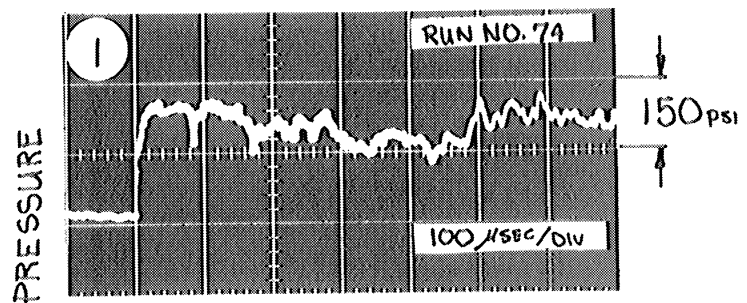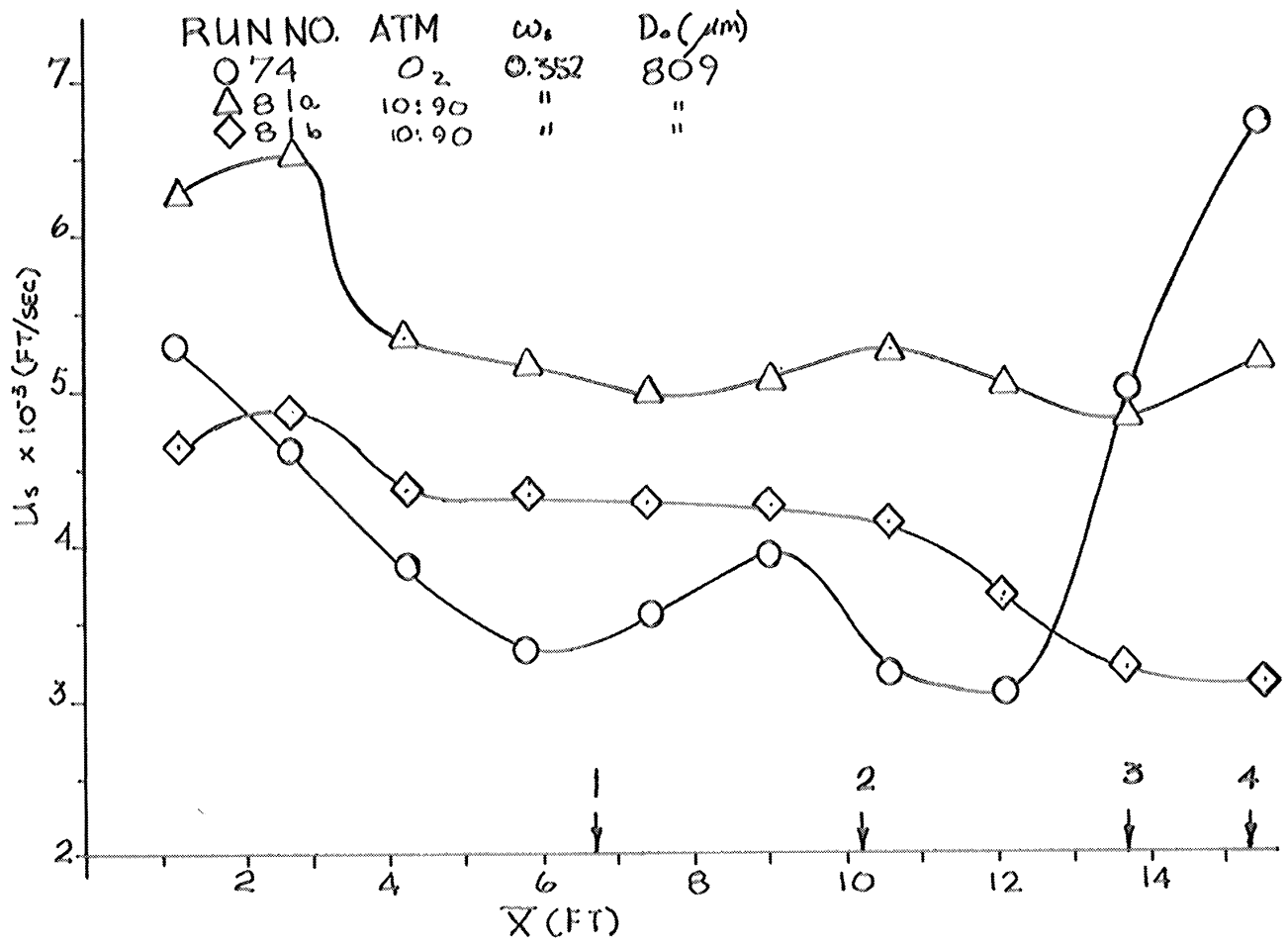
Figure 36.    Velocity and Pressure Results for Nitromethane–Runs 74, 81a, and 81b.
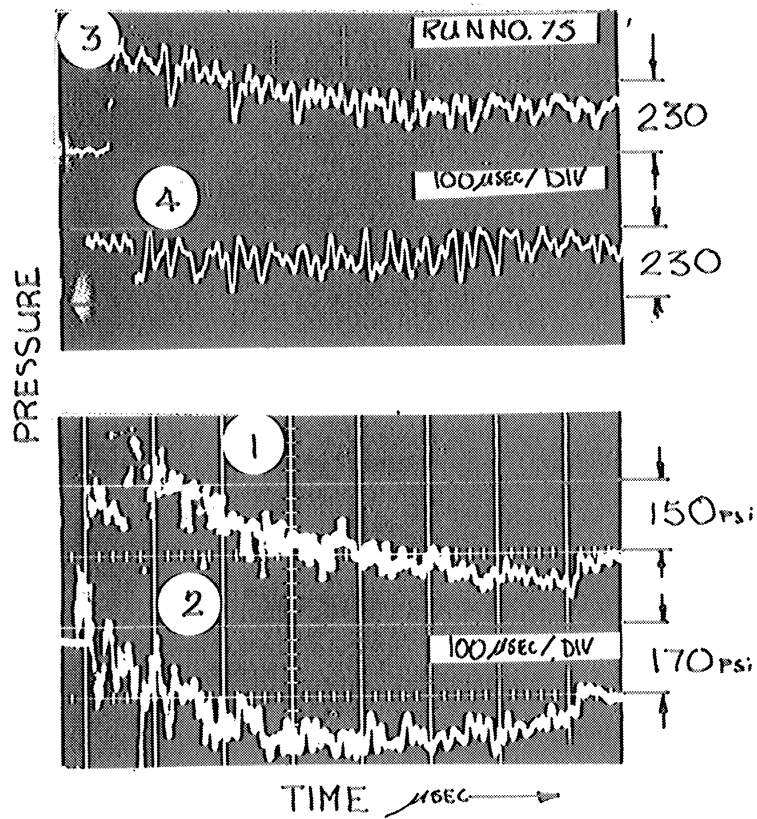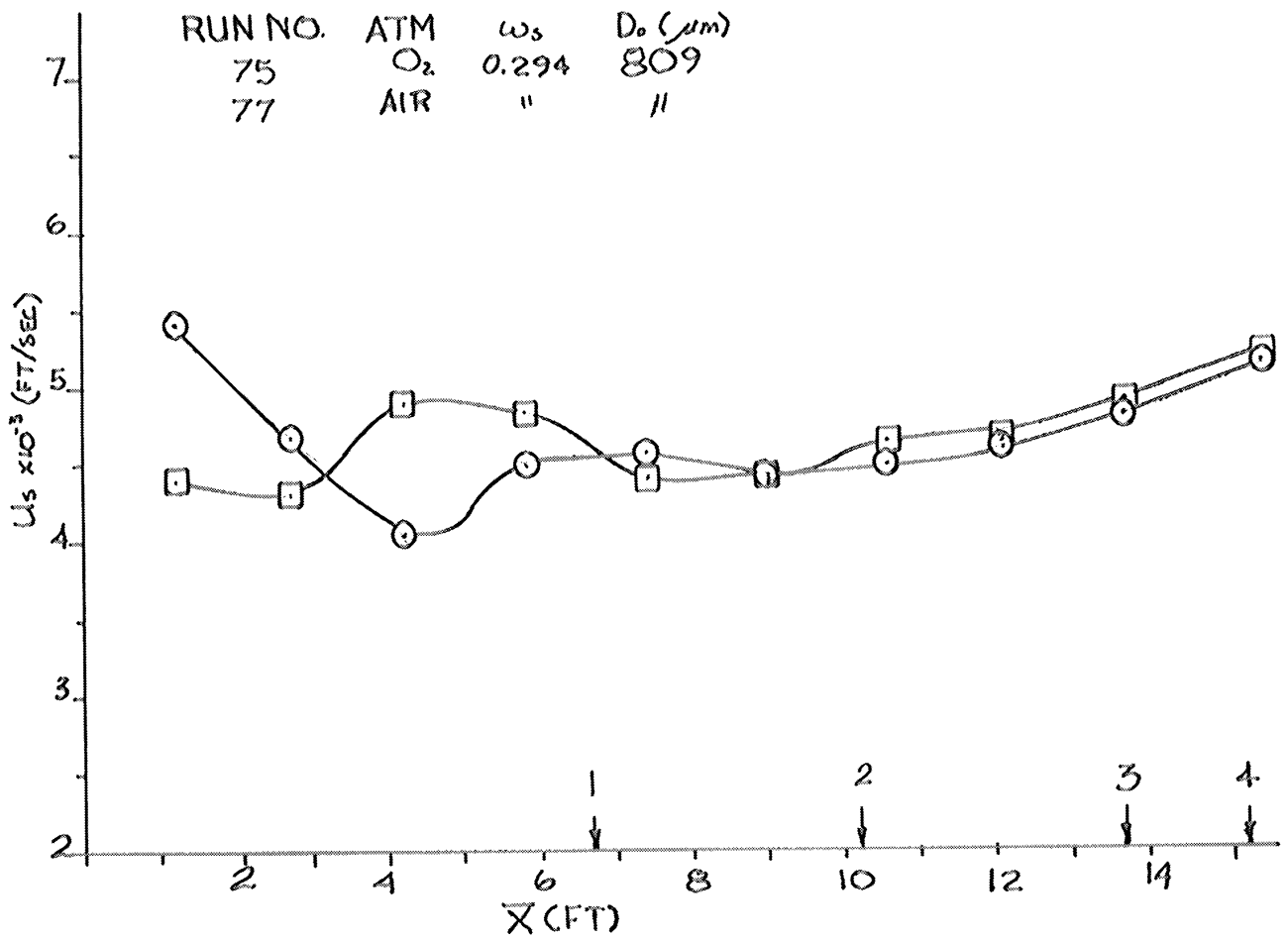
Figure 37.    Velocity and Pressure Results for Nitromethane --Runs 75 and 77.

135
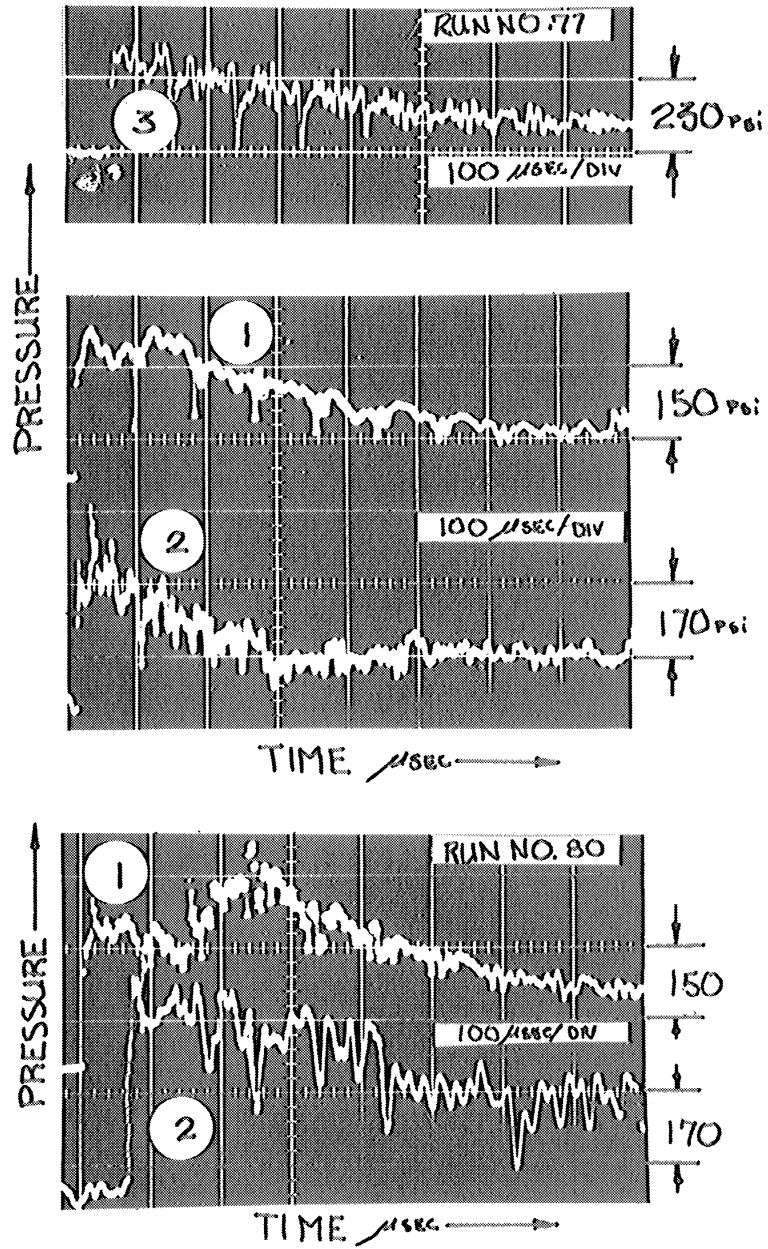
Figure 37.    (Continued) Velocity and Pressure Results for Nitromethane-
Runs 75 and 77.
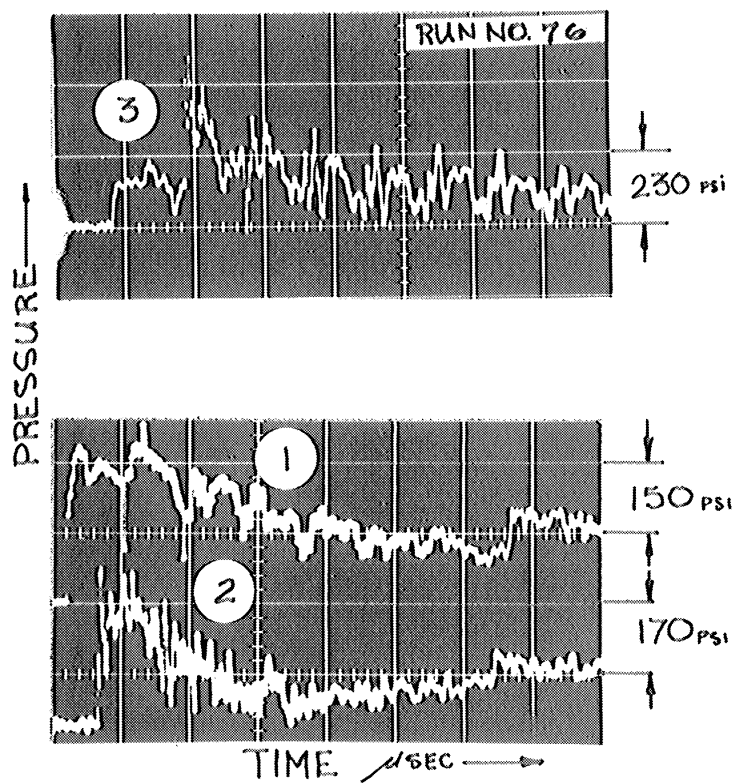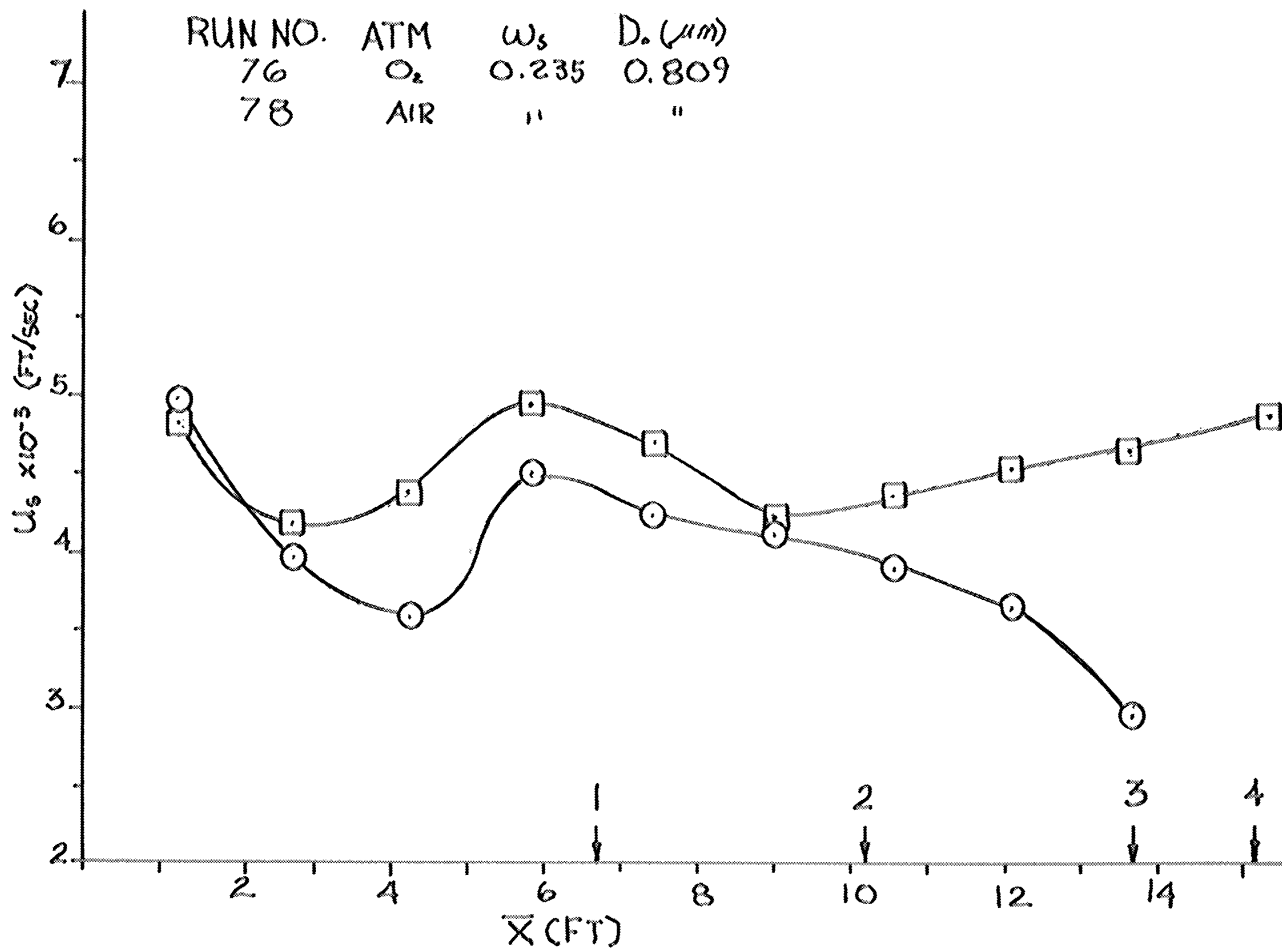
Figure 38.    Velocity and Pressure Results for Nitromethane- Runs 76 and 78.
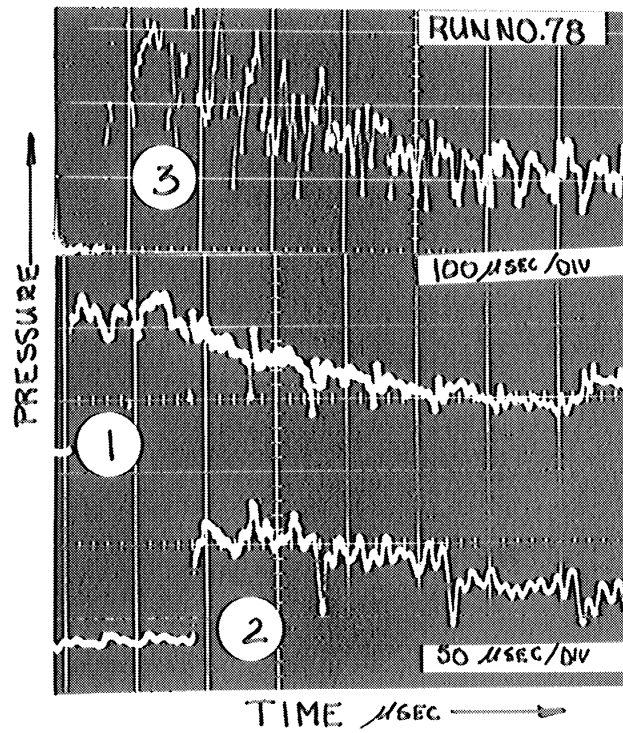
Figure 38.     (Continued) Velocity and Pressure Results for Nitromethane-
Runs 76 and 78.
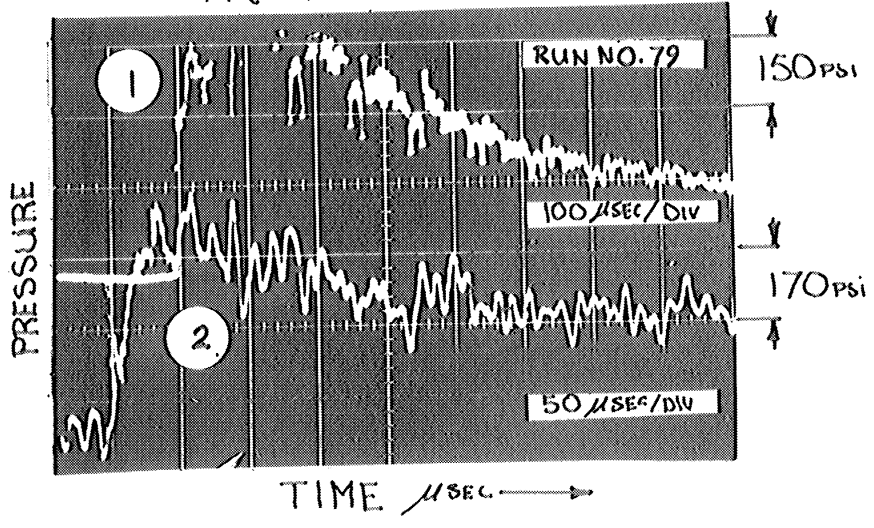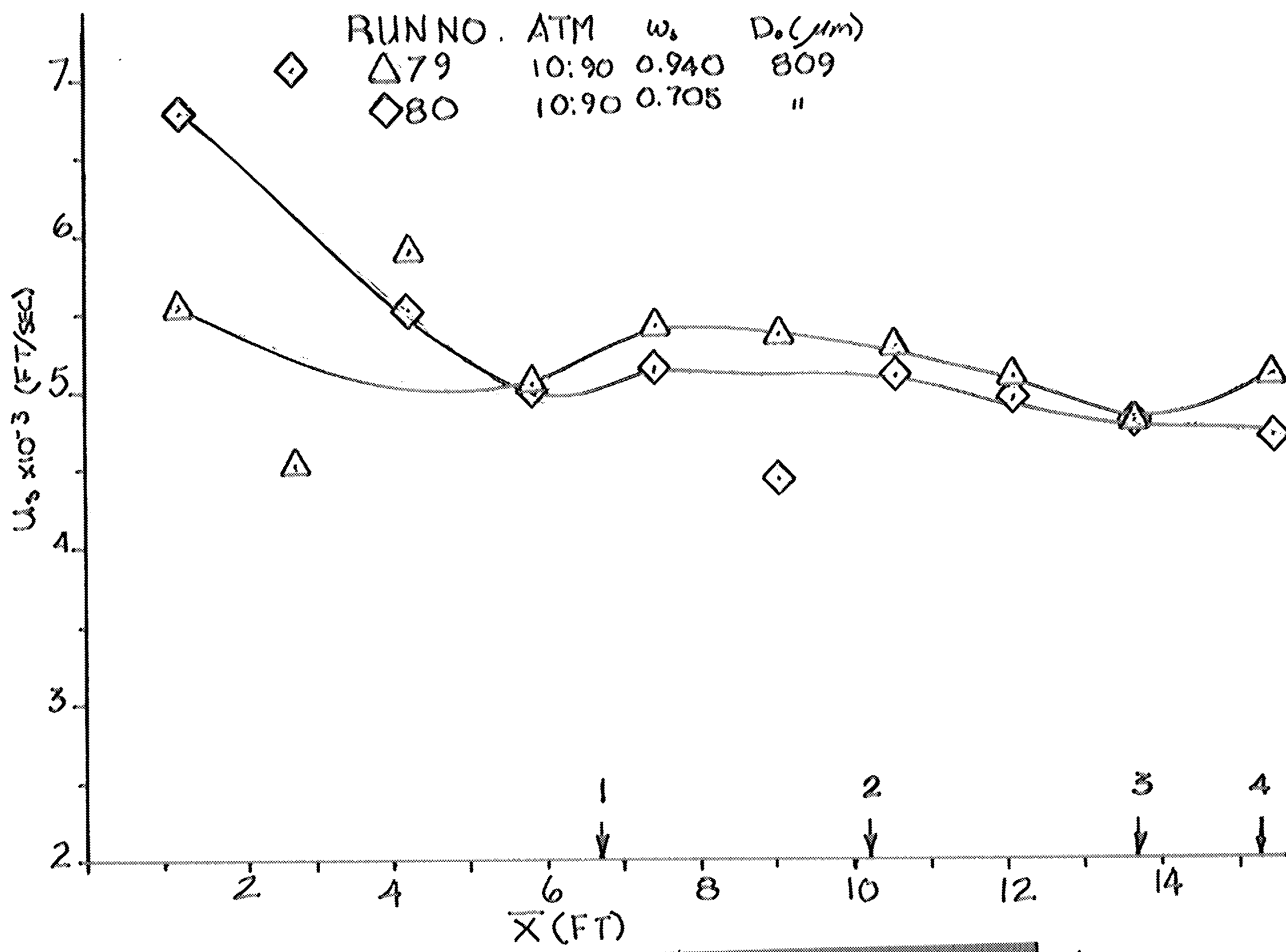
Figure 39.    Velocity and Pressure Results for Nitromethane--Runs 79 and 80.
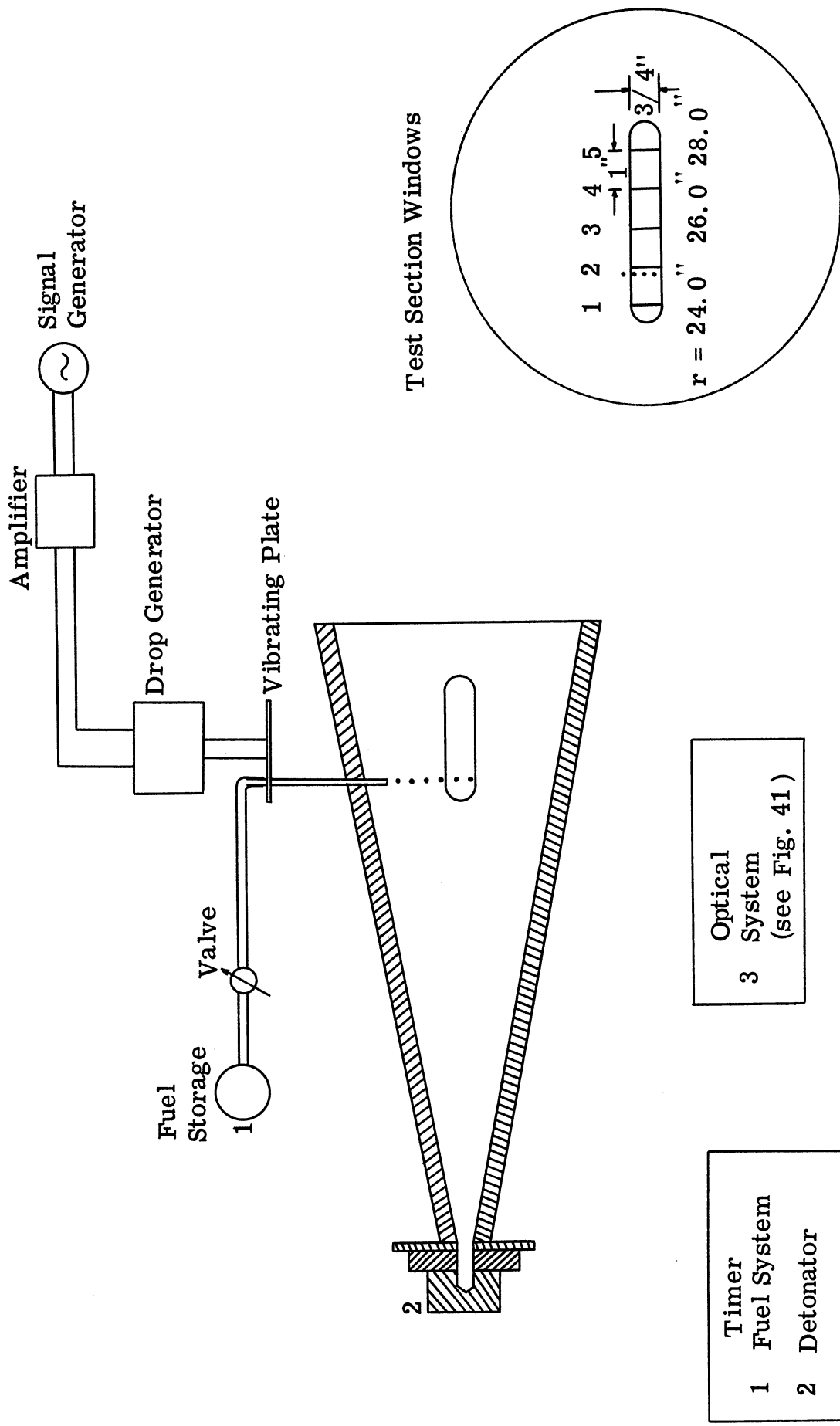
Figure 40.    Schematic of Sectored Chamber Facility.

140
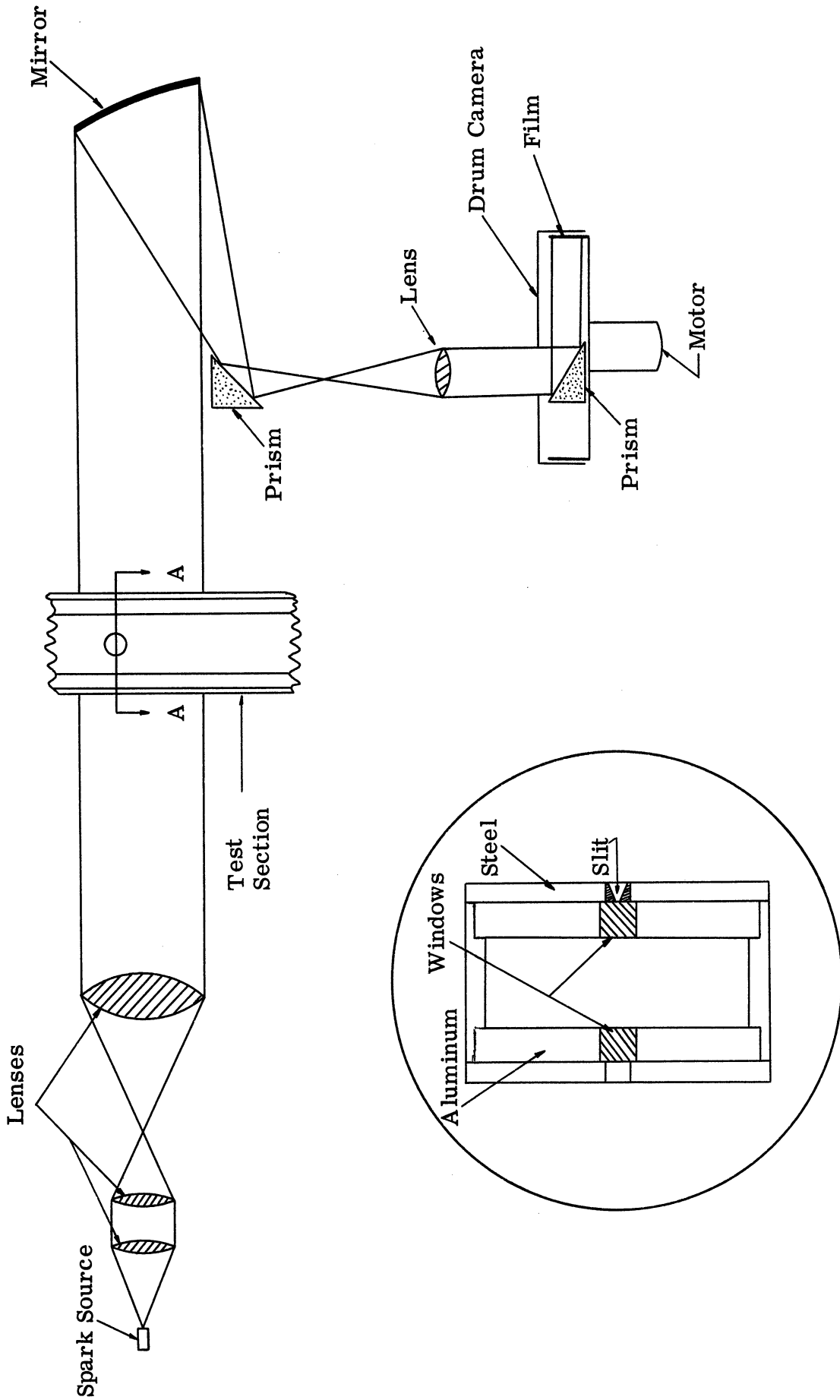
Figure 41. Streak Schlieren Optical System.
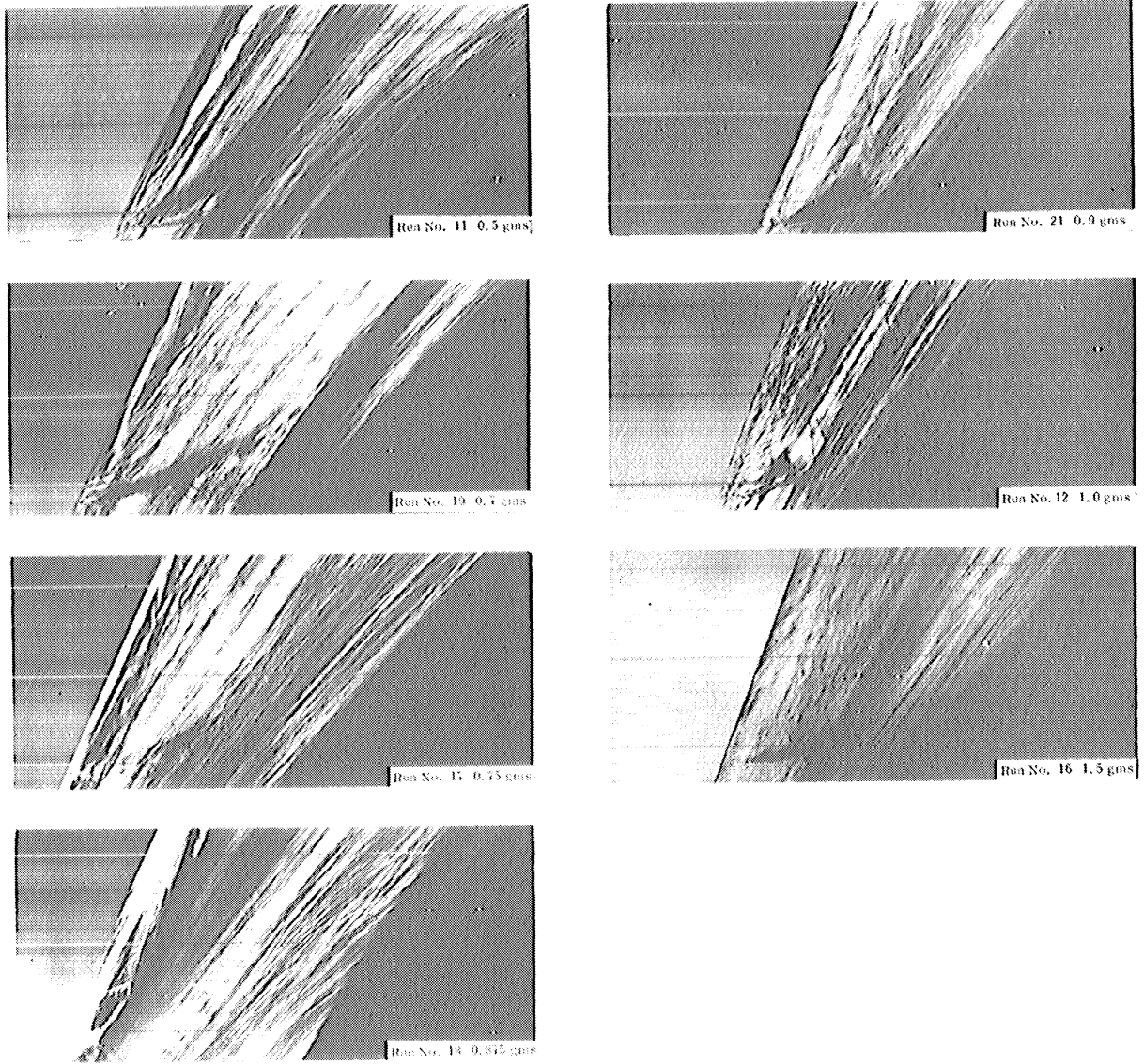
Figure 42a.   Streak Schlieren Records, n-Propyl Nitrate, 768 $\mu$m, 100%$O_2$.
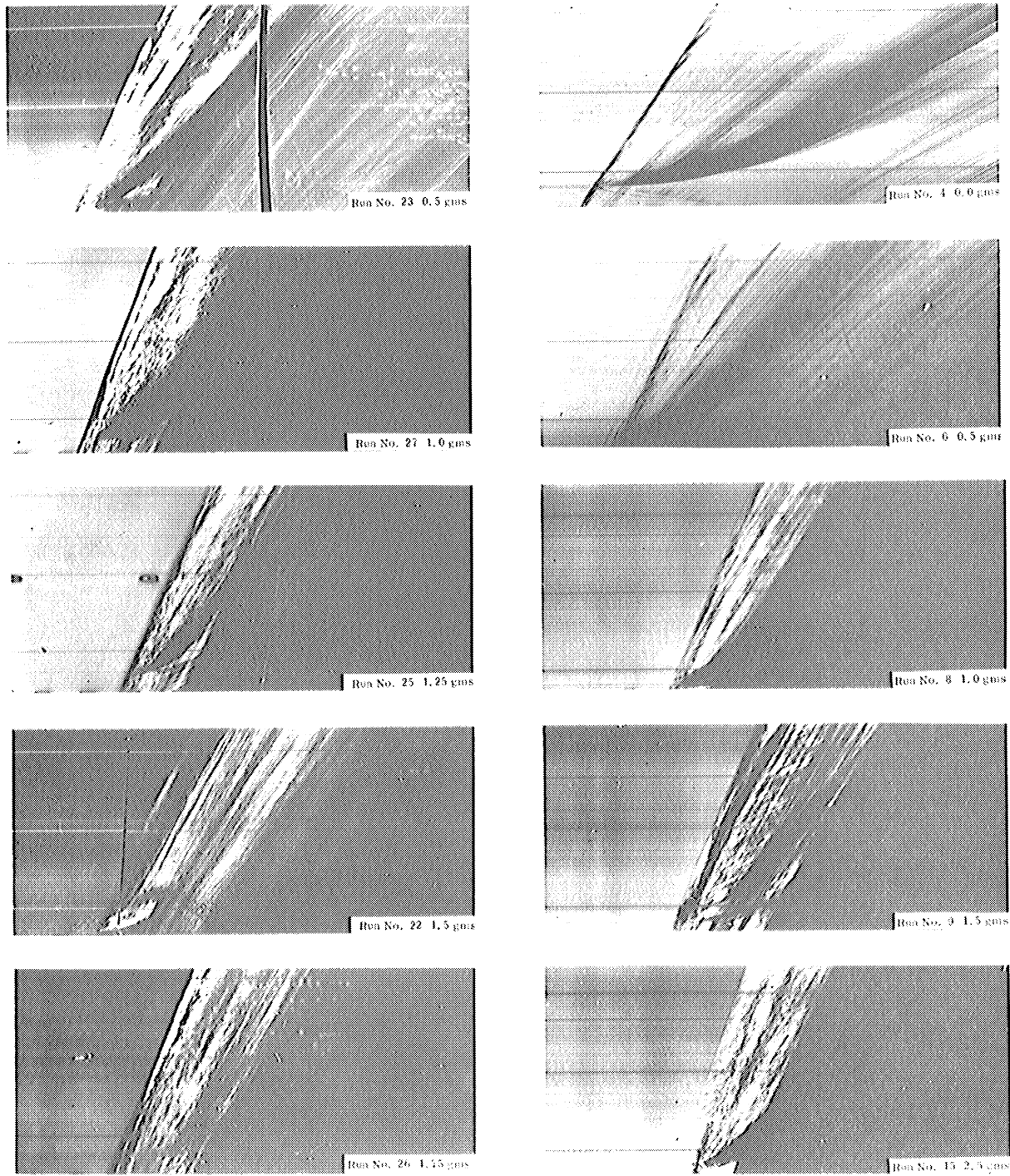
Figure 42b.    Streak Schlieren Records, left column 50% $O_2$ - 50% $N_2$, right column 100% Air.
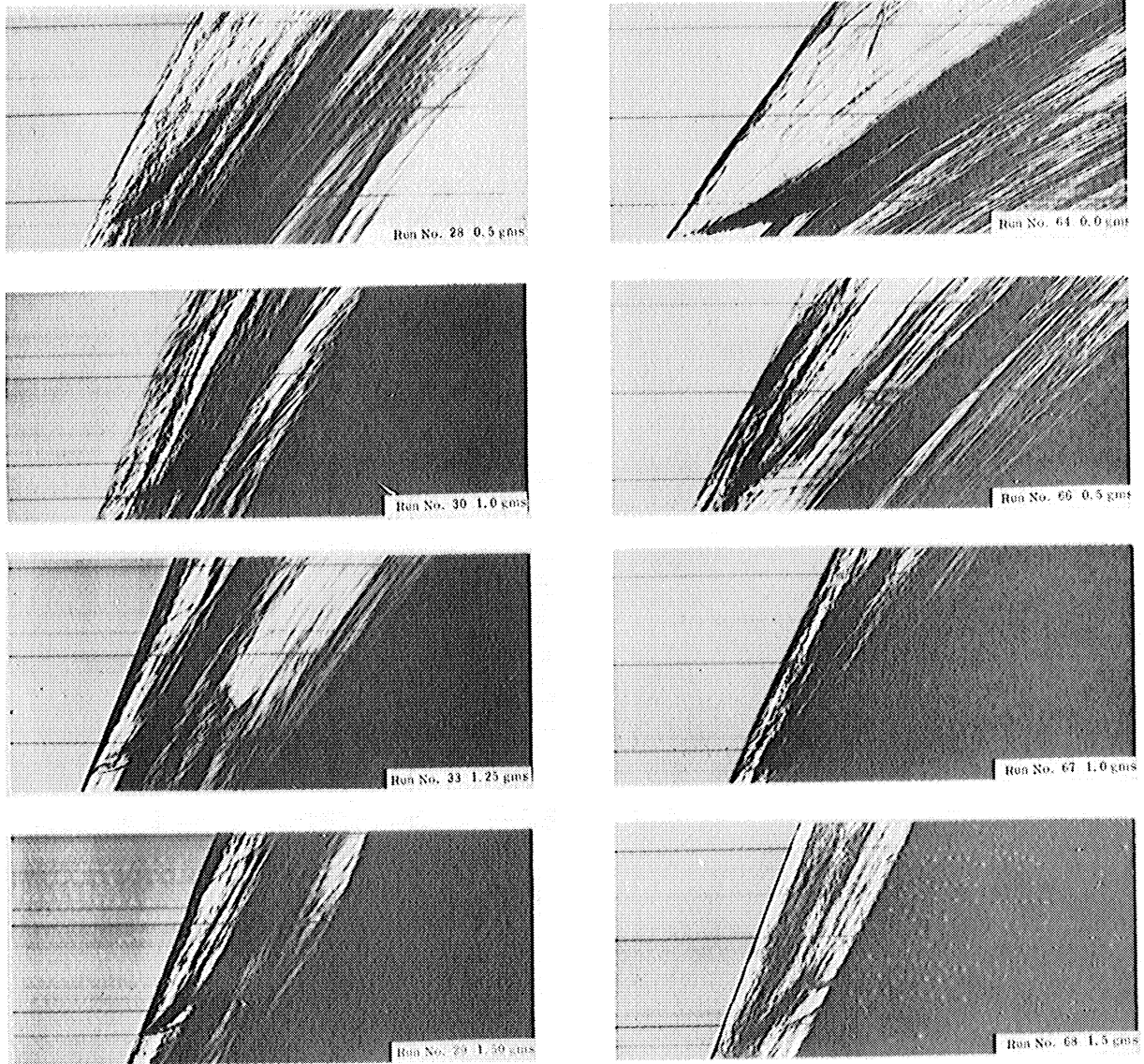
Figure 43.     Streak Schlieren Records, n-Propyl Nitrate, 384 $\mu$ m, left column, 100% $O_2$, right column 50% $O_2$ - 50% $N_2$.

144
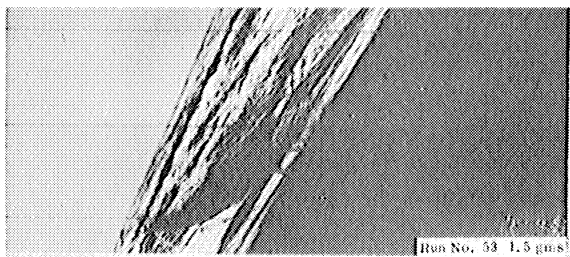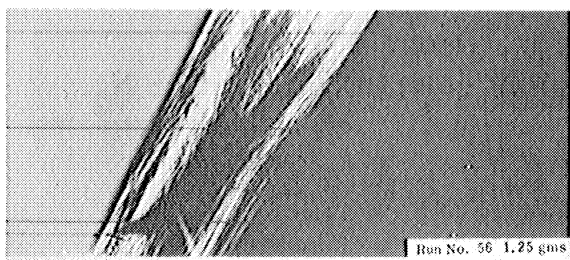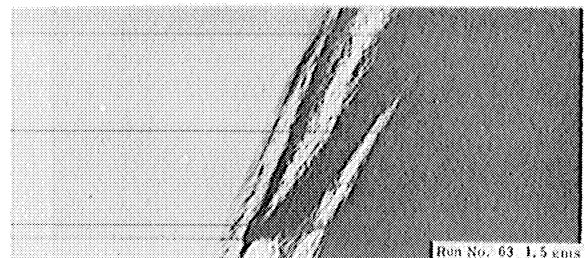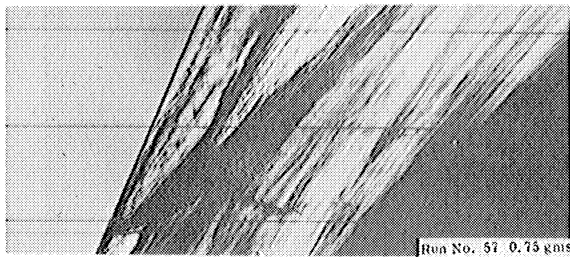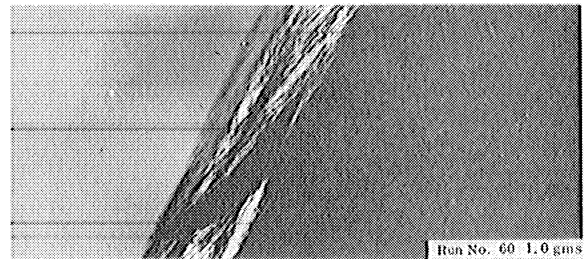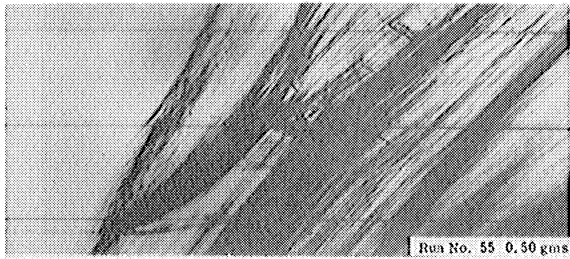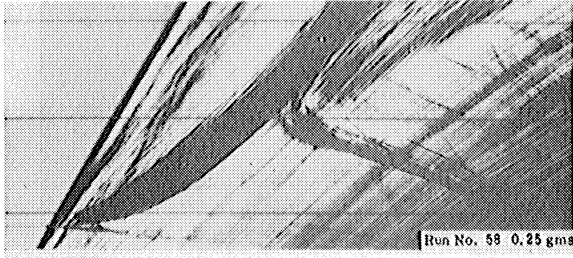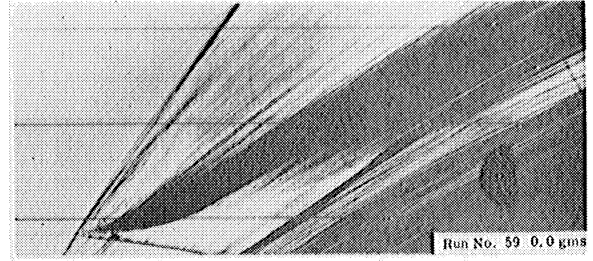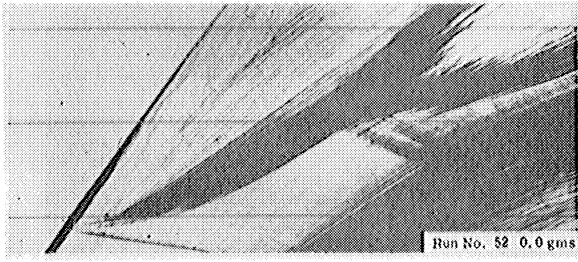
Streak Schlieren Records, Decane, 768 $\mu$ m,
left column 100% $O_2$, right column 50% $O_2$ - 50% $N_2$.
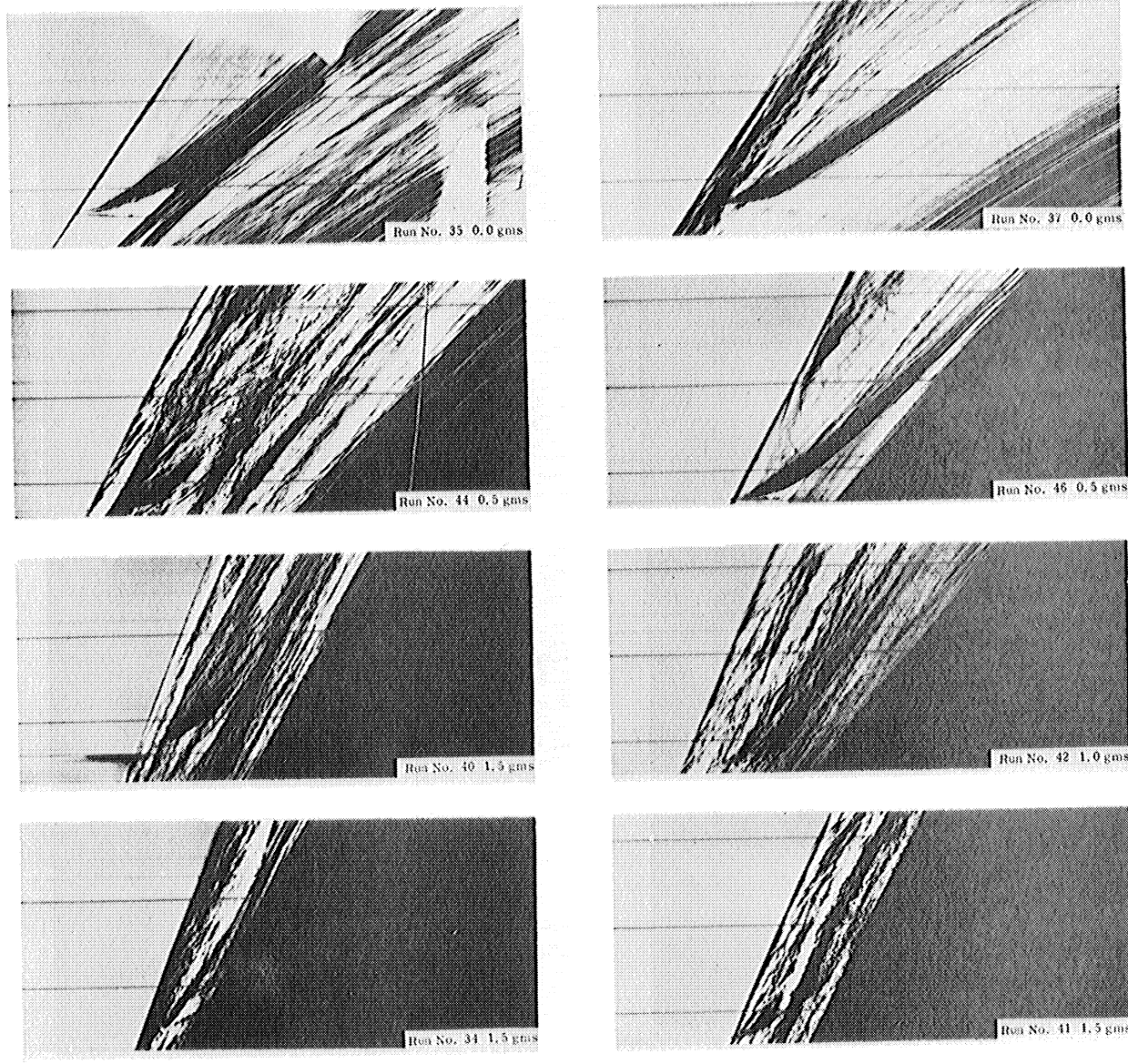
Figure 45. Streak Schlieren Records, Decane, $384 \mu m$, left column 100% $O_2$, right column 50% $O_2$-50% $N_2$.

146
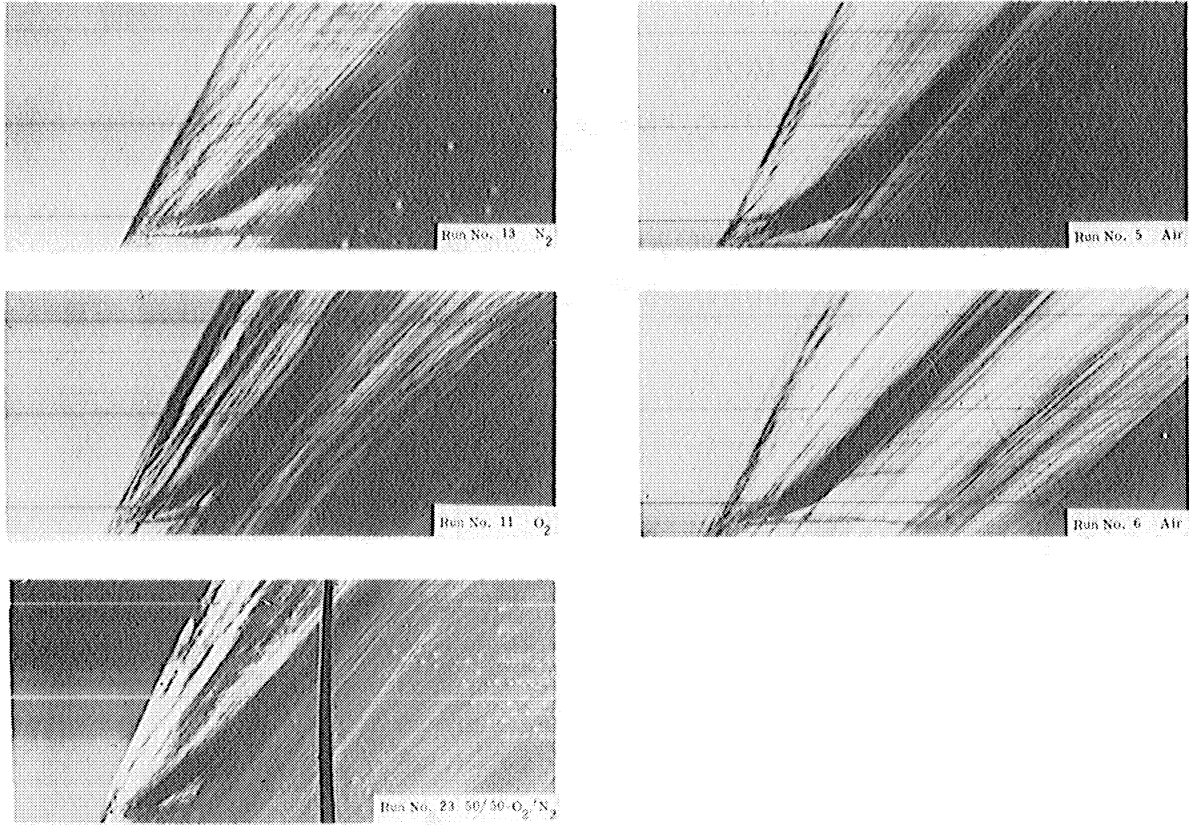
Figure 46.    Streak Schlieren Records, n-Propyl Nitrate, 768 $\mu$m, 0.5 gms Detasheet 'C'.
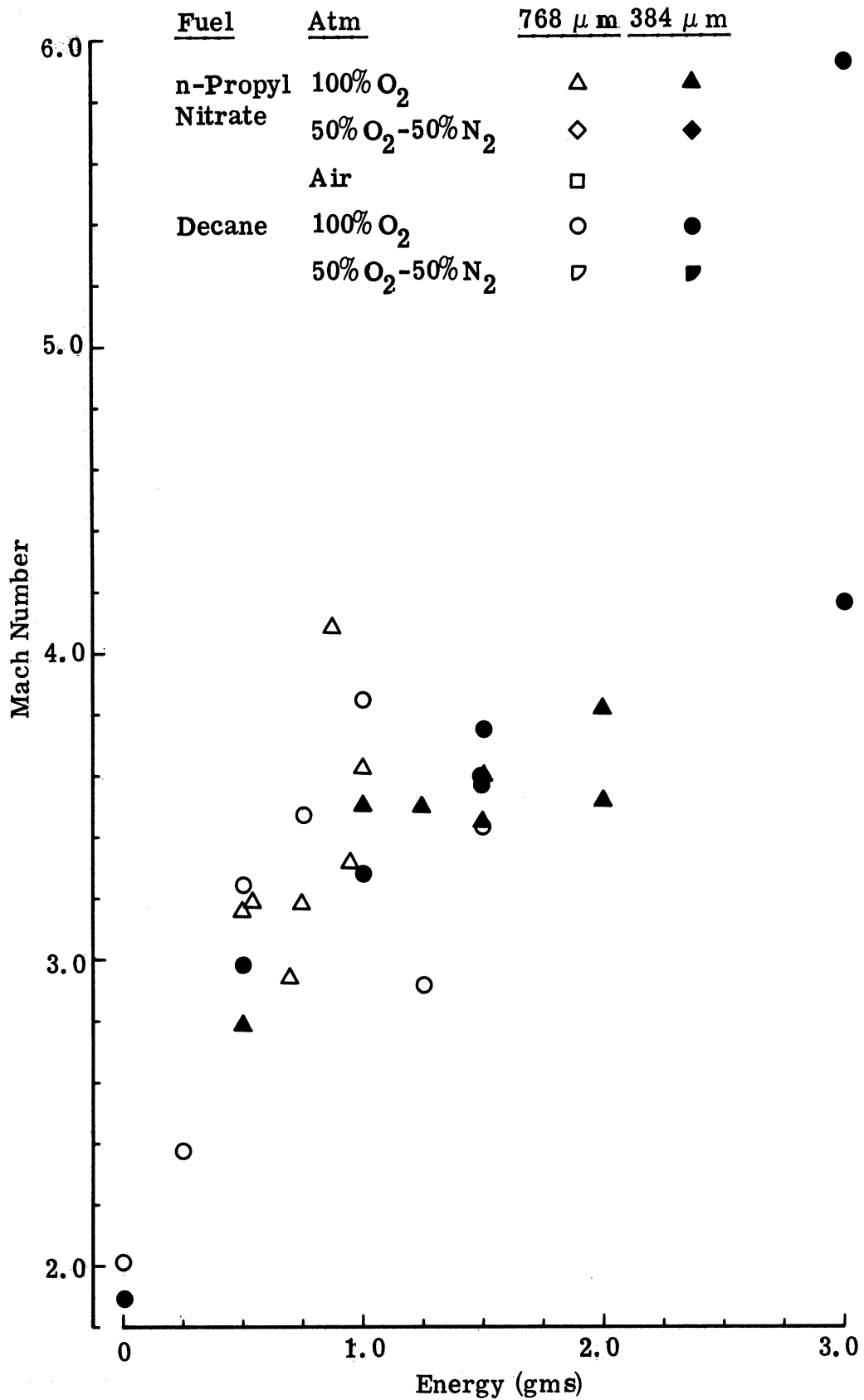
Figure 47a.    Blast Wave Mach Number at R = 24 in. vs Blast Source Energy, 100% $O_2$.
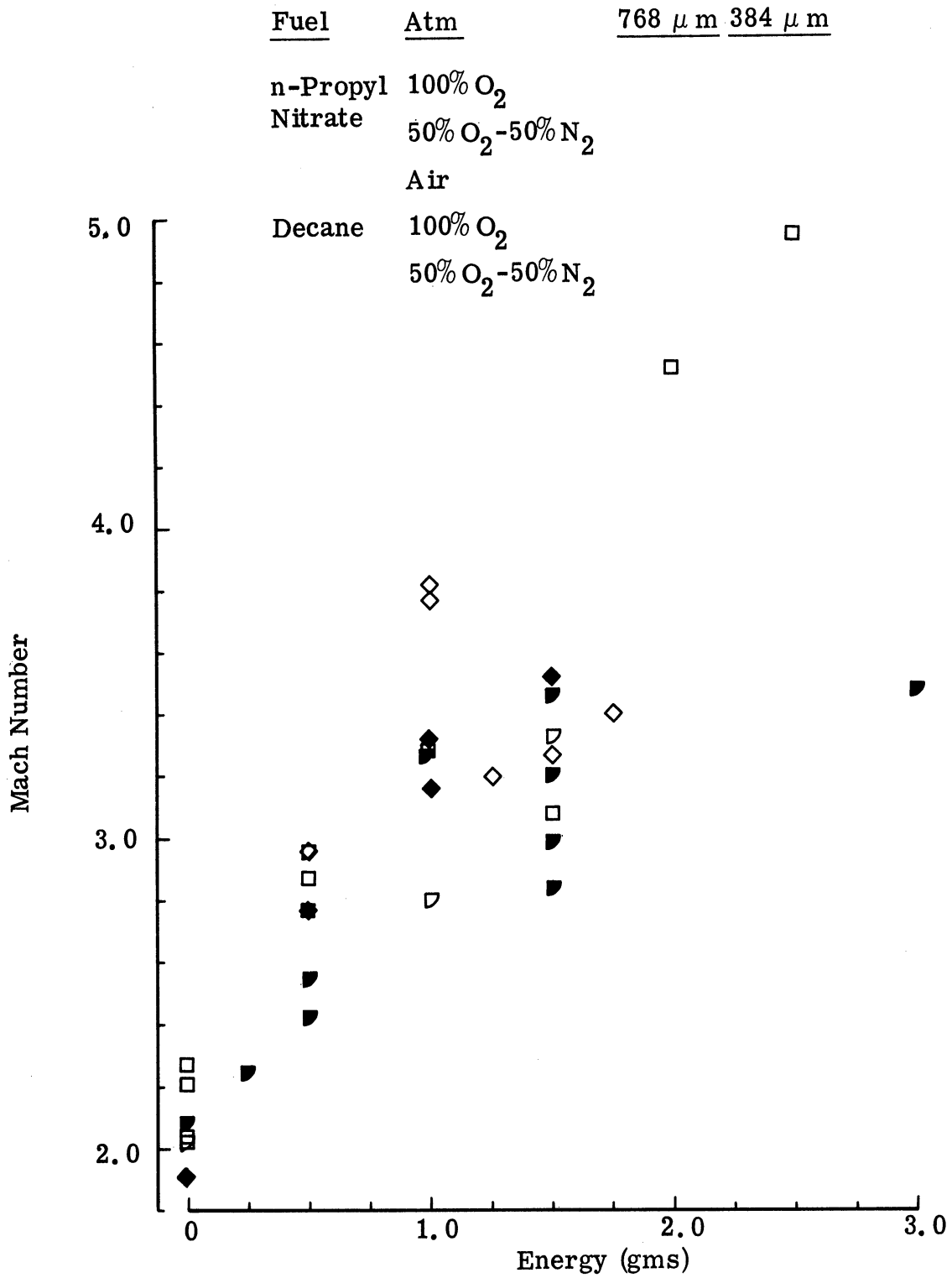
Figure 47b. Blast Wave Mach Number at R =24 in. vs Blast Source Energy, 50% $O_2$-50% $N_2$ and Air.
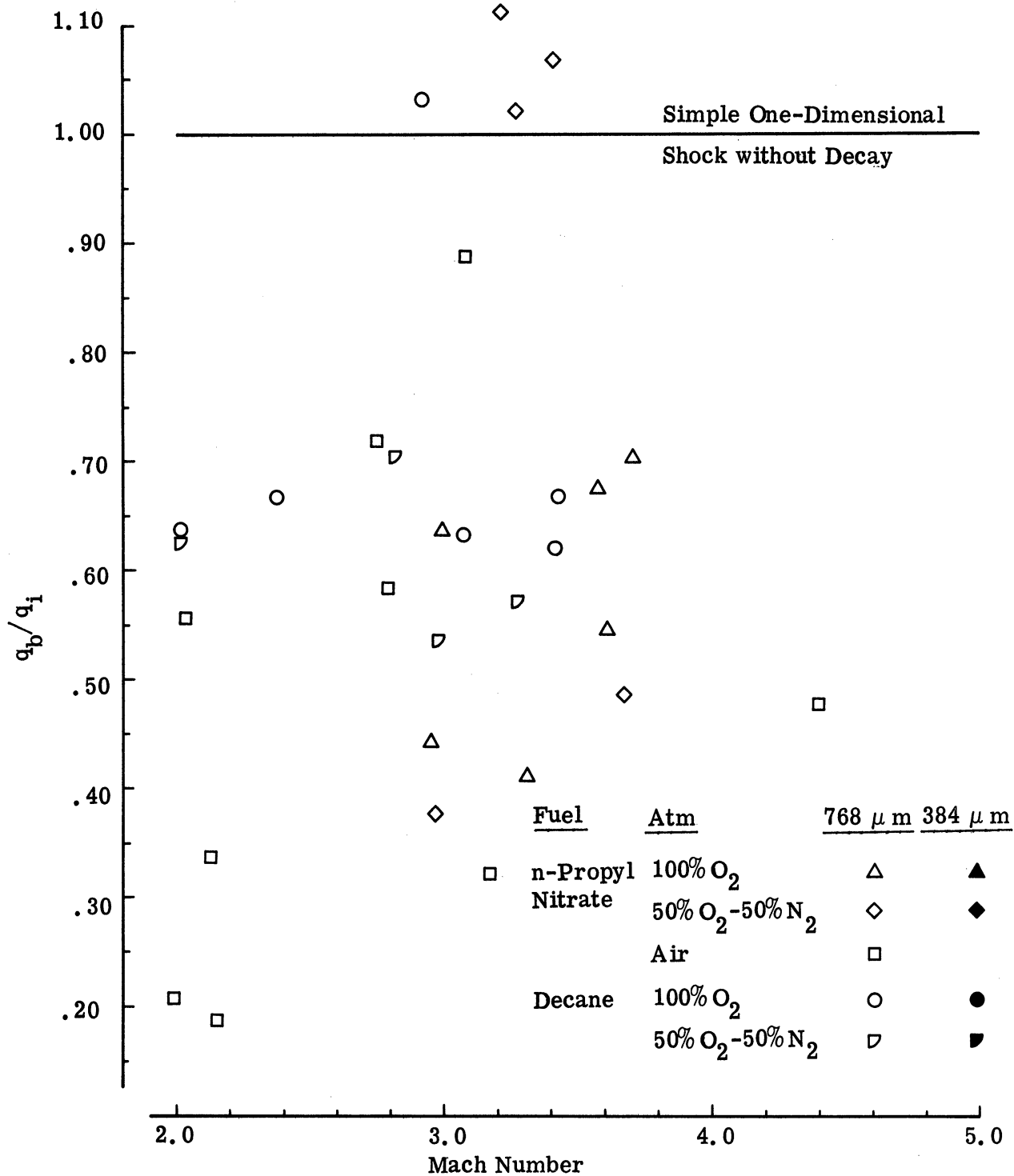
Figure 48a.  Drop Local Dynamic Pressure Ratio vs Mach Number, $D_o = 768 \, \mu$ m.
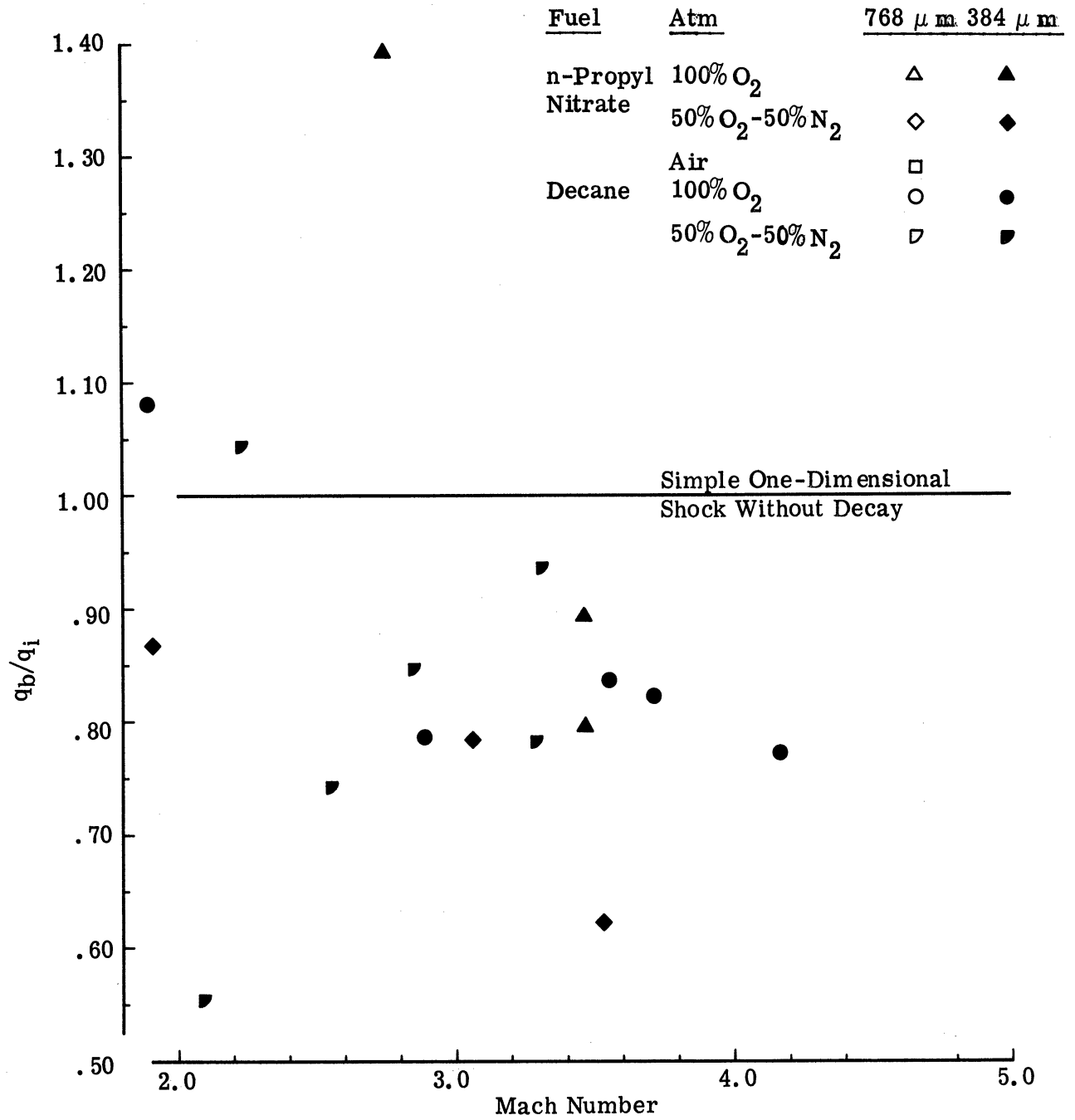
Figure 48b.    Drop Local Dynamic Pressure Ratio vs Mach Number, $D_o$ = 384 $\mu$ m.
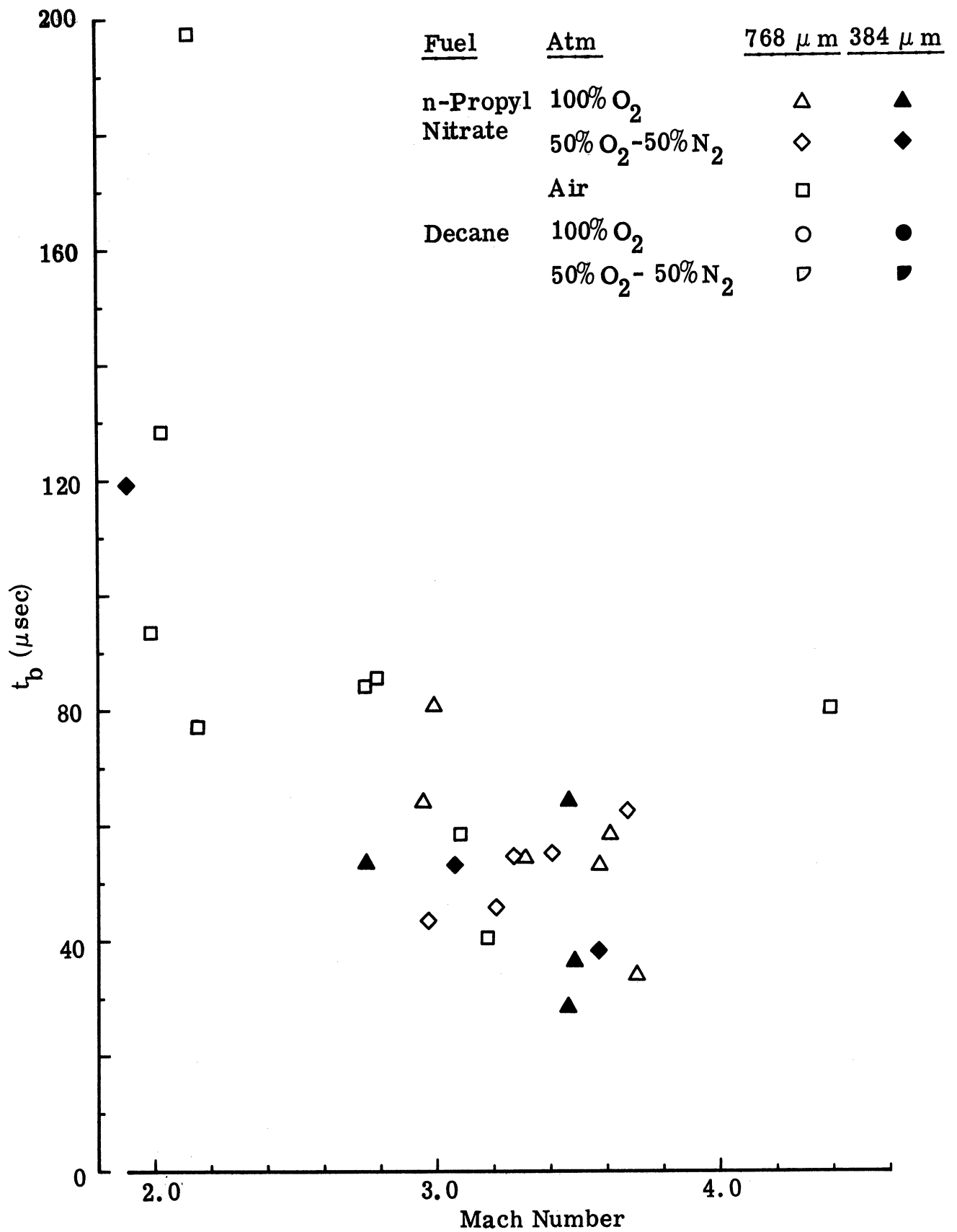
Figure 49a.    Breakup Time vs Mach Number, n-Propyl Nitrate.
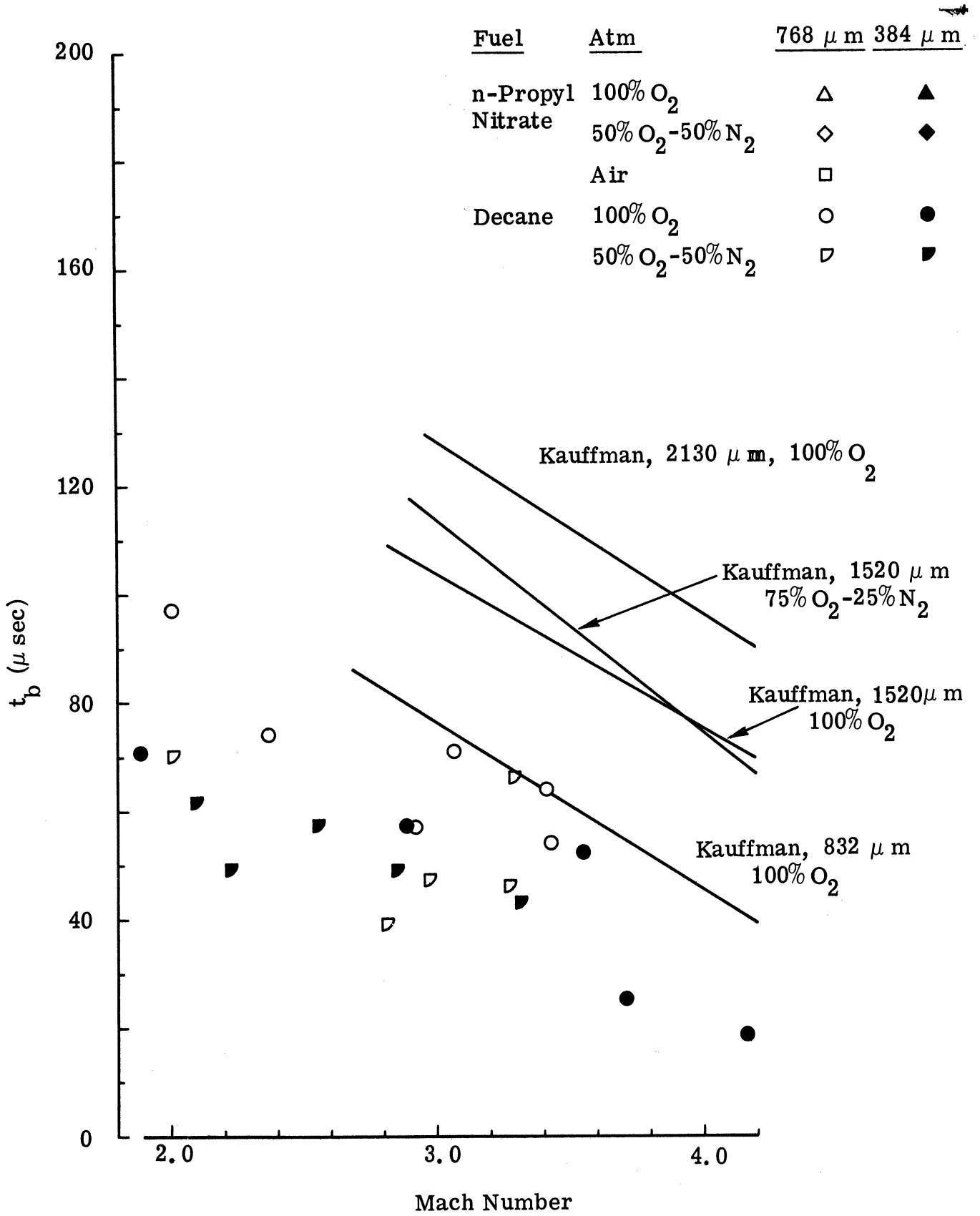
Figure 49b.    Breakup Time vs Mach Number, Decane.
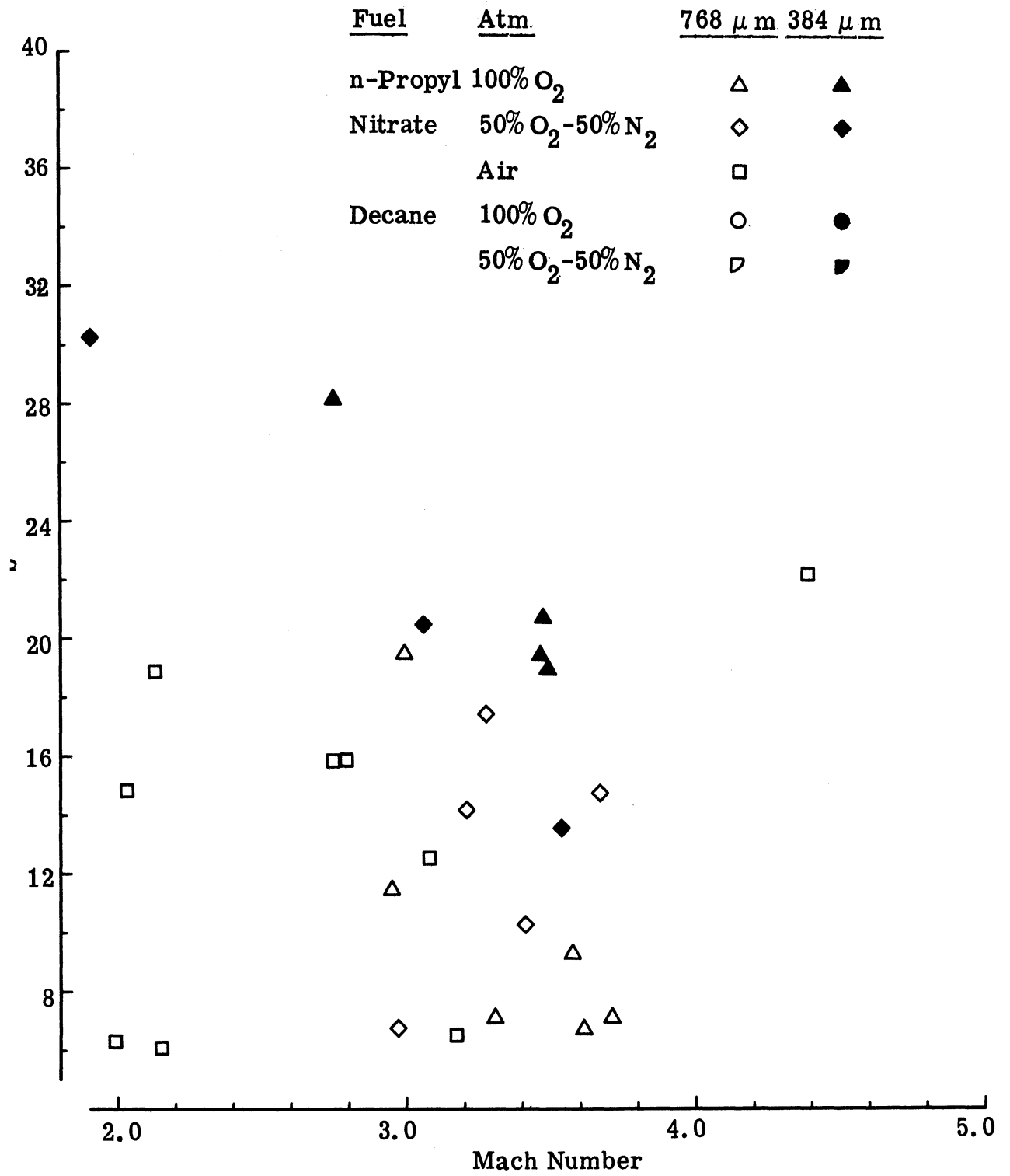
Figure 50a.    Non-Dimensional Breakup Distance vs Mach Number, n-Propyl Nitrate.
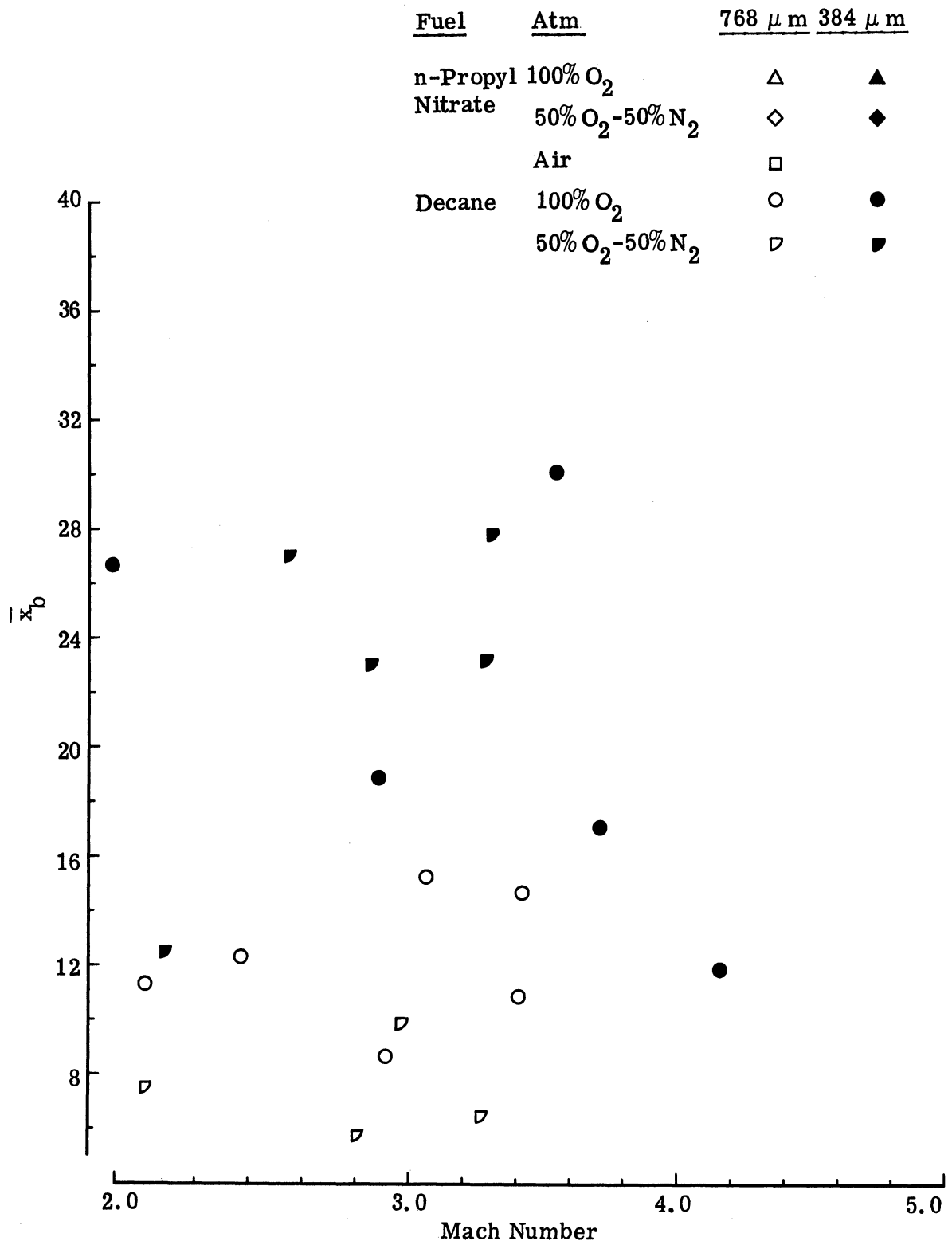
Figure 50b. Non-Dimensional Breakup Distance vs Mach Number, Decane.
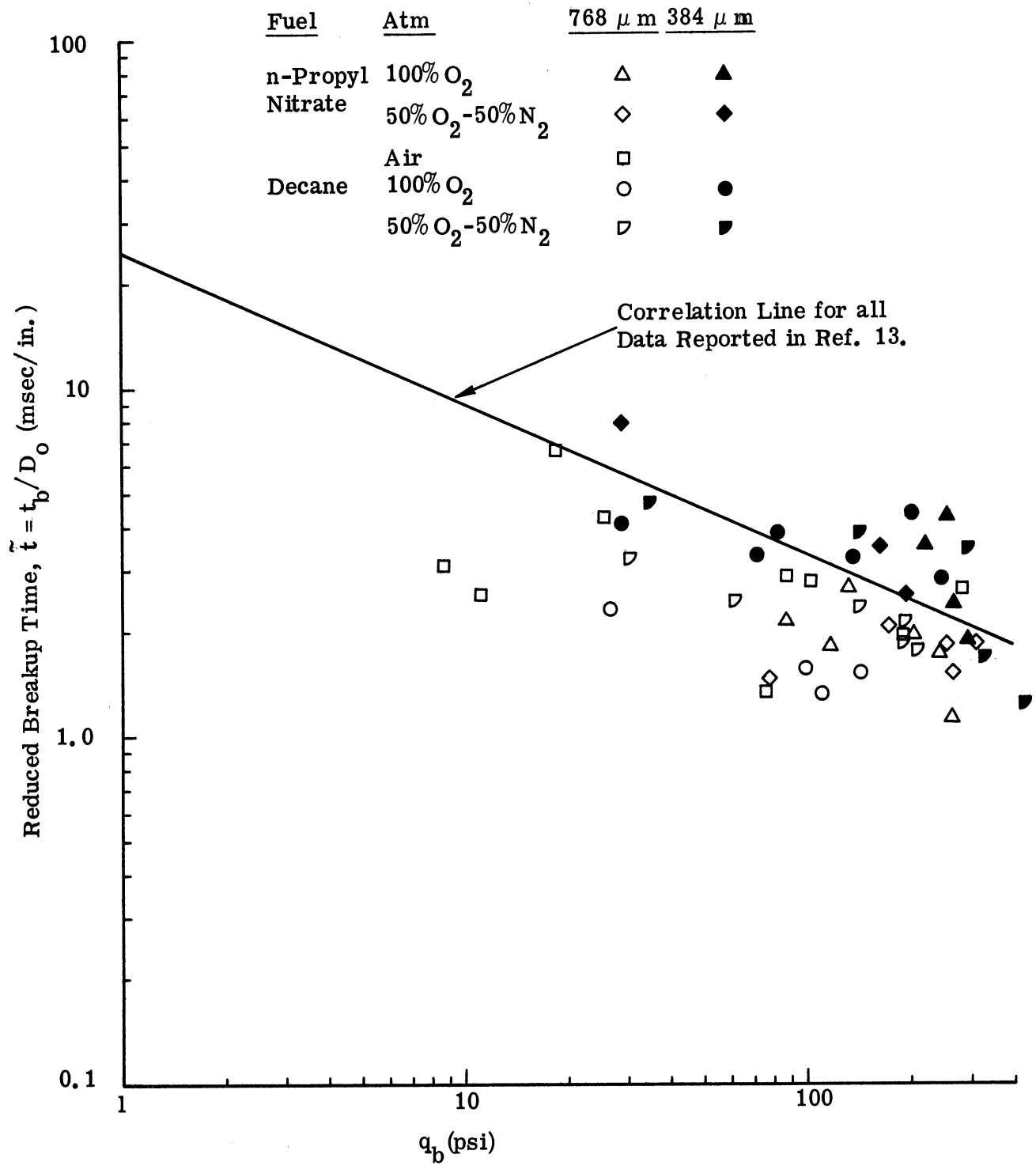
Figure 51.    Reduced Breakup Time vs Dynamic Pressure at Breakup.
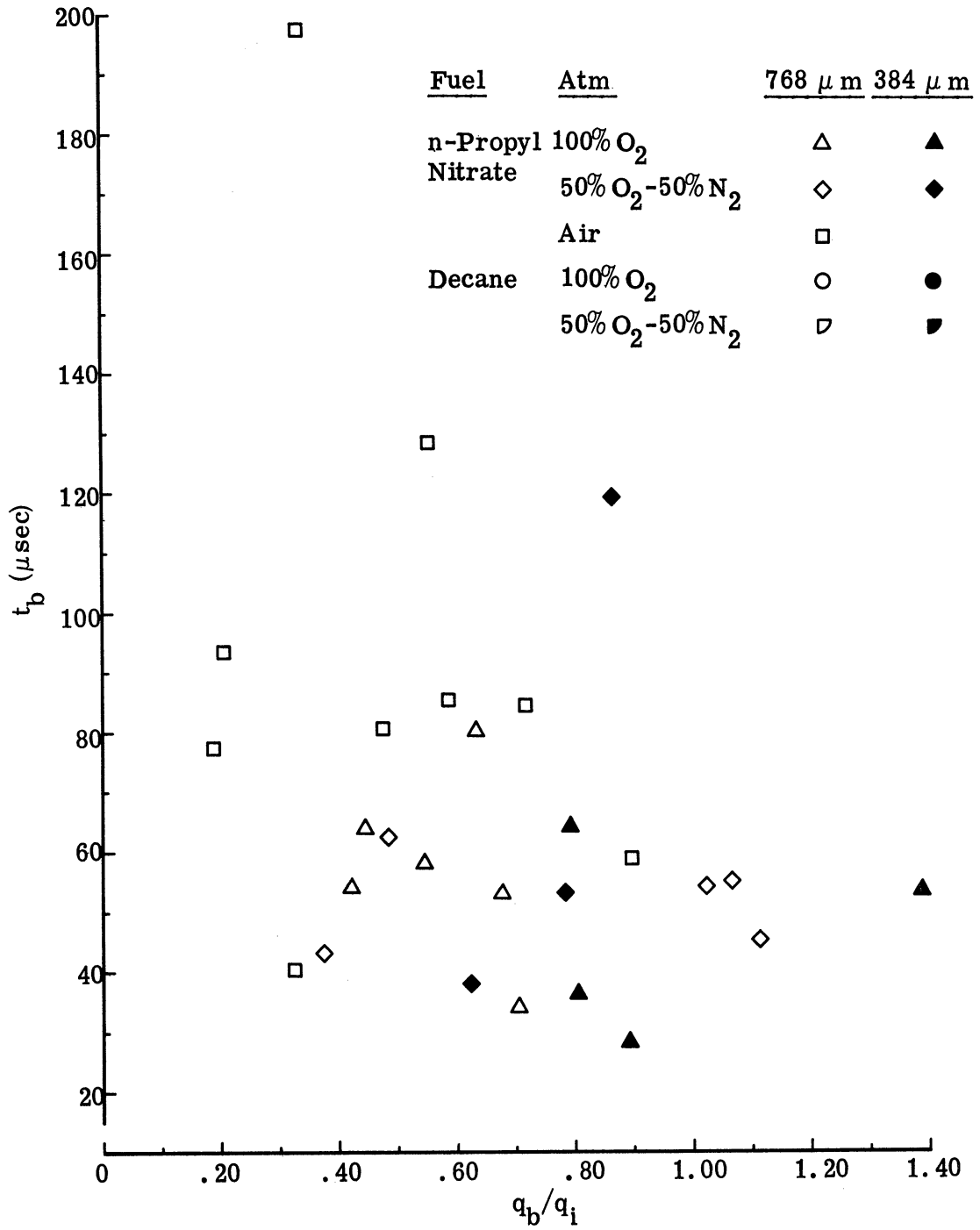
Figure 52a.    Breakup Time vs Drop Local Dynamic Pressure Ratio, n-Propyl Nitrate.
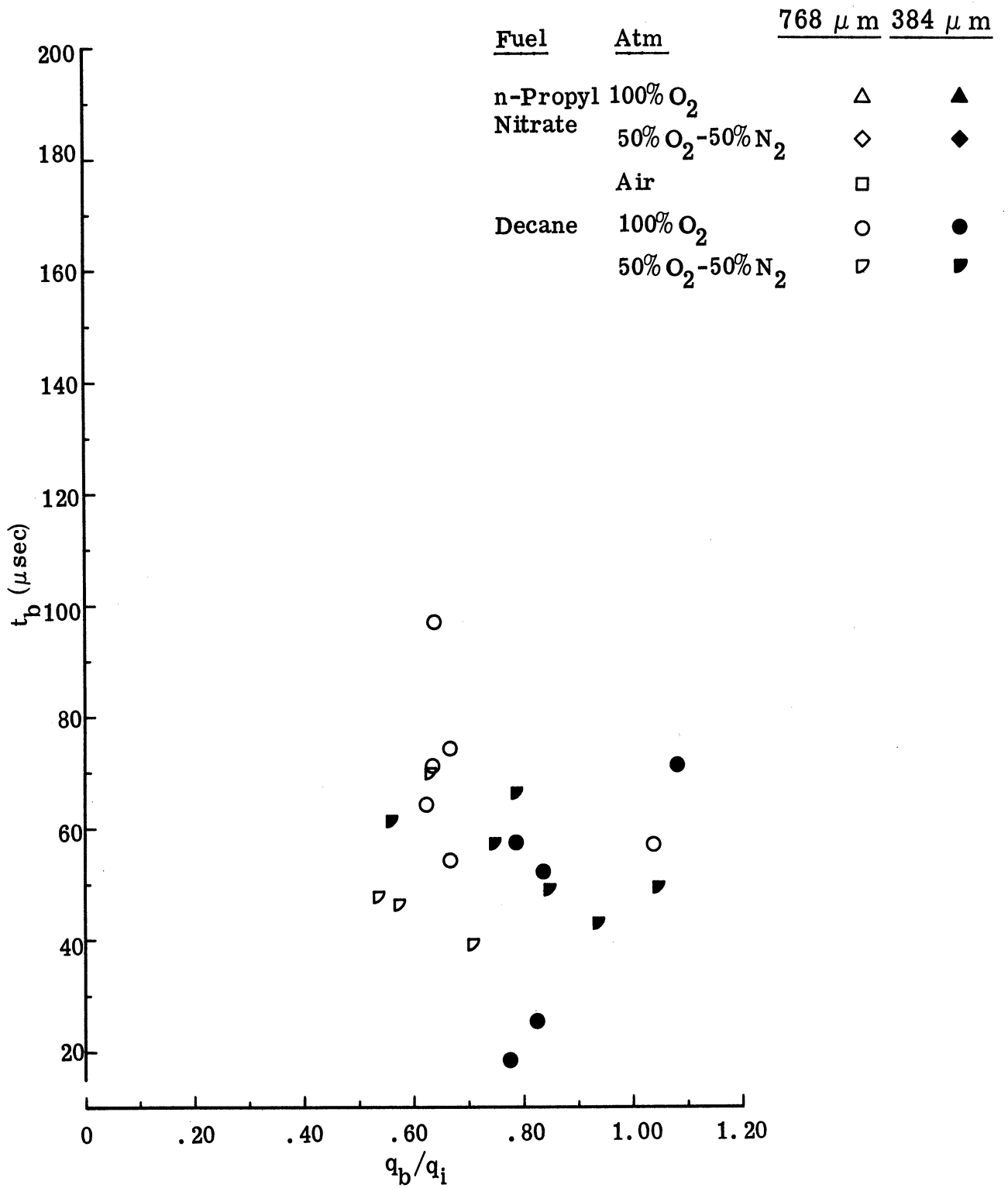
Figure 52b.    Breakup Time vs Drop Local Dynamic Pressure Ratio, Decane.
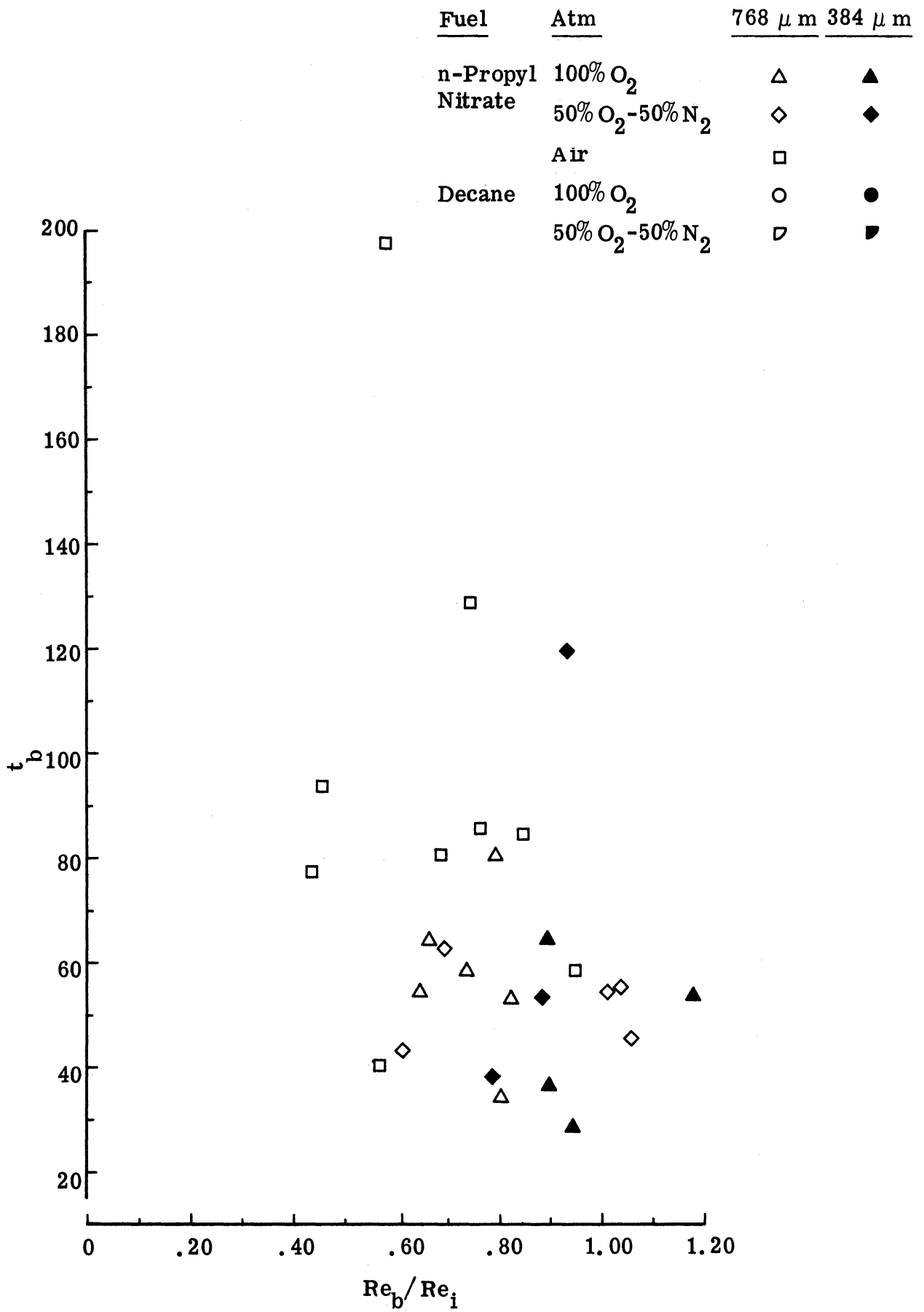
Figure 53a.    Breakup Time vs Drop Local Reynolds Number Ratio, n-Propyl Nitrate.

| Fuel | Atm. | | 768 $\mu$ m | 384 $\mu$ m |
|------|------|--|-------------|-------------|
| n-Propyl Nitrate | 100% $O_2$ | | △ | ▲ |
| | 50% $O_2$-50% $N_2$ | | ◇ | ◆ |
| | Air | | □ | |
| Decane | 100% $O_2$ | | ○ | ● |
| | 50% $O_2$-50% $N_2$ | | ◹ | ◢ |
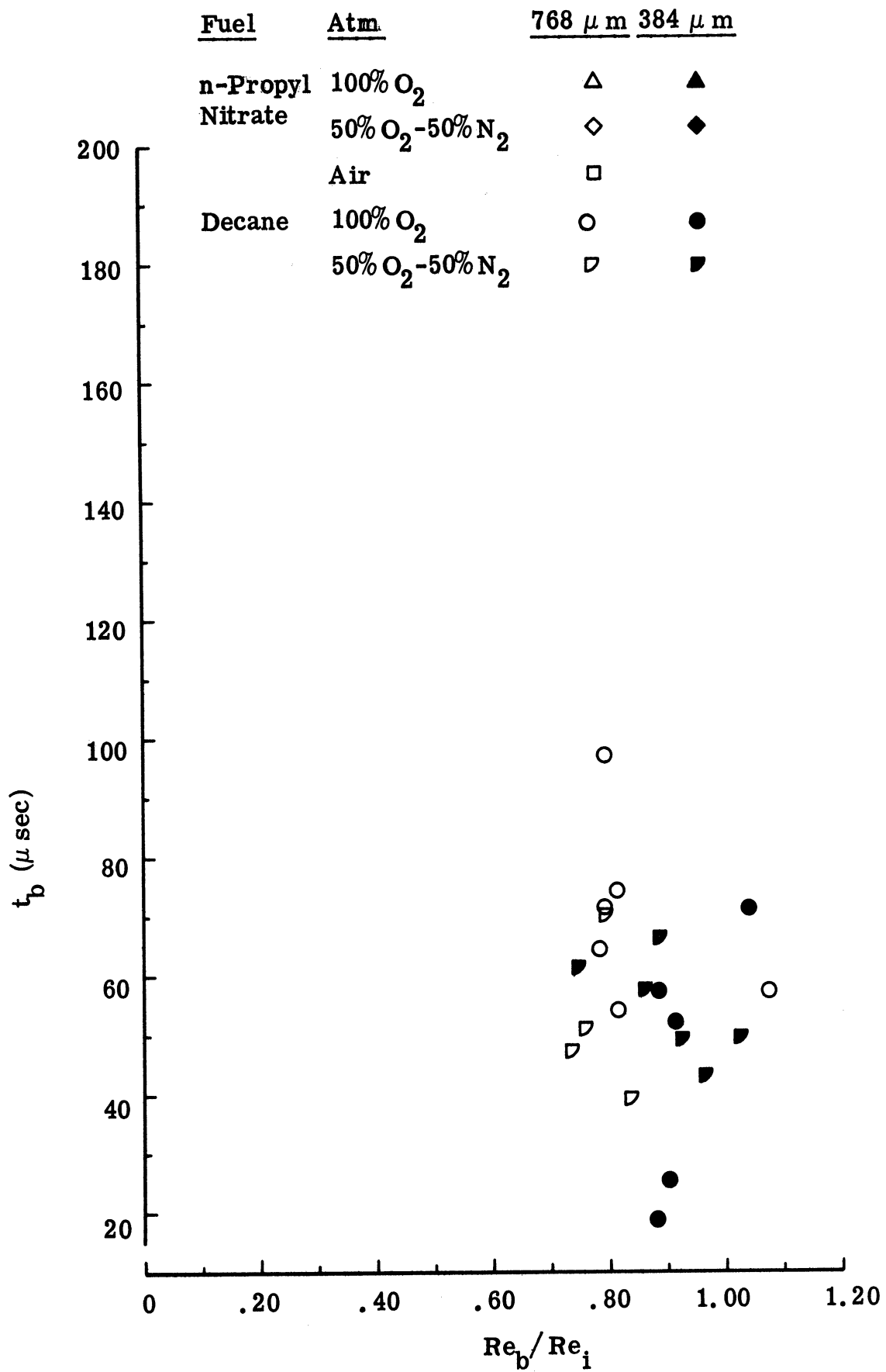
Figure 53b.    Breakup Time vs Drop Local Reynolds Number Ratio, Decane.

160
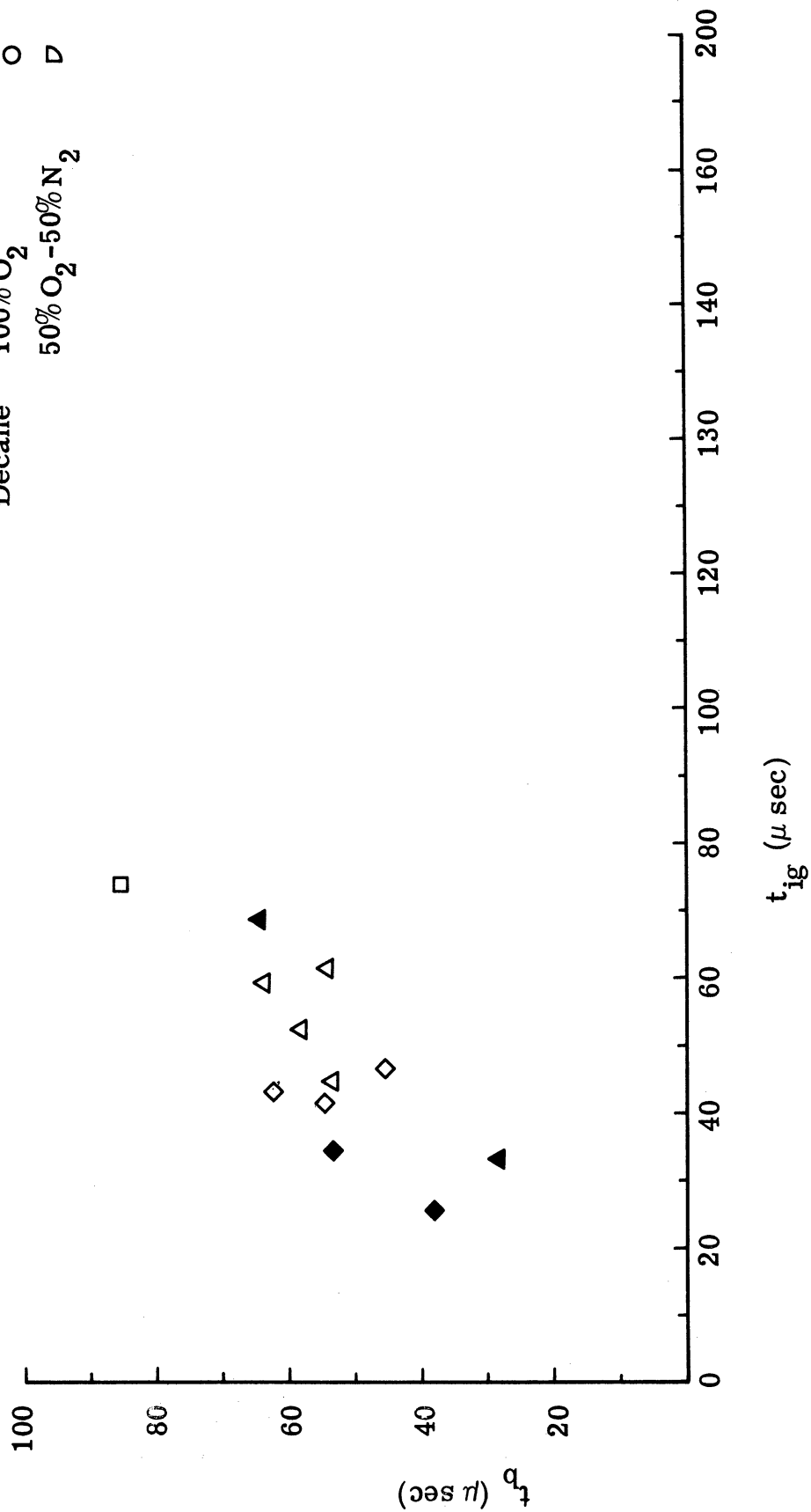
Figure 54a.　Breakup Time vs Ignition Delay Time, n-Propyl Nitrate.
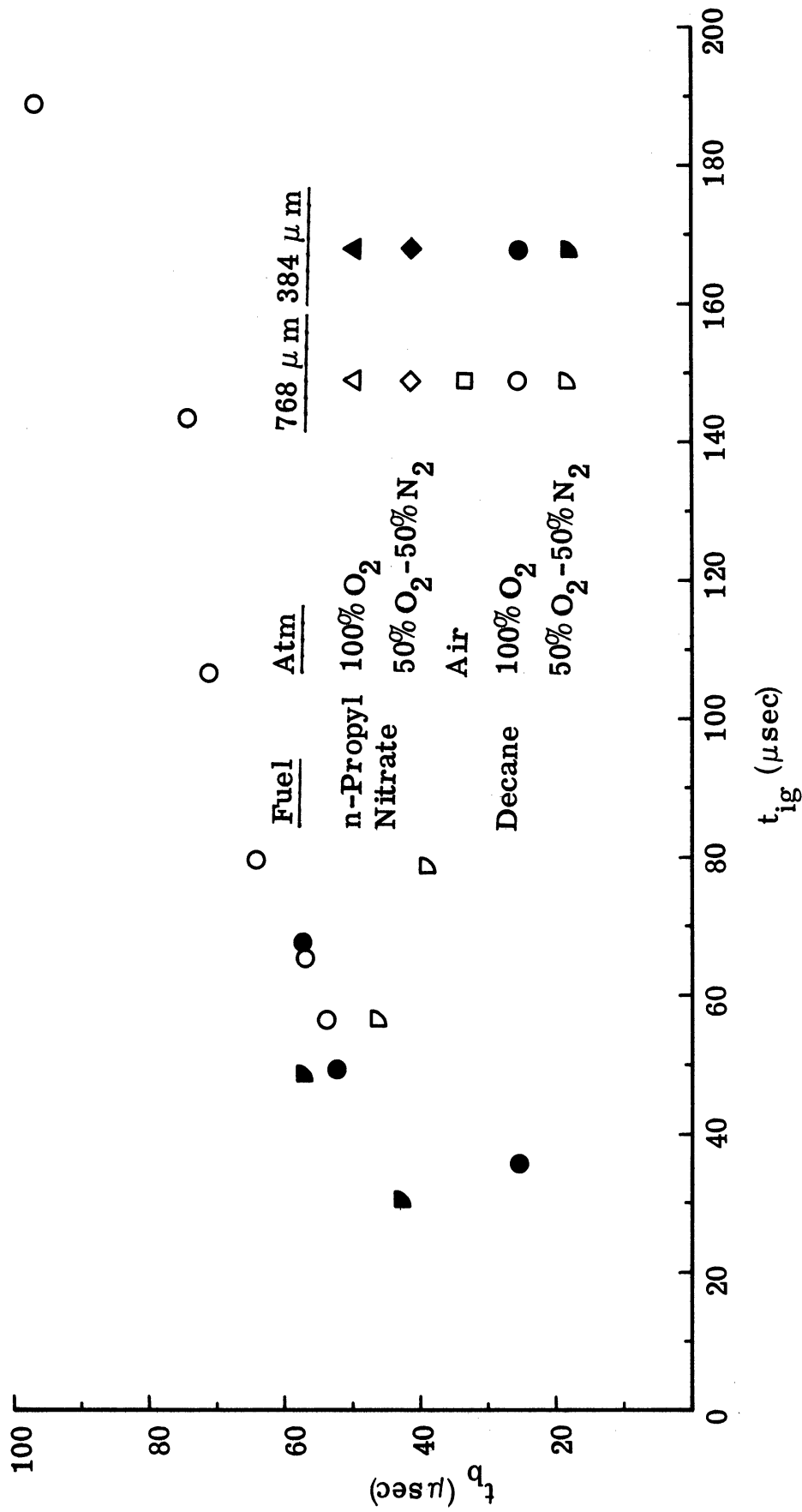
Figure 54b.    Breakup Time vs Ignition Delay Time,  Decane.
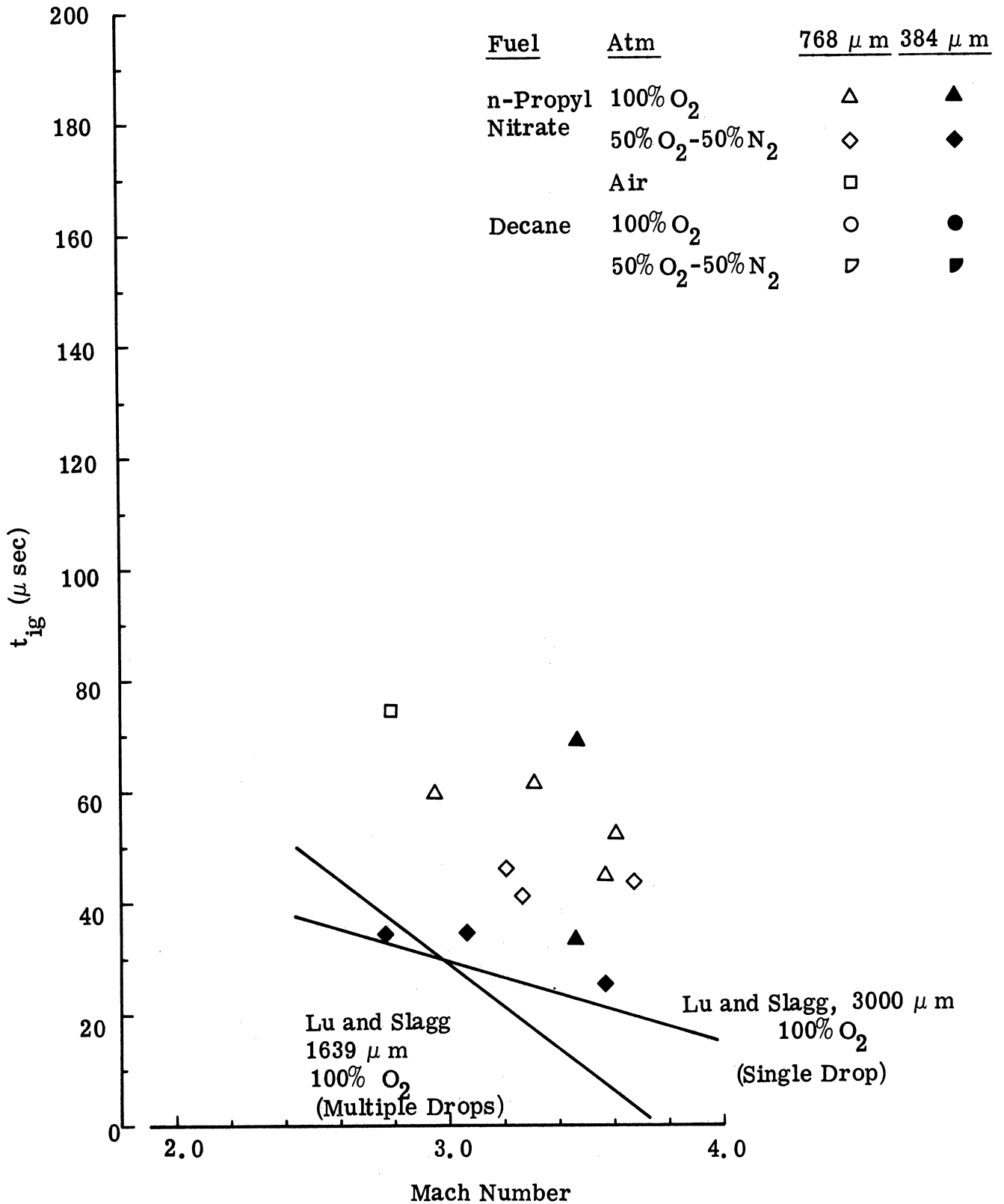
Figure 55a.    Ignition Delay Time vs Mach Number, n-Propyl Nitrate.
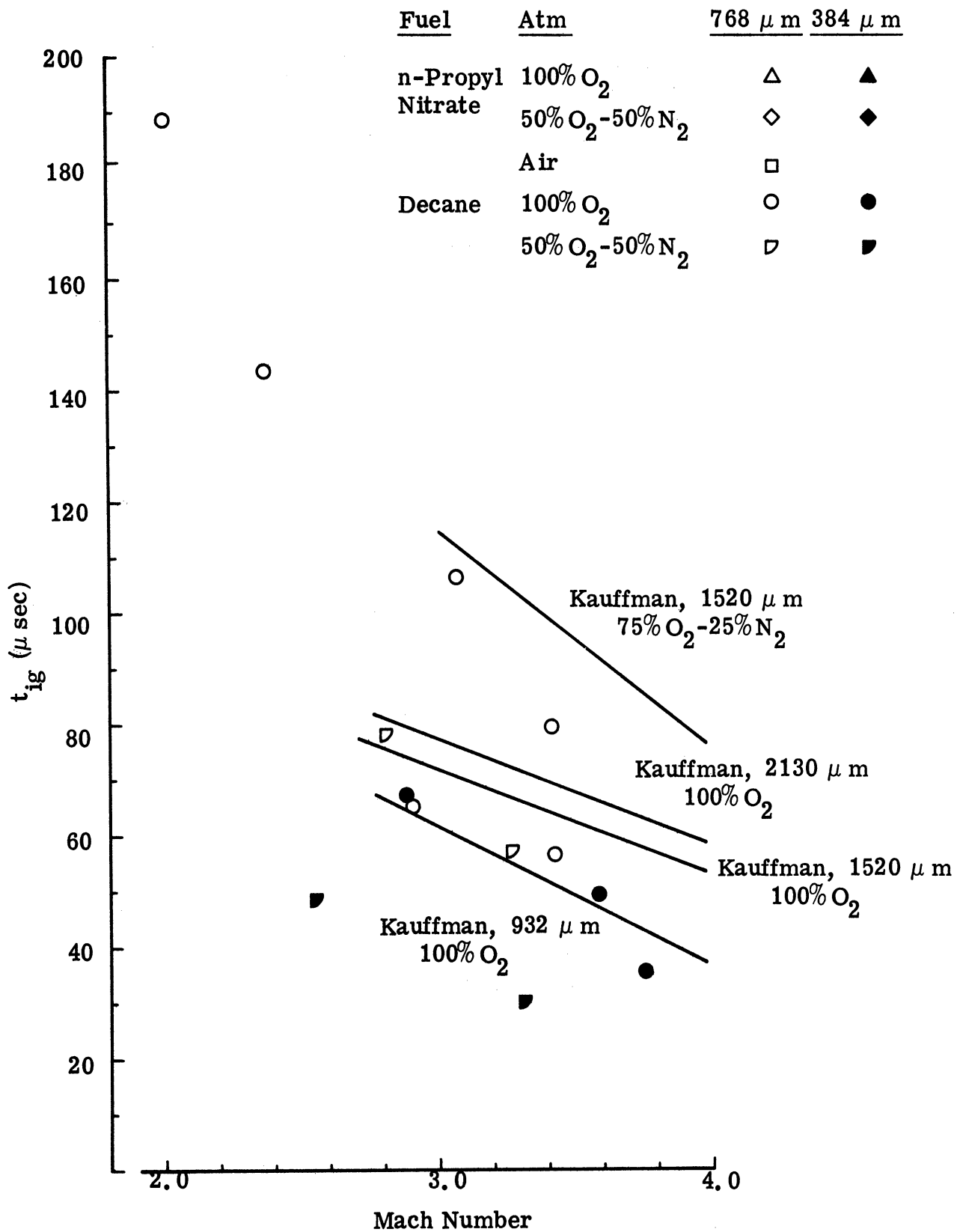
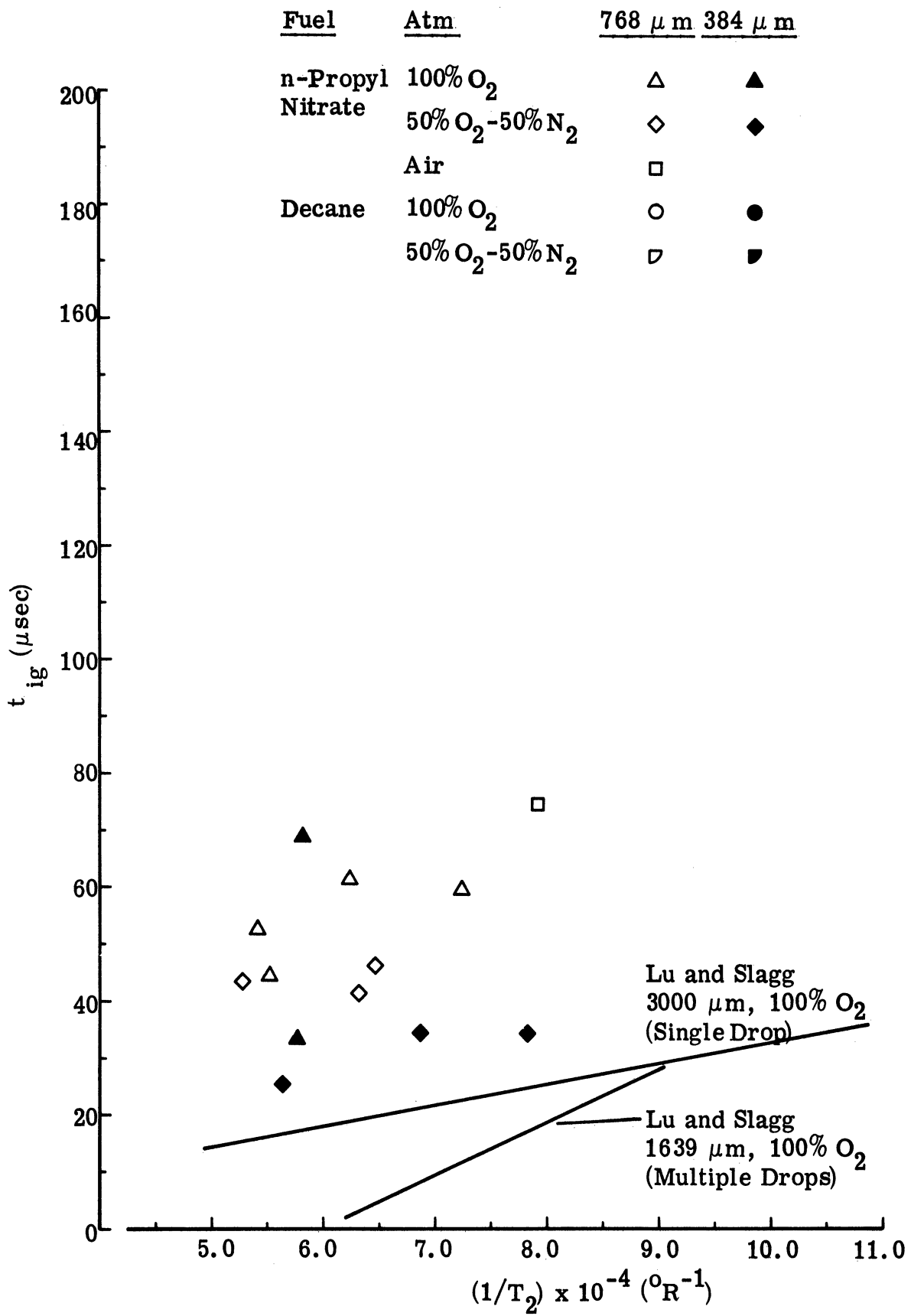Figure 55b.    Ignition Delay Time vs Mach Number, Decane.

Figure 56a.    Ignition Delay Time vs Reciprocal Static Temperature,  n-Propyl Nitrate.
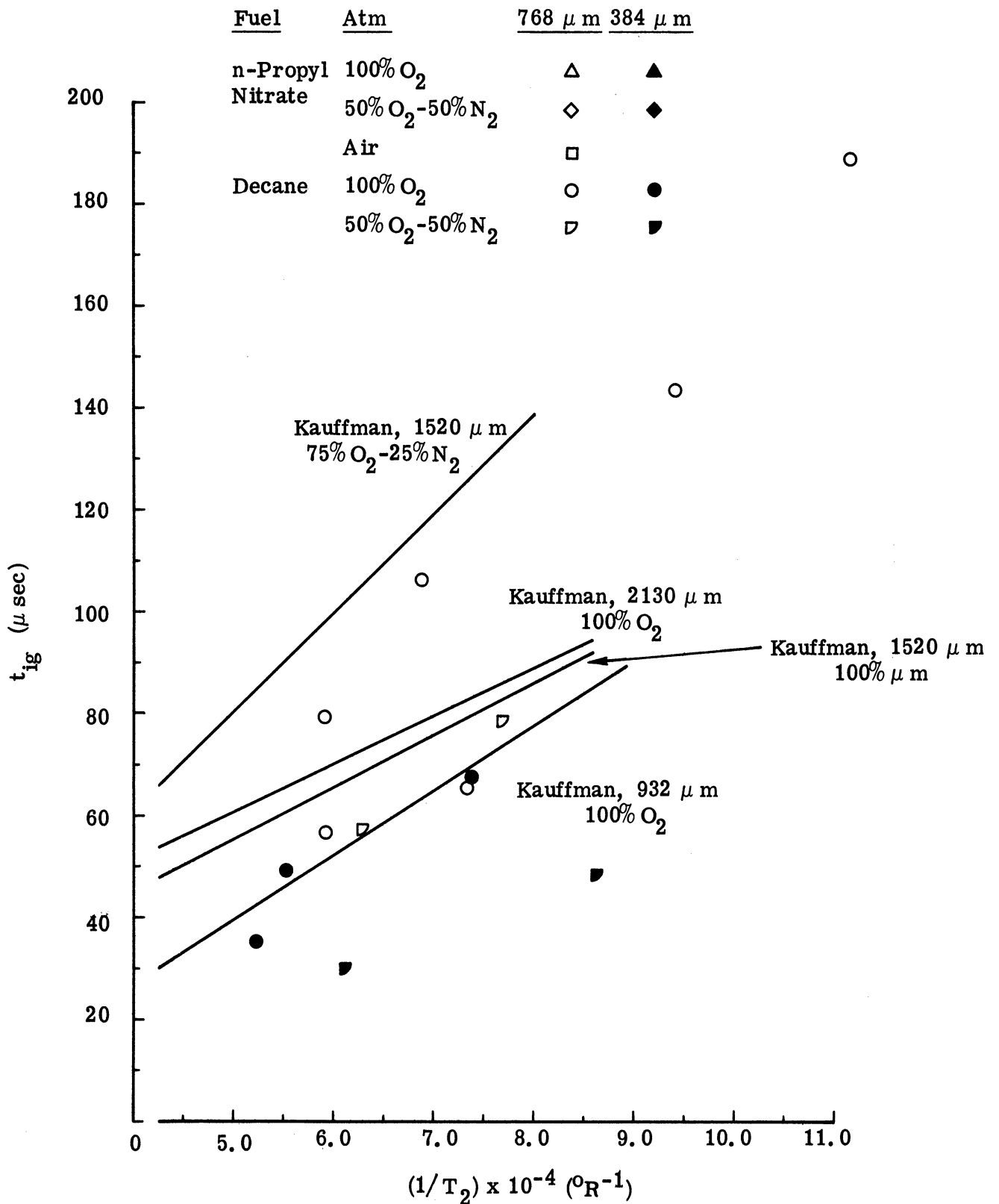
Figure 56b. Ignition Delay Time vs Reciprocal Static Temperature, Decane.
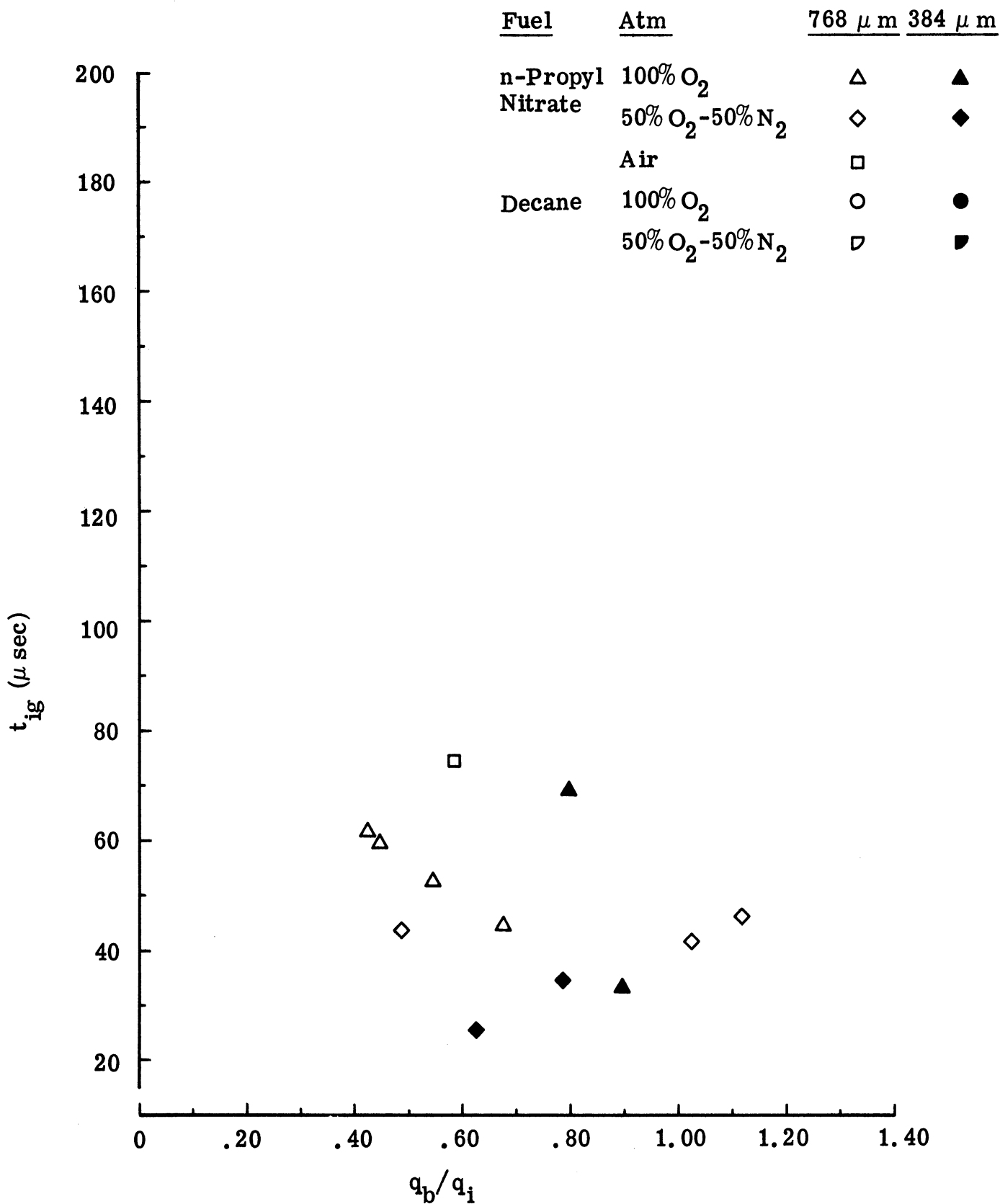
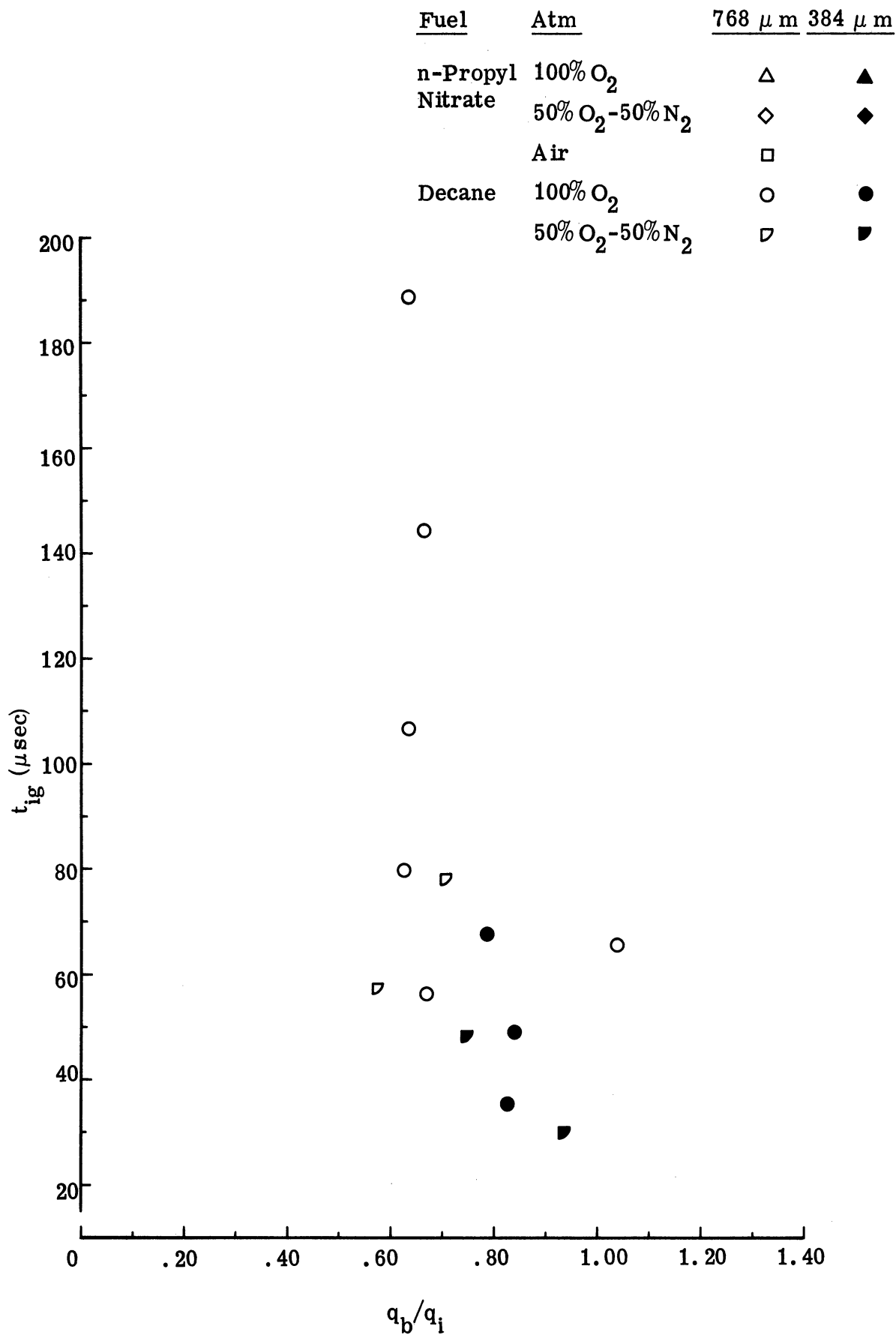Figure 57a.    Ignition Delay Time vs Drop Local Dynamic Pressure Ratio, n-Propyl
Nitrate.

167

**Figure 57b.** Ignition Delay Time vs Drop Local Dynamic Pressure Ratio, Decane.

168